

**Isolation and Structure Elucidation of Bioactive Secondary
Metabolites from the Sponge-Associated Fungus *Aspergillus* sp.**

**(Isolierung und Strukturaufklärung von Bioaktiven Sekundärmetaboliten aus
dem Schwamm Assoziierten Pilz *Aspergillus* sp.)**

**Inaugural-Dissertation
zur
Erlangung des Doktorgrades
der Mathematisch-Naturwissenschaftlichen Fakultät
der Heinrich-Heine-Universität Düsseldorf**

**vorgelegt von
Yaming Zhou
Aus Beijing, V. R. China**

Düsseldorf, 05. 2012

**Aus dem Institut für Pharmazeutische Biologie und Biotechnologie
der Heinrich-Heine Universität Düsseldorf**

**Gedruckt mit der Genehmigung der
Mathematisch-Naturwissenschaftlichen Fakultät der
Heinrich-Heine-Universität Düsseldorf**

**Gedruckt mit der Unterstützung des
China Scholarship Council, the Ministry of Education of China**

Referent: Prof. Dr. Peter Proksch

Koreferent: Prof. Dr. Matthias U. Kassack and Prof. Dr. Wenhan Lin

Tag der mündlichen Prüfung: 28. 06. 2012

Erklärung

Hiermit erkläre ich ehrenwörtlich, dass ich die vorliegende Dissertation mit dem Titel „Isolierung und Strukturaufklärung von Bioaktiven Sekundärmetaboliten aus dem Schwamm Assoziierten Pilz *Aspergillus* sp.“ selbst angefertigt habe. Außer den angegebenen Quellen und Hilfsmitteln wurden keine weiteren verwendet. Diese Dissertation wurde weder in gleicher noch in abgewandelter Form in einem anderen Prüfungsverfahren vorgelegt. Weiterhin erkläre ich, dass ich früher weder akademische Grade erworben habe, noch dies versucht habe.

Düsseldorf, den 11.05.2012

Yaming Zhou

Acknowledgements

First of all I sincerely acknowledge my appreciation to Prof. Dr. Peter Proksch for providing me this valuable opportunity to pursue the doctoral research and for the excellent work facilities in the Institute of Pharmaceutical Biology and Biotechnology, Heinrich-Heine University, Düsseldorf. I would also like to express my heartfelt gratitude and deep thanks for his genial supervision, admirable guidance, fruitful discussions, generous considerations and unforgettable support for my study in Düsseldorf.

My special thanks are to Prof. Dr. Wenhan Lin (National Research Laboratories of Natural and Biomimetic Drugs, Peking University, Health Science Center) for his valuable suggestions, constructive discussions and continuous encouragement.

I am deeply indebted to Dr. Amal Hassan for all the techniques and knowledge she taught me, together with her precious help, patient guidance and scientific advices. Without her I could not make the study until now.

I would like to express my appreciation to Dr. Victor Wray (Helmholtz Centre for Infection Research) for the distinguished NMR measurements and his significant opinion on the structure elucidation of compounds, Prof. W. E. G. Müller (University of Mainz) for conducting the cytotoxicity assays. I am also thankful to Dr. Peters and his colleagues (HHU-Düsseldorf) for 500 MHz ^1H -NMR and 125 MHz ^{13}C -NMR measurement as well as Dr. Keck and Dr. Tommes (HHU-Düsseldorf) for EI-mass spectra measurements.

I am grateful to Dr. Tibor Kurtán (Department of Organic Chemistry, University of Debrecen, Hungary) and his coworkers for their splendid CD calculation, as well as Dr. Abdessamad Debbab for valuable advices, NMR courses and generous help in structure elucidation.

I am deeply thankful to Prof. Dr. Barbara Schulz (Institut für Mikrobiologie, Technische Universität Braunschweig) for introducing me to Prof. Dr. Peter Proksch. My thankfulness is also to Prof. Dr. Bingui Wang and Dr. RuAngelie Edrada-Ebel for their fruitful discussions, constructive advices and measurements of NMR and HRMS spectra.

I would like to acknowledge Prof. Dr. Matthias U. Kassack for conducting cytotoxicity assays and estimating my PhD study as second referee.

I am grateful to Dr. Yao Wang, Dr. Sherif Elsayed and Dr. Julia Kjer for helping me to get through my life, taking care of me and instructing when I started my study at the institute. I would like to deeply thank them for the pleased conversations and for making me feel like in a family in 26. 23. U1. 25.

I am indebted to Mrs. Claudia Eckelskemper for her kind and generous help of administration, and the technical staff Mrs. Waltraud Schlag and Mrs. Katrin Rohde for their geniality and for supplying laboratory materials. My thanks are also to Mrs. Simone Miljanovic, Mr. Klaus Dieter Jansen, Mrs. Eva Müller and Mrs. Heike Goldbach-Gecke for their help.

I would like to extend my sincere thanks to my past and present colleagues Dr. M. Bayer, Dr. A. Putz, Dr. J. Xu, C. Pham, B. Lipowicz, D. Rönsberg, L. Hammerschmidt, H. Niemann, A. Ola, R. Bara, G. Daletos, M. ElAmrani, W. Ebrahim, F. Z. Kabbaj, F. Okoye, M. A. Tarabeen, M. Elnekity, M. Onyebuchi, and all the others for the nice multicultural time I spent with them, for their help and assistance whenever I needed it. My deep thanks to my colleague Andreas Marmann for his help in writing and revising the German summary in this study.

I appreciate the generous help of Dr. Jianping Wang, Dr. Zhiyong Guo, Dr. Daowan Lai, and Dr. Shushan Gao as well as Dr. Aiyong Ma and Mrs. Jin Li and their

interesting discussions. I am also thankful to Prof. Dr. Claus Paßreiter for his safety instruction.

My profound appreciation is to the China Scholarship Council, Ministry of Education of China for the financial support during my stay in Germany.

At the end, I would like to express my deepest thanks and gratitude to my family for encouraging and supporting me always in good and bad times to finish this study.

To all of you, thank you very much!

Zusammenfassung

Marine Mikroorganismen haben sich als ergiebige Quelle von strukturell interessanten und biologisch aktiven Naturstoffen erwiesen. Insbesondere haben marine Pilze die Aufmerksamkeit auf sich gezogen durch die Diversität an chemischen Inhaltsstoffen und beobachteten biologischen Aktivitäten ihrer sekundären Metaboliten. Marine Pilze wurden aus verschiedenen Organismen isoliert, einschließlich Algen, Muscheln und im besonderen, Schwämmen. Jedoch erwiesen sich schwammassoziierte Pilze als produktivste Quelle für bioaktive Stoffe. Zudem zeigten die meisten Substanzen aus schwammassoziierten Pilzen eine signifikante Biokativität in einigen pharmakologischen Bioassay Projekten. Daher könnten diese interessante Kandidaten sein, um Leitstrukturen für die Entwicklung neuer Pharmaka, primär auf dem Feld der Zytostatika, Entzündungshemmer, Antiinfektiva und Analgetika, bereitzustellen.

Folglich war es das Ziel dieser Arbeit, sekundär Metabolite aus dem marinen Pilz *Aspergillus* sp., isoliert aus dem mediterranem Schwamm *Tethya aurantium*, zu identifizieren und auf das pharmakologische Potential zu untersuchen. Die Großkultivierung des Pilzen zur Isolierung und Identifizierung von Sekundärmetaboliten wurde auf zwei unterschiedlichen Medien durchgeführt, und zwar auf Bio-Malz Agar und festem Dinkel-Gerste Medium für 21 Tage bei 22°C. Die von beiden Medien gewonnen Kulturen wurden lyophilisiert, mit Ethylacetat extrahiert und der nach dem Abrotieren zurückbleibende trocken Rückstand mit Petrolether entfettet. Die daraus resultierende Fraktion wurde anschließend unterschiedlichen chromatographischen Separierungsverfahren zugeführt um die Sekundärmetabolite zu isolieren.

Zur Identifikation von Molekulargewicht und Struktur der Sekundärmetabolite wurden in erster Linie Verfahren der Massenspektrometrie (MS) und der Magnetresonanz-Experimente (NMR) verwendet. Zudem wurde in Einzelfällen, bei

optisch aktiven Naturstoffen, eine Time-dependent Density Functional Theory Electronic Circular Dichroism (TDDFT ECD) Berechnungen durchgeführt um deren absolute Konfiguration festzustellen. Schließlich wurden alle isolierten Substanzen unterschiedlichen Bioassays zugeführt, wie z.B. Zytotoxizitäts- und antimikrobiellen Assays, um deren Bioaktivität festzustellen.

Die chromatographische Auftrennung des Rohextraktes vom schammassoziiertem Pilz *Aspergillus* sp. ergab elf bekannte Polyketide (**1-7**, **16-18**, und **28**), sechs neue Meroterpenoide (**10-14** und **29**), zwölf Alkaloide einschließlich einem neuen Thyotoquivalin (**20**), sechs neue Fumiquinazolone (**21-26**), ein neues Tryptophan-Alkaloid (**31**) als auch vier bekannte Alkaloide (**8**, **9**, **19**, und **27**), einen neuen Biphenylether (**30**) und ein bekanntes Nukleosid (**15**).

Bei den meisten in dieser Studie isolierten Polyketiden waren Citrinin-Derivate. Zusätzlich wurde Butyrolacton II (**1**) als Hauptsekundärmetabolit des untersuchten *Aspergillus* sp. isoliert. 4-Acetyl-3,4-dihydro-6,8-dihydroxy-5-methyl Isocoumarin (**5**) zeigte eine ausgeprägte Zytotoxizität gegen mehrere ausgewählte Zelllinien, wohingegen alle anderen Polyketide keine oder eine nur sehr schwache Aktivität gegen die murine Lymphomzelllinie L5178Y zeigte.

Die unbekannt meroterpenoiden Substanzen, Austalide M-R (**10-14** und **29**), zeigten sich strukturell verwandt mit den bekannten Austaliden A-L, welche zuvor aus *Aspergillus ustus* isoliert wurden. Die strukturelle Analyse der Austalide legt einen Biosyntheseweg nahe, welcher 6-Farnesyl-5,7-dihydroxy-4-methylphtalid enthält, ein wichtiges Zwischenprodukt in der Biogenese von Mycophenolsäure. Darüber hinaus wurden TDDFT ECD Berechnungen der Austalide M-Q (**10-14**), neue Metabolite von *Aspergillus* sp., vorgestellt. ECD Berechnungen gaben Aufschluss über die absolute Konfiguration und zeigten zudem, dass die Konformation des Chromophors, wie auch der charakteristische ECD-Cotton Effekt im benzyllischen Zentrum, durch das Phtalid bestimmt wird. Die Berechnungen erklärten außerdem die bemerkenswerten

Unterschiede der ECD-Spektren der strukturell verwandten Austalide und zeigen, dass die absolute Geometrie nicht durch einen einfachen Vergleich von ECD-Spektren ermittelt werden kann. Letztendlich zeigten diese Verbindungen jedoch nur eine schwache, oder keine Aktivität gegenüber der murinen Lymphomzelllinie L5178Y.

Die bekannten Alkaloide **8**, **9** und **19** wurden zum ersten Mal aus einem schwammassoziierten Pilz charakterisiert, während in frühere Studien bereits die Isolierung von *Aspergillus fumigatus* aus Meeressediment, *Aspergillus fumigatus* aus der Raumluft von Asthma-Patienten und *Trichoderma sp.* aus Bambusblättern beschrieben wurde. Verbindung **8** und **9** zeigten eine ausgeprägte Zytotoxizität gegen die Mauslymphomzelllinie L5158Y mit IC₅₀ Werte von 3,7 und 0,2 μM , während **19** nur eine schwache Aktivität in diesem Assay zeigte. Darüber hinaus zeigte **9** getestet auf menschlichen Zelllinien, eine moderate Aktivität gegen ovariale Karzinomzellen (A2780sens) und die Philadelphia Chromosom positive, chronische myeloische Leukämie Zelllinie (K562) mit IC₅₀ Werten zwischen 8,0 und 19,3 μM , während **8** nur eine moderate bis schwache Aktivität gegenüber K562, A2780sens und A2780CisR mit IC₅₀ Werten von 15,0, 18,5 und 38,8 μM zeigte.

Die Verbindungen **20-26** sind neue Tryptoquivaline- und Fumiquinazolonalalkaloide. Die wichtigsten strukturellen Unterschiede zwischen denen in dieser Studie neu erfassten Vertretern und den bereits zuvor beschriebenen Verbindungen mit gleichem molekularem Gerüst, ist die Einbeziehung eines seltenen Aminosäurerests, 1-Aminocyclopropan-1-carbonsäure, anstelle von Alanin- oder Methylalaninresten, wie es in den früher berichteten Analoga zu finden ist. Die absolute Konfiguration von Tryptoquivalin K (**20**) und Fumiquinazolone K (**21**) wurde durch TDDFT ECD Berechnungen der Lösung ihrer Konformere untersucht und die ECD letzterer wurden auch verwendet um eine strukturelle Abgrenzung der verwandten Fumiquinazolone L-P (**22-26**) vorzunehmen. Außerdem wurden die neuen Alkaloide (**20-26**) bezüglich ihrer Zytotoxizität mittels der murinen Lymphomkarzinoms L5178Y überprüft, wo sie nur eine schwach bis keine Aktivität zeigten (bis zu einer Dosis von 10 $\mu\text{g/ml}$)

Zusammenfassend kann gesagt werden, dass in dieser Studie einunddreißig Verbindungen erfolgreich aus dem schwammassoziierten Pilz *Aspergillus sp.* identifiziert wurden, von den fünfzehn nach unserem besten Wissen, neue Naturstoffe sind (Tabelle 5.1).

Table of Contents

1. Introduction	1
1.1 Natural products research and development in drug discovery	1
1.1.1 History and background of the use of natural products	1
1.1.2 General role of traditional medicine in drug discovery	3
1.1.3 Current status of natural products research	4
1.1.4 The future of natural product chemistry	5
1.2 Bioactive natural products of fungal origin	6
1.3 Marine fungi as sources of bioactive metabolites	10
1.3.1 Cytotoxic metabolites from sponge-derived fungi	13
1.3.2 Kinase inhibitors from sponge-derived fungi	14
1.3.3 Antimicrobial metabolites from sponge-derived fungi	15
1.4 Endophytic fungi as sources of bioactive products	15
1.4.1 The endophyte-host interaction	16
1.4.2 Metabolites from endophytic fungi	17
1.4.2.1 Antimicrobial compounds from endophytic fungi	17
1.4.2.2 Antiviral compounds from endophytic fungi	18
1.4.2.3 Antitumoral compounds from endophytic fungi	19
1.4.2.4 Immunosuppressive compounds from endophytic fungi	19
1.5 Aim and significance of the study	20
2. Materials and Methods	21
2.1 Materials	21
2.1.1 Fungal material	21
2.1.2 Laboratory chemicals	21
2.1.2.1 General laboratory chemicals	21
2.1.2.2 Solvents	21
2.1.2.2.1 General solvents	21
2.1.2.2.2 Solvents for HPLC and LC-MS	22
2.1.2.2.3 Solvents for optical rotation	22
2.1.2.2.4 Solvents for NMR	22
2.1.3 Chromatography	23
2.1.3.1 Stationary phase	23
2.1.3.2 Spray reagents	23
2.2 Laboratory instruments	24
2.3 Methods	25
2.3.1 Purification and identification of fungal strains	25

Table of Contents

2.3.2 Fungal cultivation and extraction	26
2.3.3 Solvent-solvent extraction	26
2.3.4 Isolation and purification of secondary metabolites from <i>Aspergillus</i> sp.	27
2.3.5 Chromatographic methods	31
2.3.5.1 Thin layer chromatography (TLC)	31
2.3.5.2 Vacuum liquid chromatography (VLC)	32
2.3.5.3 Column chromatography (CC)	32
2.3.5.4 Flash chromatography	34
2.3.5.5 Preparative high pressure liquid chromatography (HPLC)	34
2.3.5.6 Semi-preparative high pressure liquid chromatography (HPLC)	35
2.3.5.7 Analytical high pressure liquid chromatography (DAD-HPLC)	35
2.3.6 Structure elucidation of the isolated secondary metabolites	37
2.3.6.1 Mass spectrometry (MS)	37
2.3.6.1.1 Electrospray ionization mass spectrometry (ESIMS)	38
2.3.6.1.2 Electron impact mass spectrometry (EI-MS)	39
2.3.6.1.3 Fast atom bombardment mass spectrometry (FAB-MS)	40
2.3.6.1.4 High resolution mass spectrometry (HR-MS)	40
2.3.6.2 Nuclear magnetic resonance spectrometry (NMR)	40
2.3.6.3 Optical activity	42
2.3.6.4 Determination of absolute stereochemistry by Mosher reaction	43
2.3.6.5 Circular dichroism (CD) spectroscopy	44
2.3.7 Testing the biological activity	45
2.3.7.1 Antimicrobial and antifungal activity	45
2.3.7.2 Cytotoxicity test	46
3. Results	48
3.1 Secondary metabolites from the sponge-associated fungus <i>Aspergillus</i> sp.	48
3.1.1 Butyrolactone II (compound 1 , known)	49
3.1.2 Dicitrinin A (compound 2 , known)	53
3.1.3 4-Acetyl-3,4-dihydro-6,8-dihydroxy-3-methoxy-5-methylisocoumarin (compound 3 , known)	57
3.1.4 2,3,4-Trimethyl-5,7-dihydroxy-2,3-dihydrobenzofuran (compound 4 , known)	60
3.1.5 4-Acetyl-3,4-dihydro-6,8-dihydroxy-5-methylisocoumarin (compound 5 , known)	63
3.1.6 Citrinin (compound 6 , known)	66
3.1.7 Phenol A acid (compound 7 , known)	68
3.1.8 Fumiquinazoline J (compound 8 , known)	71

Table of Contents

3.1.9 Methyl 3,4,5-trimethoxy-2-(2-(nicotinamido) benzamido) benzoate (compound 9 , known)	75
3.1.10 Austalide M (compound 10 , new)	80
3.1.11 Austalide N (compound 11 , new)	90
3.1.12 Austalide O (compound 12 , new)	94
3.1.13 Austalide P (compound 13 , new)	97
3.1.14 Austalide Q (compound 14 , new)	106
3.1.15 3'- <i>O</i> -Acetylthymidine (compound 15 , known)	109
3.1.16 Dihydrocitrinin (compound 16 , known)	113
3.1.17 Dihydrocitrinone (compound 17 , known)	116
3.1.18 Decarboxydihydrocitrinone (compound 18 , known)	118
3.1.19 Pretrichodermamide A (compound 19 , known)	121
3.1.20 Tryptoquivaline K (compound 20 , new)	127
3.1.21 Fumiquinazoline K (compound 21 , new)	134
3.1.22 Fumiquinazoline L (compound 22 , new)	141
3.1.23 Fumiquinazoline M (compound 23 , new)	147
3.1.24 Fumiquinazoline N (compound 24 , new)	152
3.1.25 Fumiquinazoline O (compound 25 , new)	157
3.1.26 Fumiquinazoline P (compound 26 , new)	161
3.1.27 Cytochalasin Z17 (compound 27 , known)	165
3.1.28 Dihydroisoflavipucine (compound 28 , known)	171
3.1.29 Austalide R (compound 29 , new)	175
3.1.30 3-(4-(4-(2-Carboxyvinyl)-2-methoxyphenoxy)-3-methoxyphenyl)-2- hydroxyacrylic acid (compound 30 , new)	179
3.1.31 3-((1-Hydroxy-3-(2-methylbut-3-en-2-yl)-2-oxoindolin-3-yl)methyl)-1- methyl -3,4-dihydro-1 <i>H</i> -benzo[<i>e</i>][1,4]diazepine-2,5-dione (compound 31 , new)	184
3.2 Bioactivity test results for compounds isolated from <i>Aspergillus</i> sp.	190
4. Discussion	192
4.1 Considerations of natural products research in the present future	192
4.2 The importance of marine-associated fungi	193
4.3 The compounds isolated from <i>Aspergillus</i> sp.	194
4.3.1 Polyketides	194
4.3.2 Meroterpenoids	199
4.3.3 Alkaloids	203
5. Summary	205

Table of Contents

6. References	215
7. Attachments	233
8. List of abbreviations	264
9. Curriculum Vitae	266

1. Introduction

Natural products are organic compounds formed by living organisms in response to external stimuli such as nutritional changes, infection and competition. Biologically active natural products produced by plants, animals, insects, fungi, bacteria and protozoans have been isolated to be used in pharmaceutical drug discovery and design (Rollinger *et al.*, 2006; Willian, 2000). At the present time, natural products are commonly related to herbs, herbal concoctions, dietary supplements, traditional Chinese medicine or alternative medicine (Carter, 2011; Holt and Chandra, 2002). No rigid scheme is used to classify natural products due to their bewildering diversity in structure, function and biosynthesis. However, as chemicals, natural products mainly include the following classes of compounds: terpenoids and steroids, fatty acid-derived substances and polyketides, alkaloids, nonribosomal polypeptides, and enzyme cofactors. Natural products serve as a promising major source of drug discovery and are widely recognized in the pharmaceutical industry due to their structural diversity and the broad range of their pharmacological activities (Clark, 1996). Accordingly, they represent very useful tools for pharmacologists and biologists, and function as lead compounds for the treatment of hypercholesteremia, inflammation, microbial infections, cancer, and tissue rejection in organ transplantation (Blunt *et al.*, 2011; Carter, 2011; Ojima, 2008).

1.1 Natural products research and development in drug discovery

1.1.1 History and background of the use of natural products

Natural products generally originate from either animal sources, plants, microbes or are from prebiotic origin (Nakanishi, 1999). They are not just accidentally produced in nature, but it is much more likely that they are a natural expression of the increase in organism complexity (Jarvis, 2000). Throughout the ages nature has provided humankind with the production of foodstuffs, shelters, clothing, means of

transportation, fertilizer, flavors, fragrances, and last not least, medicines for their basic needs, together with the tools for the first attempts at therapeutic intervention. Plants have constantly been the basis of sophisticated traditional medicine systems that have existed for thousands of years (Nakanishi, 1999; Newman *et al.*, 2000). The first use of natural products on the record in medicine has been written on hundreds of clay tablets in cuneiform from Mesopotamia and dates back to nearly 2600 BC. As a matter of fact, many of these plant-derived substances are still in use today as treatments for influenza, inflammation, coughing, parasitic infection, ailments from coughs and colds (Cragg and Newman, 2001; Newman *et al.*, 2000).

The use of traditional medicine in Egypt has been found to date back to about 2900 BC, but the best known Egyptian pharmaceutical record is the Ebers Papyrus, dating from 1500 BC, which documents almost 700 different substances (mostly plants, though animal organs were also involved along with some minerals), and also includes formulation such as snuffs, poultices, gargles, infusions, pills and ointments, with beer, milk, wine and honey being normally used as vehicles (Cragg and Newman, 2001; Holt and Chandra, 2002; Newman *et al.*, 2000). The use of herbaceous plants in China goes as far back as 2000 BC. Indeed, the *Chinese Materia Medica* has been widely documented over the centuries dating from approximately 1100 BC, with the first time record in Wu Shi Er Bing Fang, including 52 prescriptions, and then followed by works such as the Shennong Herbal (~100BC; 365 drugs) and the Tang Herbal (659 AD; 850 drugs). In India, a collection of Ayurvedic hymns from 1000 BC and earlier describes the use of over 1000 different herbs and this system formed the basis for the primary text of *Tibetan medicine*, translated from Sanskrit during the eighth century (Fallarino, 1994; Newman *et al.*, 2000). In the Western world, the Greeks made a contribution to the development in use of herbal drugs. In Rome, Galen (130-200 AD), who is extensively known for his complex formulae and prescriptions in use of compounding drugs, practiced and taught medicine and pharmacy, published almost 30 books about these subjects (Newman *et al.*, 2000). As mentioned above, throughout history, the interest in natural products continues to

exist and natural products have provided many applications in the fields of medicine, pharmacy and biology as a rich source of bioactive compounds (Barron and Vanscoy, 1993; Goradliza, 2007; Kaul and Joshi, 2001). The first commercial pure natural product, generally considered to be the narcotic morphine, was introduced for therapeutic use by E. Merk in 1826. The first semi-synthetic pure drug on the basis of a natural product, aspirin, was introduced by Bayer in 1899 (Newman *et al.*, 2000).

A seminal point in the use of natural products as single, pharmaceutical entities was the well known discovery of penicillin in 1928, followed by its subsequent industrialization during World War II. The antibacterial agents chlortetracycline, chloramphenicol, streptomycin and erythromycin, the antitumor agents daunorubicin, and the antifungal drugs amphotericin B and nystatin had been discovered by 1964. All these share two key characteristics: all of them are derived from natural products and they are cornerstones of modern pharmaceutical care. These natural drug substances were crucial for therapeutic research and pivotal in stimulating the development of the modern pharmaceutical industry in drug discovery (Flisiak *et al.*, 2008; Jarvis, 2000).

1.1.2 General role of traditional medicine in drug discovery

As noted above, medicine has been closely linked with natural products for thousands of years through the use of traditional medicines and natural poisons (Butler, 2004). Natural products have provided the source of most of the active ingredients of medicines (Harvey, 2008). Plants have formed the basis for clinical, pharmacological and chemical studies of traditional medicine systems, which have been used for thousands of years in countries such as China and India as well as many other cultures (Chang and But, 1986; Kapoor, 1990; Schultes and Raffauf, 1990). These plant-based traditional medicines were the basis of most early medicines such as aspirin, digitoxin, morphine, quinine and pilocarpine (Butler, 2004) and they continue to play an important role in health care. The World Health Organization has estimated that

almost 80% of the world's inhabitants depend mainly on traditional medicines for their primary health care (Arvigo and Balich, 1993; Farnsworth *et al.*, 1985; Newman, 2008).

For the remaining 20% of the population products from plants still represent an important source for active ingredients of medicines. The analysis of data of prescriptions dispensed from community pharmacies in the United States from 1959 to 1980 revealed that approximately 25% contained plant extracts or active principle from higher plants (Newman *et al.*, 2000). At present, approximately 119 chemical substances from 90 plant species are considered as important drugs for use in one or more countries, 74% of which resulted from chemical studies that aimed at isolation of bioactive substances from plants used in traditional medicine (Arvigo and Balich, 1993). At least, 80% of drug substances were natural products or inspired by a natural compound and the comparison of information presented on sources of new drugs from 1981 to 2007 exhibited that about half of the drugs approved since 1994 are based on natural products. Likewise, more recent studies demonstrate that natural products constantly play an important role in drug development (Butler, 2008; Newman and Cragg, 2007; Sneader, 1996).

Hence, a large number of examples from medicine reveal the innovative potential of natural compounds and their impact on progress in drug discovery and development (Tejesvi *et al.*, 2007).

1.1.3 Current status of natural products research

Natural products are still providing their fair share of new clinical candidates and drugs despite competition from other drug discovery methods. This is established recently by analyzing the number of natural products-derived drugs present in the total drug launches from 1981 to 2002 (Cragg *et al.*, 1997; Newman *et al.*, 2003). In the modern research field of drug discovery, natural products continue to be valuable

targets for production by biotechnological approaches, and as sources of lead compounds derived from traditional systems of medicine (Carter, 2011; Newman, 2008).

Currently, over 100 natural-product-derived compounds are undergoing clinical trials and at least 100 similar projects are in preclinical development. Most of them are derived from leads obtained from microbial or plant sources. These projects on the basis of natural products are predominantly being studied for use in cancers or as anti-infectives. About one-third of the top-selling drugs in the world are natural products or their derivatives. Natural products have inspired many developments in organic chemistry leading to advances in synthetic methodologies and to the possibility of making analogues of the original lead compound with improved pharmacological or pharmaceutical properties (Harvey, 2008; Newman, 2008; Sunazuka *et al.*, 2008; Wilson and Danishefsky, 2006).

These facts demonstrate that natural products are indeed valuable sources for drug discovery and development. As a matter of fact, without natural products, medicine would be lacking therapeutic tools in several important clinical areas. Moreover, the continual emergence of novel natural product skeletons with interesting bioactivities, together with the potential for chemical modification and synthesis bode well for the utility of natural products. At last, the use of natural products is also expanded to agrochemical appreciated as the development of pesticides highlights (Duke *et al.*, 2000; Rishton, 2008).

1.1.4 The future of natural product chemistry

The importance of natural products in drug discovery is obvious. Novel bioactive natural products will continue to serve as lead compounds for drug development and as biochemical probes for the discovery of pharmacological and biochemical processes. The use of bioactive natural products to probe the molecular and

pharmacological processes of living organisms will go on with even greater sophistication due to the major advances being made in molecular biology (Baker *et al.*, 2007; Clark, 1996; Newman *et al.*, 2000).

The selection of a successful drug discovery paradigm has reached an important crossroad. The adoption of biochemical assays and high-throughput screening has recently created the good impression that high-throughput screening of large compound collections is more effective or more practical than natural extract screening. It is possible to make the future of natural products in drug discovery more promising than ever before, by applying the vast resources of the pharmaceutical industry together with the incredible advancements of spectroscopic analysis and purification technologies. Therefore, natural products will continue to play a vital role in improving the human condition, and this role will go on as long as there are unexplored sources of new natural products (Clark, 1996; Rishton, 2008).

Despite the obvious successes in drug discovery from natural products, pharmacologists, phytochemists, and other natural product scientists still face many challenges in future. They need to constantly improve the quality and quantity of compounds that enter the drug development phase in order to keep pace with other discovery efforts (Butler, 2008; Carter, 2011; Joseph and Priya, 2011).

1.2 Bioactive natural products of fungal origin

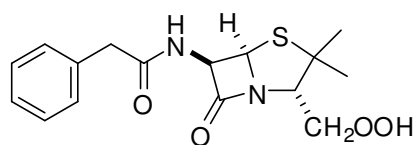
Fungi are widespread, non-photosynthetic microorganisms, and they are eukaryotic rather than prokaryotic, playing a vital role in the environment, particularly in the biodegradation of organic material. The definition of a fungus is complex because in the fungal kingdom, there is a broad range of heterotrophic organisms with diverse cellular structures, reproduction, biochemistry, physiology, and secondary metabolism. Fungi are ubiquitous and have been isolated from every conceivable organic substrate examined, wherever in the world it was collected (Hawkesworth *et al.*, 1983).

Recently, there has been an increasing understanding of microbial abundance and diversity, particularly that of fungi. It has revealed that fungal world has just been superficially scratched so far. In fact, there is still a huge unknown and untapped microbial pool, which provides the chance to discover novel, useful and economically profitable bioactive compounds (Joseph and Priya, 2011; Rateb and Ebel, 2011).

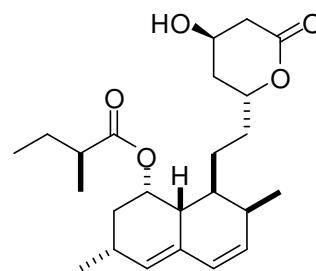
The study of fungal metabolites has made important contributions to the overall development of chemistry. On the other hand, the microbiological chemist is interested in their structure, chemistry and biological activity. Fungi are extraordinary organisms that yield a broad range of secondary metabolites and their chemical activities have a long history (Hanson, 2008). Fungi have historically been a gold mine of lead compounds in drug discovery for pharmaceutical industry. The discovery of penicillin (**1**) isolated from *Penicillium notatum* by Fleming in the autumn of 1928, and which he reported in 1929, revolutionized medicinal chemistry after a lengthy gestation period. And then, the outbreak of the Second World War increased the urgency with which the study was carried on to success. The yield of penicillin had been increased by 1940 and sufficient material was used for the first human trial in February of 1941, which resulted in a breakthrough in the treatment of bacterial infections. After the exciting discovery of penicillin, more attention of pharmaceutical companies and academic laboratories was put on fungi as a source of lead compounds. Thus, fungi became a vital source of drug discovery for the treatment of various diseases (Butler, 2004; 2005).

Since then, many novel metabolites with quite diverse carbon skeletons have been isolated from fungi. The main driving force has been the search for bioactive fungal metabolites for pharmaceutical use, not only as antibiotics but also for other therapeutic areas, and this has led to several compounds that have achieved commercial importance. Success stories include, lovastatin (**2**) isolated from *Aspergillus terreus* which is used as a cholesterol-lowering agent (Endo, 1979), cyclosporine A (**3**) isolated from *Cylindrocarpon lucidum* and *Tolypocladium inflatum*

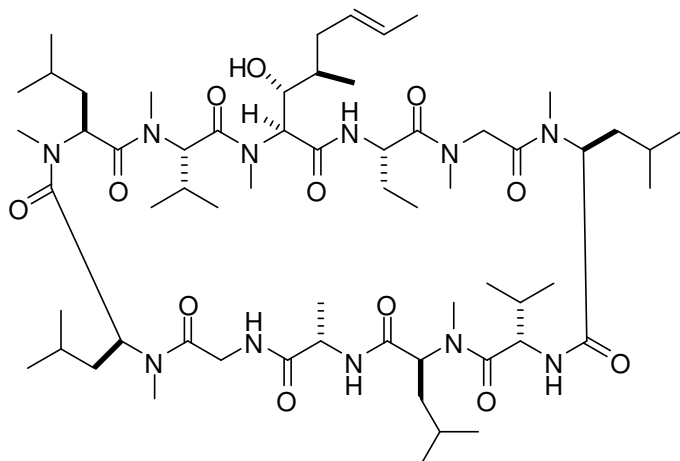
used widely as an immunosuppressive agent (Traber *et al.*, 1982; 1987), aphidicolin (4) isolated from *Cephalosporium aphidicola* used as a potent inhibitor of DNA polymerase alpha which has been examined as a potential tumour inhibitor and anti-viral agent, pleuromutilin (5) from *Pleurotus mutilus* which is the core for the antibiotic thiamulin (Hanson, 2008), in addition to well known antimicrobial agents fusidic acid (6), griseofulvin (7), and mycophenolic acid (8) used as immunosuppressive agents (Butler, 2008; Flisiak *et al.*, 2008). Despite this, fungi will still be responsible for the next big breakthrough in medicine (Carter, 2011).



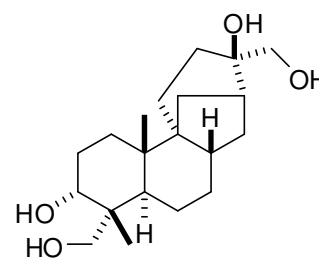
penicillin G (1)



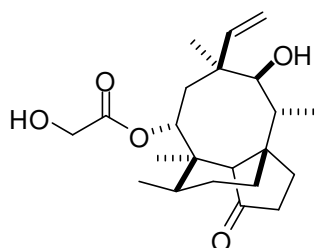
lovastatin (2)



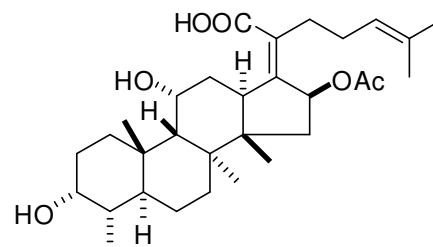
cyclosporine A (3)



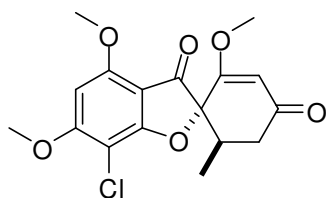
aphidicolin (4)



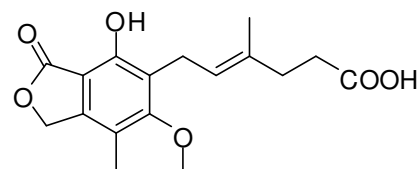
pleuromutilin (5)



fusidic acid (6)



griseofulvin (7)



mycophenolic acid (8)

Figure 1.2.1 Bioactive metabolites of fungal origin used in medicine

1.3 Marine fungi as sources of bioactive metabolites

Approximately three quarters of the earth's surface are occupied by seas and oceans. Marine microorganisms have become an important source of pharmacologically active and structurally diverse metabolites (Haefner, 2003). Because marine-derived fungi live in a significantly different environment from those of terrestrial organisms, it is reasonable to suppose that their secondary metabolites will also differ considerably (Bugni and Ireland, 2004; Molinski *et al.*, 2009).

Marine fungi are an ecologically rather than physiologically or taxonomically defined group of organisms. On the basis of the "classic" definition that appears to be universally accepted in the scientific community, marine fungi are separated into two groups, obligate and facultative marine fungi. The *obligate* marine fungi are those that grow and sporulate exclusively in a marine or estuarine habitat, while *facultative* marine fungi are those from freshwater or terrestrial milieus able to grow in the marine environment (Kohlmeyer and Kohlmeyer, 1979). Marine fungal strains have been isolated from virtually every possible marine habitat, including inorganic matter, marine microbial communities, marine plants, marine invertebrates and vertebrates (Rateb and Ebel, 2011).

In recent years, natural products obtained from marine-associated fungi have attracted considerable attention, because many of them are structurally unique and possess promising biological and pharmacological properties. Since the discovery of cephalosporin C isolated from a culture of a *Cephalosporium* species, it took another thirty years for marine-associated fungi to be more systematically evaluated for their chemical potential. Studies reporting chemistry from marine-associated fungi were rare until the 1990s. Since then research on the chemistry of marine-associated fungi have experienced a tremendous increase owing to the need for compounds possessing bioactivity with possible pharmaceutical applications or other economically useful properties such as fine chemical, drugs, cosmetics, and functional personal-care

products. Consequently, 272 new natural products were discovered, many of which having novel carbon skeletons. Overall, the total number of natural products from marine-associated fungi currently exceeds 1000, including polyketides, terpenes, steroids and peptides (Rateb and Ebel, 2011). Hence, the rapid growth in the chemistry of marine-associated fungi led to the discovery of a surprisingly large number of novel structures and provided the evidence that marine-associated fungi have the potential to be a promising source of pharmaceutical leads (Bugni and Ireland, 2004; Saleem *et al.*, 2007).

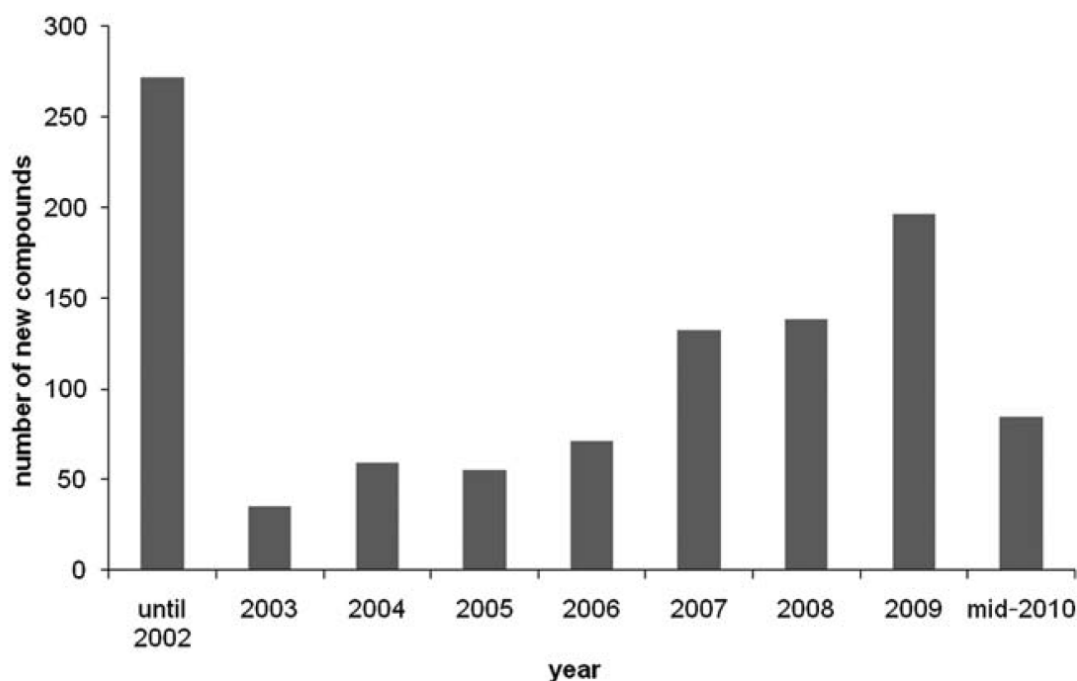


Figure 1.3.1 New compounds from marine-derived fungi (Rateb and Ebel, 2011)

Additionally, biological assays are mostly focusing on the areas of antibiotic and anticancer properties, and also other selective bioactivities including cell cycle inhibition, antagonism of platelet activating factor, antiviral activity, neuritogenic activity, phosphatase inhibition, kinase inhibition, and radical scavenging activities (Bugni and Ireland, 2004; Debbab *et al.*, 2011).

Sponges are first-class sources of marine fungal diversity, as shown by the number of novel structures reported therefrom. Sponge-associated fungi were found to represent a vast untapped reservoir of metabolic diversity and have drawn increasing attention to the discovery of bioactive natural products in recent years. The distribution of fungi has been graphically summarized according to the number of distinct genera presented from a marine source in the natural product literature, and thus showing that sponges have produced the greatest taxonomic diversity (see Fig. 1.3.2). Interestingly, sponge-associated fungi have yielded the overall greatest number (28%) of novel metabolites (see Fig. 1.3.3) (Bugni and Ireland, 2004; Debbab *et al.*, 2011; Paz *et al.*, 2010; Rateb and Ebel, 2011). Herein, a selection of some interesting compounds yielded by sponge-derived fungi and grouped based on their bioactivity is shown below.

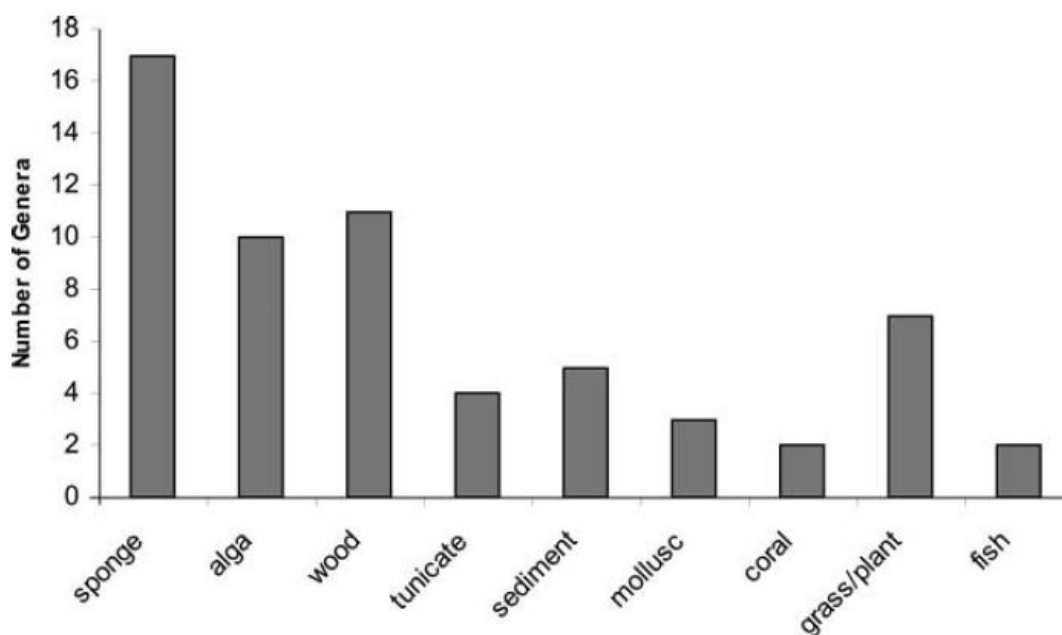


Figure 1.3.2 The number of distinct fungal genera based on the marine source (Bugni and Ireland, 2004; Rateb and Ebel, 2011).

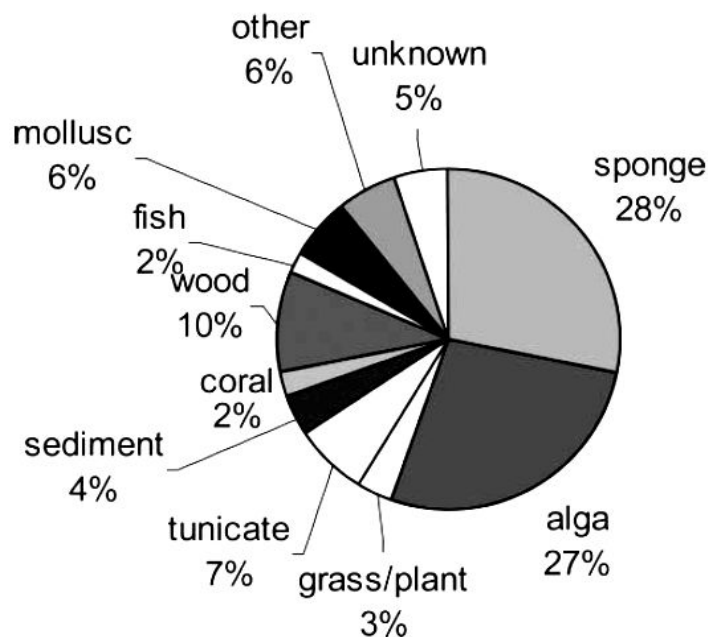


Figure 1.3.3 The distribution of new compounds from marine-associated fungi

(Bugni and Ireland, 2004; Rateb and Ebel, 2011).

1.3.1 Cytotoxic metabolites from sponge-derived fungi

Asperazine (**9**), an unusual unsymmetrical diketopiperazine dimer obtained from *Hyrtios proteus* sponge-associated *Aspergillus niger*, displayed selective cytotoxicity towards leukemia cells, implying that asperazine has a specific mammalian target. Gymnastatin B (**10**), obtained from the ascomycete strain *Gymnascella dankaliensis* derived from the sponge *Halichondria japonica*, exhibited potent cytotoxicity against P388 lymphocytic leukemia cells (Bugni and Ireland, 2004; Varoglu and Crews, 2000).

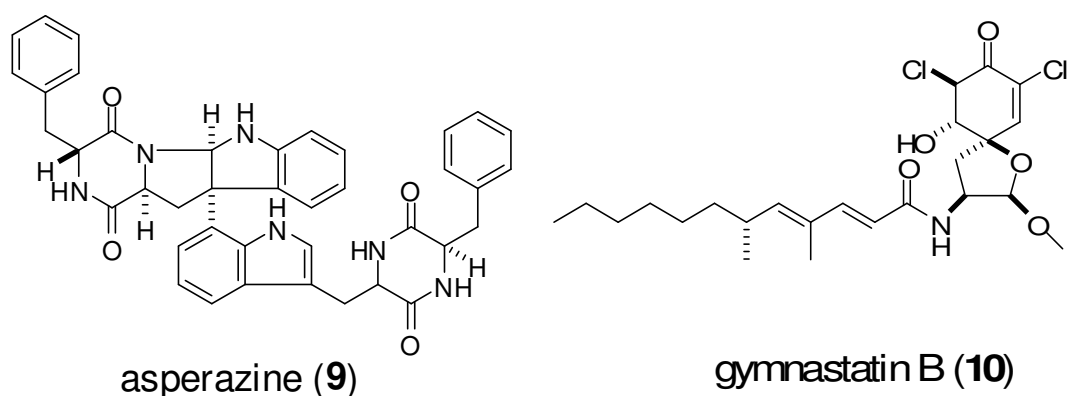


Figure 1.3.4 Cytotoxic compounds from sponge-derived fungi

1.3.2 Kinase inhibitors from sponge-derived fungi

A p56^{lck} tyrosine kinase inhibitor, ulocladol (11), was obtained from a culture of *Ulocladium botrytis* isolated from the sponge *Myxilla incrustans*. The p56^{lck} is necessary for T-cell activation and inhibitors of the kinase could be useful for treating autoimmune diseases. Cathestatin A (12) was obtained from a culture of sponge-derived *Microascus longirostris*, and the amino acid-derived compound was found to be an irreversible nanomolar inhibitor of cysteine proteases (Bugni and Ireland, 2004; Holler *et al.*, 1999; Yu *et al.*, 1996).

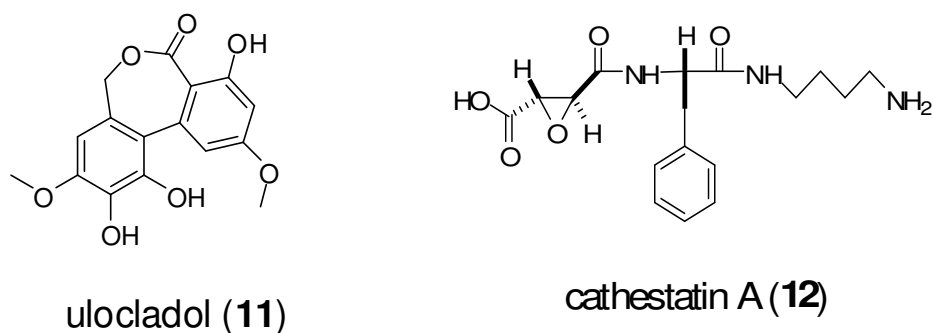


Figure 1.3.5 Kinase inhibitors from sponge-derived fungi

1.3.3 Antimicrobial metabolites from sponge-derived fungi

The fermentation broth of a marine-derived fungus *Aspergillus* sp. isolated from the sponge *Xestospongia testudinaria* collected from the South China was shown to yield (-)-sydonol (**13**) and this compound exhibited strong inhibitory activity against *Staphylococcus albus* and *Micrococcus tetragenus*. Varixanthone (**14**) was obtained from a sponge-derived *Emericella variecolor* (anamorph *Aspergillus variecolor*) and displayed promising antimicrobial activity against *Escherichia coli*, *Proteus* sp., *Bacillus subtilis*, and *Staphylococcus aureus* (Li *et al.*, 2012; Malmstrom *et al.*, 2002; Wang *et al.*, 1998).

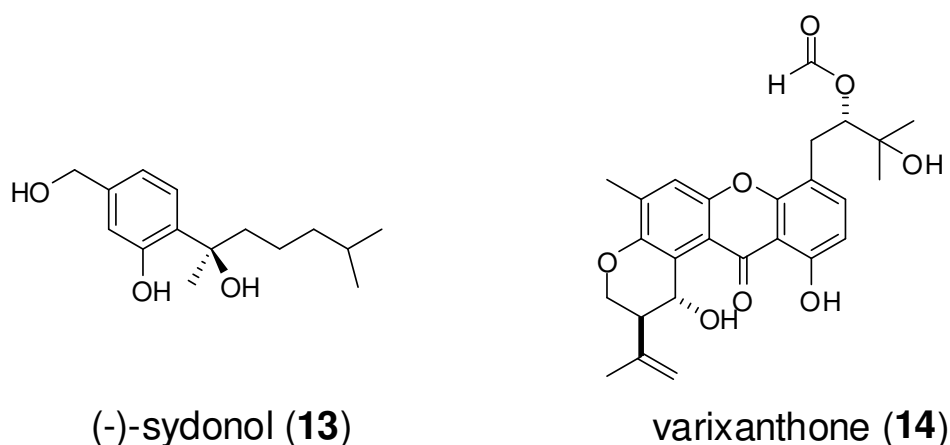


Figure 1.3.6 Antimicrobial compounds from sponge-derived fungi

1.4 Endophytic fungi as sources of bioactive products

An endophyte is a bacterial (including actinomycete) or fungal microorganism, which spends the whole or part of its life cycle colonizing inter- and/or intra-cellularly within the healthy tissues of the host plant, typically without causing any noticeable symptoms of disease (Aly *et al.*, 2011; Bacon and White, 2000; Hyde and Soyong, 2008). Endophytes have been found in all parts of plants including xylem and phloem

and they can be isolated from mildly surface-sterilized plant tissues and cultivated on nutrient agar (Bacon and White, 2000; Tan and Zou, 2001).

Endophytic fungi are being gradually recognized as an ecological assemblage of microorganisms that provides potential sources for new secondary metabolites with useful bioactivities owing to the world's urgent need for new antibiotics, chemotherapeutic agents and agrochemicals to cope with increasing medicinal and environmental problems (Aly *et al.*, 2010; Blunt *et al.*; 2011; Debbab *et al.*, 2010; Joseph and Priya, 2011; Rateb and Ebel, 2011; Strobel and Daisy, 2003; Tejesvi *et al.*, 2007). Theoretically, the probability of discovering novel bioactive metabolites will be higher in endophytes than in common genera of soil fungi because endophytes are relatively unstudied (Bill and Polishook, 1992; Carter, 2011; Tejesvi *et al.*, 2007). This has prompted a worldwide scientific effort to isolate endophytic fungi and to study their natural products since they may present a vital area for bioactive metabolites in drug discovery (Joseph and Priya, 2011; Strobel *et al.*, 2004). The majority of isolated endophytic species have been found to belong to the ascomycete and deuteromycete classes of fungi (Gusman and Vanhaelen, 2000; Joseph and Priya, 2011).

1.4.1 The endophyte-host interaction

The relationship between the endophyte and its host plant is described as a balanced symbiotic continuum ranging from mutualism through commensalism to parasitism (Tan and Zou, 2001; Kogel *et al.*, 2006). It is believed that endophytism may have evolved from time that higher plants first appeared on the earth millions of years ago, which is proved by the fact that plant-associated microbes have been discovered in the fossilized tissues of stems and leaves. It is plausible that some endophytes may have developed genetic systems allowing for transfer of information between themselves and the higher plants and vice versa owing to long-held association (Strobel, 2002). Moreover, plants may provide compounds necessary for the completion of the life

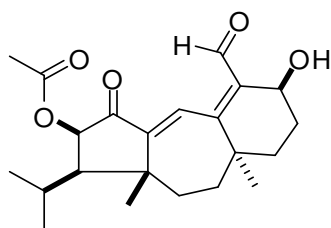
cycle of the inhabiting microorganism, and in some cases endophytes could be responsible for degradation of the dead or dying host plant to start the process of nutrient re-cycling (Guo *et al.*, 2008; Metz *et al.*, 2000; Joseph and Priya, 2011).

1.4.2 Metabolites from endophytic fungi

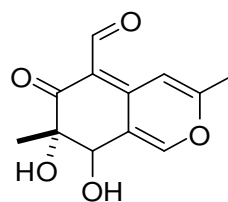
Endophytic fungi are capable of synthesizing bioactive natural products that can be used by plants for defense against pathogens and some of these natural products have been proven to be promising for use in drug discovery. Recent research on endophytic fungi exhibited hundreds of natural products including substance of alkaloids, terpenoids, flavonoids, steroids, etc. Until now, most of the reported natural products are of therapeutic potential including antibiotics, anticancer agents, and biological control agents. Therefore, the role of endophytic fungi in the production of novel structures for exploitation in medicine is receiving increased interest (Gunatilaka, 2006; Joseph and Priya, 2011). Herein, a selection of some interesting metabolites yielded by endophytic fungi is shown below grouped according to their bioactivity.

1.4.2.1 Antimicrobial compounds from endophytic fungi

Guanacastepene A (**15**) isolated from an unidentified endophytic fungus from Costa Rica has revealed antibiotic activity against methicillin-sensitive and methicillin-resistant *Staphylococcus aureus* and vancomycin-resistant *Enterococcus faecalis* (Brady *et al.*, 2000). Studies have also shown that guanacastepene A lysed human red blood cells and caused leakage of intracellular potassium (Singh *et al.*, 2000). Moreover, 7-epiaustdiol (**16**) obtained from the mangrove derived endophytic fungus *Talaromyces* sp. ZH-154 isolated from the stem of *Kandelia candel* (L.), displayed significant inhibitory activity against *Pseudomonas aeruginosa*, a multidrug resistant opportunistic pathogen (Liu *et al.*, 2010; Liu *et al.*, 2010b).



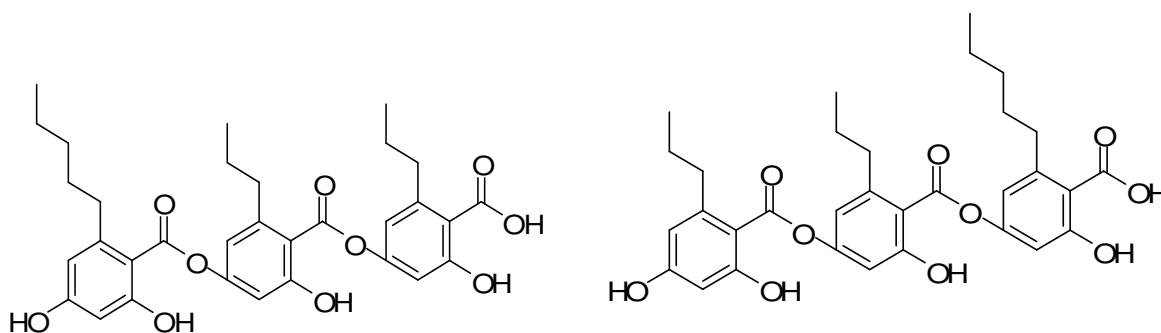
guanacastepene A (15)



7-epiaustdiol (16)

Figure 1.4.1 Antimicrobial compounds of endophytic fungi**1.4.2.2 Antiviral compounds from endophytic fungi**

Cytonic acids A (17) and B (18), produced by the endophytic fungus *Cytonaema* sp., isolated from *Quercus* sp. are two human cytomegalovirus (hCMV) protease inhibitors. The hCMV is a ubiquitous opportunistic pathogen that infects congenitally immunodeficient patients (Guo *et al.*, 2000; Tejesvi *et al.*, 2007).



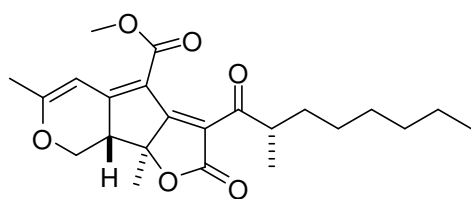
cytonic acid A (17)

cytonic acid B (18)

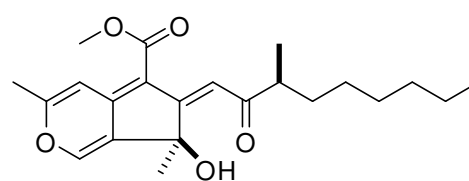
Figure 1.4.2 Antiviral compounds from endophytic fungi

1.4.2.3 Antitumoral compounds from endophytic fungi

Sequoiatones A (**19**) and B (**20**) produced by *Aspergillus parasiticus* isolated from the coastal redwood (*Sequoia sempervirens*), revealed moderate and selective inhibition of human tumor cells, with the strongest activity against breast cell lines (Saleem *et al.*, 2007; Stierle *et al.*, 1999).



sequoiatone A (**19**)

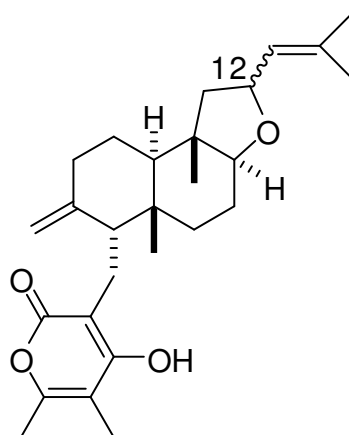


sequoiatone B (**20**)

Figure 1.4.3 Antimicrobial compounds from endophytic fungi

1.4.2.4 Immunosuppressive compounds from endophytic fungi

The immunosuppressive noncytotoxic metabolites, subglutinol A (**21**) and B (**22**) were obtained from the endophytic fungus *Fusarium subglutinans* isolated from the perennial twining vine *Tripterygium wilfordii* (Lee *et al.*, 1995; Tan and Zou, 2001).



subglutinol A 12=S (**21**)
subglutinol B 12=R (**22**)

Figure 1.4.4 Immunosuppressive compounds from endophytic fungi

1.5 Aim and significance of the study

As mentioned above, sponge-derived fungi are of considerable interest and represent a vital source of chemically new metabolites in new drug discovery with pharmaceutical and agrochemical potential.

The primary aim of this study were to characterize the compounds responsible for biological activity from a marine-derived endophytic *Aspergillus* strain, isolated from a specimen of the Mediterranean sponge *Tethya aurantium* and to carry out a preliminary evaluation of their pharmaceutical potential. Based on the previous findings, this study has focused on the isolation and structural elucidation of secondary metabolites from sponge-derived fungi, either known or preferentially new ones.

Moreover, fractions and pure compounds were subjected to various bioassays such as antimicrobial and cytotoxic inhibitory activities, to test their pharmaceutical potential.

2. Materials and Methods

2.1 Materials

2.1.1 Fungal material

The marine-derived endophytic fungus *Asperillus* sp., isolated from a specimen of the Mediterranean sponge *Tethya aurantium*, was investigated in this study.

2.1.2 Laboratory chemicals

2.1.2.1 General laboratory chemicals

- | | |
|---|---------|
| ➤ (-)-2-Butanol | Merck |
| ➤ (R)-(-)-Methoxy- α -trifluoromethylphenylacetyl chloride | Aldrich |
| ➤ (S)-(-)-Methoxy- α -trifluoromethylphenylacetyl chloride | Aldrich |
| ➤ 2-Aminoethyl diphenylboronate | Fluka |
| ➤ Anisaldehyde (4-methoxybenzaldehyde) | Merck |
| ➤ Concentrated ammonia solution | Fluka |
| ➤ Concentrated sulphuric acid | Merck |
| ➤ Dimethylsulfoxide | Merck |
| ➤ Formic acid | Merck |
| ➤ Trifluoroacetic acid (TFA) | Merck |

2.1.2.2 Solvents

2.1.2.2.1 General solvents

- Acetone
- Acetonitrile

- Dichloromethane
- Ethanol
- Ethyl acetate
- Hexane
- Methanol

The solvents were purchased from the Institute of Chemistry, University of Duesseldorf. They were distilled before using and special grades were used for spectroscopic measurements.

2.1.2.2.2 Solvents for HPLC and LC-MS

- Acetonitrile LiChroSolv HPLC grade (Merck)
- Methanol LiChroSolv HPLC grade (Merck)
- Nanopure water distilled and heavy metals free water obtained by passing distilled water through nano- and ion-exchange filter cells (Barnstead, France).

2.1.2.2.3 Solvents for optical rotation

- Chloroform Spectral grade (Sigma)
- Ethanol Spectral grade (Sigma)
- Methanol Spectral grade (Sigma)
- Water Spectral grade (Fluka)

2.1.2.2.4 Solvents for NMR

- Chloroform-*d* Uvasol, Merck
- DMSO-*d*₆ Uvasol, Merck
- Methanol-*d*₄ Uvasol, Merck

- Pyridine-*d*₅ Uvasol, Merck

2.1.3 Chromatography

2.1.3.1 Stationary phase

Diaion HP20	Supelco
Pre-coated TLC plates, Silica Gel 60 F ₂₅₄ , layer thickness 0.2 mm	Merck
Pre-coated TLC plates, RP-18, F ₂₅₄ S, layer thickness 0.25 mm	Merck
RP-18, 0.04 – 0.063 mm mesh size	Merck
Sephadex LH 20, 0.25-0.1 mm mesh size	Merck
Silica Gel 60, 0.04-0.063 mm mesh size	Merck

2.1.3.2 Spray reagents

The reagents were stored in amber-colored bottles and kept refrigerated until being used. TLC was used to monitor the identity of each of the fractions and the qualitative purity of the isolated compounds. It was also utilized to optimize the solvent system that would be applied for column chromatography.

Anisaldehyde/H₂SO₄ Spray Reagent

Methanol	85 mL
Glacial acetic acid	10 mL
Conc.H ₂ SO ₄	5 mL (added slowly)
Anisaldehyde	0.5 mL

Vanillin/H₂SO₄ Spray Reagent

Methanol	85 mL
Conc.H ₂ SO ₄	15 mL (added slowly)
Vanillin	1 g

2.2 Laboratory instruments

General instruments

Analytical balances MC -1	Sartorius
Half-micro and analytical balance MC-1	Sartorius
pH-meter inoLab, pH-Electrode Sen Tix 21	WTW
Desiccator	Glaswerk Wertheim
Hot plate and magnetic stirrer: IKA-Combimag RCH	Janke & Kunkel KG
Glass ware	Schott Duran
Drying oven	ET6130 Heraeus
Ultra sonicator RK 510 H	Bandelin
UV- lamp (254 and 366 nm)	Camag
Rotary evaporator	Büchi Rotavapor R-200
Vacuum pump CVC 2000	Vacuubrand
Centrifuge Pico	Heraeus
Nitrogen generator UHPN3001	Nitrox
Air generator ZA20	WGA
Fraction collector retriever II	ISCO
Lyvac GT2 (Freeze dryer)	Steris
Vacuum pump Trivag D10E (Freeze dryer)	Leybold
Cooling trap RVT 400 (Speedvac)	Savant
Vacuum pump VLP80 (Speedvac)	Savant
Syringe	Hamilton 1701 RSN

Semipreparative HPLC

Pump: L -7100	Merck/Hitachi
Detector: UV-L7400 (Photodiode array detector)	Merck/Hitachi
Printer: Chromato-Intergartor D-2000	Merck/Hitachi
Column: Eurospher 100-C18, [10 μ m; 300 mm \times 8 mm]	Knauer
Pre-column: Eurospher 100-C18, [10 μ m; 30 mm \times 8 mm]	Knauer

Analytical HPLC

Pump: P 580A LPG	Dionex
Autosampler: ASI-100T (injection volume= 20 μ L)	Dionex
Detector: UVD 340S (photodiode array detector)	Dionex
Column oven: STH 585	Dionex
Column: Eurospher 100-C18, [5 μ m; 125 mm \times 4 mm]	Knauer
Pre-column: Vertex column, Eurospher100- 5 C18 [5-4 mm]	Knauer
Software: Chromeleon (V. 6.30)	

HPLC-MS

Analytical HPLC: Agilent 1100 series (photodiode array detector)	Agilent
MS: Finigan LCQ-DECA	Thermoquest
Ionizer: ESI and APCI	Thermoquest
Vacuum pump: Edwards 30	BOC
Column: Eurospher 100-C18, [5 μ m; 227 mm \times 2 mm]	Knauer
Pre-column: Vertex column, Eurospher 100-5 C18 [5- 4 mm]	Knauer

NMR

ARX - 400	Brucker
DRX - 500	Brucker
DMX- 600	Brucker

2.3 Methods

2.3.1 Purification and identification of fungal strains

The sponge *Tethya aurantium*, collected from the Mediterranean Sea near Italy, was surface sterilized by immersing in 70% ethanol for 30 sec. followed by rinsing three times in sterilized artificial sea water. Then, the sponge was cleaved aseptically into small segments (\approx 1.5 x 1.5 mm). The material was placed on a potato carrot agar

medium and incubated at room temperature (25°C). After several days hyphae growing from the sponge material were transferred to fresh plates with the same medium, incubated again and periodically checked for culture purity. The fungus was identified as *Aspergillus* sp. (Moniliaceae) using a molecular biological protocol as well as by morphological characterization.

2.3.2 Fungal cultivation and extraction

Mass growth of the fungus for the isolation and identification of secondary metabolites was carried out on two different media, namely biomalt agar and spelt barley (composed of 200 g barley, 200 g spelt, 2 g soy protein, 2 mg MnCl₂ und 250 mL distilled water) solid media for 21 days at 22 °C. The cultures obtained from both media were then lyophilized, extracted with ethyl acetate, and the dry residues left after evaporation were defatted with petroleum ether to afford 35 g of extract after removal of solvent under reduced pressure.

2.3.3 Solvent -solvent extraction

Solvent-solvent extraction is a broadly employed technique for the separation of organic compounds from a mixture. It involves the separation of compounds in two immiscible solvents. Since the technique is based on the basis of an unequal distribution of solutes between two solvents with a different polarity, the solutes will be more soluble in one solvent compared to the other. The distribution of a component A between two phases can be expressed as distribution coefficient (K):

$$K = \frac{[A]_{\text{top phase}}}{[A]_{\text{lower phase}}}$$

where, [A] is the concentration of solute A.

The following general principles should be considered in choosing a solvent for the system:

- the solvents involved in the extraction must be immiscible
- the solvents must not react with the components that will be separated
- the solvents should be easily removed by evaporation after the process

In this study, the solvent extraction was used for the first step in the whole separation process. It was meant to “clean” the ethyl acetate extract from salts and other undesirable polar constituents by water-ethylacetate extraction. Subsequently, the methanol-*n*-hexane extraction was applied to remove fatty acids and other undesirable non polar components yielding 18.0 g dry residue.

2.3.4 Isolation and purification of secondary metabolites from *Aspergillus* sp.

The 90 % MeOH fraction was used for further isolation and purification of natural products in this study because secondary metabolites are more easily separated and isolated through available chromatography techniques and methods than those in *n*-hexane and water extracts. The details of the schematic isolation and purification of secondary metabolites from large scale fermentation of *Aspergillus* sp. by using chromatography techniques were displayed as follow.

Figure 2.1 Secondary metabolites isolated from fermentation of *Aspergillus* sp.

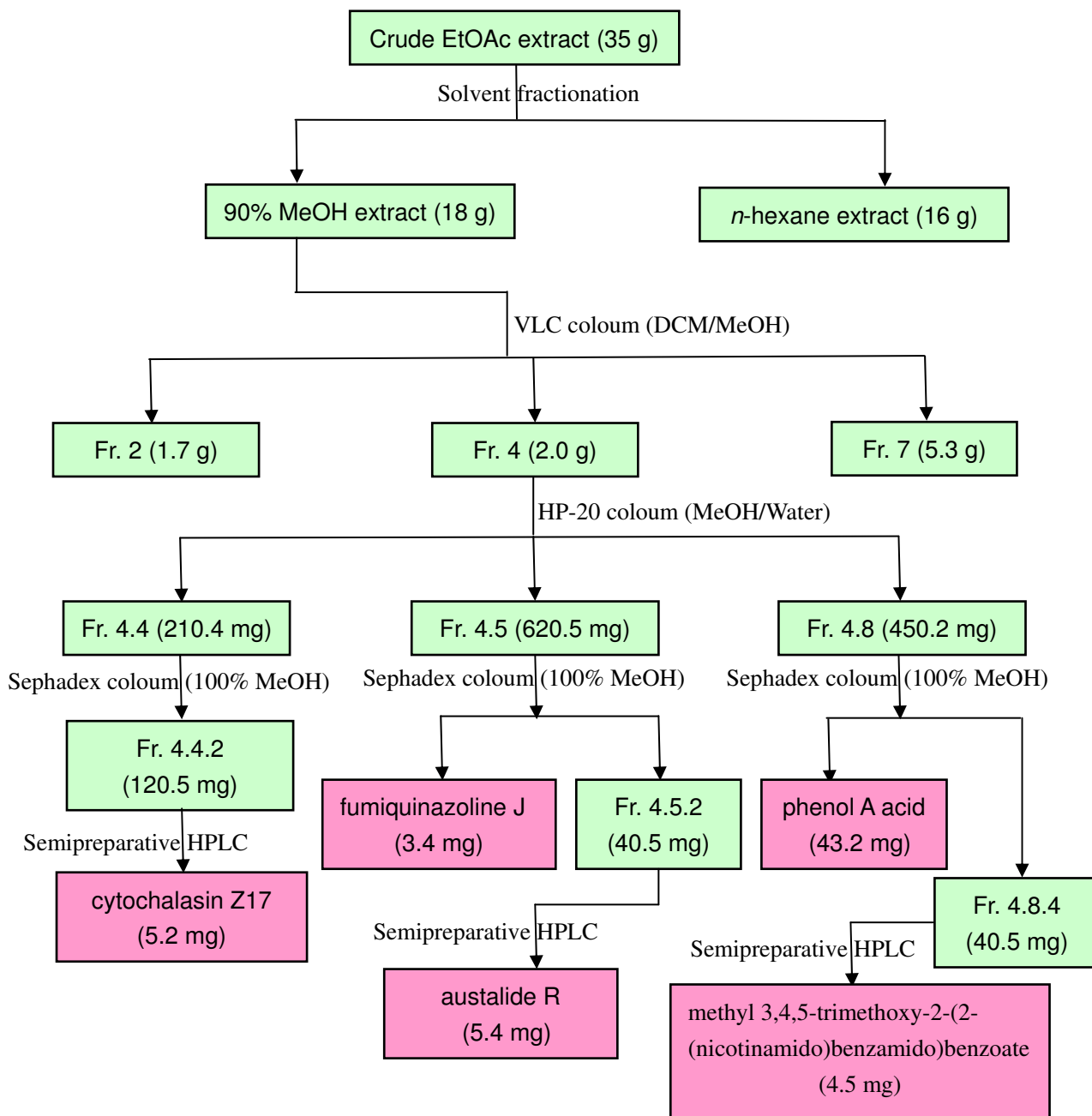


Figure 2.2 Secondary metabolites isolated from fermentation of *Aspergillus* sp.

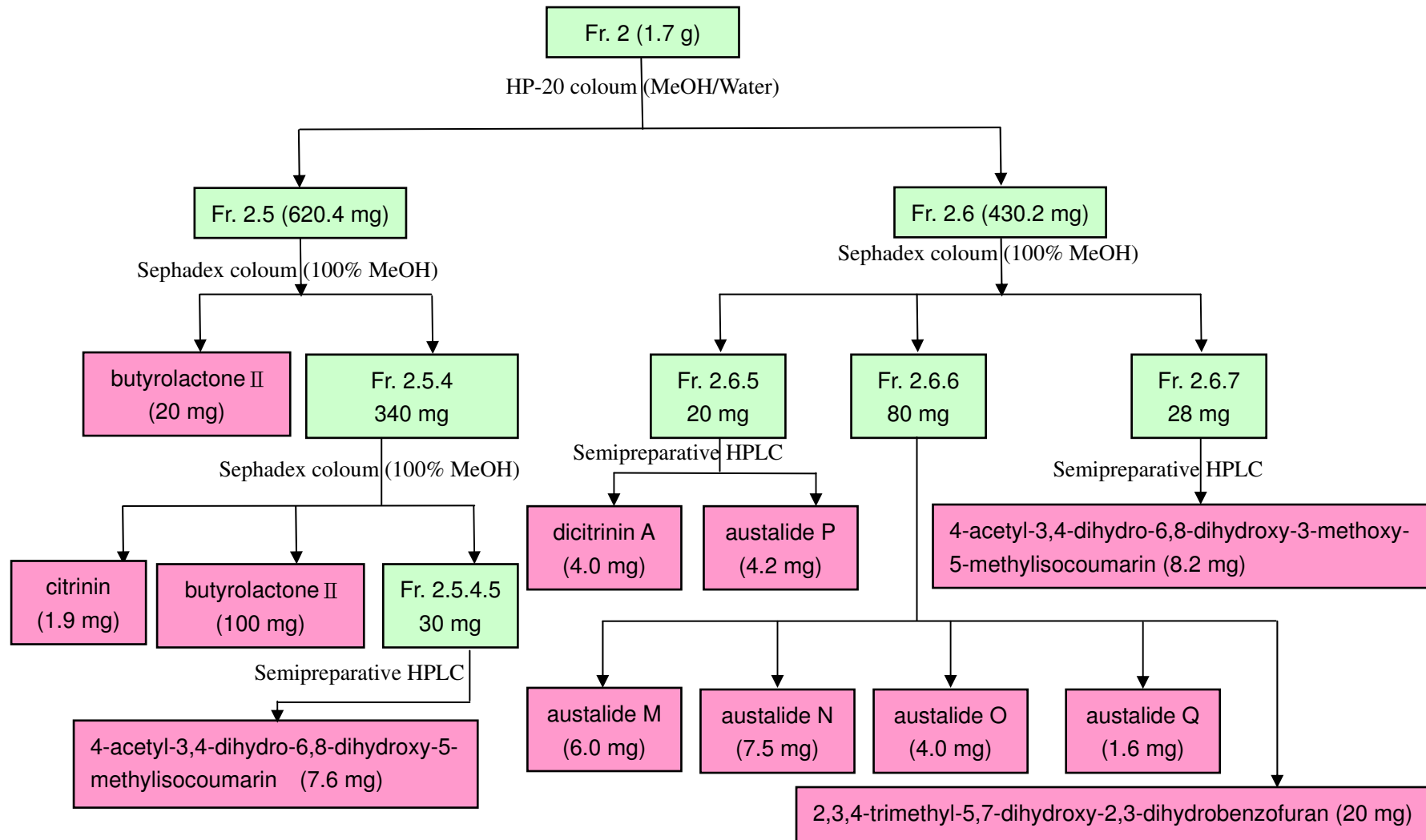
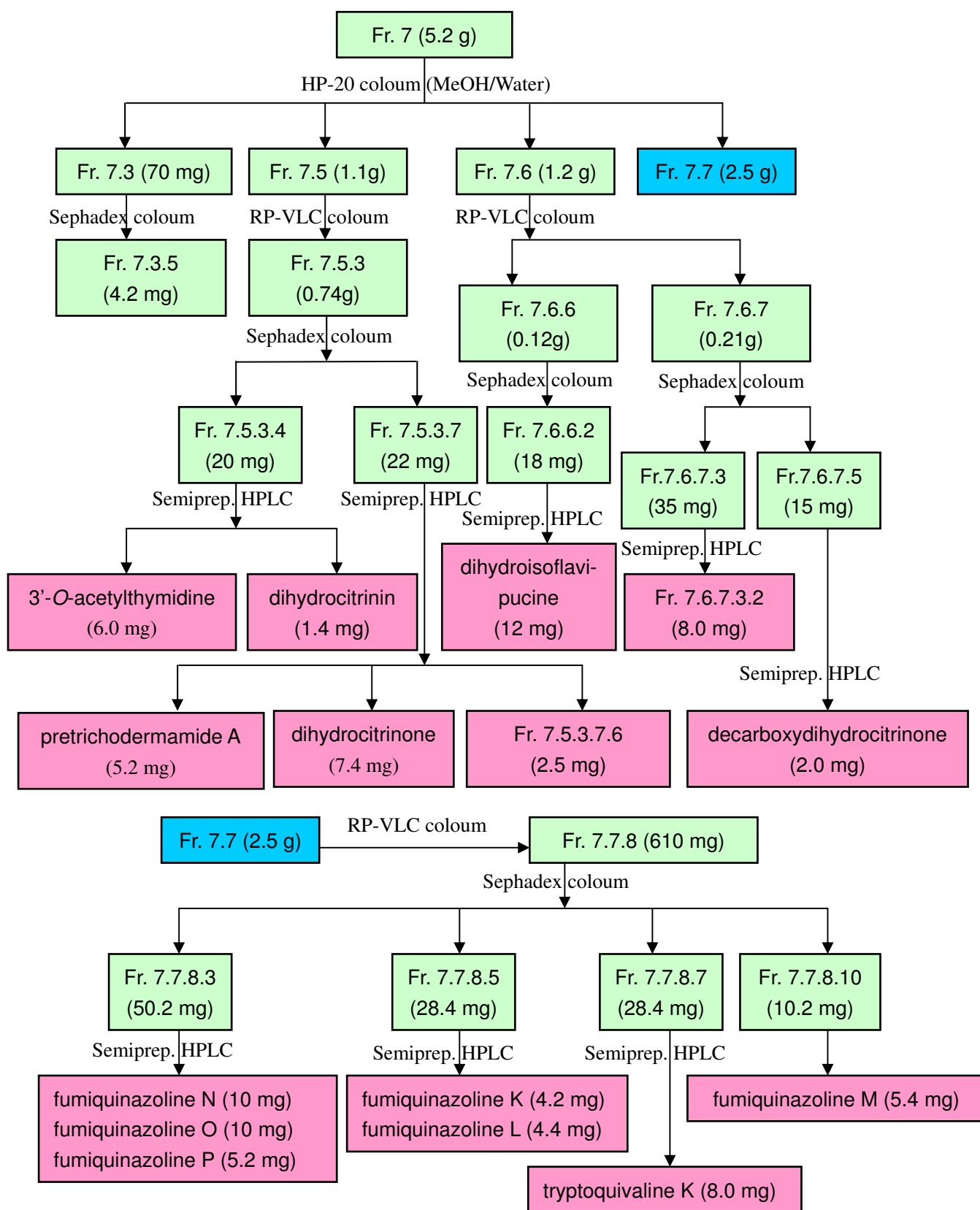


Figure 2.3 Secondary metabolites isolated from fermentation of *Aspergillus* sp.



2.3.5 Chromatographic methods

2.3.5.1 Thin layer chromatography (TLC)

Thin layer chromatography (TLC) is a simple and quick method of chromatography for analysis of the components in the mixtures and for the determination of the purity of a substance. Chromatography refers to any separation method in which the components are distributed between two different phases, stationary phase and mobile phase. The components separate because of having different affinities for these two phases. Sometimes, TLC is also applied for the preparative separation and purification of the components in mixtures (preparative TLC).

TLC was applied for the detection and monitoring of compounds through the separation processes, and was used to optimize solvent systems for column chromatography. It was performed on pre-coated TLC plates with silica gel 60 F₂₅₄ (layer thickness 0.2 mm, Merck, Darmstadt, Germany). The band separation on the TLC describing the separation of compounds was detected under UV absorbance at 254 nm (fluorescence absorption) and 366 nm (fluorescence), followed by spraying the TLC plates with anisaldehyde-H₂SO₄ reagent and subsequent heating at 110 °C. TLC was conducted prior to further work to track the identity of each fraction and the qualitative purity of the isolated compounds. The following solvent systems were used as mobile phase.

For polar compounds: EtOAc:MeOH:H₂O (30:5:4, 30:6:5, and 30:7:6)
For semi-polar compounds: DCM:MeOH (95:5, 90:10, 85:15, 80:20, and 70:30)
DCM:MeOH:EtOAc (90:10:5, and 80:20:10)
For non-polar compounds: *n*-Hexane:EtOAc (95:5, 90:10, 85:15, 80:20, and 70:30)
n-Hexane:MeOH (95:5, and 90:10)

TLC on reversed phase RP18 F₂₅₄ (layer thickness 0.25 mm, Merck, Darmstadt, Germany) was used for polar substances using different solvent systems of MeOH:H₂O (90:10, 80:20, 70:30, and 60:40). The band separation on TLC was detected under UV lamp at 254 and 366 nm, followed by spraying TLC plates with anisaldehyde/H₂SO₄ reagent and they were heated subsequently at 110°C.

2.3.5.2 Vacuum liquid chromatography (VLC)

Vacuum liquid chromatography is a useful method as an initial isolation step employing extracts or fractions with relatively large weights. The apparatus consists of a 500 cm sintered glass filter funnel with an inner diameter of 12 cm. Silica gel 60 was packed to a hard cake at a height of 5-10 cm under applied vacuum. The sample used as adsorbed onto a small amount of silica gel using volatile solvents. The resulting sample mixture was then packed onto top of the column. Using step gradient elution with non-polar solvent (e.g. *n*-Hexane or DCM) and increasing amounts of polar solvents (e.g. EtOAc or MeOH) successive fractions were collected. The flow was produced by vacuum and the column was allowed to run dry after each fraction collected.

2.3.5.3 Column chromatography (CC)

Open column chromatography plays a vital role in the separation of compounds from natural product extracts. The separation takes place through selective distribution of the components between a mobile phase and a stationary phase. Different choice of packing material and mobile phase can be applied depending on the class of compounds or fractions. Fractions derived from VLC were subjected to repeated separation through column chromatography using appropriate stationary and mobile phase solvent systems previously determined by TLC. The following types of separation systems were used in this study:

- ✧ Normal phase chromatography using a polar stationary phase, typically silica gel, in conjunction with a non-polar mobile phase (e.g. *n*-Hexane, DCM) with gradually increasing amount of a polar solvent (e.g. EtOAc or MeOH). Therefore, hydrophobic compounds elute quicker than hydrophilic compounds.
- ✧ Reversed phase (RP) chromatography using a non-polar stationary phase and a polar mobile phase (e.g. H₂O, MeOH). The stationary phase consists of silica with covalently bound *n*-alkyl chains. For instance, C-8 signifies an octanyl chain and C-18 an octadecyl ligand in the matrix. The more hydrophobic the matrix on each ligand, the greater the tendency of the column to retain hydrophobic moieties. Thus, hydrophilic compounds elute more quickly than do hydrophobic compounds. Elution was performed using H₂O with gradually increasing amount of MeOH.
- ✧ Size exclusion chromatography involves separations based on molecular size of compounds being analyzed. The stationary phase consists of porous beads (Sephadex LH-20). Compounds having larger molecular size will be excluded from the interior of the bead and thus will firstly elute, while compounds with smaller molecular size will enter the beads and elute according to their ability to exit from the small sized pores where they were trapped. Elution was performed using MeOH or MeOH:DCM (1:1).
- ✧ Ion exclusion chromatography uses ion exchange resin beds (Diaion HP-20) that act as a charged solid separation medium. The components of the processed sample have different electrical affinities to this medium and are, as a result, differently retained by the resins due to these different affinities. Therefore, by elution, these components can be recovered separately at the outlet of the resins bed. Elution was performed using H₂O with gradually increasing amounts of MeOH and acetone.

2.3.5.4 Flash chromatography

Flash chromatography is a preparative column chromatography based on an optimized pre-packed column and an eluent at a high flow rate driven by air pressure. It is a simple and quick technique widely used for the separation of various organic compounds. Normally, the column, pre-packed by a dried Silica Gel 60 GF₂₅₄ at a height of 18 cm, is filled and saturated with the desired mobile phase just prior to the sample loading on the top of the column. The mobile phase, an isocratic or gradient solvent, is then pumped through the column with the help of air pressure. This process results in the separation of samples on the column. This technique, only considered as a technique under low to medium pressure, is applied for the separation of samples of the range from milligram to some gram of sample.

2.3.5.5 Preparative high pressure liquid chromatography (HPLC)

HPLC is a robust, versatile, and usually rapid technique to purify compounds from complex mixtures. The reversed-phase C-18 chromatography was used as the exclusive stationary phase of HPLC in this study. This method was used for the isolation and purification of compounds from fractions previously separated by column chromatography. The most appropriate solvent systems were established before running the HPLC separation. The mobile phase combination was MeOH or acetonitrile and nanopure water with or without 0.1% TFA or 0.1% formic acid, pumped in gradient or isocratic manner depending on the compounds retention time. Each injection consisted of 20–80 mg of the fraction dissolved in 400 mL of the solvent system. The solvent system was pumped through the column at a rate of 20 mL/min. The eluted peaks were detected by the online UV detector and collected separately in Erlenmeyer flasks.

Preparative HPLC system specifications are described as follows:

Pump	Varian, PrepStar 218
Detector	Varian, ProStar 320 UV-Vis detector
HPLC Program	Varian Star (V.6)
Column	Varian Dynamax (250×4.6 mm, ID and 250×21.4mm, ID), pre-packed with Microsorb 60-8 C-18, with integrated pre-column

2.3.5.6 Semi-preparative high pressure liquid chromatography (HPLC)

All samples for semi-preparative HPLC must be analyzed thoroughly and pretreated to make the separation optimal and maintain the life-span of the HPLC system. The eluant used in semi-preparative HPLC comprises a mixture of nanopure water and methanol. The isocratic conditions were always the premier, even the only choice to achieve separations. 50 µL of approximately 40 mg/mL solution of the substance was injected each time. The flow rate was stabilized at 5 mL/min, and the paper speed of the recorder was 5 mm/min. The eluted peaks were collected respectively by manual work based on the records of a UV-vis detector.

Semi-preparative HPLC system specifications are described as follows:

Pump	Merck Hitachi L-7100
Detector	Merck Hitachi UV detector L-7400
Column	Knauer (300×8 mm, ID), pre-packed with Eurosphere 100–10 C-18, with integrated pre-column

2.3.5.7 Analytical high pressure liquid chromatography (DAD-HPLC)

Analytical HPLC which is HPLC coupled to a PDA (photodiode array) detector, is extremely useful for the analysis of natural products to identify the distribution of peaks either from extracts or fractions, as well as to evaluate the purity of isolated

compounds. It can help to analyze individual HPLC peaks, and to obtain complete UV spectra of individual components. The HPLC retention time and the UV spectrum of a component (HPLC peak) can be characteristic of a certain compound. The whole system was run by the sophisticated software (Chromeleon[®] Version 6.30) that allows building up of spectral libraries for reference compounds and automated compound search.

The solvent gradient used started with MeOH:nanopure water (10:90), adjusted to pH 2 with phosphoric acid, and reached to 100 % MeOH in 35 minutes. The autosampler injected 20 μ L sample. All peaks were detected by UV-VIS photodiode array detector. In some cases, special gradient were used. The HPLC instrument consists of a pump, a detector, an injector, a separation column and a reservoir of mobile phase. The separation column (125 \times 2 mm, ID) was pre-filled with Eurospher-100 C18 (5 μ m), with an integrated pre-column (Knauer, Berlin, Germany).

The conditions of analytical HPLC are described as follows:

Flow rate:	1 mL/min
Injection volume:	20 μ L
Sample concentration:	ca. 0.1 mg/mL
Column temperature:	20 °C
UV detection wavelengths:	235, 254, 280, and 340 nm

LC/UV system specifications are described as follows:

Pump	Dionex P580A LPG
Detector	Dionex Photodiode Array Detector UVD 340S
Column thermostat	STH 585
Autosampler	ASI-100T
HPLC Program	Chromeleon (V. 6.3)
Column	Knauer (125 \times 4 mm, ID), pre-packed with Eurosphere 100–5 C18, with integrated pre-column

Standard gradient for analytical HPLC

Time (min)	Acidic water (%)	MeOH (%)
0	90	10
5	90	10
35	0	100
45	0	100
50	0	10
60	0	10

2.3.6 Structure elucidation of the isolated secondary metabolites**2.3.6.1 Mass spectrometry (MS)**

Mass spectroscopy (MS) is an analytical technique for the determination of the elemental composition of a molecule and for elucidating the chemical structures of molecules. It is a very sensitive technique and even from micro gram amounts good spectra can be obtained. A mass spectrometer is an analytical instrument used for determining the molecular weight of a compound. Technically, mass spectrometers are divided into three parts: ionization source, analyser, and detector, which should be maintained under high vacuum conditions so as to maintain the ions travel through the instrument without any hindrance from air molecules. The sample is ionized in the ionization source and the rising ions are sorted and separated according to their mass (m) to charge (z) ratio (m/z) in the mass analyser. Both negative and positive charged ions can be observed. Once the separated ions flow into the detector, the signals are transmitted to the data system where the mass spectrum is recorded. The molecular ion (parent ion) has to be identified giving the molecular weight of the compound. From the fragmentation patterns of the compound information about substructures can be attained. Therefore, mass spectrometry is used to determine the molecular weights of pure compounds or compounds in a mixture.

2.3.6.1.1 Electrospray ionization mass spectrometry (ESIMS)

In ESI method, a solution of a substance is sprayed through a capillary into a chamber. Charged droplets are produced by an applied potential of a few kV, and in the following are driven by the electric field to move into the pre-analyser region. ESIMS is a powerful analytical method, because it allows one to analyse the molecular ions of polar and higher molecular compounds in aqueous solution.

Liquid chromatography mass spectrometry (LC/MS)

High pressure liquid chromatography is a useful and powerful method for the separation of complex mixtures, especially when many of the components may have similar polarities. If a mass spectrum of each component can be recorded as it elutes from the LC column, quick characterization of the components is greatly facilitated. Generally, ESI-MS is interfaced with LC to make an effective on-line LC/MS. HPLC/ESI-MS was carried out using a Finnigan LCQ-DECA mass spectrometer connected to a UV detector. The samples were dissolved in water/MeOH mixtures and injected to HPLC/ESI-MS set-up. For standard MS/MS measurements, a solvent gradient that started with MeOH:nanopure water (10:90), adjusted with 0.1 % HCOOH, and reached to 100 % MeOH in 35 minutes was used.

LC/UV/MS system specifications are described as follows:

HPLC system	Agilent 1100 series (pump, detector and autosampler) Finnigan LC Q-DECA
MS spectrometer	Knauer, (250 × 2 mm, ID), prepacked with Eurosphere 100-5
Column	C18, with integrated pre-column

Standard gradient for LC/MS

Time (min)	Acidic water (%)	MeOH (%)
0	90	10
5	90	10
35	0	100
45	0	100
50	0	10
60	0	10

2.3.6.1.2 Electron impact mass spectrometry (EI-MS)

Electron impact mass spectrometry (EI-MS) yields a molecular ion M^+ , named radical cation, through the collision of an electron with the sample in gas phase. The sample is vaporized and then directly injected into a high vacuum chamber where the sample is ionized by bombarding with neutral molecules, which have energy of 70 eV and are accelerated in a 8 kV electric field. The ionization process is then accelerated by vacuum condition in a magnet field and ions are sorted by the ratios of mass to charge in a continued change of magnetic field.

Since the samples must be volatile and thermally stable, the measurement of EI-MS is limited to compounds with low molecular weight of 600 Da or less. Some classes of compounds, only generating molecular ion M^+ , are not ideal for this measurement. In most cases, the information of molecular structure can be deduced from the extensive fragments occurring in the analysis. The determination of molecular weight using this method is conducted by Dr. Keck and Dr. Tommes at the Institute of Inorganic Chemistry, University of Düsseldorf. The EI mass spectrometer type is Finnegan MAT 8200.

2.3.6.1.3 Fast atom bombardment mass spectrometry (FAB-MS)

This was the first broadly accepted method that employs energy sudden ionization. FAB is powerful for compounds, especially polar molecules, unresponsive to either EI or CI mass spectrometry. It enables both non-volatile and high molecular weight compounds to be analyzed. In this technique, a sample is dissolved or dispersed in a polar and relatively non-volatile liquid matrix, introduced into the source on a copper probe tip. Then, this matrix is bombarded with a beam of atoms of about 8 Kev. It uses a beam of neutral gas (Ar or Xe atoms) and both positive and negative ion FAB spectra can be obtained.

Low resolution FAB-MS was measured by a Finnigan MAT 8430 mass spectrometer. Measurements were conducted by Dr. Peter Tommes, Institute for Inorganic and Structural Chemistry, Heinrich-Heine University, Duesseldorf.

2.3.6.1.4 High resolution mass spectrometry (HR-MS)

High resolution is achieved by passing the ion beam through an electrostatic analyzer before it enters the magnetic sector. In such a double focusing mass spectrometer, ion masses can be measured with an accuracy of about 1 ppm. With measurement of this accuracy, the atomic composition of the molecular ions can be determined.

HRESI-MS was measured on a Micromass Qtof 2 mass spectrometer at Helmholtz Centre for Infection Research, Braunschweig. The time-to-flight analyzer separates ions according to their mass-to-charge ratios (m/z) by measuring the time it takes for ions to travel through a field free region known as the flight.

2.3.6.2 Nuclear magnetic resonance spectrometry (NMR)

The NMR phenomenon is based on the fact that nuclei of atoms have magnetic

properties that can be utilized to generate chemical information. Some nuclei experience this phenomenon, and others do not, depending upon whether they possess a property called spin. It is used to study physical, chemical, and biological properties of matter. As a consequence, NMR spectroscopy finds applications in several areas of science. NMR spectroscopy is routinely used by chemists to study chemical structure using simple one dimensional technique. Two dimensional techniques were used to determine and confirm the structure of more complicated molecules.

This technique utilizes the atomic nuclei spinning behavior of atoms with an odd number of nucleons, e. g. ^1H and ^{13}C . An NMR spectrum is acquired by varying the magnetic field that is applied to the sample dissolved in a deuterated solvent over a small range while observing the resonance signal from the sample. Depending on the electron density around each proton they obtain different shielding and deshielding effects appearing in different parts of the resulting NMR spectrum and thus provide information about the environment of each proton. The resulting frequency where the nuclei resonate, the so-called chemical shift, is given in ppm and the coupling constants between adjacent nuclei in Hertz (Hz). NMR experiments can be conducted in a one (1D) or two (2D) dimensional manner. 2D NMR spectra can be either measured between two equal (H,H-COSY) or two different (H,C-COSY) frequency axes. For the H,H-2D experiments the connection between two adjacent protons (COSY), between two protons through space (NOESY, nuclear Overhauser enhancement spectroscopy; ROESY, rotatingframe enhancement spectroscopy) or between all protons in one spin system (TOCSY, total correlation spectroscopy) are given. H,C-2D experiments measure the direct correlation between a proton and a carbon (HMQC, heteronuclear multiple quantum correlation) or the connection of protons over two, three and even four bonds to carbon atoms, so-called long range coupling (HMBC, heteronuclear multiple bond correlation). Correlations are shown as cross peaks in the plane between two axes containing the 1D NMR shifts.

NMR spectra were recorded on a Bruker ARX-500 by Dr. Peter Tommes, Institute for

Inorganic and Structural Chemistry, Heinrich-Heine University, Duesseldorf. Some measurements were also performed at the Helmholtz Centre for Infection Research, Braunschweig, by Dr. Victor Wray using an AVANCE DMX-600 NMR spectrometer. All 1D and 2D spectra were obtained using the standard Bruker software. The samples were dissolved in different solvents, the choice of which was dependent on the solubility of the samples. Residual solvent signals were used as internal standards (reference signal). The observed chemical shift (δ) values were given in ppm and the coupling constants (J) in Hz.

2.3.6.3 Optical activity

When a polarized light is passed through a chiral molecule, the direction of polarization can be changed. This phenomenon is called optical rotation or optical activity. The measurement of this change in polarization orientation is called polarimetry and the instrument used to measure this phenomenon is called a polarimeter.

This measurement is used to study the structure of anisotropic compounds and to check the purity of chiral mixtures. If the sample contains only one enantiomer of its chiral molecule, the sample is said to be optically pure. An enantiomer is called as a levorotatory (l) or (-) enantiomer if it rotates light to the left (counterclockwise). On the contrary, if an enantiomer rotates light to the right (clockwise), it is said to be as a dextrorotary (d) or (+) enantiomer.

Since the degree of optical rotation depends on the number of optically active species (chiral) in which the light passes, the measurement of optical rotation depends on concentration (c) and light path length (l) of the sample. The specific rotation, $[\alpha]$, expresses the optical rotation degree after correction of concentration and path length. Thus the specific rotation is a specific quantity for a chiral molecule at certain temperature T and wavelength λ .

$$[\alpha]_{\lambda}^T = 100 \alpha / cl$$

where:

$[\alpha]_{\lambda}^T$ is specific rotation at certain temperature T and wavelength

l is optical path length in dm

λ is wavelength

T is temperature

α is measured optical rotation degree at certain temperature T and wavelength λ

c is concentration in g/100 mL

In this study, the measurement of optical rotation was recorded on Perkin-Elmer 241 MC polarimeter. The substance was stored in a 0.5 mL cuvette with 1 dm length. $[\alpha]_{\text{D}}^{20}$ is the specific optical rotation at the wavelength of Sodium-D-lamp, 589 nm, at a temperature of 20 °C.

2.3.6.4 Determination of absolute stereochemistry by Mosher reaction

The reaction was performed based on a modified Mosher ester procedure described by Su et al. (Ohtani *et al.*, 1991; Su *et al.*, 2002).

Reaction with (*R*)-(-)- α -(trifluoromethyl) phenylacetyl chloride

The compounds (1 mg of each) were transferred into NMR tubes and were dried under vacuum. Deuterated pyridine (0.5 mL) and (*R*)-MTPA chloride were added immediately under a N₂ gas stream. The reagent was added in the ratio of 0.14 mM reagent to 0.10 mM of the compound (Dale and Mosher, 1973). The NMR tubes were shaken carefully to mix the samples and MTPA chloride evenly. The reaction NMR tubes were permitted to stand at room temperature and monitored by ¹H-NMR until the reaction was completed. ¹H-¹H COSY was measured to confirm the assignment of the signals.

Reaction with (S)-(-)- α -(trifluoromethyl) phenylacetyl chloride

Another portion of each compound (1 mg) was transferred into NMR tube. The reaction was performed in the same manner as described before to yield the (S)-MTPA ester.

2.3.6.5 Circular dichroism (CD) spectroscopy

Circular dichroism is based on the difference between the absorption of left-handed circularly polarised light (L-CPL) and right-handed circularly polarised light (R-CPL). It occurs when a molecule contains one or more chiral chromophores (light-absorbing groups).

$$\text{Circular dichroism} = \Delta A(\lambda) = A(\lambda)_{\text{LCPL}} - A(\lambda)_{\text{RCPL}}$$

where λ is the wavelength.

Circular dichroism (CD) spectroscopy is a spectroscopic method. The CD of molecules is recorded over a range of wavelengths. CD spectroscopy is widely used to study chirality of molecules.

Measurements are carried out in the visible and ultra-violet region of the electro-magnetic spectrum to monitor electronic transitions. If the molecule under investigation contains chiral chromophores, one CPL state will be absorbed to a greater extent than the other and the CD signal over the corresponding wavelengths will be non-zero. A circular dichroism signal can be positive or negative, depending on whether L-CPL is absorbed to a greater extent than R-CPL (CD signal positive) or to a lesser extent (CD signal negative).

Circular dichroism spectra are measured using a circular dichroism spectrometer,

which is a highly specialised derivative of an ordinary absorption spectrometer. CD spectrometers alternately measure the absorption of L- and R-CPL, usually at a frequency of 50 KHz, and then calculate the circular dichroism signal.

In this study, the CD spectra were recorded on a J-810 CD spectropolarimeter. Conformational searches were carried out by means of the MacroModel 9.7.211 (MacroModel *et al.*, 2009) software using Merck Molecular Force Field (MMFF) with implicit solvent model for chloroform. Geometry reoptimizations at B3LYP/6-31G(d) level of theory followed by TDDFT calculations using various functionals (B3LYP, BH&HLYP, PBE0) and TZVP basis set were performed by the Gaussian 03 (Frisch *et al.*, 2004) package. Boltzman distributions were estimated from the ZPVE corrected B3LYP/6-31G(d) energies. CD spectra were generated as the sum of Gaussians (Stephens and Harada, 2010) with 3000 cm⁻¹ half-height width (corresponding to ca. 16 nm at 230 nm), using dipole-velocity computed rotational strengths for conformers above 5%. The MOLEKEL (Varetto, 2009) software package was used for visualization of the results.

2.3.7 Testing the biological activity

2.3.7.1 Antimicrobial and antifungal activity

Extracts and pure compounds were evaluated in a 96 well plates primary screening assay against the following resistant pathogens: *Escherichia coli*, *Enterococcus faecium*, *Staphylococcus aureus*, *Streptococcus pneumonia*, *Pseudomonas aeruginosa*, *Klebsiella pneumonia*, *Candida albicans*, *Candida krusei*, *Aspergillus fumigatus*, *Aspergillus faecius*.

Pure compounds were diluted from 250 to 62.5 µg/mL and extracts from 1250 to 312 µg/mL in Müller Hinton Bouillon (Merck, Germany) for bacterial screening and in RPMI (PAA, Austria), enriched with 2% glucose (PAA, Austria), for fungal screening.

Afterwards the substance/extract solution was overlaid with the microbes (105 CFU/mL) and cultivated for bacteria 24 h for fungi 48h at 35°C. As negative control an antibiotic/antimycotic mix (PAA, Austria) was used in addition to a non treated infected control (positive). The result was analysed by checking the microbial growth with the visible eye and by measurement of the turbidity at 650 nm. All procedures were done under aseptic conditions in a sterile laminar air flow according to good laboratory practice.

Substances with an activity around 125 g/ml and extracts with 625 µg/ml were considered as possible candidates for further antimicrobial screening. With these positive candidates a MIC (minimal inhibition concentration) assay was performed to identify the exactly minimal inhibition concentration. Therefore, the substances/extracts were diluted from 250 g/mL to 0.24 g/mL and screened in the same manner as in the primary screening.

2.3.7.2 Cytotoxicity test

Microculture tetrazolium (MTT) assay

Cytotoxicity assays were performed by Prof. Dr. W. E. G. Müller, Institute for Physiological Chemistry and Pathobiochemistry, University of Mainz, Mainz. Cytotoxicity was evaluated against L5178Y mouse lymphoma cells using microculture tetrazolium (MTT) assay, and compared to that of untreated controls (Carmichael *et al.*, 1987).

Cell cultures

L5178Y mouse lymphoma cells were grown in Eagle's minimal essential medium supplement with 10 % horse serum in roller tube culture. The medium contained 100 units/mL penicillin and 100µg/mL streptomycin. The cells were maintained in a

humidified atmosphere at 37 °C with 5 % CO₂.

MTT colorimetric assay

Of the test samples, stock solutions in ethanol 96% (v/v) were prepared. Exponentially, growing cells were harvested, counted, and diluted appropriately. Of the cell suspension, 50 μ L containing 3750 cells were pipetted into 96-well microtiter plates. Subsequently, 50 μ L of a solution of the test samples containing the appropriate concentration was added to each well. The concentration range was 3 and 10 μ g/mL. The small amount of ethanol present in the wells did not affect the experiments. The test plates were incubated at 37 °C with 5% CO₂ for 72 h. A solution of 3-(4,5-dimethylthiazol-2-yl)-2,5-diphenyltetrazolium bromide (MTT) was prepared at 5 mg/mL in phosphate buffered saline (PBS; 1.5 mM KH₂PO₄, 6.5 mM Na₂HPO₄, 137 mM NaCl, 2.7 mM KCl; pH 7.4) and from the solution, 20 μ L was pipetted into each well. The yellow MTT penetrates the healthy living cells and in the presence of mitochondrial reductase, MTT is transformed to its blue formazan complex. After an incubation period of 3 h 45 min at 37 °C in a humidified incubator with 5 % CO₂, the medium was centrifuged (15 min, 20 °C, 210 x g) with 200 μ L DMSO, the cells were lysed to liberate the formed formazan product. After thorough mixing, the absorbance was measured at 520 nm using a scanning microtiter-well spectrophotometer. The colour intensity is correlated with the number of healthy living cells. Cell survival was calculated using the formula:

$$\text{Survival \%} = 100 \times \frac{\text{Absorbance of treated cells} - \text{Absorbance of culture medium}}{\text{Absorbance of untreated cells} - \text{Absorbance of culture medium}}$$

All experiments were carried out in triplicates and repeated three times. As controls, media with 0.1% EGMME/DMSO were included in the experiments.

3. Results

3.1 Secondary metabolites from the sponge-associated fungus *Aspergillus* sp.

Bioactive natural products from marine-derived fungi were reported for the first time back in the 1940s from a fungal strain of *Acremonium chrysogenum*, which yielded cephalosporin C, the parent compound of cephalosporin antibiotics. Meanwhile, marine-derived fungi have been isolated from various organisms, including algae, mollusks and particularly sponges (Bringmann *et al.*, 2004; Lopez-Gresa *et al.*, 2009). However, sponge-derived fungi were found to be among the most prolific sources of bioactive compounds (Daferner and Sterner, 2002).

The genus *Aspergillus* (Moniliaceae) contains approximately 180 species which survive in various climates worldwide in both terrestrial and marine environments (He *et al.*, 2004). *Aspergillus* species and their chemical profiles have been studied by numerous research groups. The genus has proven to be a rich source of secondary metabolites with novel structures and interesting bioactivities (Liu *et al.*, 2009). Examples of isolated metabolites include meroterpenoids, isochroman derivatives, drimane sesquiterpenoids, and cyclic tripeptides, which in most cases exhibited interesting biological activities, such as plant growth inhibition, cytotoxic activity against tumor cell lines, selective antifungal activity, as well as inhibition of endothelin-type B receptors (Liu *et al.*, 2009; Newman, 2008; Yaming *et al.*, 2011).

With the goal of isolation and identification of novel biologically active metabolites from marine-associated fungi, we have investigated the bioactive constituents from a sponge-derived fungal *Aspergillus* strain, isolated from a specimen of the Mediterranean sponge *Tethya aurantium*. Chromatographic separation of the crude extract obtained from this fungal strain, yielded 31 compounds including 15 new natural products.

3.1.1 Butyrolactone II (compound 1, known)

Butyrolactone II	
Biological Source	<i>Aspergillus</i> sp.
Sample Code	Fr.2.5.5, Fr.2.5.4.6
Sample Amount	120 mg
Molecular Formula	C ₁₉ H ₁₆ O ₇
Molecular Weight	356 g/mol
Solubility	MeOH
Physical Description	Colorless amorphous powder
Optical Rotation	[α] _D ²⁰ + 16.2° (c 1.0, EtOH)
HPLC Retention Time	22.8 min (standard gradient)

Butyrolactone II (**1**) was isolated as a colorless amorphous powder (120 mg) and it revealed UV absorbances at λ_{\max} (MeOH) 202.0, 223.8, and 307.1 nm. The compound was optically active with an $[\alpha]_D^{20}$ value of $+16.2^\circ$ (c 1.0, EtOH). Its molecular weight was indicated as 356 g/mol based on the molecular ion peaks observed at m/z 357 $[M+H]^+$ (base peak) and 355 $[M-H]^-$ (base peak) upon positive and negative ionization by ESI-MS, respectively. ^{13}C NMR and DEPT spectra of **1** displayed 19 carbon signals assigned for one methoxy group, one methylene group, eight aromatic methine groups including four overlapping ones, and nine quaternary carbon atoms including two ester carbonyl carbons (Table 3.1.1). The ^1H -NMR spectra of **1** displayed signals corresponding to eight aromatic protons at δ_{H} 6.59 ppm (H-5/9), 6.50 ppm (H-6/8), 7.52 ppm (H-5'/9'), and 6.87 ppm (H-6'/8'). A signal at δ_{H} 3.74 ppm revealed the presence of one methoxy group (OCH₃-1a) and the signal at δ_{H} 3.40 ppm belonged to the methylene group (CH₂-3). At last, the remaining signals revealed the presence of three hydroxy groups at δ_{H} 10.56 ppm (2'-OH), 9.93 ppm (7'-OH), and 9.22 ppm (7-OH). The HMBC correlations of the methylene protons with C-2 (δ_{C} 84.7 ppm), C-4 (δ_{C} 123.1 ppm), C-3' (δ_{C} 127.4 ppm), C-5/9 (δ_{C} 131.1 ppm), and C-1 (δ_{C} 169.7 ppm) suggested that the protons were positioned at C-3 (δ_{C} 38.0 ppm) and connected the aromatic ring to the lactone ring. The correlation of H-1a with C-1 indicated that the methoxy group was attached to C-1. The remaining HMBC correlations are shown in Figure 3.1.1 and Figure 3.1.2. Therefore, compound **1** was finally confirmed as butyrolactone II by analysis of all data as mentioned above together with comparing the data with reported data of butyrolactone II (Table 3.1.1) (Nitta *et al.*, 1983; Rao *et al.*, 2000).

Table 3.1.1 NMR data for butyrolactone II (1)

Position	1 DMSO- <i>d</i> ₆ , δ (ppm), <i>J</i> in Hz		Reference, δ (ppm), <i>J</i> in Hz	
	¹ H (300 MHz)	¹³ C (75 MHz)	¹ H (60 MHz) ^a (Nitta <i>et al.</i> , 1983)	¹³ C (50 MHz) ^b (Rao <i>et al.</i> , 2000)
1a	3.74 s	53.5	3.71 s	53.5
1		169.7		169.9
2		84.7		84.9
3	3.40 s	38.0	3.43 s	38.2
4		123.1		123.4
5	6.59 d (8.6)	131.1	6.63 d (9.0)	131.3
6	6.50 d (8.6)	114.6	6.43 d (9.0)	114.8
7		156.3		156.4
7-OH	9.22			
8	6.50 d (8.6)	114.6	6.43 d (9.0)	114.8
9	6.59 d (8.6)	131.1	6.63 d (9.0)	131.3
1'		167.9		168.1
2'		138.1		138.3
2'-OH	10.56			
3'		127.4		127.7
4'		121.0		121.2
5'	7.52 d (8.8)	128.8	7.51 d (9.0)	129.0
6'	6.87 d (8.8)	115.8	6.85 d (9.0)	116.0
7'		157.9		158.1
7'-OH	9.93			
8'	6.87 d (8.8)	115.8	6.85 d (9.0)	116.0
9'	7.52 d (8.8)	128.8	7.51 d (9.0)	129.0

^a acetone-*d*₆ ^b DMSO-*d*₆

Results

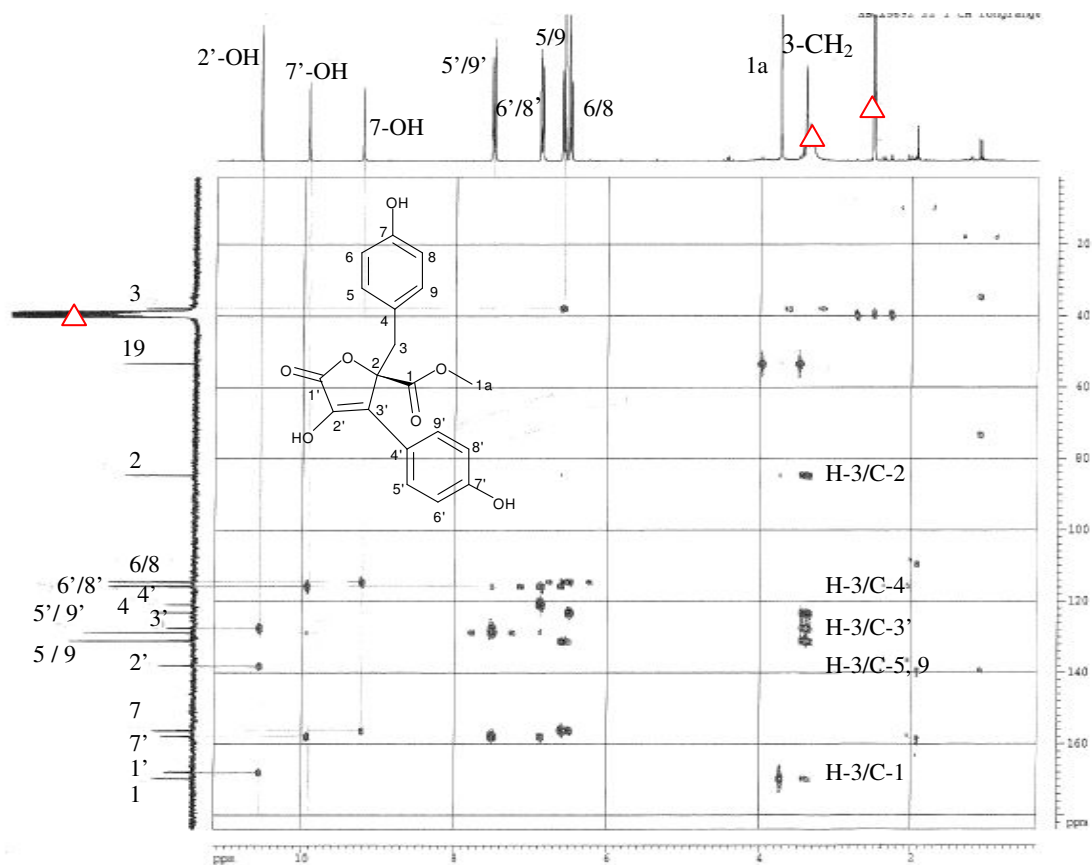


Figure 3.1.1 HMBC correlations of butyrolactone II (1).

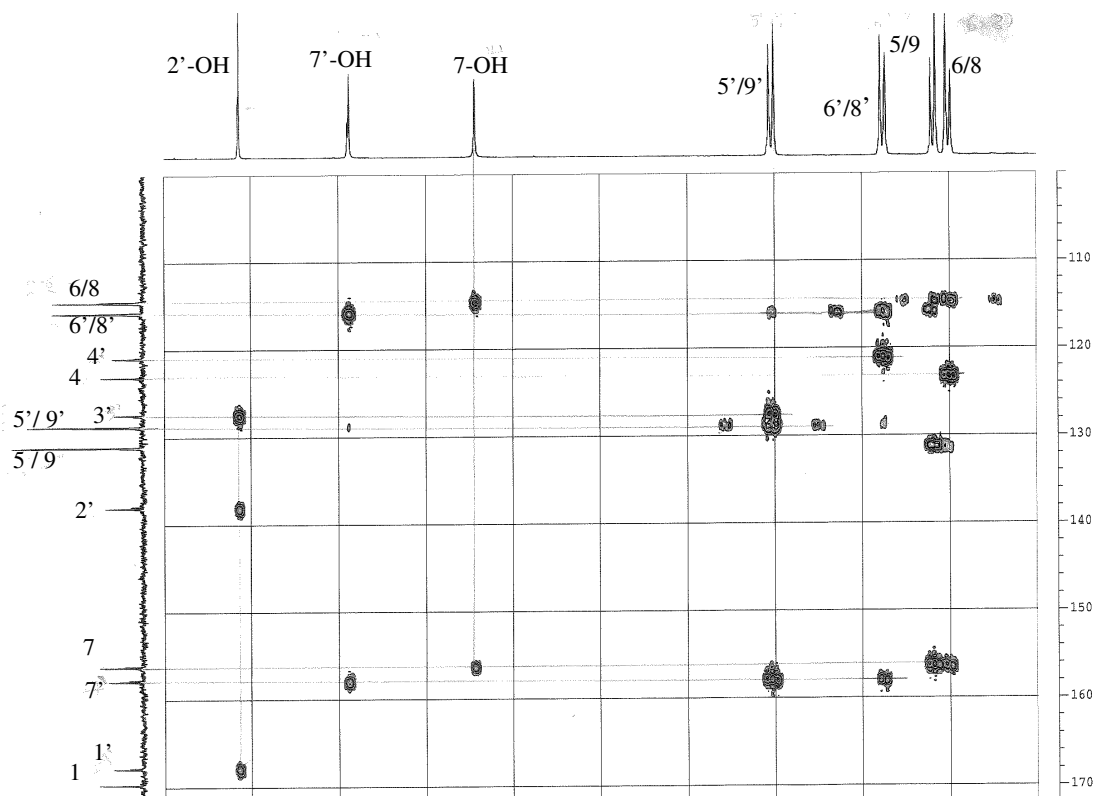
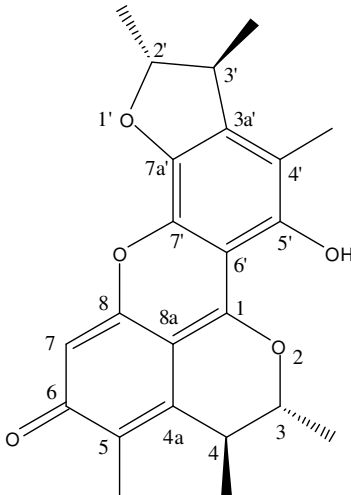
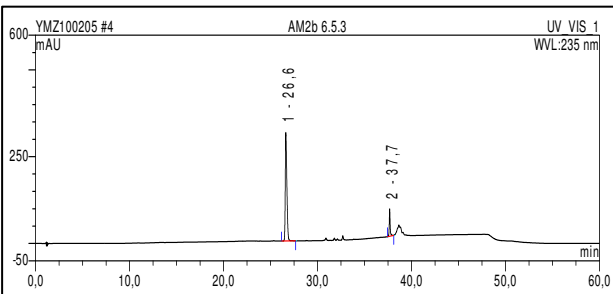
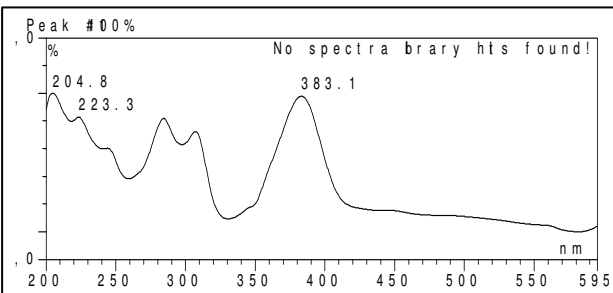
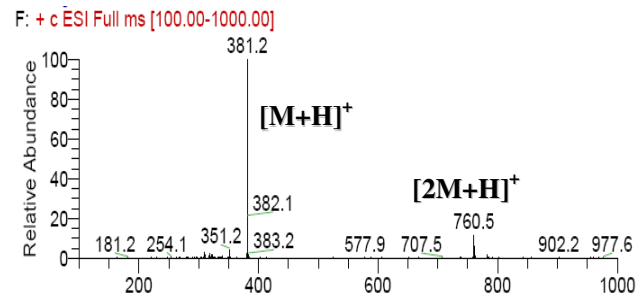
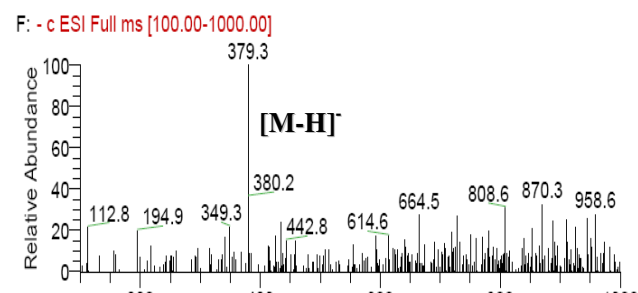


Figure 3.1.2 HMBC correlations of butyrolactone II (1)

3.1.2 Dicitrinin A (compound 2, known)

Dicitrinin A	
Biological Source	<i>Aspergillus</i> sp.
Sample Code	Fr.2.6.5.3
Sample Amount	4.5 mg
Molecular Formula	C ₂₃ H ₂₄ O ₅
Molecular Weight	380 g/mol
Solubility	MeOH
Physical Description	Red solid
Optical Rotation	$[\alpha]_D^{20} + 76.0^\circ$ (<i>c</i> 0.016, CDCl ₃)
HPLC Retention Time	26.6 min (standard gradient)
	
	
	
	
	

Dicitrinin A (**2**) was isolated as a red solid (4.5 mg) with an $[\alpha]_D^{20}$ value of $+76.0^\circ$ (c 0.016, CHCl_3). It revealed UV absorbances at λ_{max} (MeOH) 204.8, 223.3, and 383.1 nm. Its molecular weight was determined as 380 g/mol according to the molecular ion peaks observed at m/z 381.2 $[\text{M}+\text{H}]^+$ (base peak) and 379.2 $[\text{M}-\text{H}]^-$ (base peak) upon positive and negative ionization by ESI-MS, respectively. The ^{13}C NMR of **2** (Table 3.1.2) showed six methyl carbons, four sp^3 methine carbons, a sp^2 methine carbon, and 12 quarternary carbons including one carbonyl carbon. Furthermore, the ^1H -NMR of **2** (Table 3.1.2) displayed four tertiary methyl signals, two aromatic methyl signals, two sets each composed of two sp^3 methine protons, and an aromatic proton singlet at δ_{H} 5.95 ppm (H-7). The detailed analysis of ^1H - ^1H COSY and HMBC spectra confirmed the planar structure of dicitrinin A. HMBC correlations were observed from H-3 (δ_{H} 5.03 ppm) to C-1 (δ_{C} 156.2 ppm) and C-4a (δ_{C} 132.3 ppm), and from H-4 (δ_{H} 3.16 ppm) to C-8a (δ_{C} 98.6 ppm) and C-5 (δ_{C} 128.2 ppm), from H-7 (δ_{H} 5.95 ppm) to C-5 and C-8a. Moreover, HMBC correlations were observed from CH_3 -2' (δ_{H} 1.29 ppm) to C-2' (δ_{C} 87.2 ppm) and C-3' (δ_{C} 43.7 ppm), from CH_3 -3' (δ_{H} 1.25 ppm) to C-2', C-3' and C-3a' (δ_{C} 139.2 ppm), and from CH_3 -4' (δ_{H} 2.14 ppm) to C-6' (δ_{C} 102.6 ppm), C-4' (δ_{C} 116.9 ppm), C-7' (δ_{C} 134.9 ppm), C-7a' (δ_{C} 136.8 ppm), C-3a' and C-5' (δ_{C} 148.3 ppm) (Figure 3.1.3 and Figure 3.1.4). Consequently, compound **2** was determined as dicitrinin A by interpretation of COSY and HMBC spectra in addition to comparison of UV, ^1H , ^{13}C NMR, mass spectral data and $[\alpha]_D$ value with published data (Daigo *et al.*, 2006; Benjamin *et al.*, 2006). In spite of deviations of our NMR data from those reported for dicitrinin A in literature (Table 3.1.2), structural confirmation was achieved by thorough interpretation of 2D NMR spectra, mass spectral analysis and measurement of optical rotation. It is to note that such deviations were observed even among published data for the same substance (Daigo *et al.*, 2006; Benjamin *et al.*, 2006).

Table 3.1.2 NMR data for dicitrinin A (2)

Position	2 DMSO- <i>d</i> ₆ , δ (ppm), <i>J</i> in Hz		Reference DMSO- <i>d</i> ₆ , δ (ppm), <i>J</i> in Hz (Benjamin <i>et al.</i> , 2006)	
	¹ H (400 MHz)	¹³ C (100 MHz)	¹ H (600 MHz)	¹³ C (150 MHz)
1		156.2		169.8
2				
3	5.03 q (6.7)	81.1	5.46 q (6.8)	84.9
3-CH ₃	1.32 d (6.5)	21.4	1.37 d (6.8)	18.2
4	3.16 q (7.2)	33.9	3.55 q (7.2)	33.3
4-CH ₃	1.20 d (7.1)	18.8	1.26 d (7.2)	18.8
4a		132.3		137.5
5		128.2		124.1
5-CH ₃	1.95 s	10.2	2.22 s	10.0
6		169.1		170.4
7	5.95 s	101.2	7.03 s	99.4
8		157.2		157.6
8a		98.6		102.4
1'				
2'	4.57 dq (3.9, 6.3)	87.2	4.75 dq (3.6, 6.4)	87.9
2'-CH ₃	1.29 d (6.5)	18.0	1.36 d (6.4)	20.6
3'	3.22 dq (3.8, 7.0)	43.7	3.42 dq (3.6, 7.0)	44.2
3'-CH ₃	1.25 d (7.0)	18.5	1.30 d (7.0)	18.7
3a'		139.2		144.9
4'		116.9		119.1
4'-CH ₃	2.14 s	11.6	2.27 s	12.0
5'		148.3		149.1
6'		102.6		104.7
7'		134.9		137.3
7a'		136.8		137.2

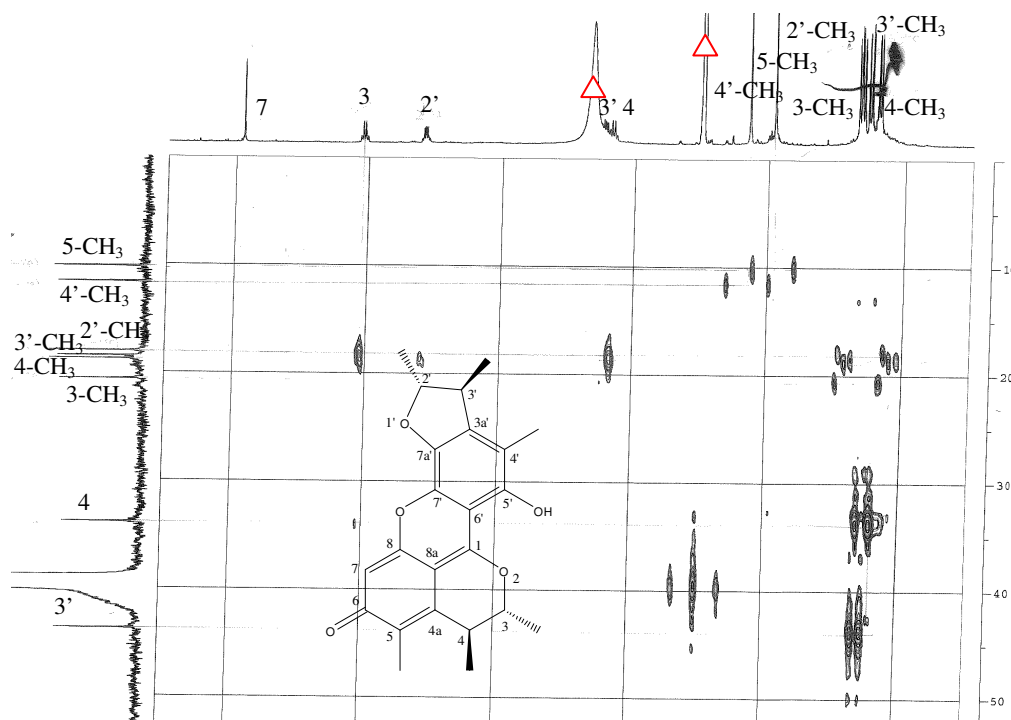


Figure 3.1.3 HMBC correlations of dicitrinin A (2)

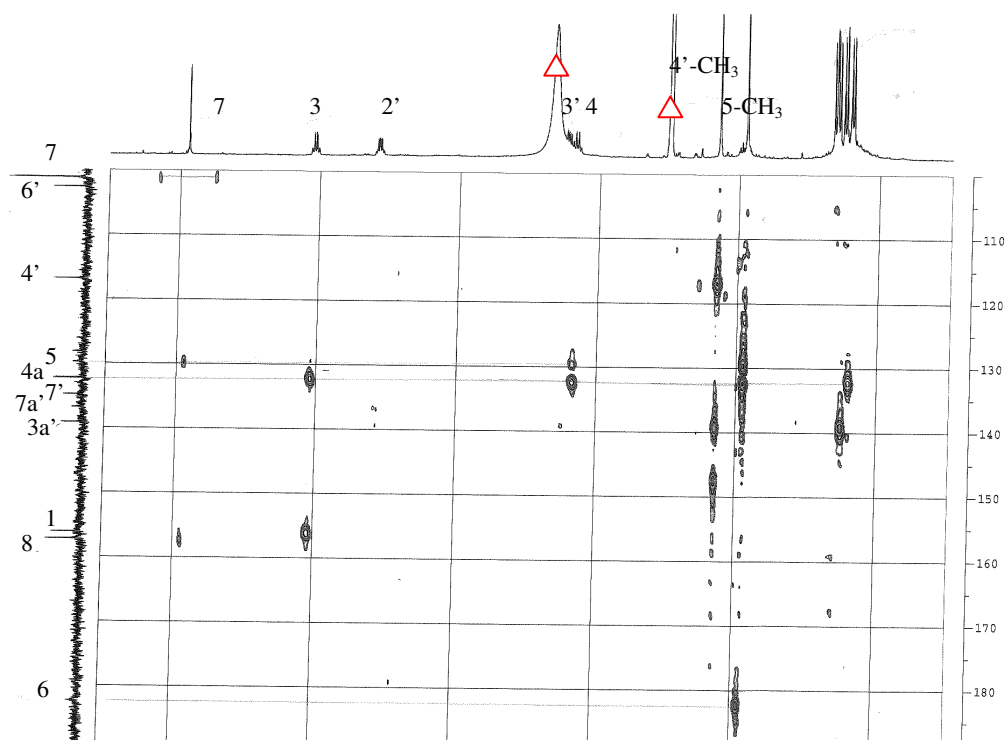
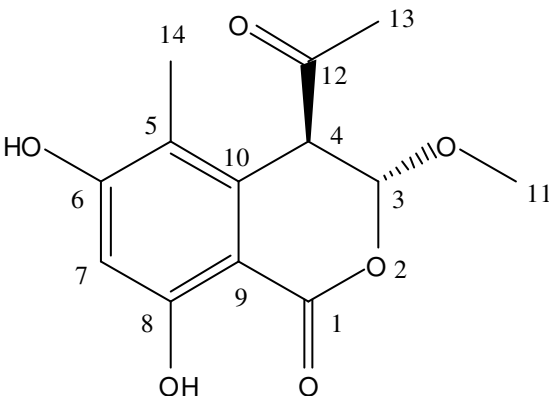
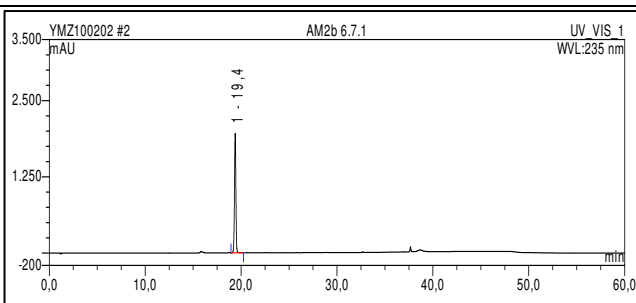
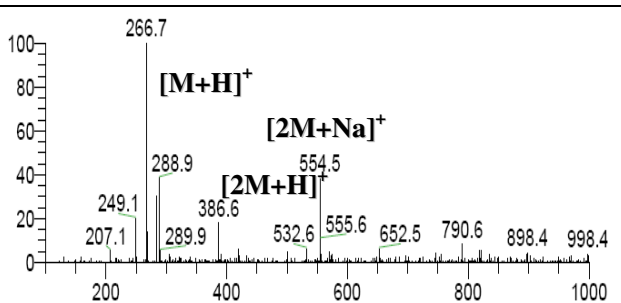
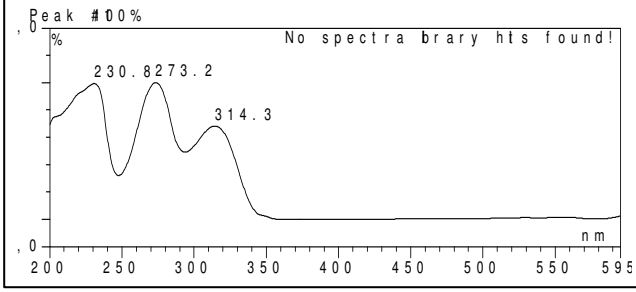
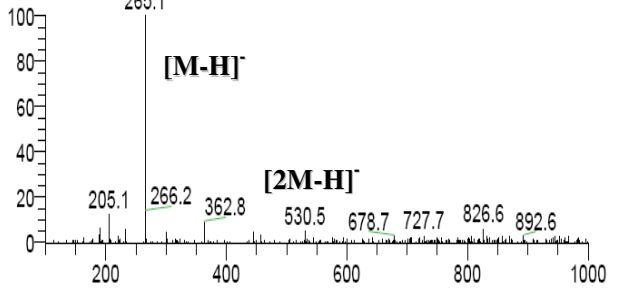


Figure 3.1.4 HMBC correlations of dicitrinin A (2)

3.1.3 4-Acetyl-3,4-dihydro-6,8-dihydroxy-3-methoxy-5-methylisocoumarin (compound 3, known)

4-Acetyl-3,4-dihydro-6,8-dihydroxy-3-methoxy-5-methylisocoumarin	
Biological Source	<i>Aspergillus</i> sp.
Sample Code	Fr.2.6.7.1
Sample Amount	11.7 mg
Molecular Formula	C ₁₃ H ₁₄ O ₆
Molecular Weight	266 g/mol
Solubility	MeOH
Physical Description	Yellow amorphous solid
Optical Rotation	$[\alpha]_D^{20} - 5.7^\circ$ (<i>c</i> 1.0, MeOH)
HPLC Retention Time	19.4 min (standard gradient)
	
	
	
	
	

4-Acetyl-3,4-dihydro-6,8-dihydroxy-3-methoxy-5-methylisocoumarin (**3**) was obtained as a yellow amorphous solid (11.7 mg) with an $[\alpha]_D^{20}$ value of -5.7° (c 1.0, MeOH). It displayed UV absorbances at λ_{\max} (MeOH) 230.8, 273.2, and 314.3 nm. Its molecular weight was suggested as 266 g/mol according to the molecular ion peaks observed at m/z 266.7 $[M+H]^+$ (base peak) and 288.9 $[M+Na]^+$ in the positive mode and at m/z 265.1 $[M-H]^-$ (base peak) in the negative mode by ESI-MS analysis. The 1H NMR spectrum (Table 3.1.3) exhibited an aromatic methine singlet at δ_H 6.35 ppm (H-7), two methine doublets at δ_H 5.84 ppm and 4.48 ppm (H-3 and H-4), a methoxy group at δ_H 3.45 ppm (H-11), two methyl singlets at δ_H 2.27 ppm and 1.94 ppm (H-13 and H-14), and two hydroxyl singlets at δ_H 10.93 ppm and 10.83 ppm (8-OH and 6-OH), respectively. In the ^{13}C NMR spectrum (Table 3.1.3) 13 carbon signals were clearly observed and they were assigned to a ketone carbonyl carbon at δ_C 202.8 ppm (C-12), an ester carbonyl carbon at δ_C 167.2 ppm (C-1), two oxygenated sp^2 carbons at δ_C 163.2 ppm and 161.2 ppm (C-6 and C-8, respectively), one aromatic methine carbon at δ_C 100.8 ppm (C-7), three sp^2 quaternary carbons at δ_C 135.0 ppm, 115.5 ppm and 99.7 ppm (C-10, C-5 and C-9, respectively), an acetal carbon at δ_C 101.0 ppm (C-3), a methine carbon at δ_C 52.8 ppm (C-4), a methoxyl carbon at δ_C 56.3 ppm (C-11), and two methyl carbons at δ_C 29.4 ppm and 10.8 ppm (C-13 and C-14, respectively). The structure of **3** was determined based on analysis of the HMBC spectrum (Figure 3.1.5), which revealed correlations from the methine proton H-7 to C-5, 6, 8, and 9, as well as the omega correlation to C-1, from the methyl protons CH₃-14 to C-5, 6, and 10, from the acetal proton H-3 to C-1, 10, 11, and 12, from the methine proton H-4 to C-3, 5, 9, 10, and 12, from the methyl protons CH₃-11 to C-3, and from the methyl protons CH₃-13 to C-4 and the carbonyl carbon C-12. Furthermore, the coupling constant of $J_{3,4}=1.3$ Hz suggested a *trans*-bisequatorial arrangement of the substituents at C-3 and C-4 on the pyranone ring. Therefore, the structure of **3** was determined as 4-acetyl-3,4-dihydro-6,8-dihydroxy-3-methoxy-5-methylisocoumarin on the basis of HMBC correlations (Figure 3.1.5) in addition to comparison with reported data (Krohn *et al.*, 2001, 2004).

Table 3.1.3 NMR data for 4-acetyl-3,4-dihydro-6,8-dihydroxy-3-methoxy-5-methylisocoumarin (3)

Position	3 DMSO- <i>d</i> ₆ , δ (ppm), <i>J</i> in Hz		Reference CD ₃ OD, δ (ppm), <i>J</i> in Hz (Krohn <i>et al.</i> , 2001)	
	¹ H (400 MHz)	¹³ C (100 MHz)	¹ H (200 MHz)	¹³ C (50 MHz)
1		167.2		168.3
3	5.84 d (1.3)	101.0	5.65 d (1.3)	102.2
4	4.48 d (1.3)	52.8	4.24 d (1.3)	53.8
5		115.5		116.4
6		163.2		164.1
6-OH	10.83 br s			
7	6.35 s	100.8	6.26 s	101.2
8		161.2		162.7
8-OH	10.93 s			
9		99.7		100.0
10		135.0		135.1
11	3.45 s	56.3	3.46 s	56.1
12		202.8		203.5
13	2.27 s	29.4	2.11 s	28.1
14	1.94 s	10.8	1.96 s	10.1

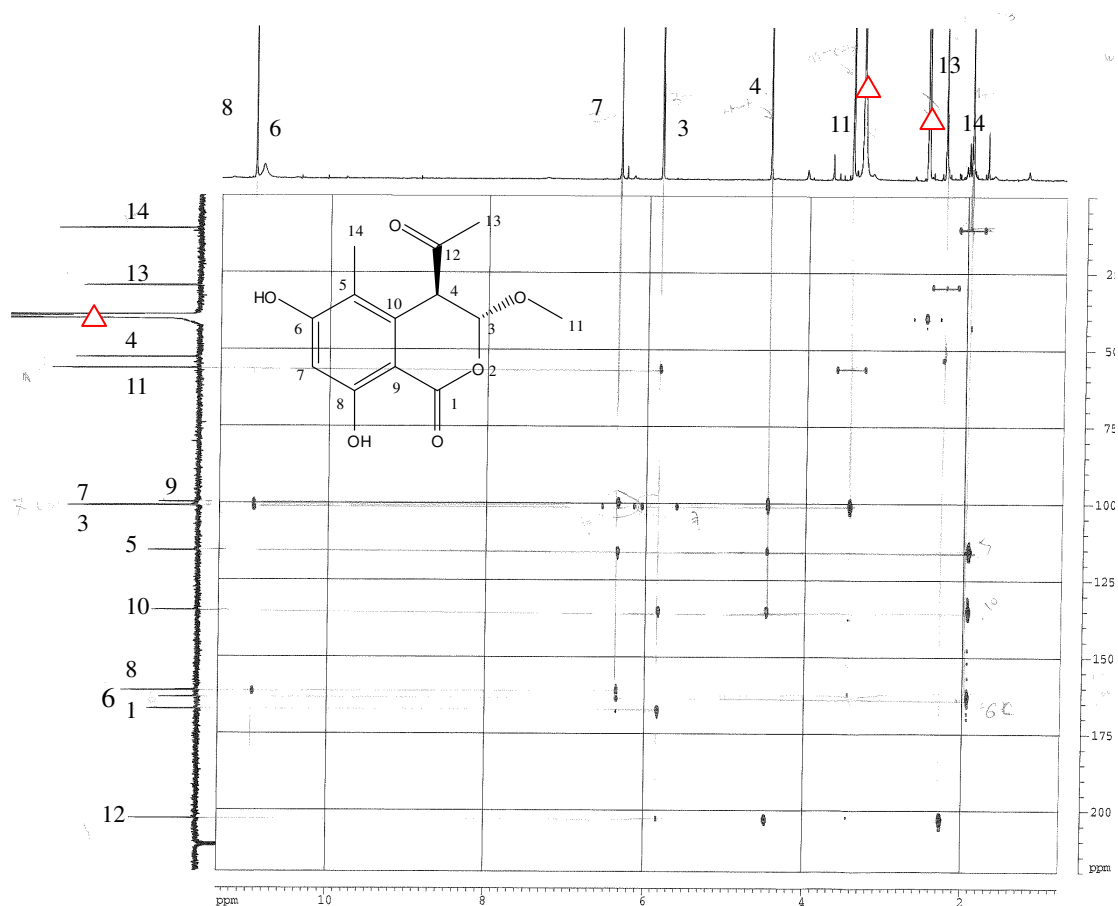
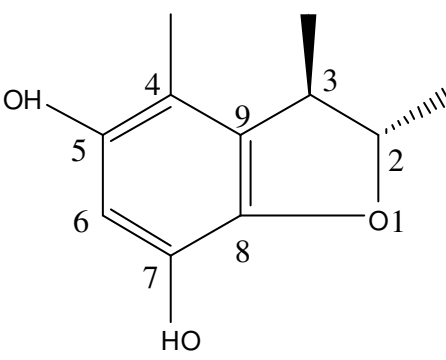
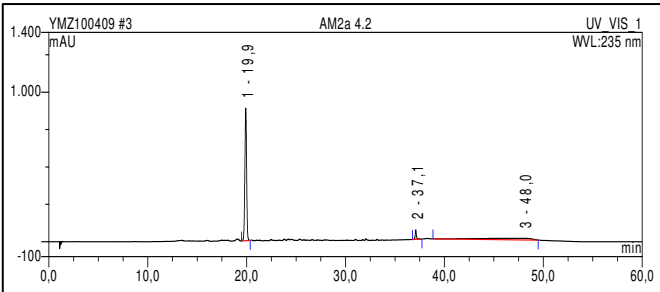
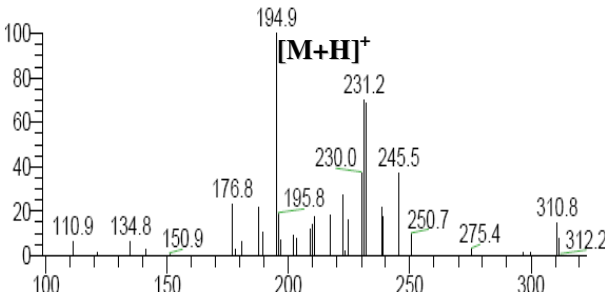
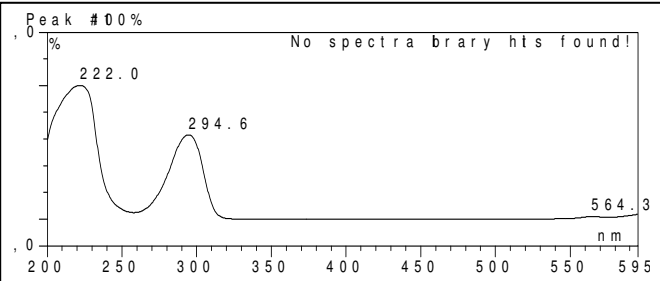


Figure 3.1.5 HMBC correlations of 4-acetyl-3,4-dihydro-6,8-dihydroxy-3-methoxy-5-methylisocoumarin (3)

3.1.4 2,3,4-Trimethyl-5,7-dihydroxy-2,3-dihydrobenzofuran (compound 4, known)

2,3,4-Trimethyl-5,7-dihydroxy-2,3-dihydrobenzofuran	
Biological Source	<i>Aspergillus</i> sp.
Sample Code	Fr.2.4.2
Sample Amount	20.0 mg
Molecular Formula	C ₁₁ H ₁₄ O ₃
Molecular Weight	194 g/mol
Solubility	MeOH
Physical Description	Brown solid
Optical Rotation	$[\alpha]_D^{20} + 30^\circ$ (c 0.1, MeOH)
HPLC Retention Time	19.9 min (standard gradient)
	
	
	
	

2,3,4-Trimethyl-5,7-dihydroxy-2,3-dihydrobenzofuran (**4**) was isolated as a brown solid (20.0 mg) with an $[\alpha]_D^{20}$ value of $+30^\circ$ (c 0.1, MeOH). It displayed UV absorbances at λ_{max} (MeOH) 222.0, and 294.6 nm. Its molecular formula was assigned as $\text{C}_{11}\text{H}_{14}\text{O}_3$ on the basis of its ESI-MS showing molecular ion peak at m/z 194.9 $[\text{M}+\text{H}]^+$ in the positive mode, ^1H and ^{13}C NMR data (Table 3.1.4). Both ^1H and ^{13}C NMR of **4** contained well-separated and clearly assigned resonances and led to believe that the compound possessed a dihydrobenzofuran-like skeleton. Analysis of the ^{13}C NMR and DEPT spectra of **4** implied the presence of three methyl groups, one sp^2 aromatic methine, two sp^2 methines one of which being oxygenated, two aromatic quaternary carbons, and three oxygenated aromatic quaternary carbons. The ^1H NMR spectrum of **4** revealed signals at δ_{H} 1.15 ppm (CH_3 -3), 1.22 ppm (CH_3 -2), 2.92 ppm (H-3), and 4.26 ppm (H-2), assigned to two methyl groups, one methine signal, and one oxymethine signal, respectively, and thus building the furan ring of the dihydrobenzofuran skeleton. These protons were correlated with the carbon signals at δ 19.2 ppm (CH_3 -3), 20.7 ppm (CH_3 -2), 43.6 ppm (C-3), and 85.3 ppm (C-2), respectively, in the HMQC spectrum, which is in agreement with a 2,3- dimethyl-2,3-dihydrobenzofuran unit. The ^1H NMR spectrum also revealed the presence of one aromatic proton at δ_{H} 6.14 ppm (H-6), thus indicativng a pentasubstituted benzene ring, also carrying the methyl group at δ_{H} 1.93 ppm (CH_3 -4). The HMBC correlations of CH_3 -3 to C-2, C-3, and C-9; of CH_3 -2 to C-2 and C-3; of H-2 to CH_3 -3, C-8, and C-9; of H-3 to C-2, C-3, C-8, and C-9; of CH_3 -4 to C-4, C-5, C-6, C-8, and C-9; and of H-6 to C-4, C-5, C-7, C-8, and C-9 confirmed the substitution of the benzene ring (Figure 3.1.6). The relative stereochemistry of **4** was established from a 1D NOE experiment. NOEs were observed from CH_3 -2 to H-3, and from CH_3 -3 to H-2 and CH_3 -4 thus suggesting a *trans* relationship for CH_3 -2 and CH_3 -3. Therefore, all of the above data are in agreement with the structure of 2,3,4-trimethyl-5,7-dihydroxy-2,3-dihydrobenzofuran which was also confirmed by comparison with reported data (Chen *et al.*, 2002).

Table 3.1.4 NMR data for 2,3,4-trimethyl-5,7-dihydroxy-2,3-dihydrobenzofuran (4)

Position	4 DMSO- <i>d</i> ₆ , δ (ppm), <i>J</i> in Hz		Reference CD ₃ OD, δ (ppm), <i>J</i> in Hz (Chen <i>et al.</i> , 2002)	
	¹ H (500 MHz)	¹³ C (125 MHz)	¹ H (500 MHz)	¹³ C (125 MHz)
2-CH ₃	1.22 d (6.3)	20.7	1.30 d (6.5)	20.1
2	4.26 m	85.3	4.37 m	86.7
3-CH ₃	1.15 d (6.8)	19.2	1.25 d (6.5)	18.7
3	2.92 m	43.6	3.00 m	44.3
4-CH ₃	1.93 s	11.3	2.05 s	10.5
4		110.1		111.8
5-OH	8.40 s			
5		148.8		149.0
6	6.14 s	102.8	6.20 s	102.8
7-OH	8.65 s			
7		138.6		138.9
8		138.1		138.7
9		131.6		132.0

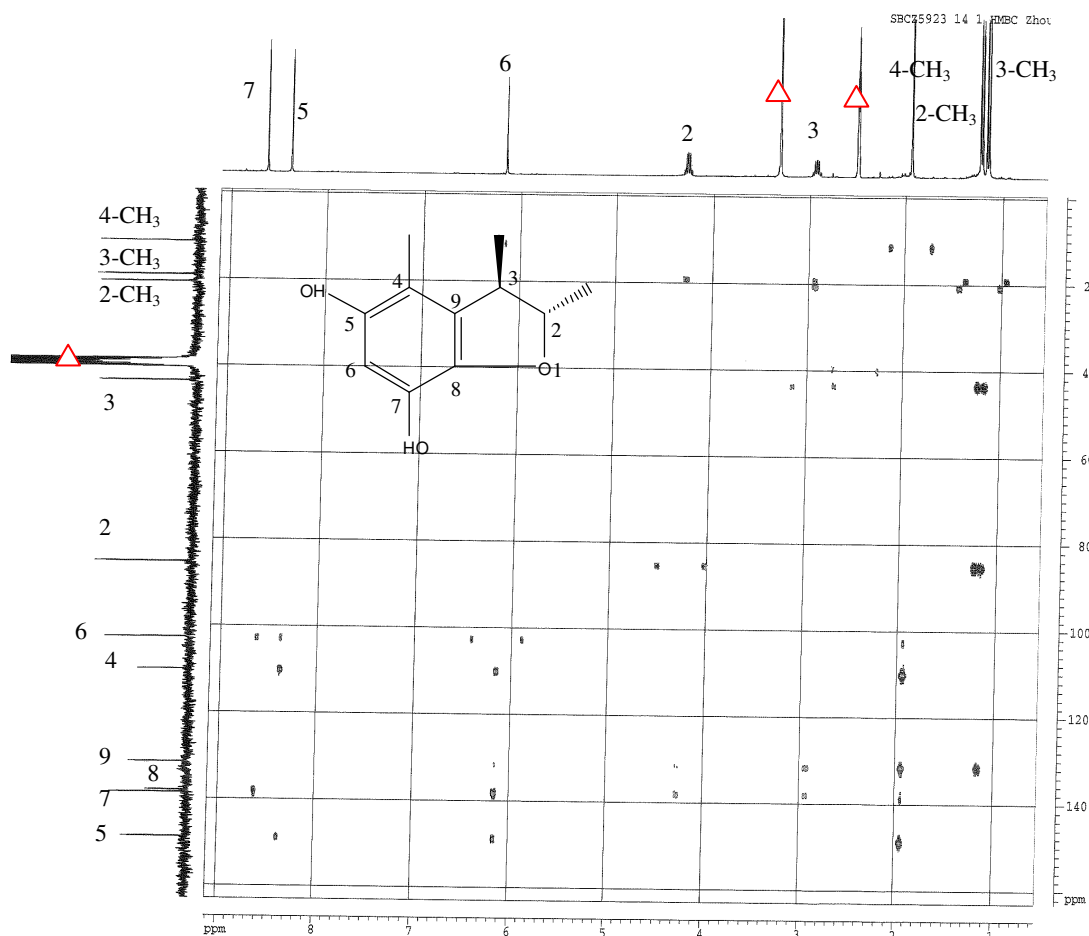
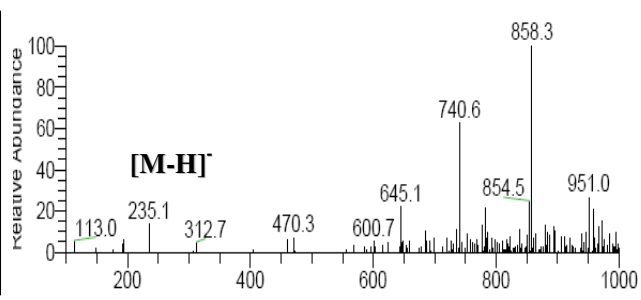
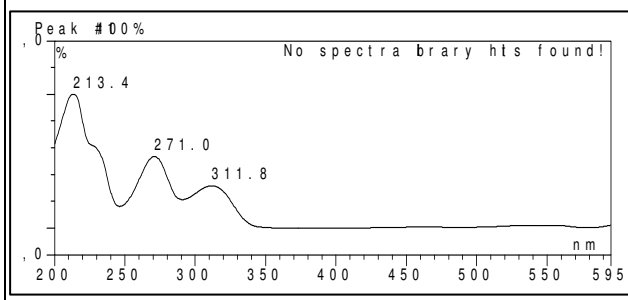
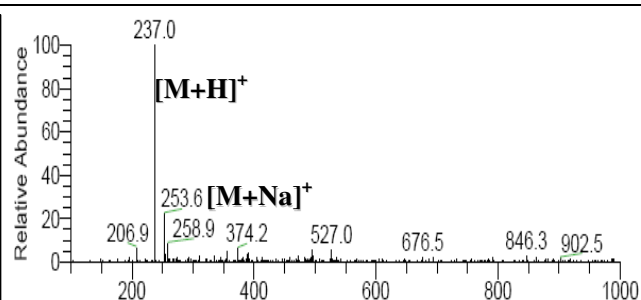
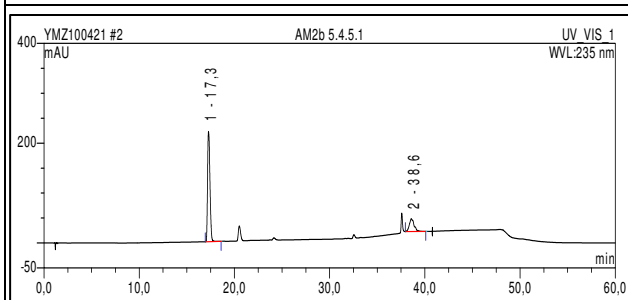
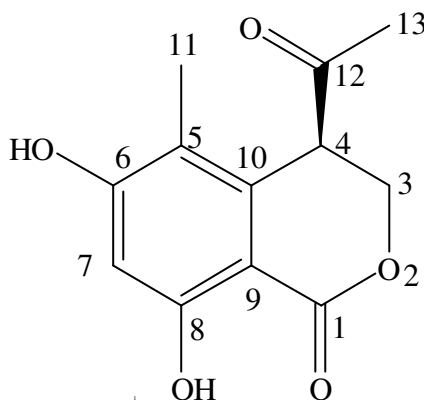


Figure 3.1.6 HMBC correlations of 2,3,4-trimethyl-5,7-dihydroxy-2,3-dihydrobenzofuran (4)

3.1.5 4-Acetyl-3,4-dihydro-6,8-dihydroxy-5-methylisocoumarin (compound 5, known)

4-Acetyl-3,4-dihydro-6,8-dihydroxy-5-methylisocoumarin	
Biological Source	<i>Aspergillus</i> sp.
Sample Code	Fr.2.5.4.5.1
Sample Amount	7.6 mg
Molecular Formula	C ₁₂ H ₁₂ O ₅
Molecular Weight	236 g/mol
Solubility	MeOH
Physical Description	Yellow amorphous solid
Optical Rotation	[α] _D ²⁰ - 8.0° (c 0.07, MeOH)
HPLC Retention Time	17.3 min (standard gradient)



4-Acetyl-3,4-dihydro-6,8-dihydroxy-5-methylisocoumarin (**5**) was obtained as a yellow amorphous solid (7.6 mg) with an $[\alpha]_D^{20}$ value of -8.0° (c 0.07, MeOH). It displayed UV absorbances at λ_{\max} (MeOH) 213.4, 271.0, and 311.8 nm. Its molecular weight was suggested as 236 g/mol according to the molecular ion peaks observed at m/z 237.0 $[M+H]^+$ (base peak) and 258.9 $[M+Na]^+$ in positive mode and at m/z 235.1 $[M-H]^-$ (base peak) in negative mode by ESI-MS analysis. The 1H NMR spectrum (Table 3.1.5) exhibited two hydroxyl singlets at δ 11.0 ppm and 10.8 ppm (8-OH and 6-OH, respectively), an aromatic methine singlet at δ 6.36 ppm (H-7), two oxygenated methylene protons at δ 4.90 ppm and 4.59 ppm (CH₂-3), a methine proton at δ 4.27 ppm (H-4), one acetyl methyl group at δ 2.26 ppm (CH₃-13), and one aromatic methyl group at δ 1.91 ppm (CH₃-11). In the ^{13}C NMR and DEPT spectra (Table 3.1.5) 12 carbon signals were observed and were assigned to ketone carbonyl carbon at δ 205.1 ppm (C-12), ester carbonyl carbon at δ 169.0 ppm (C-1), two oxygenated sp² carbons at δ 162.9 ppm and 161.3 ppm (C-6 and C-8, respectively), the aromatic methine carbon at δ 101.1 ppm (C-7), three sp² quaternary carbons at δ 137.7 ppm, 114.5 ppm and 100.3 ppm (C-10, C-5 and C-9, respectively), the methylene carbon at δ 68.0 ppm (C-3), the methine carbon at δ 47.7 ppm (C-4), and two methyl carbons at δ 28.5 ppm and 10.7 ppm (C-13 and C-11, respectively). The structure of **5** was deduced from the HMBC spectrum (Figure 3.1.7), which exhibited correlations from the methine proton H-7 to C-5, 6, 8, and 9, as well as to C-1 and C-11 via omega correlation, from the methyl protons CH₃-11 to C-5, 6, 7, 9, 10, and 12, from the methylene protons CH₂-3 to C-1, 4, 10, 12, and to C-5 via omega correlation, from the methine proton H-4 to C-3, 5, 9, 10, and 12, and from the methyl protons CH₃-13 to C-4 and the carbonyl carbon C-12. Moreover, the structure of **5** was very similar to that of **3**. Therefore, based on analysis of the HMBC spectrum, comparison with reported data in literature (Krohn *et al.*, 2001, 2004) and those obtained for **3**, compound **5** was finally determined as 4-acetyl-3,4-dihydro-6,8-dihydroxy-5-methylisocoumarin (Figure 3.1.7).

Table 3.1.5 NMR data for 4-acetyl-3,4-dihydro-6,8-dihydroxy-5-methylisocoumarin (5)

Position	5 DMSO- <i>d</i> ₆ , δ (ppm), <i>J</i> in Hz		Reference CD ₃ OD, δ (ppm), <i>J</i> in Hz (Krohn <i>et al.</i> , 2001)	
	¹ H (500 MHz)	¹³ C (125 MHz)	¹ H (200 MHz)	¹³ C (50 MHz)
1		169.0		170.1
3	4.59 dd (11.8, 3.9) 4.90 d (11.8)	68.0	4.60 dd (11.7, 3.8) 4.97 dd (11.7, 1.3)	68.7
4	4.27 d (3.0)	47.7	4.18 dd (3.8, 1.3)	48.7
5		114.5		115.4
6		162.9		163.9
6-OH	10.8 s			
7	6.36 s	101.1	6.38 s	101.5
8		161.3		162.9
8-OH	11.0			
9		100.3		100.4
10		137.7		137.7
11	1.91 s	10.7	2.07 s	10.0
12		205.1		205.7
13	2.27 s	28.5	2.27 s	27.7

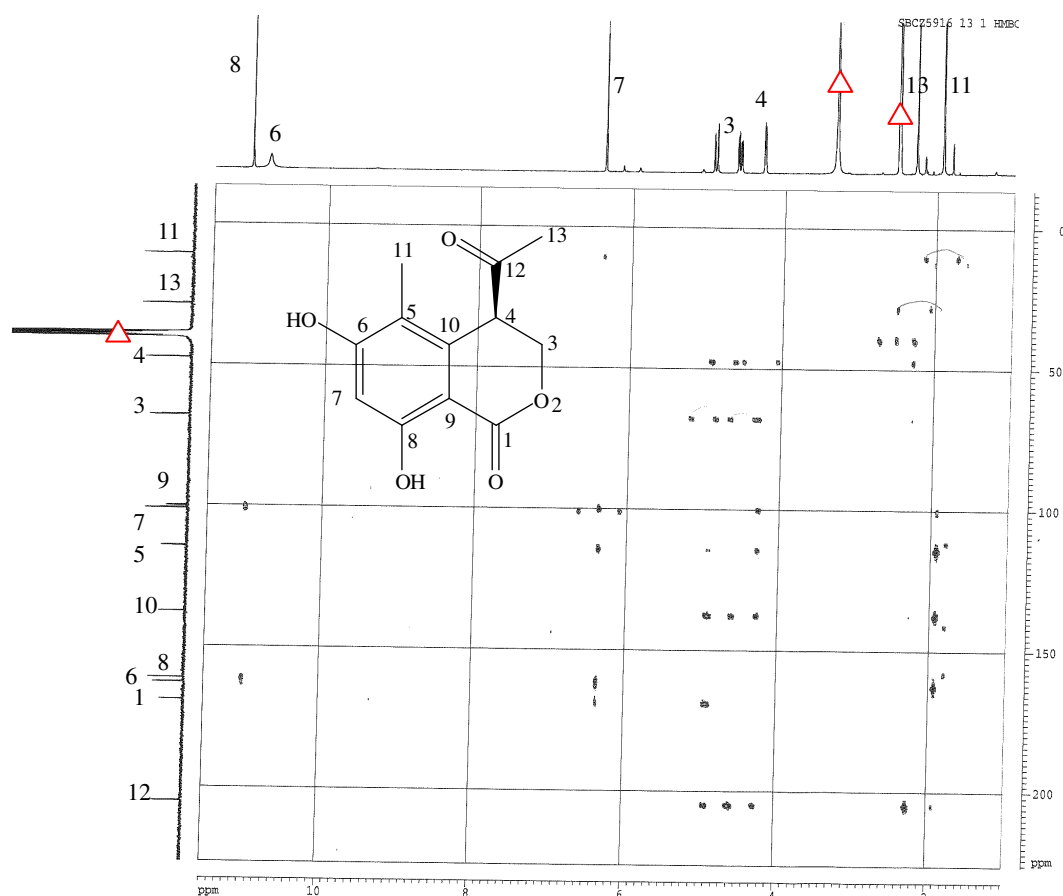
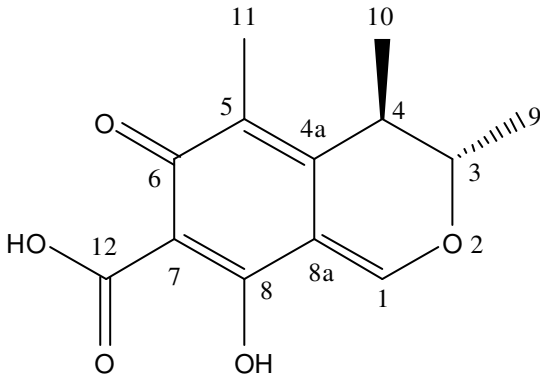
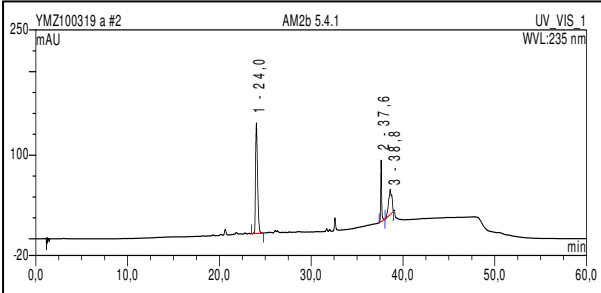
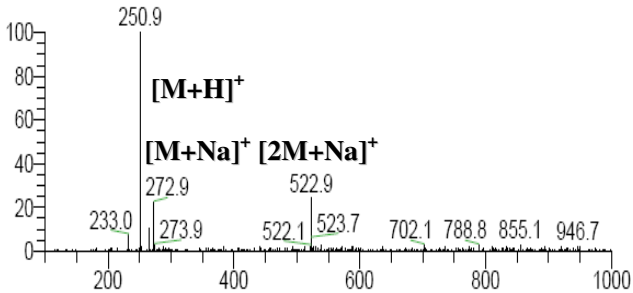
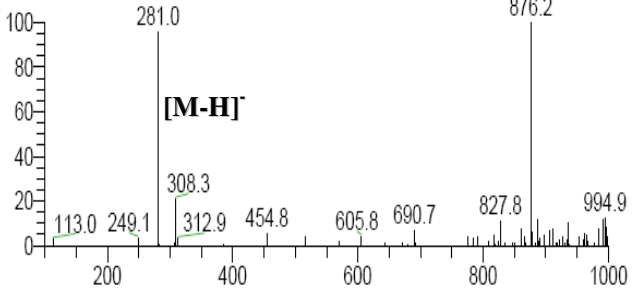
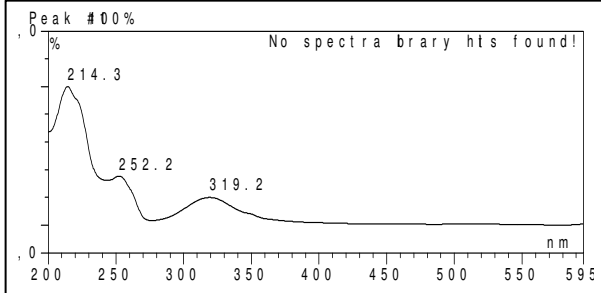


Figure 3.1.7 HMBC correlations of 4-acetyl-3,4-dihydro-6,8-dihydroxy-5-methylisocoumarin (5)

3.1.6 Citrinin (compound 6, known)

Citrinin	
Biological Source	<i>Aspergillus</i> sp.
Sample Code	Fr.2.5.4.1
Sample Amount	1.9 mg
Molecular Formula	C ₁₃ H ₁₄ O ₅
Molecular Weight	250 g/mol
Solubility	MeOH
Physical Description	Yellow amorphous solid
Optical Rotation	$[\alpha]_D^{20} - 40^\circ$ (<i>c</i> 0.05, CHCl ₃)
HPLC Retention Time	24.0 min (standard gradient)
	
	
	
	
	

Citrinin (**6**) was obtained as a yellow amorphous solid (1.9 mg) with an $[\alpha]_D^{20}$ value of -40° (c 0.05, CHCl_3) and UV absorbances at λ_{max} (MeOH) 214.3, 252.2, and 319.2 nm. Its molecular weight was established as 250 g/mol on the basis of the molecular ion peaks observed at m/z 250.9 $[\text{M}+\text{H}]^+$ (base peak), 272.9 $[\text{M}+\text{Na}]^+$, and 522.8 $[2\text{M}+\text{Na}]^+$ in positive mode and at m/z 249.0 $[\text{M}-\text{H}]^-$ (base peak) in negative mode by ESI-MS analysis. Moreover, analysis of the fragmentation pattern indicated the presence of both a hydroxyl group, evident from the peak at m/z 233.0 $[\text{M}+\text{H}-\text{H}_2\text{O}]^+$, and a carboxylic group, demonstrated by the loss of CO_2 in the negative ionization mode (m/z 204.9). The ^1H NMR spectrum (Table 3.1.6) exhibited one olefinic methine singlet at δ 5.54 ppm (H-1), two aliphatic methine units at δ 3.94 ppm and 2.66 ppm (H-3 and H-4, respectively), and three methyl groups at δ 2.04 ppm, 1.32 ppm and 1.13 ppm (H-11, H-9, and H-10, respectively). The ^1H NMR and MS data (Table 3.1.6) as well as the optical rotation was in excellent agreement with reported data for citrinin (Barber *et al.*, 1987). This compound was first isolated from *Penicillium citrinum* and later reported from other sources like *Penicillium* or *Aspergillus* spp. (Barber *et al.*, 1987).

Table 3.1.6 NMR data for citrinin (6)

Position	6 CD_3OD , δ (ppm), J in Hz	Reference CD_3OD , δ (ppm), J in Hz (Barber <i>et al.</i> , 1987)
	^1H (500 MHz)	^1H (300 MHz)
1	5.54 s	6.00 s
3	3.94 q (6.1)	4.10 q (6.5)
4	2.66 q (6.6)	2.75 q (6.5)
9	1.32 d (6.6)	1.25 d (6.4)
10	1.13 d (6.7)	1.18 d (6.8)
11	2.04 s	2.01 s

3.1.7 Phenol A acid (compound 7, known)

Phenol A acid	
Biological Source	<i>Aspergillus</i> sp.
Sample Code	Fr.4.8.3
Sample Amount	43.2 mg
Molecular Formula	C ₁₂ H ₁₆ O ₅
Molecular Weight	240 g/mol
Solubility	MeOH
Physical Description	Colorless solid
Optical Rotation	$[\alpha]_D^{20} - 50^\circ$ (c 3.0, EtOH)
HPLC Retention Time	20.4 min (standard gradient)

Phenol A acid (**7**) was isolated as a colorless solid (43.2 mg) with an $[\alpha]_D^{20}$ value of -50° (c 3.0, EtOH) and it showed UV absorbances at λ_{\max} (MeOH) 213.5, 252.8, and 314.9 nm. Its molecular weight was established as 240 g/mol according to the molecular ion peaks observed at m/z 240.8 $[M+H]^+$ (base peak), 262.9 $[M+Na]^+$, and 502.8 $[2M+Na]^+$ in the positive mode and at m/z 239.1 $[M-H]^-$ (base peak), and 478.8 $[2M-H]^-$ in the negative mode by ESI-MS analysis. The 1H and ^{13}C NMR data (Table 3.1.7) in addition to analysis of COSY, DEPT, and HMQC spectra, revealed the presence of a penta substituted benzene ring, three hydroxyl groups, three methyl groups, and a carboxyl group. The connectivity and assignment of the carbon and proton resonances for **7**, which led to the elucidation of the planar structure of this metabolite, were deduced from interpretation of the HMBC spectrum (Figure 3.1.8). Diagnostic HMBC correlations were observed from 2'-CH₃ to C-2', from 1'-CH₃ to C-1' and C-4, from 3-CH₃ to C-2, C-3, and C-4, from H-5 to C-1, C-3, and C-6, from 6-OH to C-1, C-5, and C-6, and from 2-OH to C-1, C-2, and C-3, confirmed the structure of phenol A acid (**7**). On the basis of all the foregoing evidence in addition to comparison with reported data (Brown *et al.*, 1949; Roedel and Gerlach, 1995) **7** was identified as phenol A acid. Chemical shift differences observed upon comparing our NMR data with those published (Table 3.1.7) may be due to the use of different solvents or the difference in magnetic field strength of the NMR spectrometers used for recoding the data.

Results

Table 3.1.7 NMR data for phenol A acid (7)

Position	7 DMSO- <i>d</i> ₆ , δ (ppm), <i>J</i> in Hz		Reference acetone- <i>d</i> ₆ , δ (ppm), <i>J</i> in Hz (Roedel and Gerlach, 1995)	
	¹ H (500 MHz)	¹³ C (125 MHz)	¹ H (270.2 MHz)	¹³ C (67.9 MHz)
1		101.8		98.7
1-COOH		175.6		172.5
2		159.8		160.5
2-OH	14.72			
3		110.9		116.2
3-CH ₃	1.95 s	10.5	2.11 s	10.7
4		146.9		153.6
5	6.00 s	102.7	6.50 s	106.1
6		159.2		157.9
6-OH	14.00			
1'	2.91 q (6.4)	41.7	3.08 q (6.6)	43.3
1'-CH ₃	1.03 d (6.0)	15.4	1.15 d (6.6)	17.0
2'	3.69 q (6.3)	70.0	3.90 q (6.6)	76.4
2'-OH				
2'-CH ₃	0.94 d (6.3)	19.6	1.13 d (6.6)	20.9

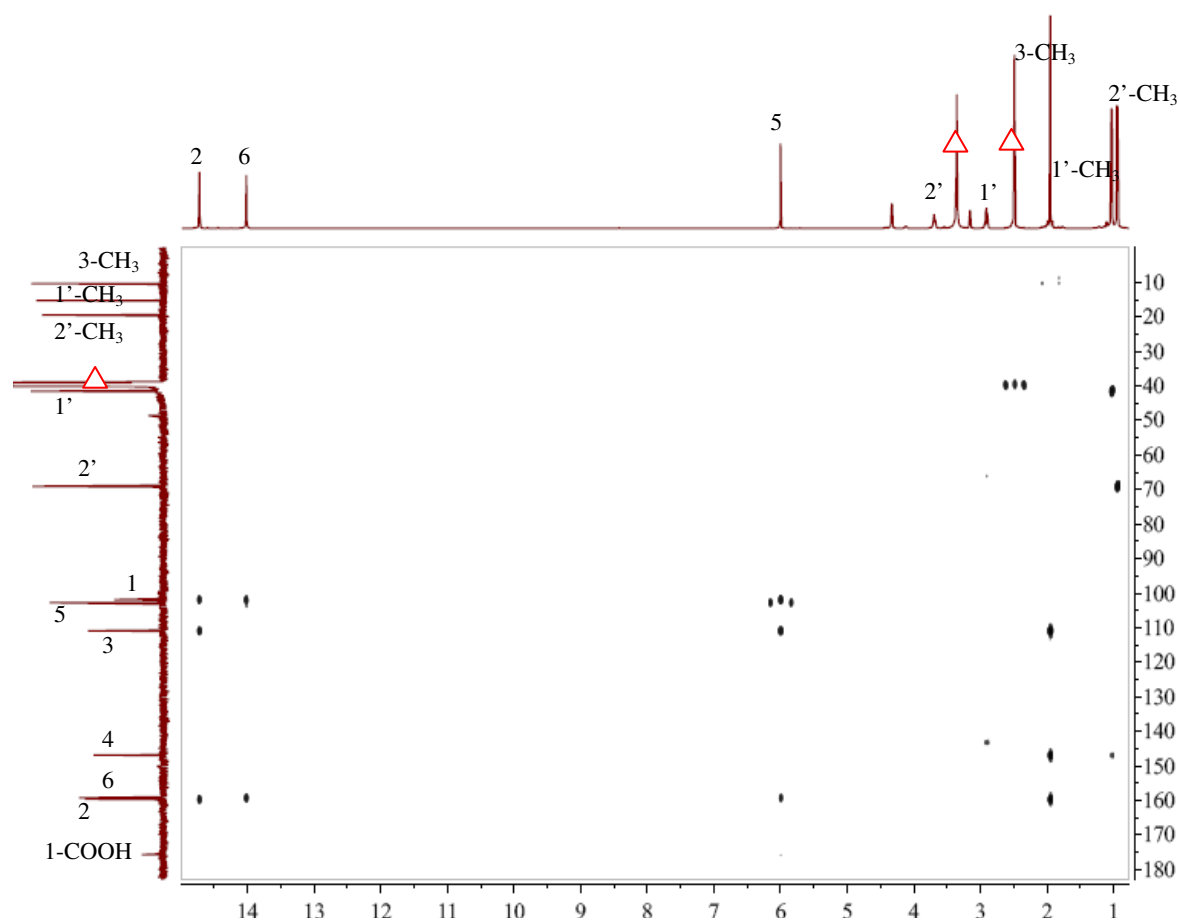
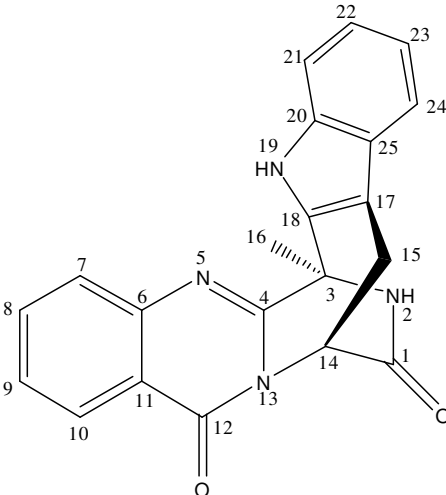
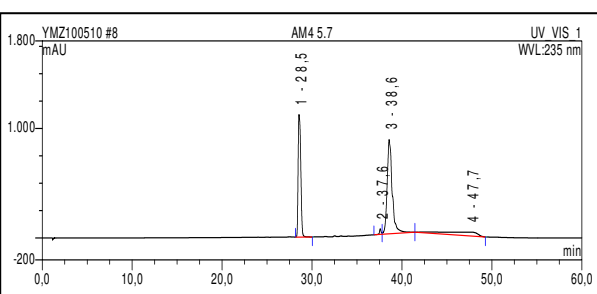
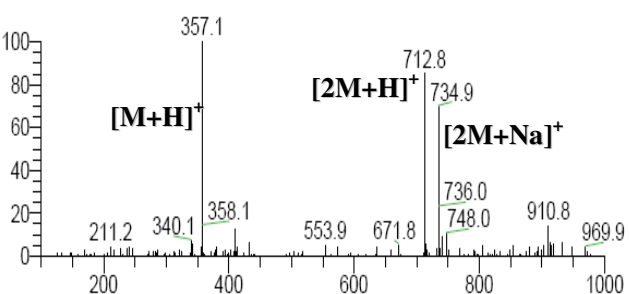
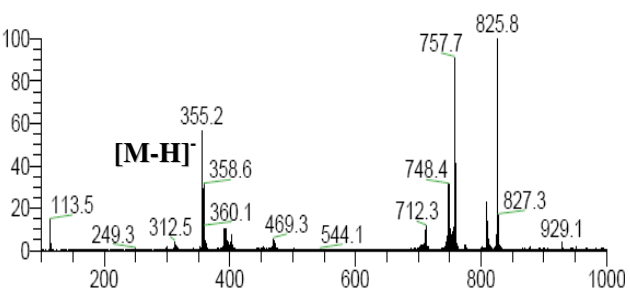
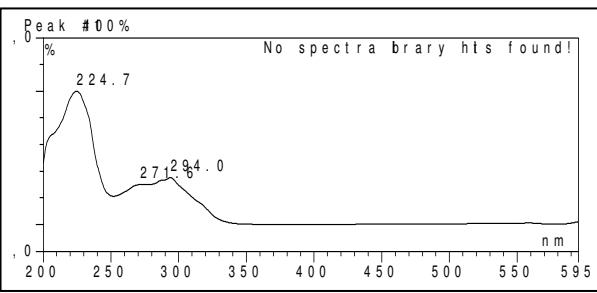


Figure 3.1.8 HMBC correlations of phenol A acid (7)

3.1.8 Fumiquinazoline J (compound 8, known)

Fumiquinazoline J	
Biological Source	<i>Aspergillus</i> sp.
Sample Code	Fr.4.5.7
Sample Amount	3.4 mg
Molecular Formula	C ₂₁ H ₁₆ N ₄ O ₂
Molecular Weight	356 g/mol
Solubility	MeOH
Physical Description	White amorphous powder
Optical Rotation	$[\alpha]_D^{20}$ -148° (c 0.32, MeOH)
HPLC Retention Time	28.5 min (standard gradient)
	
	
	
	
	

Fumiquinazoline J (**8**) was obtained as a white amorphous powder (3.4 mg) with an $[\alpha]_D^{20}$ value of -148° (c 0.32, MeOH) and it showed UV absorbances at λ_{\max} (MeOH) 224.7, 271.6, and 294.0 nm. Its molecular formula was determined as $C_{21}H_{16}N_4O_2$ with the molecular weight of 356 g/mol on the basis of the molecular ion peaks observed at m/z 357.1 $[M+H]^+$ (base peak), 712.8 $[2M+H]^+$, and 734.9 $[2M+Na]^+$ in the positive mode, and at m/z 355.2 $[M-H]^-$ (base peak) in the negative mode by ESI-MS analysis, which was fully supported by the 1H and ^{13}C NMR data (Table 3.1.8). In the 1H NMR, signals corresponding to eight aromatic methine protons, one aliphatic methine group, one methylene group, two exchangeable protons, and one methyl group were detected. The COSY spectrum of **8** revealed two ABCD spin systems with H-7 to H-10 (δ_H 7.63, 7.80, 7.52, 8.13 ppm, respectively) and H-21 to H-24 (δ_H 7.35, 7.11, 6.98, 7.39 ppm, respectively), as well as correlations between the methine proton H-14 (δ_H 5.70 ppm) and the methylene protons CH_2 -15 (δ_H 3.22/3.41 ppm) (Figure 3.1.9). The remaining proton signals were assigned to CH_3 -16 (δ_H 2.10 ppm), H-2 (δ_H 9.57 ppm), and H-19 (δ_H 11.2 ppm). The ^{13}C NMR spectrum indicated the presence of 21 carbon atoms in the structure of **8**. Together with the DEPT experiment and interpretation of the HMQC spectrum, the presence of ten quaternary carbon atoms were revealed and proton signals were assigned to the corresponding proton-bearing carbon atoms. Accordingly, the following signals were identified: two amide carbonyl carbon atoms at δ_C 169.5 ppm and 159.7 ppm (C-1 and C-12, respectively), two 1,2-disubstituted benzene rings (C-6 to C-11 and C-20 to C-25), two quaternary sp^2 carbons at δ_C 154.7 ppm (C-4) and 134.4 ppm (C-18) bearing one nitrogen, one quaternary carbon at δ_C 54.9 ppm (C-3), and one quaternary sp^2 -carbon at δ_C 105.9 ppm (C-17), one methyl carbon at δ_C 18.3 ppm (C-16), one methylene carbon at δ_C 25.6 ppm (C-15), and one methine carbon at δ_C 54.1 ppm (C-14).

The structure of **8** was deduced from inspection of its HMBC spectrum (Figure 3.1.10). The methyl protons CH_3 -16 resonated as a singlet and share correlations with C-3, C-4, and C-18. Besides, the methylene protons (CH_2 -15) coupling with the methine proton (H-14) further correlations with C-14, C-17, C-18, and C-1 were

observed in the HMBC spectrum, thus proving the linkage between C-17 and C-14 through the methylene group within the planar structure of **8**. HMBC correlations of H-2 with C-3, C-4, and C-14, and of H-19 with C-17, C-18, C-20, and C-25, established the location of the exchangeable protons. Furthermore, HMBC correlations were observed from H-7 to C-9 and C-11, from H-8 to C-6 and C-10, from H-9 to C-7 and C-11, from H-10 to C-6, C-8, and C-12, from H-21 to C-23 and C-25, from H-22 to C-20 and C-24, from H-23 to C-21 and C-25, and from H-24 to C-20 and C-22. Therefore, based on the foregoing evidence in addition to comparison with reported data (Han *et al.*, 2007; Heredia *et al.*, 2002) the structure of **8** was identified as fumiquinazoline J.

Table 3.1.8 NMR data for fumiquinazoline J (8)

Position	8 DMSO- <i>d</i> ₆ , δ (ppm), <i>J</i> in Hz		Reference CDCl ₃ , δ (ppm), <i>J</i> in Hz	
	¹ H (500 MHz)	¹³ C (125 MHz)	¹ H (600 MHz) (Han <i>et al.</i> , 2007)	¹³ C (63 MHz) (Heredia <i>et al.</i> , 2002)
1		169.5		170.5
2	9.57 s		7.38 br s	
3		54.9		54.6
4		154.7		153.1
5				
6		147.0		146.9
7	7.63 d (8.2)	127.7	7.63 br d (8.2)	127.7
8	7.80 t (7.4)	135.2	7.72 ddd (8.2, 7.0, 1.0)	134.4
9	7.52 t (7.7)	127.6	7.47 dd (8.0, 7.0)	127.5
10	8.13 d (7.9)	126.7	8.27 dd (8.0, 1.0)	126.8
11		120.5		120.6
12		159.7		160.1
13				
14	5.70 br s	54.1	6.10 br t	54.4
15	3.41 dd (17.4, 2.6) 3.22 dd (17.4, 4.6)	25.6	3.56 dd (17.2, 2.6) 3.42 dd (17.2, 4.7)	25.8
16	2.10 s	18.3	2.27 s	17.9
17		105.9		107.5
18		134.4		132.2
19	11.2 br s		8.13 br s	
20		135.3		134.5
21	7.35 d (8.2)	112.1	7.33 br d (7.6)	111.2
22	7.11 t (7.2)	122.7	7.20 br t (7.6)	123.4
23	6.98 t (7.8)	119.8	7.10 br t (7.6)	120.5
24	7.39 d (7.9)	118.5	7.42 br d (7.6)	118.3
25		127.4		127.3

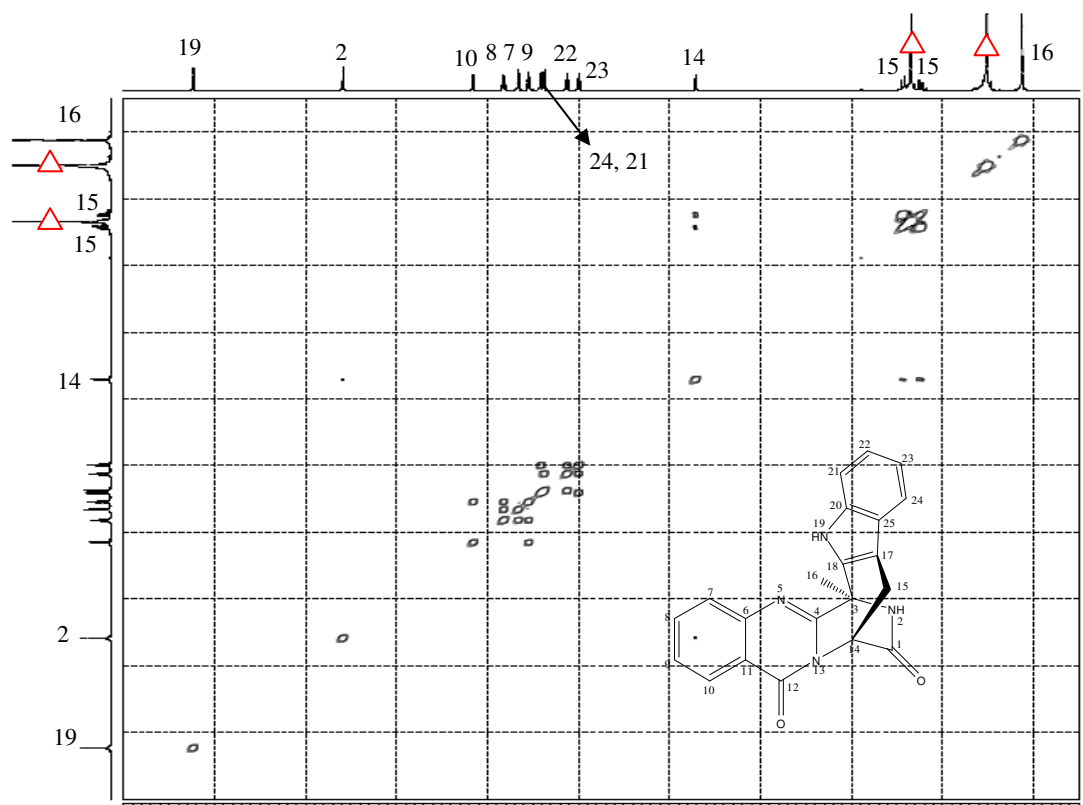


Figure 3.1.9 COSY correlations of fumiquinazoline J (8)

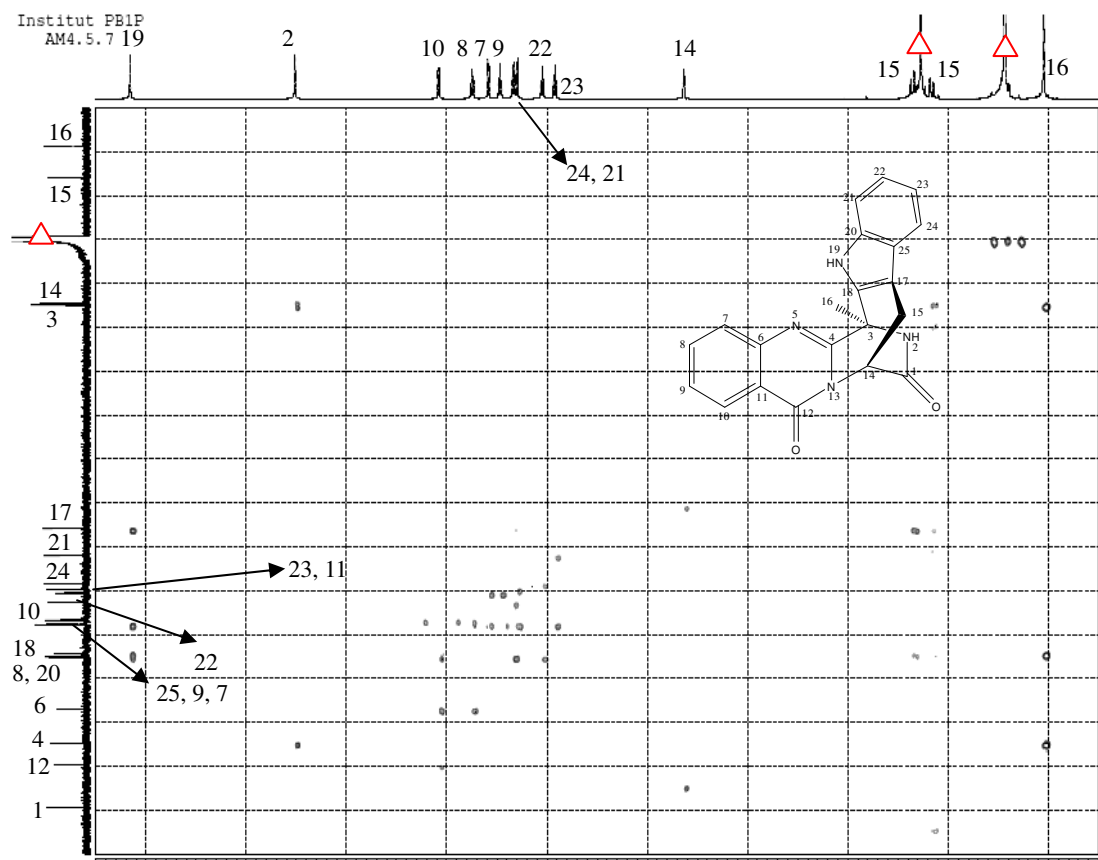


Figure 3.1.10 HMBC correlations of fumiquinazoline J (8)

3.1.9 Methyl 3,4,5-trimethoxy-2-(2-(nicotinamido) benzamido) benzoate (compound 9, known)

Methyl 3,4,5-trimethoxy-2-(2-(nicotinamido) benzamido) benzoate	
Biological Source	<i>Aspergillus</i> sp.
Sample Code	Fr.4.8.4
Sample Amount	4.5 mg
Molecular Formula	C ₂₄ H ₂₃ N ₃ O ₇
Molecular Weight	465 g/mol
Solubility	MeOH
Physical Description	Colorless solid
HPLC Retention Time	25.6 min (standard gradient)

Methyl 3, 4, 5-trimethoxy-2-(2-(nicotinamido) benzamido) benzoate (**9**) was isolated as a colorless solid (4.5 mg). It showed UV absorbances at λ_{max} (MeOH) 218.1, 260.1, and 310.0 nm. Its molecular formula was determined as $\text{C}_{24}\text{H}_{23}\text{N}_3\text{O}_7$ with the molecular weight of 465 g/mol according to the molecular ion peaks observed at m/z 465.7 $[\text{M}+\text{H}]^+$ (base peak), 930.9 $[2\text{M}+\text{H}]^+$, and 952.8 $[2\text{M}+\text{Na}]^+$ in the positive mode, and at m/z 464.1 $[\text{M}-\text{H}]^-$ (base peak) in the negative mode by ESI-MS analysis, which was fully supported by the ^1H and ^{13}C NMR data (Table 3.1.9). In the ^1H NMR spectrum, signals appeared for nine aromatic methine protons, four methoxyl groups, and two exchangeable protons. The singlets at δ_{H} 12.13 ppm and 10.22 ppm were assigned to the NH-7' and NH-7 groups, respectively. The COSY spectrum revealed one ABCD four-proton spin system with H-3' to H-6' (δ_{H} 8.08, 7.33, 7.68, 8.60 ppm, respectively), which suggested the presence of an *o*-disubstituted aromatic ring, and one ABCX spin system with H-4'', H-5'', H-6'', and H-2'' (δ_{H} 8.20, 7.60, 8.79, 9.03 ppm, respectively), the chemical shifts and spin-spin couplings of the latter implied the presence of a pyridine ring substituted with a carbonyl group at position 3'' (Figure 3.1.11). Moreover, the remaining signals were assigned to H-5 (δ_{H} 7.28 ppm), OCH₃-9 (δ_{H} 3.88 ppm), OCH₃-10 (δ_{H} 3.78 ppm), OCH₃-11 (δ_{H} 3.90 ppm), and OCH₃-13 (δ_{H} 3.65 ppm). The ^{13}C NMR spectrum revealed the presence of 24 carbon atoms. Moreover, the DEPT experiment revealed the presence of eleven quaternary carbon atoms and interpretation of the HMQC spectrum supported the assignment of proton signals to the corresponding proton-bearing carbon atoms. Accordingly, carbon signals were assigned as follow: two amide carbon atoms at δ_{C} 162.9 ppm and 168.2 ppm (C-8' and C-8), an ester carbonyl carbon at δ_{C} 165.4 ppm (C-12), nine methine sp^2 -carbon atoms at δ_{C} 108.7, 128.8, 123.4, 132.5, 120.6, 152.6, 134.6, 123.9, and 147.9 ppm (C-5, C-3', C-4', C-5', C-6', C-2'', C-4'', C-5'', and C-6'', respectively), four methoxyl carbon atoms at δ_{C} 60.9, 56.1, 60.6, and 51.9 ppm (C-9, C-10, C-11, and C-13, respectively), and eight quaternary sp^2 -carbon atoms at δ_{C} 123.9, 145.5, 149.6, 151.5, 123.3, 138.8, 121.1, and 129.9 ppm (C-1, C-2, C-3, C-4, C-6, C-1'', C-2'', and C-3'', respectively).

The structure of **9** was deduced from inspection of its HMBC spectrum (Figure 3.1.12). Correlations obtained from OCH₃-11 to C-4, from OCH₃-10 to C-3, from OCH₃-9 to C-2, and from OCH₃-13 to C-12 suggested that methoxyl groups were placed on the respective carbons. The correlations of H-3' to C-1', C-5', and C-8, of H-7 to C-3 and C-8 revealed the linkage between C-1 and C-2' through an amide carbonyl group. The correlations of H-4'' to C-2'', C-6'', C-8', of H-7' to C-2'', C-6' and C-8', of H-2'' to C-3'' and C-4'', and H-6' to C-1', C-2', C-4', C-5', and C-8 confirmed the linkage between C-3'' and C-1' through an amide carbonyl group as well. Moreover, HMBC correlations were observed from H-5 to C-1, C-2, C-3, C-4, C-6, and C-12. Consequently, on the basis of the foregoing evidence along with comparison with reported data (Arai *et al.*, 1981) the structure of **9** was indicated as methyl 3,4,5-trimethoxy-2-(2-(nicotinamido) benzamido) benzoate.

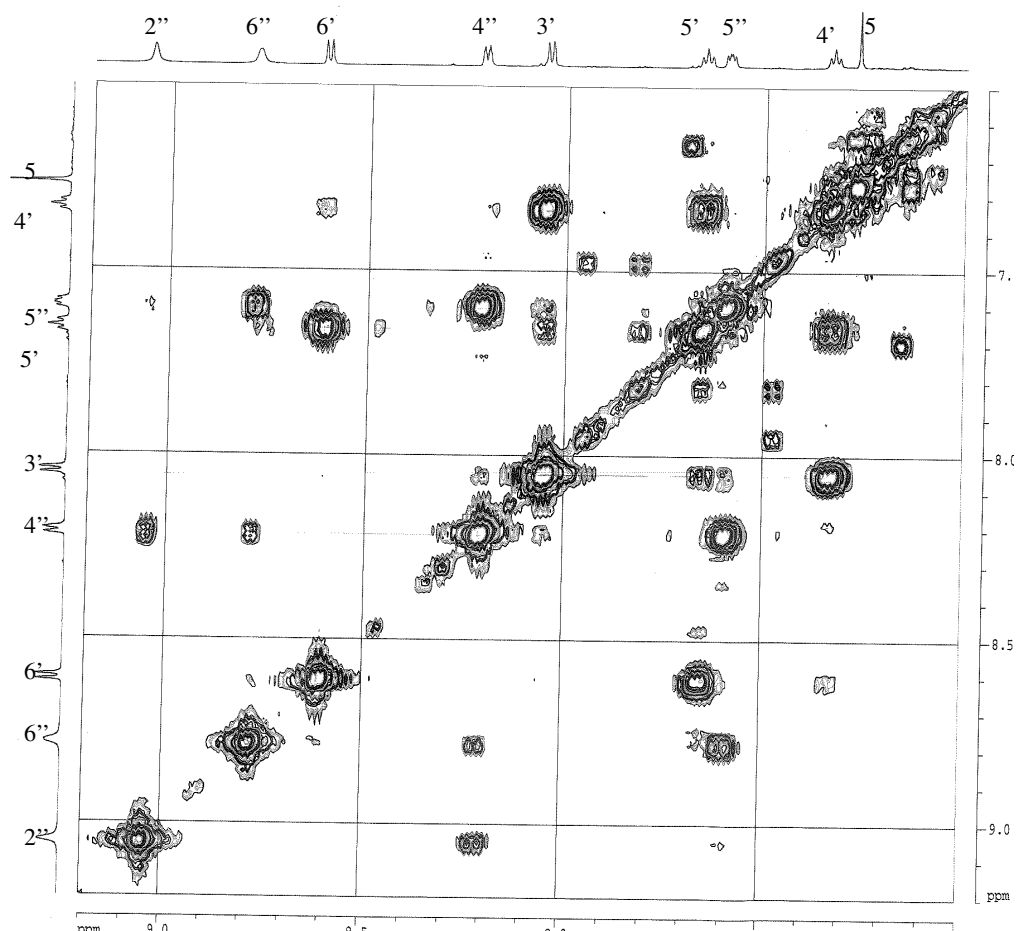


Figure 3.1.11 COSY correlations of methyl 3,4,5-trimethoxy-2-(2-(nicotinamido) benzamido) benzoate (**9**)

Table 3.1.9 NMR data for methyl 3,4,5-trimethoxy-2-(2-(nicotinamido) benzamido) benzoate (9)

Position	9 DMSO- <i>d</i> ₆ , δ (ppm), <i>J</i> in Hz	Reference acetone- <i>d</i> ₆ , δ (ppm), <i>J</i> in Hz (Arai <i>et al.</i> , 1981)		
		¹ H (600 MHz)	¹³ C (150 MHz) ^a	¹ H (100 MHz)
1			123.9	
2			145.5	
3			149.6	
4			151.5	
5	7.28 s		108.7	7.33
6			123.3	
7	10.22 s			9.55
8			168.2	
9	3.88 s		60.9	
10	3.78 s		56.1	
11	3.90 s		60.6	
12			165.4	
13	3.65 s		51.9	
1'			138.8	
2'			121.1	
3'	8.08 d (7.9)		128.8	8.14
4'	7.33 t (7.6)		123.4	7.28
5'	7.68 t (7.4)		132.5	7.65
6'	8.60 d (8.2)		120.6	8.85
7'	12.13 s			12.40
8'			162.9	
1''				
2''	9.03 s		152.6	9.17
3''			129.9	
4''	8.20 d (7.9)		134.6	8.25
5''	7.60 t (7.4)		123.9	7.53
6''	8.79 s		147.9	8.75
7''				

^a ¹³C NMR data were reported here for the first time.

Results

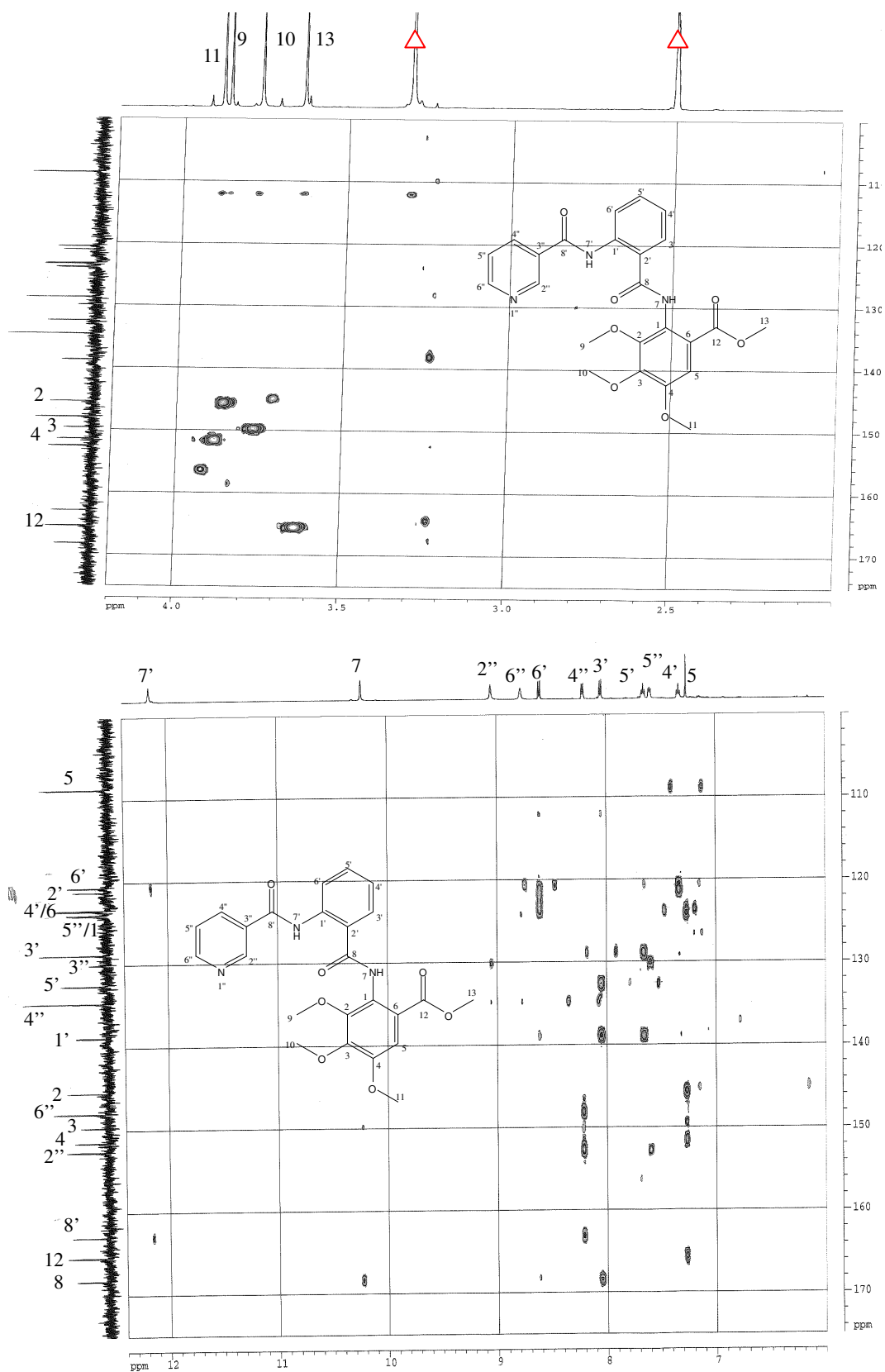
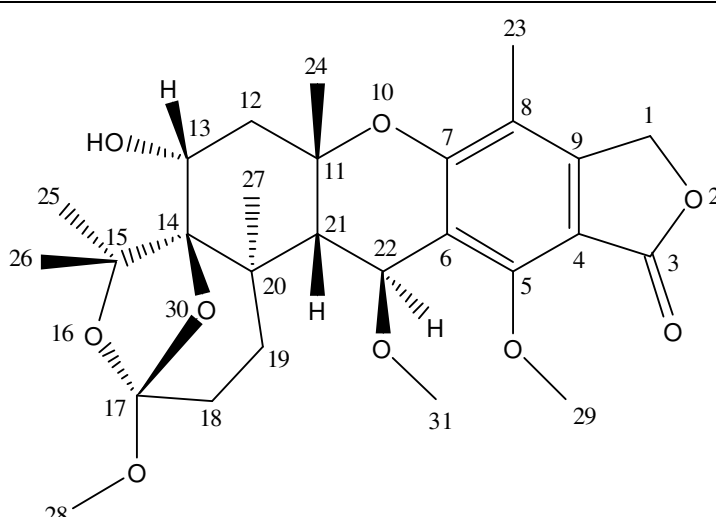
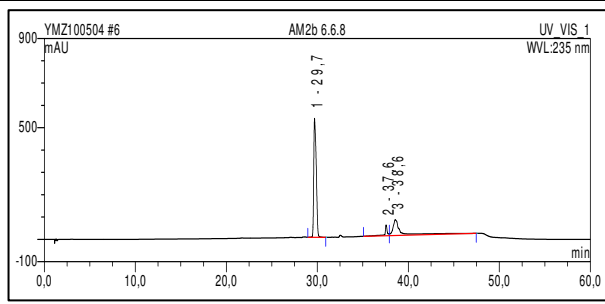
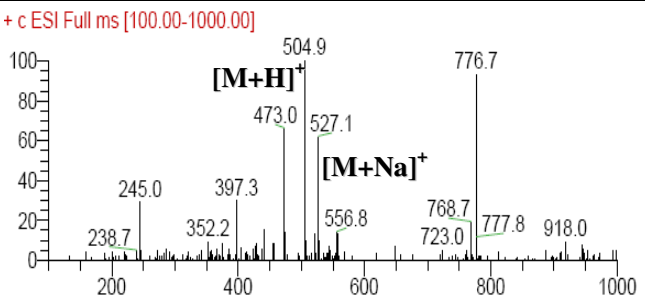
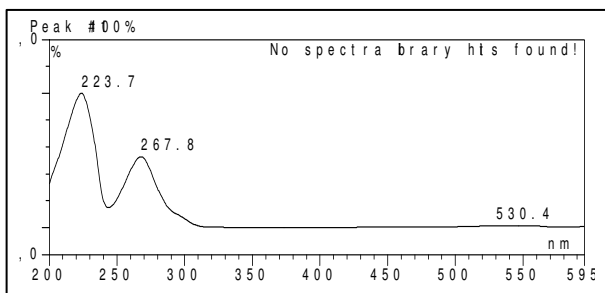


Figure 3.1.12 HMBC correlations of methyl 3,4,5-trimethoxy-2-(2-(nicotinamido)benzamido)benzoate (9)

3.1.10 Austalide M (compound 10, new)

Austalide M	
Biological Source	<i>Aspergillus</i> sp.
Sample Code	Fr.2.6.6.8
Sample Amount	6.0 mg
Molecular Formula	C ₂₇ H ₃₆ O ₉
Molecular Weight	504 g/mol
Solubility	MeOH
Physical Description	Brown amorphous solid
Optical Rotation	$[\alpha]_D^{20} - 43^\circ$ (c 0.35, MeOH)
HPLC Retention Time	29.7 min (standard gradient)
	
<div style="display: flex; justify-content: space-between;"> <div style="width: 45%;">  </div> <div style="width: 45%;"> <p style="color: red;">+ c ESI Full ms [100.00-1000.00]</p>  </div> </div> <div style="margin-top: 10px;">  </div>	

Austalide M (**10**) was obtained as a brown amorphous solid (6.0 mg) with an $[\alpha]_D^{20}$ value of -43° (c 0.35, MeOH) and its molecular formula was established as $C_{27}H_{36}O_9$ on the basis of the $[M+H]^+$ signal at m/z 505.2423 in the HRESIMS. Its UV spectrum showed maxima at $\lambda_{max} = 223$ and 267 nm, which is characteristic of a substituted phthalide moiety (Horak *et al.*, 1985). The 1H and ^{13}C NMR spectra (Table 3.1.10) indicated the presence of eight methyl groups, appearing as singlets in the 1H NMR spectrum, including three methoxy groups resonating at δ_H 3.40, 3.50 and 4.13 ppm (CH₃-28, -31 and -29, respectively), one aromatic methyl group at δ_H 2.08 ppm (CH₃-23), and four aliphatic methyl groups at δ_H 0.90, 1.33, 1.48 and 1.60 ppm (CH₃-27, -24, -26 and -25, respectively). In addition, four methylene groups were observed, one of which was attributed to the oxygenated benzylic methylene group at C-1 (δ_H 5.23 ppm, s), as well as three methine groups, two of which are situated on oxygen-bearing carbon atoms as indicated by their chemical shift values at δ_H 4.11 and 4.44 ppm (H-13 and H-22, respectively). The ^{13}C NMR spectrum of **10** (Table 3.1.10) confirmed the presence of 27 carbon atoms in the structure. Furthermore, the DEPT experiment revealed the presence of 12 quaternary carbon atoms. Analysis of the 1H - 1H COSY spectrum of **10** (Table 3.1.10, Figure 3.1.13) established the presence of three spin systems which included the correlations observed for the methylene protons resonating at δ_H 2.19 and 2.32 ppm (CH₂-12) to the deshielded methine group at C-13, and for the methine proton appearing at δ_H 2.50 ppm (H-21) to the deshielded methine group at C-22. Moreover, the correlation between the protons of both methylene groups at C-18 and C-19 verified the third spin system. Interpretation of the HMQC spectrum allowed the assignment of proton signals to the corresponding proton-bearing carbon atoms.

The connection between the different substructures of **10** was determined by inspection of the HMBC spectrum (Table 3.1.10, Figure 3.1.14). The tertiary methyl group CH₃-27 (δ_C 19.2) correlated with the quaternary carbon C-20 (δ_C 39.8), CH₂-19 (δ_C 31.4), CH-21 (δ_C 43.6), and an oxygenated quaternary carbon resonating at δ_C 87.7, which was assigned to C-14. The C-14 signal further correlated with the methyl

groups CH₃-25 and CH₃-26 (δ_C 26.5 and 29.2, respectively), which were found to constitute a geminal dimethyl moiety, as indicated by their correlation with each other as well as with an oxygenated quaternary carbon resonating at δ_C 86.1 (C-15). Furthermore, the methoxy group OCH₃-28 (δ_C 49.0) correlated with a highly deshielded quaternary carbon resonating at δ_C 120.3, which was assigned to C-17, in agreement with reported chemical shifts observed for the carbon atom of *ortho* esters (Horak *et al.*, 1985). H-21 correlated with C-20, C-22, CH₃-27, and an aromatic quaternary carbon at δ_C 119.4 (C-6). The location of OCH₃-31 (δ_C 56.4) was established based on its correlation with C-22. H-22 correlated with C-20, C-31, C-6, as well as with three oxygenated quaternary carbons, two aromatic ones overlapping at δ_C 158.9, and an aliphatic one at δ_C 77.3, which was assigned to C-5, C-7 and C-11, respectively. Correlations of the tertiary methyl group CH₃-24 (δ_C 28.8) with C-11, C-21 and CH₂-12 (δ_C 43.8) provided the remaining connections of the spin systems previously observed in the ¹H-¹H COSY spectrum (Table 3.1.10, Figure 3.1.13). The methoxy group OCH₃-29 (δ_C 63.3) was attached to C-5, as indicated by the respective HMBC correlation. The aromatic CH₃-23 (δ_C 10.7) correlated to the quaternary aromatic carbons C-7, C-8 (δ_C 116.2), and C-9 (δ_C 149.3), and hence, was placed at C-8. The remaining ¹³C resonances at δ_C 108.9 and 171.5 were attributed to the remaining sp² carbon atom of the completely substituted benzene ring (C-4) and the carbonyl carbon C-3, respectively. This was further confirmed by correlation of C-9 with the oxygenated benzylic methylene group CH₂-1 (δ_C 70.0), which, in turn, correlated with C-4 and C-3.

The relative configuration of **10** was deduced from analysis of the ROESY spectrum (Table 3.1.10). Correlations were observed for CH₃-24 to H-21 indicating that rings C and D are *cis*-fused. This was further confirmed by OCH₃-31 correlations to H-21 and CH₃-24. The correlation observed between CH₃-27 and H-22, but not to H-21, indicated a *trans* relationship between CH₃-24 and CH₃-27. CH₃-25 and CH₃-27, as well as CH₃-26 and H-13, are *cis*-oriented based on the correlations observed between them. Consequently, ring C is *cis*-fused with ring B and *trans*-fused with the

seven-membered ring. Thus, the relative stereochemistry of **10** was established as (11*S**,13*R**,14*R**,20*R**,21*S**,22*S**). For the determination of the absolute configuration, the solution ECD spectrum of **10** was recorded in acetonitrile and TDDFT ECD calculation of solution conformers was carried out. The experimental ECD spectrum is dominated by the strong negative Cotton effect (CE) at 217 nm ($\Delta\epsilon=16.00$) accompanied by a positive CE at 196 nm ($\Delta\epsilon=5.61$) and three weaker transitions at 262, 295 and 301 nm (Figure 3.1.15). The MMFF conformational search followed by B3LYP/6-31G (d) DFT reoptimization afforded two conformational isomers (conformer A and B in Figure 3.1.16 with 77.2% and 19.5% populations, respectively) above 3% population. The two conformers showed minor differences in the orientations of methoxy and hydroxy groups and the conformation of the fused phthalide moiety. In both conformers, the benzylic 22-OMe group adopted axial orientation to relieve the *peri* interaction with the 5-OMe group, and the pyran ring of the chroman chromophore had *M* helicity. The weak coupling between H-22 and the contiguous H-21, indicating a torsion angle close to 90° between these vicinal protons (Karplus, 1963), corroborated the axial orientation of the 22-OMe group. In spite of their similarities, however, the computed ECD spectra of the two conformers were significantly different (Figure 3.1.17 and Figure 3.1.18), *i.e.* the major conformer reproduced well the two intense high-energy CEs, whereas the minor one seems responsible for the negative CE at 262 nm. The different ECDs of the conformers were attributed to the different orientation of the C-3 carbonyl relatively to the benzene ring ($\omega_{O3,C3,C4,C9}$). The torsional angle $\omega_{O3,C3,C4,C9}$ was found to be -178.8° for the major conformer and $+174.3^\circ$ for the minor one. The Boltzman-weighted ECD spectra of the two conformers reproduced well the two strong CEs of the high-energy region, which allowed determining the absolute configuration of **10** as (–)-(11*S*, 13*R*, 14*R*, 20*R*, 21*S*, 22*S*). However, the agreement was quite poor for the weak transitions above 250 nm, which could be improved by setting the ratio of the two conformers to 1:1 (Figure 3.1.19). The CD calculation revealed that the $\omega_{O3,C3,C4,C9}$ torsional angle and ratio of the conformers, which are determined by the central chirality elements, are decisive for the observed CEs; this makes the application of the chroman helicity

rule (Antus *et al.*, 2001) not relevant. Attempts to determine the absolute configuration of **10** by a modified Mosher procedure (Ohtani, *et al.*, 1991; Su *et al.*, 2002) proved inconclusive. The observed chemical shift differences (500 MHz, C₅D₅N) between the (2' *S*)-2'-methoxy-2'-trifluoromethyl-2'-phenylacetic acid (MTPA) ester and its (2' *R*)-MTPA diastereomer were too small to allow unambiguous assignment (Table 3.1.11). A plausible explanation may be the presence of multiple conformers for MPTA esters of **10**, which may be due to the axial orientation of the sterically hindered 13-OH in **10**.

The absolute configuration of **10** corroborates those determined for austalides A and B by X-ray analysis and enantioselective synthesis, respectively, and represent the first austalide with a benzylic C-22 chirality center (Dillen *et al.*, 1989; Paquette *et al.*, 1994). Thus, **10** was identified as the 22- OMe derivative of austalide B and named austalide M. Because the austalide skeleton is derived from 6-[(2*E*, 6*E*)-farnesyl]-5,7-dihydroxy-4-methyl-phthalide, which is biosynthesized through a mixed polyketide-terpenoid pathway with subsequent cyclization and oxidative modification (De Jesus *et al.*, 1983, 1987; Dillen *et al.*, 1989), the C-22 benzylic substituent must be introduced after the cyclization.

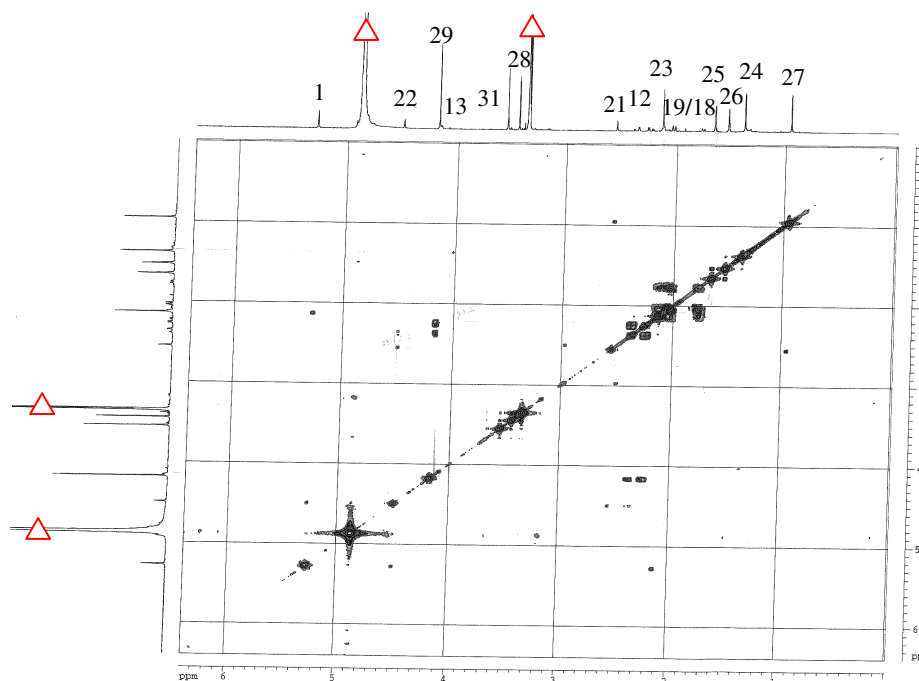


Figure 3.1.13 COSY correlations of austalide M (**10**)

Table 3.1.10 NMR data for austrialide M (10)

Position	10 CD ₃ OD, δ (ppm), J in Hz		Correlation		
	¹ H (500 MHz)	¹³ C (100 MHz)	COSY	HMBC	ROESY
1	5.23 s	70.0		3, 4, 9	
3		171.5			
4		108.9			
5		158.9			
6		119.4			
7		158.9			
8		116.2			
9		149.3			
11		77.3			
12	2.19 dd (4.3, 15.6) 2.32 dd (2.2, 15.7)	43.8	13		
13	4.11 dd (2.3, 4.3)	69.9	12		26
14		87.7			
15		86.1			
17		120.3			
18	1.71 brd (8.6) 1.98 brd (8.4)	32.0	19		
19	1.98 brd (8.4) 2.06 m	31.4	18		
20		39.8			
21	2.50 brs	43.6	22	6, 20, 22, 27	24
22	4.44 brs	72.2	21	5, 6, 7, 11, 20, 31	27
23	2.08 s	10.7		7, 8, 9	
24	1.33 s	28.8		11, 12, 21	21
25	1.60 s	26.5		14, 15, 26	27
26	1.48 s	29.2		14, 15, 25	
27	0.90 s	19.2		14, 19, 20, 21	25, 22
28	3.40 s	49.0		17	
29	4.13 s	63.3		5	
31	3.50 s	56.4		22	

Results

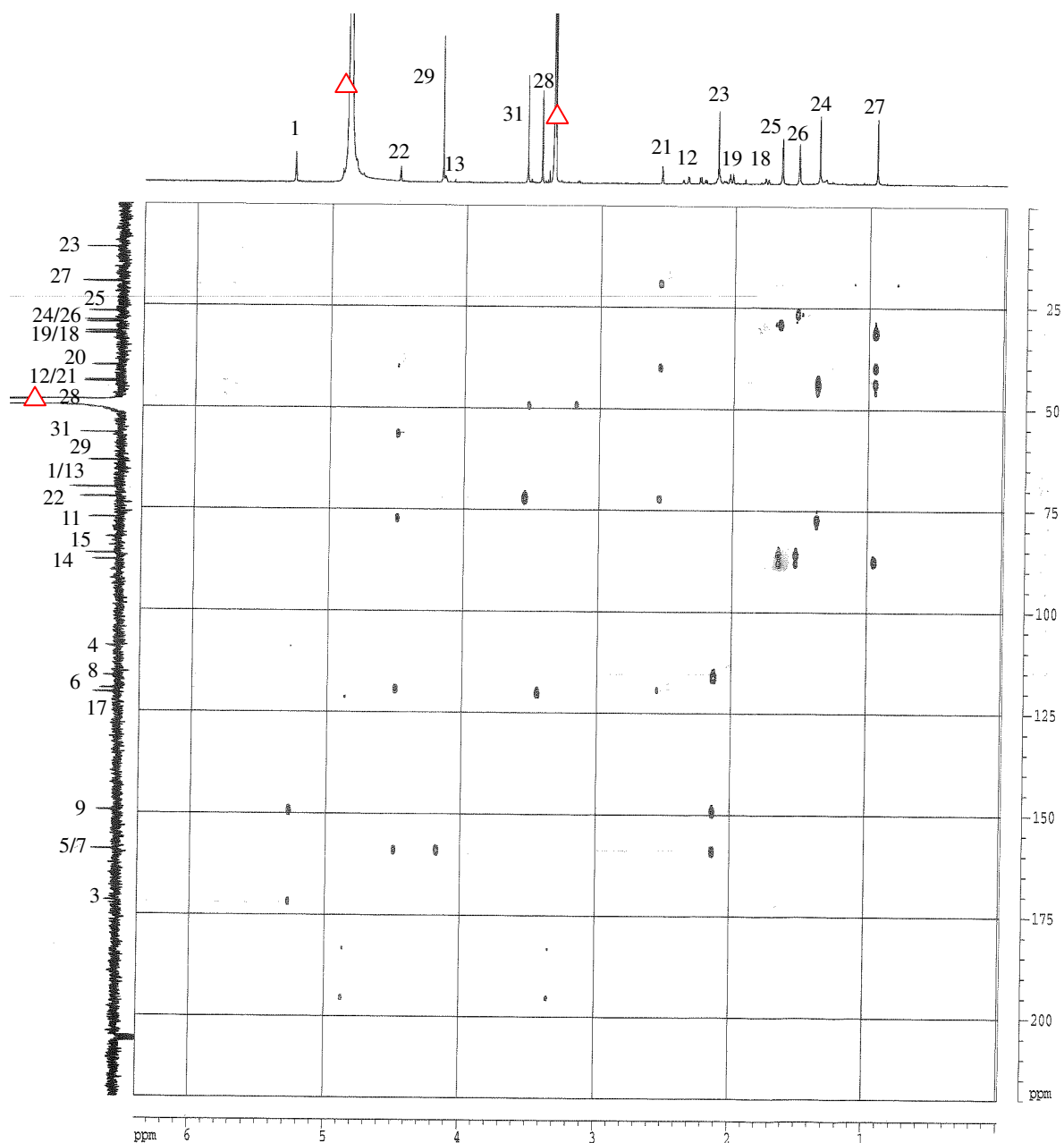
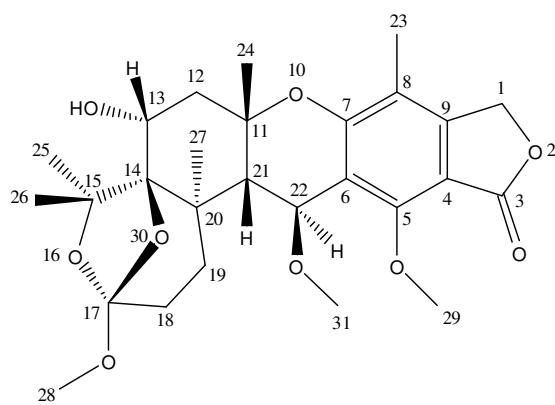


Figure 3.1.14 HMBC correlations of austalide M (10)



(10)

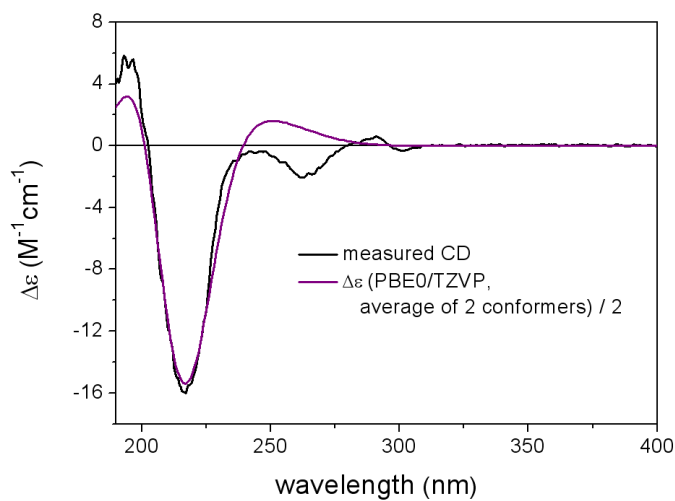


Figure 3.1.15 Experimental ECD spectrum of **10** in acetonitrile compared with the Boltzmann-weighted PBE0/TZVP spectrum calculated for the two lowest-energy conformers of the (11*S*,13*R*,14*R*,20*R*,21*S*,22*S*)-enantiomer

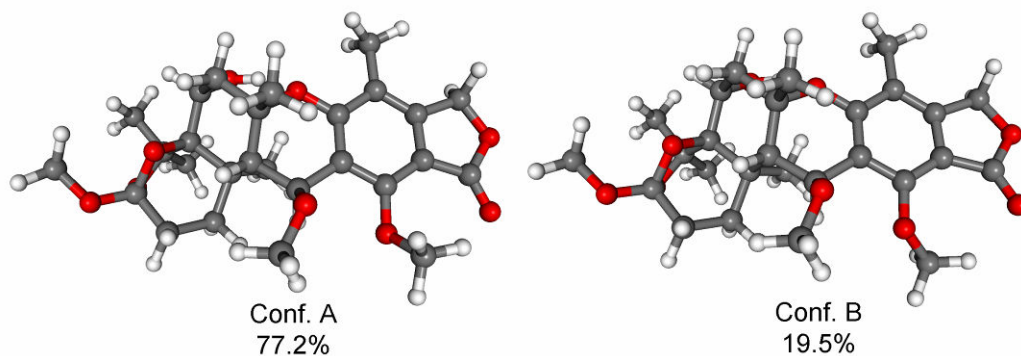


Figure 3.1.16 DFT optimized geometries of the two lowest-energy conformers of (11*S*,13*R*,14*R*,20*R*,21*S*,22*S*)-**10** with torsional angle $\omega_{O3,C3,C4,C9} = -178.8^\circ$ and $+174.3^\circ$, respectively

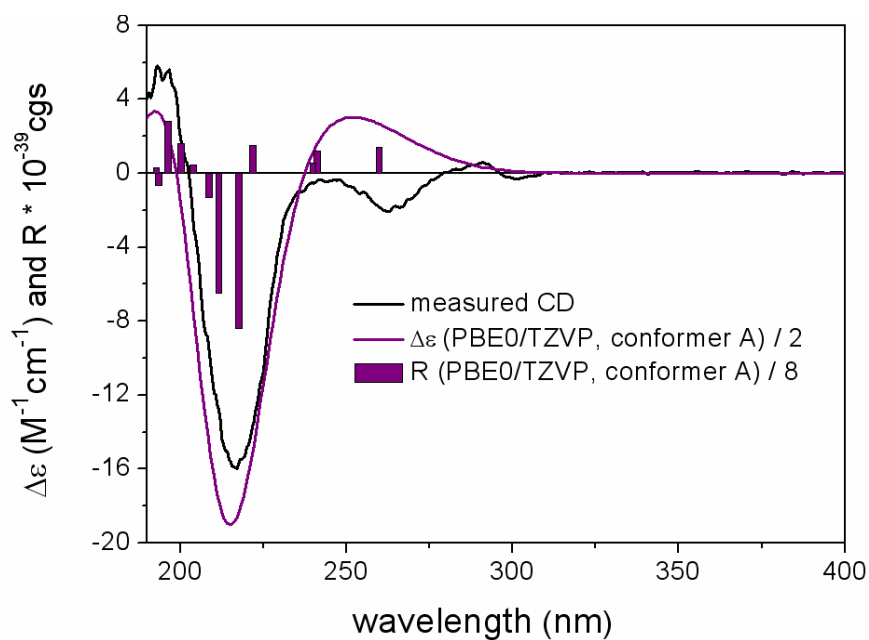


Figure 3.1.17 Experimental ECD spectrum of 10 compared with the PBE0/TZVP spectrum of the lowest-energy (11*S*,13*R*,14*R*,20*R*,21*S*,22*S*)-conformer (conformer A, 77.2% population). Bars represent rotational strengths (*R*)

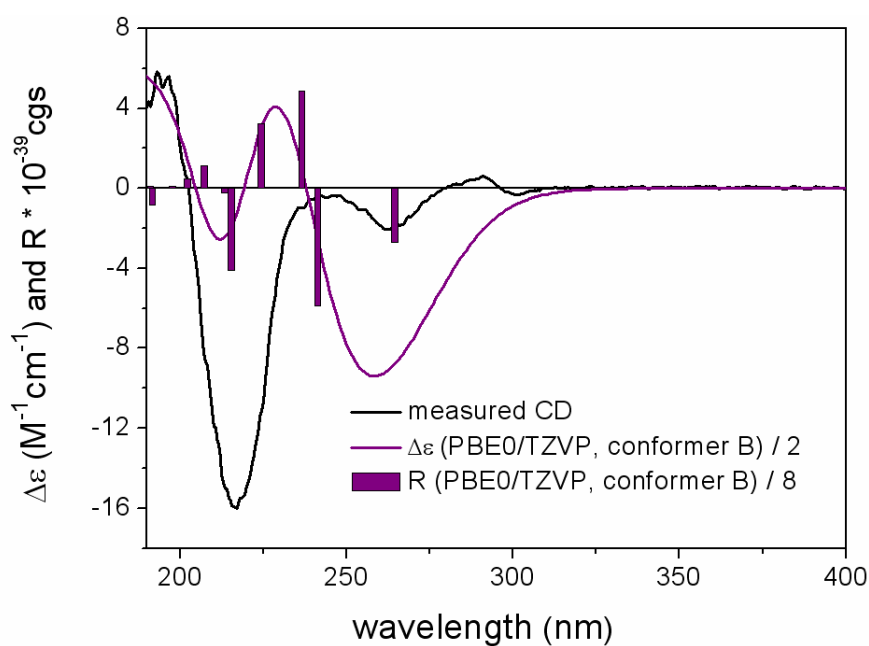


Figure 3.1.18 Experimental ECD spectrum of 10 compared with the PBE0/TZVP spectrum of (11*S*,13*R*,14*R*,20*R*,21*S*,22*S*)-conformer B (19.5% population). Bars represent rotational strengths (*R*)

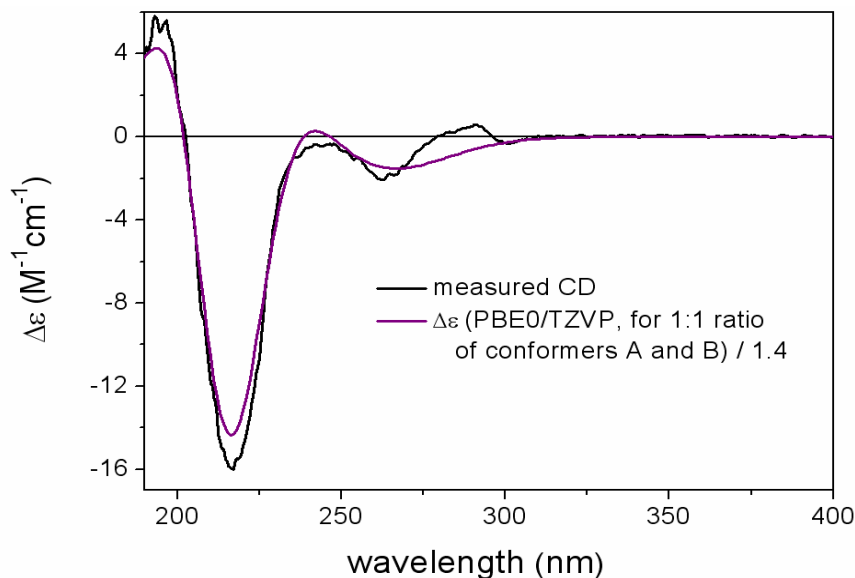


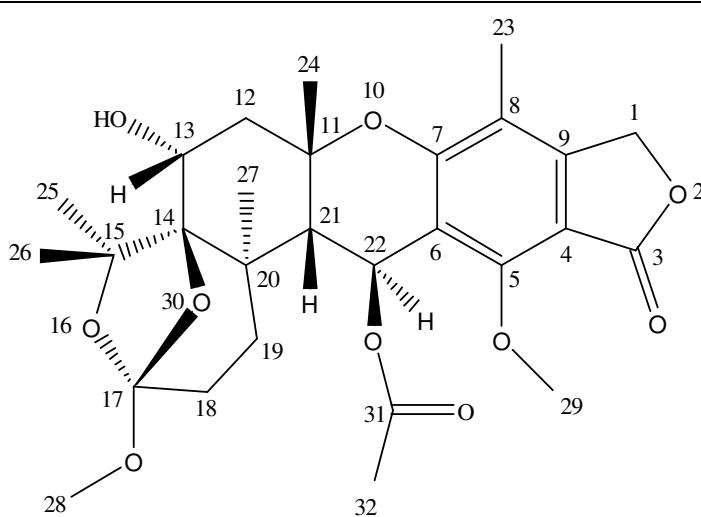
Figure 3.1.19 Experimental ECD spectrum of **10** compared with the PBE0/TZVP spectrum of the two lowest-energy (11*S*,13*R*,14*R*,20*R*,21*S*,22*S*)-conformers supposing their 1:1 ratio

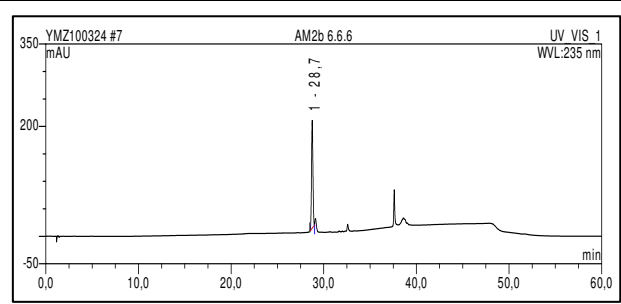
Table 3.1.11 Chemical shift difference between the (*S*)- and (*R*)-MTPA esters of compound **10**

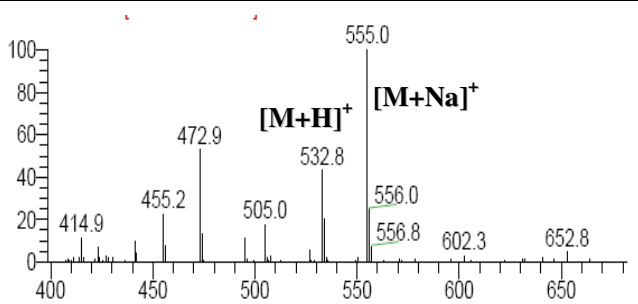
Position	Chemical shift (δ_{H} , in $\text{C}_5\text{D}_5\text{N}$, at 500 MHz)			Δ
	10	(<i>S</i>)-MTPA ester	(<i>R</i>)-MTPA ester	
12	2.3959	2.3913	2.2914	-0.0001
	2.5938	2.5985	2.5983	0.0002
13	4.4496	4.4558	4.4557	0.0001
	2.2054	2.0221	2.0223	-0.0002
18	2.1326	2.1276	2.1274	0.0002
	2.1530	2.1486	2.1487	-0.0001
19	2.2984	2.2936	2.2937	-0.0001
	2.7423	2.7379	2.7380	-0.0001
22	4.6709	4.6664	4.6666	-0.0002
	1.9793	1.9783	1.9781	0.0002
24	1.5375	1.5322	1.5324	-0.0002
	1.8343	1.8302	1.8303	-0.0001
27	1.2875	1.2831	1.2833	-0.0002
	3.5370	3.5322	3.5323	-0.0001
29	4.3979	4.3921	4.3923	-0.0002
	3.6170	3.6216	3.6115	0.0101

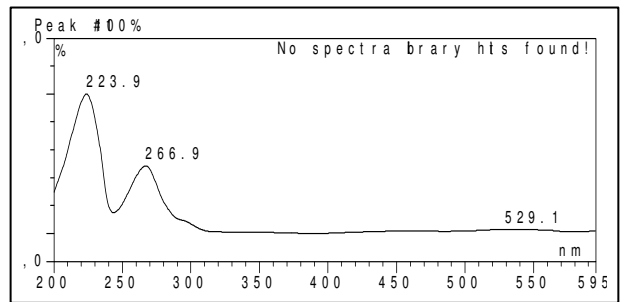
3.1.11 Austalide N (compound 11, new)

Austalide N	
Biological Source	<i>Aspergillus</i> sp.
Sample Code	Fr.2.6.6.6
Sample Amount	7.5 mg
Molecular Formula	C ₂₈ H ₃₆ O ₁₀
Molecular Weight	532 g/mol
Solubility	MeOH
Physical Description	Brown amorphous solid
Optical Rotation	$[\alpha]_D^{20} - 15^\circ$ (c 0.40, MeOH)
HPLC Retention Time	28.7 min (standard gradient)









Austalide N (**11**) was obtained as a brown amorphous solid (7.5 mg) with an $[\alpha]_D^{20}$ value of -15° (c 0.40, MeOH). Similar to **10**, the UV spectrum of **11** showed maxima at $\lambda_{\max} = 223.9$ and 266.9 nm. Compound **11** displayed similar spectroscopic data to those of **10**, suggesting that both compounds have the same basic molecular framework. The HRESIMS indicated the molecular formula $C_{28}H_{36}O_{10}$, in accordance with the $[M+H]^+$ signal at m/z 533.2388, thus revealing a 28 amu increase in the molecular weight compared with **10**. 1H , ^{13}C NMR and DEPT spectra of **11** were identical with those of **10** (Table 3.1.12) except for the replacement of the benzylic C-2 methoxyl group by a methyl ester group resonating at δ_H 2.07 ppm and δ_C 21.3 ppm (CH_3 -32). The respective ester carbonyl carbon was detected at δ_C 171.6 ppm (C-31). This was further confirmed by the observed downfield chemical shift of the H-22 signal (δ_H 6.21) caused by the acetyl substituent. Inspection of COSY, HMQC and HMBC spectra (Table 3.1.12, Figure 3.1.20 and Figure 3.1.21) revealed that, apart from the methyl ester function at C-22, the two compounds were identical. Based on the ROESY spectrum, **11** has (11*S**,13*R**,14*R**,20*R**,21*S**,22*S**) relative configuration in accordance with the corresponding chirality centers of **10**. Accordingly, compound **11** was finally characterized as a new natural product and was named austalide N.

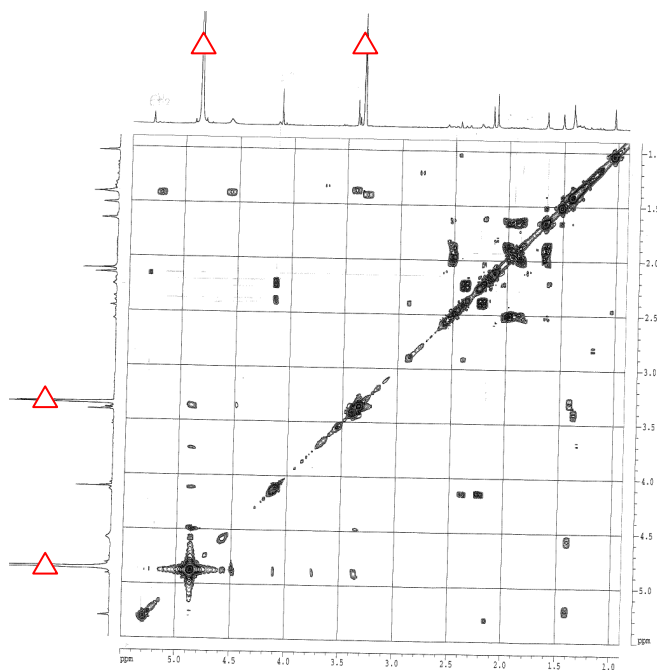


Figure 3.1.20 COSY correlations of austalide N (**11**)

Table 3.1.12 NMR data for austalide N (11)

Position	11 CD ₃ OD, δ (ppm), J in Hz		Correlation		
	¹ H (500 MHz)	¹³ C (100 MHz)	COSY	HMBC	ROESY
1	5.25 s	69.9		3, 9	
2					
3		171.2			
4		108.5			
5		158.4			
6		116.0			
7		159.6			
8		116.4			
9		150.1			
10					
11		77.1			
12	2.17 dd (4.3, 15.6) 2.33 dd (1.7, 15.7)	43.7	13		
13	4.08 dd (2.1, 4.0)	69.6	12		26
14		87.6			
15		85.1			
16					
17		120.6			
18	1.57 m	32.0	19		
	1.83 dt (5.2, 12.9)				
19	1.93 dt (6.1, 12.6) 2.45 dd (4.5, 14.2)	31.6	18		
20		40.9			
21	2.40 brs	46.3	22	6, 20, 22, 27	24
22	6.21 brs	65.3	21	5, 6, 7, 11, 20, 21, 31	27
23	2.10 s	10.6		6, 7, 8, 9	
24	1.36 s	28.8		11, 12, 14, 21	21
25	1.60 s	26.4		14, 15, 26	27
26	1.46 s	29.2		14, 15, 25	
27	0.98 s	19.2		14, 19, 20, 21	22, 25
28	3.36 s	50.1		17	
29	4.06 s	63.1		5	
30					
31		171.6			
32	2.07 s	21.3		6, 31	

Results

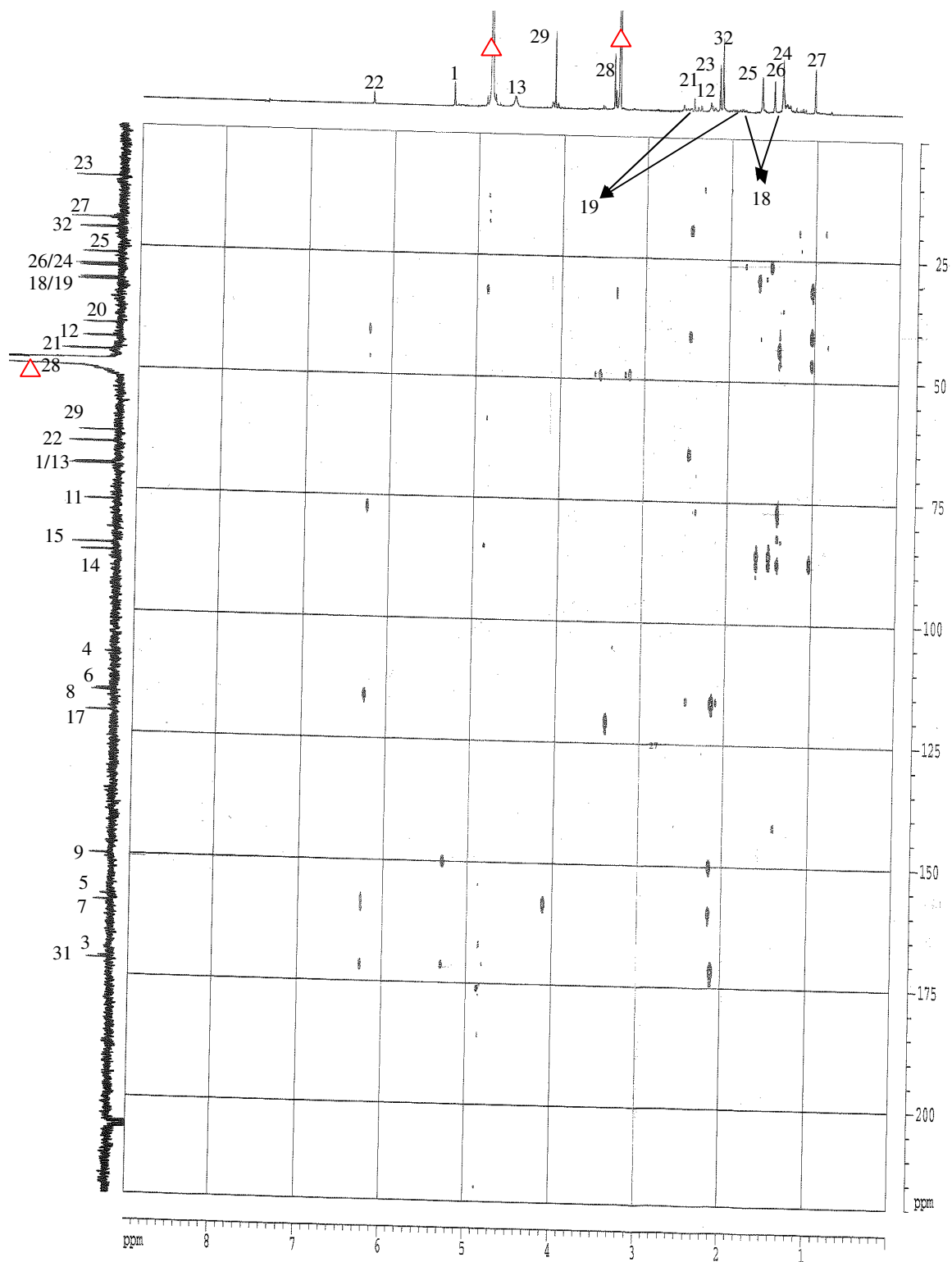
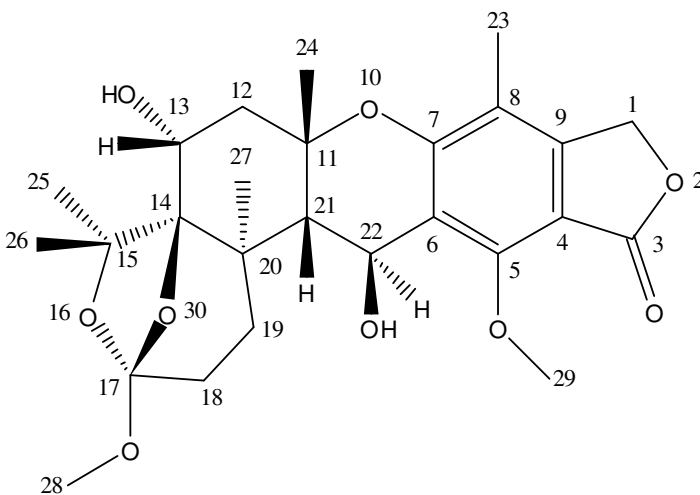
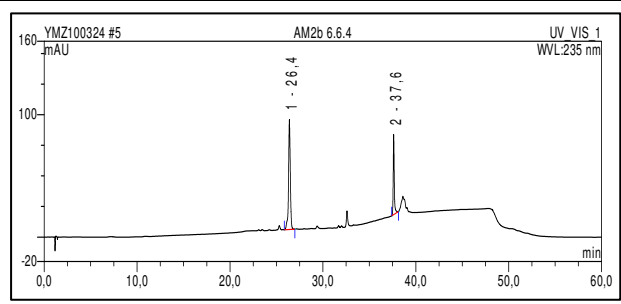
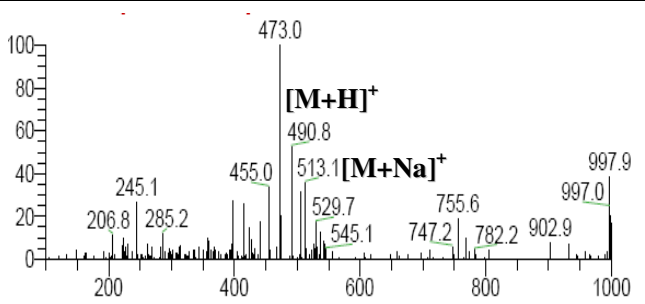
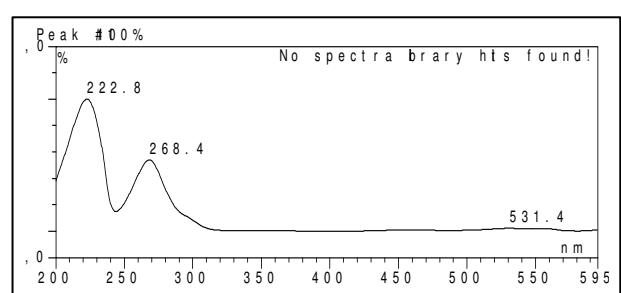


Figure 3.1.21 HMBC correlations of austalide N (11)

3.1.12 Austalide O (compound 12, new)

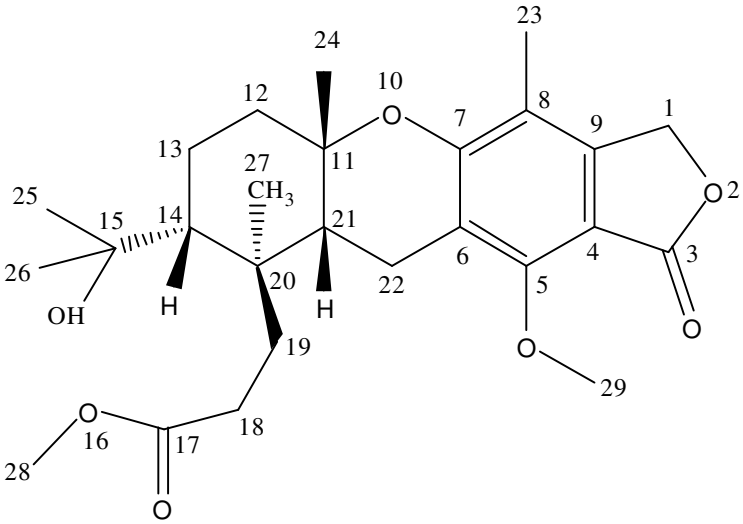
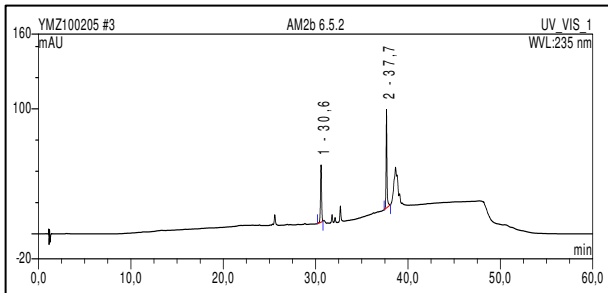
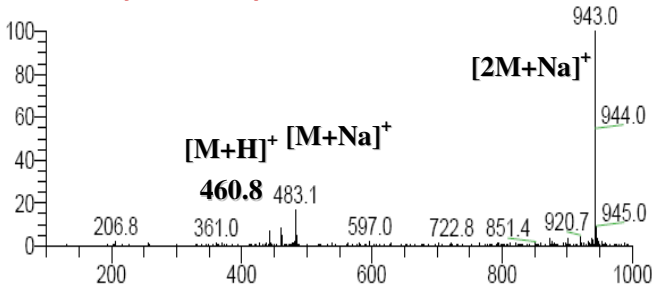
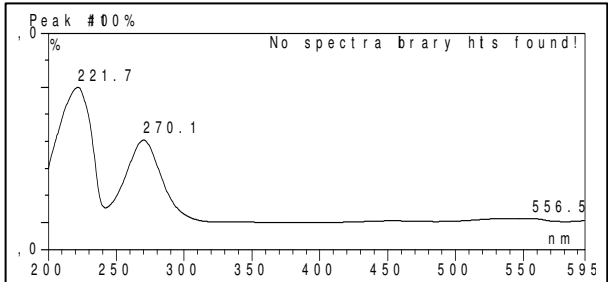
Austalide O	
Biological Source	<i>Aspergillus</i> sp.
Sample Code	Fr.2.6.6.4
Sample Amount	4.0 mg
Molecular Formula	C ₂₆ H ₃₄ O ₉
Molecular Weight	490 g/mol
Solubility	MeOH
Physical Description	Brown amorphous solid
Optical Rotation	$[\alpha]_D^{20} - 41^\circ$ (<i>c</i> 0.15, MeOH)
HPLC Retention Time	26.4 min (standard gradient)
	
	
	
	

Austalide O (**12**) was obtained as a brown amorphous solid (4.0 mg) with an $[\alpha]_D^{20}$ value of -41° (c 0.15, MeOH) and its UV spectrum showed maxima at $\lambda_{\max} = 222.8$ and 268.4 nm. The molecular formula of **12** was determined as $C_{26}H_{34}O_9$, from the prominent signal at m/z 491.2293, corresponding to $[M+H]^+$ in the HRMS (ESI), indicating a loss of 14 amu compared with **10**. The physicochemical and NMR data of **12** were almost identical to those of **10**, apart from the disappearance of the C-22 methoxy group in the NMR spectra of **12** (Table 3.1.13). This suggested that **12** possessed the same skeleton as **10** but with a benzylic 22-OH group instead of the 22-OCH₃, which accounts for the 14 amu molecular weight difference. Accordingly, slight downfield and large upfield shifts were observed for H-22 (δ_H 4.97 ppm) and C-22 (δ_C 62.0 ppm), respectively, in the 1H and ^{13}C NMR spectra of **12**. As with **11**, further confirmation of the planar structure was achieved by analysis of the DEPT, COSY, HMQC, and HMBC spectra (Table 3.1.13). Moreover, the ROESY spectrum indicated a ($11S^*,13R^*,14R^*,20R^*,21S^*,22S^*$) relative configuration, in agreement with those of **10** and **11**. Therefore, compound **12** was identified as a new natural product and was named austalide O. When compound **12** was kept in ethyl acetate for more than 48 hours, no formation of the acetate derivative **11** was detected. Thus, we conclude that compound **11** is a genuine natural product and not an artefact resulting from acetylation of **12**.

Table 3.1.13 NMR data for austalide O (12)

Position	12 CD ₃ OD, δ (ppm), J in Hz		Correlation		
	¹ H (500 MHz)	¹³ C (100 MHz)	COSY	HMBC	ROESY
1	5.23 s	69.9		3, 9	
2					
3		172.0			
4		108.5			
5		158.5			
6		116.0			
7		159.2			
8		116.1			
9		149.2			
10					
11		77.1			
12	2.20 dd (4.4, 15.6) 2.32 dd (2.1, 15.7)	43.8	13		
13	4.09 dd (2.3, 4.3)	70.0	12		26
14		87.6			
15		86.2			
16					
17		120.5			
18	1.64 m 1.96 m	31.8	19		
19	1.96 m 2.13 m	31.8	18		
20		40.1			
21	2.48 brs	48.0		20,22,27	24
22	4.97 brs	62.0		11	27
23	2.09 s	10.8		7, 8, 9	
24	1.37 s	29.2		11,12, 21	21
25	1.60 s	26.4		14,15, 26	27
26	1.47 s	29.0		14,15, 25	
27	0.92 s	19.0		14,19, 20, 21	25, 22
28	3.38 s	50.0		17	
29	4.16 s	62.2		5	

3.1.13 Austalide P (compound 13, new)

Austalide P	
Biological Source	<i>Aspergillus</i> sp.
Sample Code	Fr.2.6.5.2
Sample Amount	4.2 mg
Molecular Formula	C ₂₆ H ₃₆ O ₇
Molecular Weight	460 g/mol
Solubility	MeOH
Physical Description	Brown amorphous solid
Optical Rotation	$[\alpha]_D^{20}$ - 35° (c 0.15, MeOH)
HPLC Retention Time	30.6 min (standard gradient)
	
	
	
	

Austalide P (**13**) was obtained as a brown amorphous solid (4.2 mg) with an $[\alpha]_D^{20}$ value of -35° (c 0.15, MeOH) and its UV spectrum showed maxima at $\lambda_{\max} = 221.7$ and 270.1 nm. Compound **13** was determined from the HRMS (ESI) to have the molecular formula $C_{26}H_{36}O_7$, with a prominent peak at m/z 483.2349 $[M+Na]^+$. Its physical characteristics were comparable to those of **10**, suggesting the same basic molecular framework. The 1H and ^{13}C NMR spectra of **13** (Table 3.1.14) indicated the presence of seven methyl groups, appearing as singlets in the 1H NMR spectrum, including two methoxy groups resonating at δ_H 3.68 ppm and 4.04 ppm (CH_3 -28 and -29, respectively), one aromatic methyl group at δ_H 2.08 ppm (CH_3 -23), and four aliphatic methyl groups at δ_H 0.70, 1.20, 1.19 and 1.27 ppm (CH_3 -27, -24, -25 and -26, respectively). In addition, six methylene groups were observed, one of which was attributed to the oxygenated benzylic methylene group at C-1 (δ_H 5.21 ppm, s), as well as two methine groups. The ^{13}C NMR spectrum (Table 3.1.14) confirmed the presence of 26 carbon atoms in the structure. Furthermore, the DEPT experiment revealed the presence of 11 quaternary carbon atoms. Analysis of the 1H - 1H COSY spectrum of **13** (Table 3.1.14, Figure 3.1.22) established the presence of three spin systems which included the fragment $CH_2(12)CH_2(13)CH(14)$ based on the correlations observed between the corresponding protons resonating at δ_H 1.61 (CH_2 -12), 1.52 and 1.83 (CH_2 -13), as well as 2.14 (H-14) ppm, thus indicating the loss of the hydroxyl group substituent at C-13 present in **10-12** as well as of the oxo-bridge connecting C-14 to C-17. Moreover, the correlations observed between the protons of the methylene groups at C-18 (δ_H 2.32 and 2.60 ppm) and C-19 (δ_H 1.80 and 2.42 ppm), and between the methylene protons appearing at δ_H 2.78 and 3.03 ppm (CH_2 -22) and the methine group at C-21 (δ_H 1.70 ppm) verified the remaining two spin systems. Proton signals were assigned to their corresponding carbon atoms by analysis of the HMQC spectrum.

The structural units identified in **13** were connected on the basis of correlations observed in the HMBC spectrum (Table 3.1.14, Figure 3.1.23). The tertiary methyl group CH_3 -27 (δ_C 19.5) correlated with the quaternary carbon C-20 (δ_C 41.6), CH_2 -19

(δ_C 34.9), CH-21 (δ_C 41.2), and CH-14 (δ_C 40.1). C-14 further correlated with the methyl groups CH₃-25 and CH₃-26 (δ_C 28.0 and 33.2, respectively), which were found to constitute a geminal dimethyl moiety, as indicated by their correlation with each other as well as with an oxygenated quaternary carbon resonating at δ_C 75.7 (C-15). The upfield chemical shift of C-15 in **13** compared to that observed in **10-12** and indicated its location within a side chain and not as part of a seven-membered ring as in **10-12**. Furthermore, the methoxy group OCH₃-28 (δ_C 52.0) correlated with an ester carbonyl carbon resonating at δ_C 177.7 which was assigned to C-17. H-21 correlated with CH₂-19, C-20, CH₃-27, CH₂-22 (δ_C 18.5), and C-6 (δ_C 118.0). CH₂-22 correlated with C-20, CH-21, C-6, as well as with the oxygenated quaternary carbons C-5 (δ_C 158.1), C-7 (δ_C 160.0) and C-11 (δ_C 78.3). Correlations of the tertiary methyl group CH₃-24 (δ_C 27.9) with C-11, C-21 and CH₂-12 (δ_C 40.2) provided the remaining connections of the spin systems previously observed in the ¹H-¹H COSY spectrum. The methoxy group OCH₃-29 (δ_C 62.1) was attached to C-5 as indicated by the respective HMBC correlation. The aromatic CH₃-23 (δ_C 10.6) correlated to the quaternary aromatic carbons C-7, C-8 (δ_C 117.3), and C-9 (δ_C 148.0), and hence, was placed at C-8. The remaining ¹³C resonances at δ_C 108.0 and 172.1 were attributed to C-4 and C-3, respectively. This was further confirmed by the observed correlation of C-9 with CH₂-1 (δ_C 69.8), which, in turn, correlated with C-8, C-4 and C-3. Accordingly, **13** shows familiar features to **10-12**, except for that the seven-membered ring of **10-12** was opened at the oxo-bridges, giving rise to two side chains located at C-20 and C-14.

The relative configuration of **13** was established by interpretation of the ROESY spectrum. By analogy with **10**, CH₃-24 correlated with H-21 thus denoting *cis*-fusion of rings C and D. This was further confirmed by correlations observed for H-21 with H-14 and CH₃-24, indicating the *cis* orientation of H-21 and H-14. A *trans* relationship between CH₃-24 and CH₃-27 was assumed from the absence of correlations between CH₃-27 and H-14, H-21 or CH₃-24. Accordingly, the relative stereochemistry of **13** was determined as (11*S**,14*R**,20*S**,21*R**). Compound **13** lacked the benzylic

chirality center and its ECD spectrum was completely different from that of **10**, which implied that ECD calculation was required for the configurational assignment. The ECD spectrum of **13** showed four main ECD bands at 267, 228, 212 and 194 nm with alternating negative, positive, negative, positive CEs, respectively (Figure 3.1.24). The MMFF conformational search followed by B3LYP/6-31G(d) DFT reoptimization of 31 conformers afforded four conformational isomers with 40.0%, 23.5%, 16.8% and 15.1% populations above 2% populations. Besides slightly different orientations of the side-chains, the value of the torsional angle $\omega_{O3,C3,C4,C9}$ was identified as the main difference among the conformers (Figure 3.1.25). In contrast to the situation for austalide M (**10**), the two lowest-energy conformers had positive torsional angle $\omega_{O3,C3,C4,C9}$, whereas the two higher-energy conformers had negative angles. In accordance, conformers A and B gave nearly identical calculated ECDs, which was different from those of conformer C and D, which were similar. The Boltzmann-weighted ECD spectra of (11*S*,14*R*,20*S*,21*R*)-**13** computed with TZVP basis set and three different functionals (B3LYP, BH&HLYP, PBE0) reproduced well the experimental ECD spectrum, with PBE0 giving the best agreement (Figure 3.1.25). Thus, the absolute configuration of **13** was unambiguously determined as (-)-(11*S*,14*R*,20*S*,21*R*) and it was named as austalide P. The ECD calculation also revealed that the sign of the torsional angle $\omega_{O3,C3,C4,C9}$, i.e., the conformation of the benzene-fused phthalide ring, is decisive for the ECD parameters. The major conformers of austalide M (**10**) and P (**13**) had oppositely signed torsional angles $\omega_{O3,C3,C4,C9}$, which resulted in markedly different ECD spectra. The torsional angle $\omega_{O3,C3,C4,C9}$ of the conformers and their populations are clearly determined by the central chirality elements and the benzylic C-22 chirality center has obviously a determining role. The results of the ECD calculation also explain the fact that the ECD spectra (Figure 3.1.26) of austalide N (**11**) and O (**12**) were different from that of austalide M (**10**), although they are homochiral and they differ only in the nature of the benzylic C-22 substituent. The nature of the benzylic C-22 substituent (methoxy, acetoxy or hydroxyl) has an effect on the torsional angle $\omega_{O3,C3,C4,C9}$ of the conformers and their populations, which in turn determines the ECD parameters. The examples of

austalides studied here suggest that a general procedure to determine absolute configuration for structurally related compounds by simple comparison of their ECD spectra cannot be used safely in the presence of a chirally perturbed benzene-fused phthalide chromophore. Austalide P is similar to the reported austalide G and H, in which the oxygen-bridged bicyclic A/B rings are also opened, but it lacks the C-13 chiral center (Horak *et al.*, 1985).

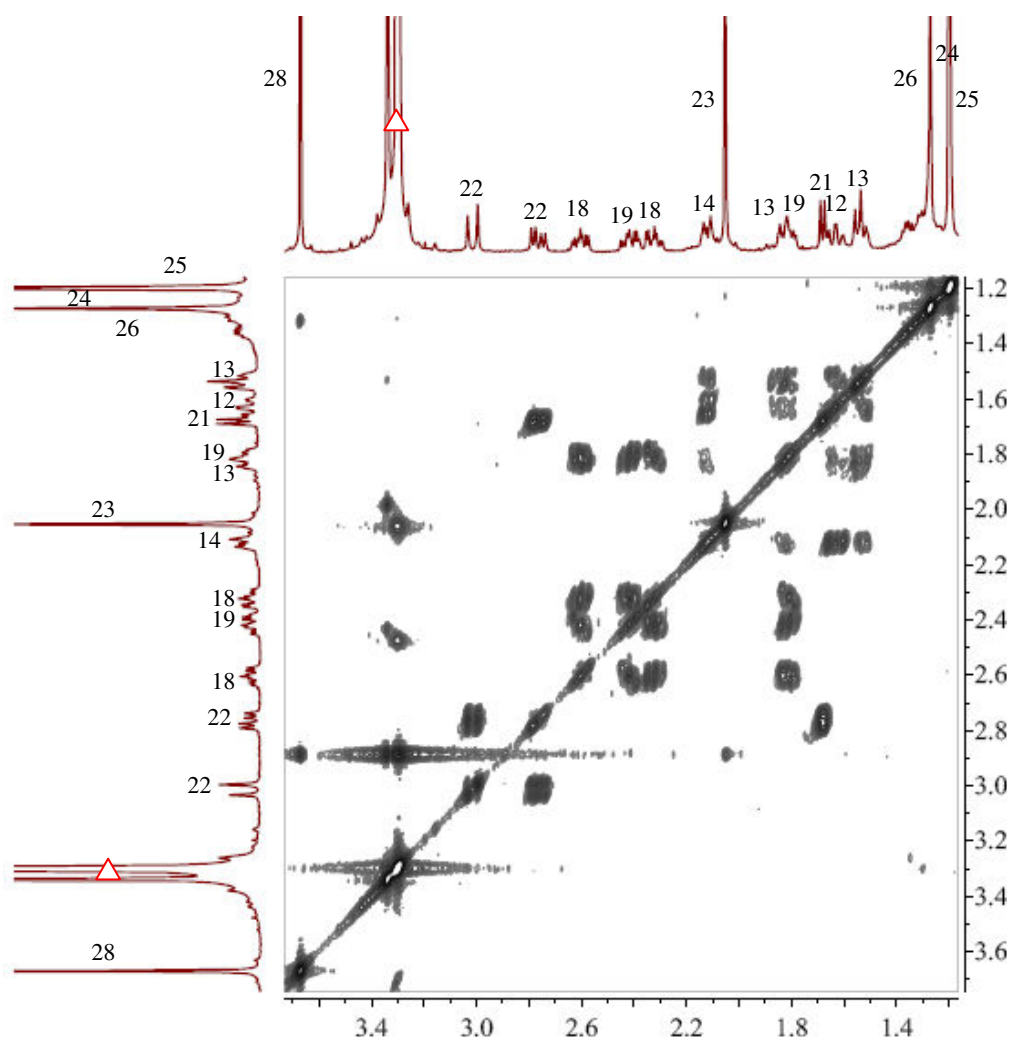


Figure 3.1.22 COSY correlations of austalide P (13)

Table 3.1.14 NMR data for austalide P (13)

Position	13 CD ₃ OD, δ (ppm), <i>J</i> in Hz		Correlation		
	¹ H (500 MHz)	¹³ C (150 MHz)	COSY	HMBC	ROESY
1	5.21 s	69.8		3, 4, 8,9	
2					
3		172.1			
4		108.0			
5		158.1			
6		118.0			
7		160.0			
8		117.3			
9		148.0			
10					
11		78.3			
12	1.61 dt (3.8, 14.3)	40.2	13		
13	1.52 t (10.7) 1.83 m	22.4	12,14	15, 20, 25, 26, 27	
14	2.14 dd (3.4, 13.7)	40.1	13		21
15		75.7			
15-OH					
16					
17		177.7			
18	2.32 m, 2.60 m	30.0	19	17, 19	
19	1.80 m, 2.42 m	34.9	18	14, 17, 18, 20, 21	
20		41.6			
21	1.70 d (8.1)	41.2	22	6, 19, 20, 22, 27,	24,14
22	2.78 dd (8.1, 18.5) 3.03 d (18.6)	18.5	21	5, 6, 7, 11, 20 21	
23	2.08 s	10.6		7, 8, 9	
24	1.20 s	27.9		11, 12, 21	21
25	1.19 s	28.0		14, 15, 26	
26	1.27 s	33.2		15, 14, 25	
27	0.70 s	19.5		14, 19, 20, 21,	
28	3.68 s	52.0		17	
29	4.04 s	62.1		5	

Results

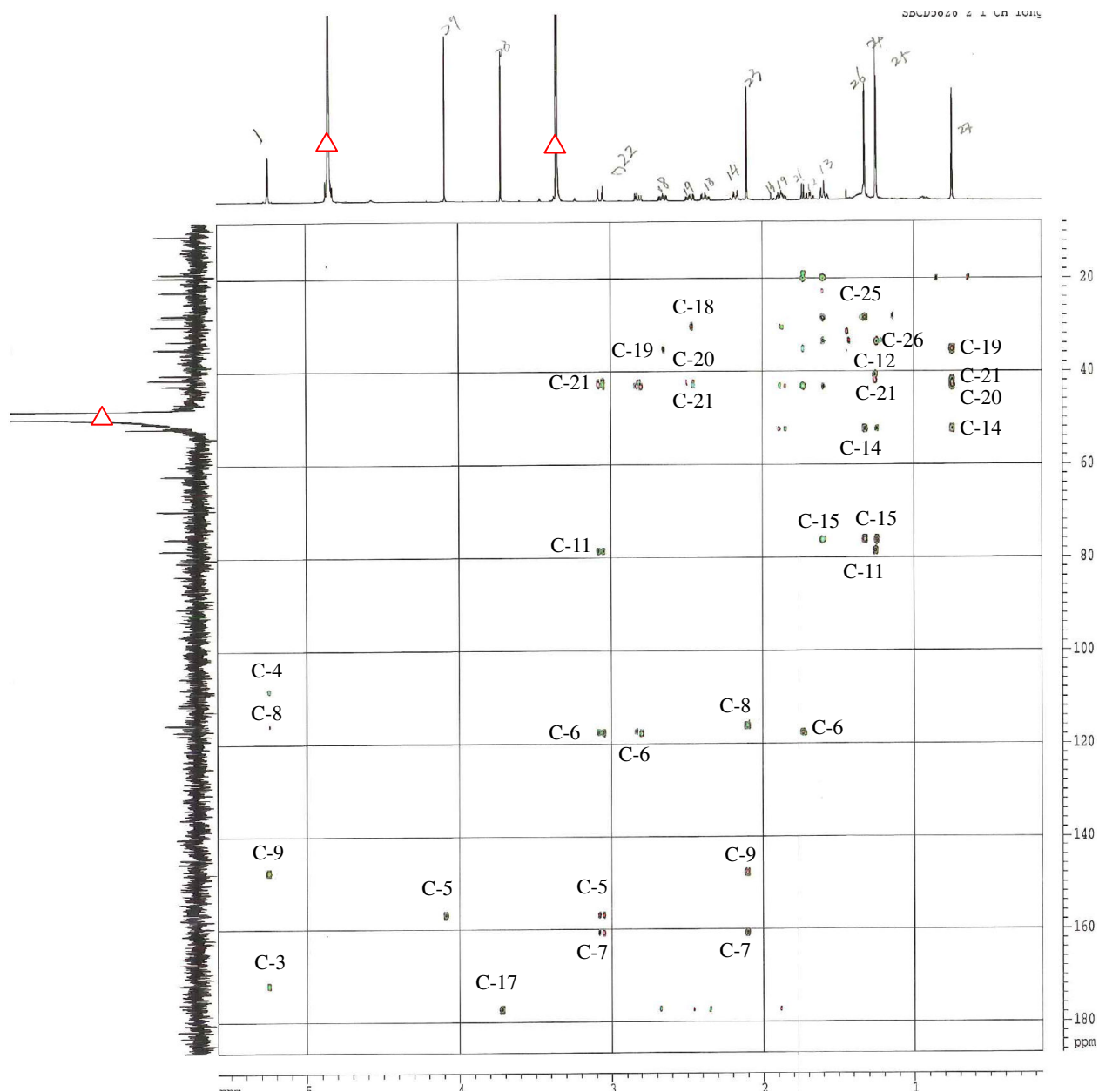


Figure 3.1.23 HMBC correlations of austalide P (13)

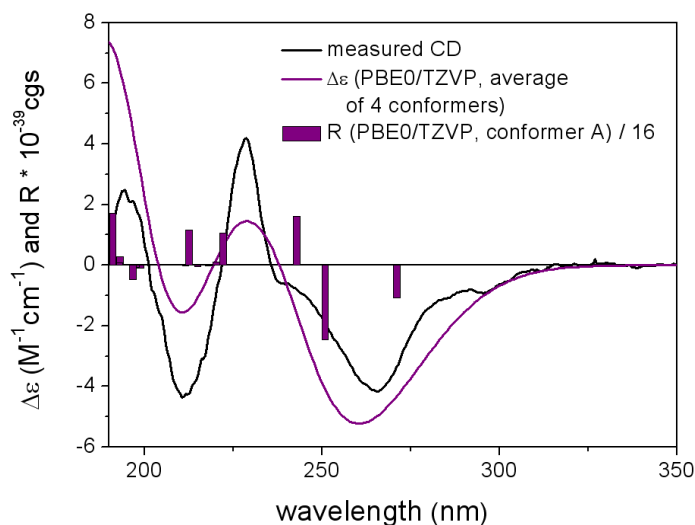


Figure 3.1.24. Experimental ECD spectrum of 13 in acetonitrile compared with the Boltzmann-weighted PBE0/TZVP spectrum calculated for the four lowest-energy conformers with (11*S*,14*R*,20*S*,21*R*) absolute configuration. Bars represent rotational strengths (*R*) of the lowest-energy conformer (40.0%)

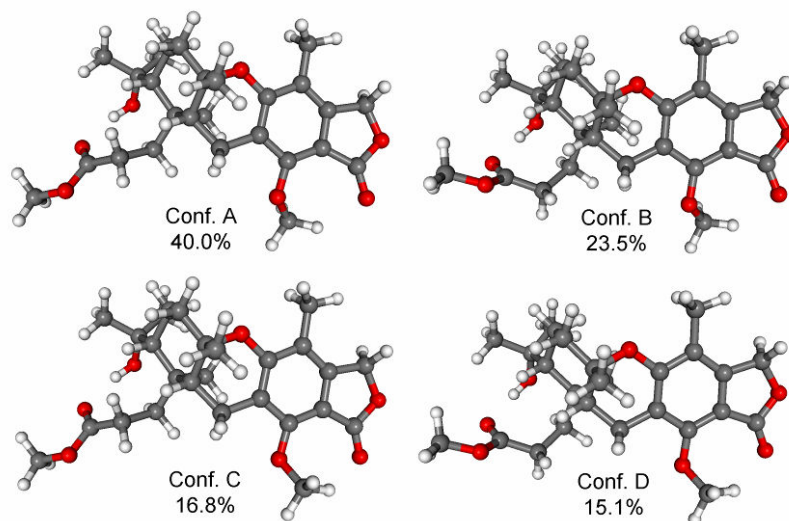


Figure 3.1.25 DFT optimized geometries and populations of the four lowest-energy conformers of (11*S*,14*R*,20*S*,21*R*)-13 with torsional angle $\omega_{O3,C3,C4,C9} +174.61^\circ$, $+174.92^\circ$, -176.28° and -175.94° , respectively

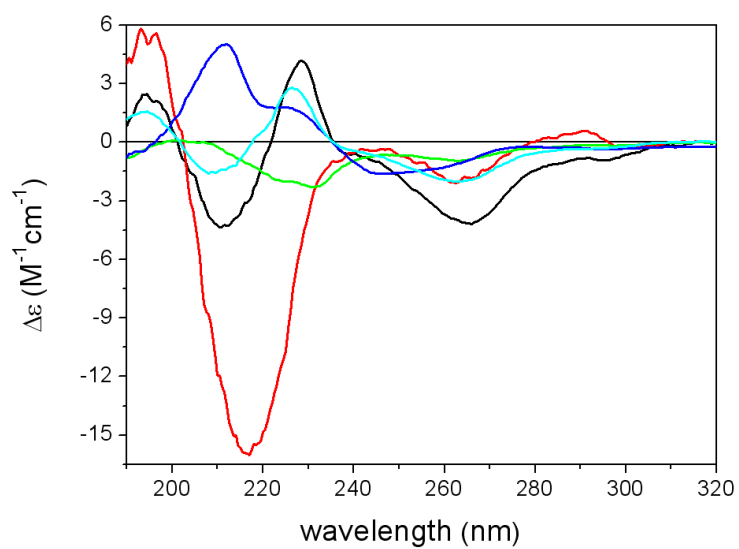
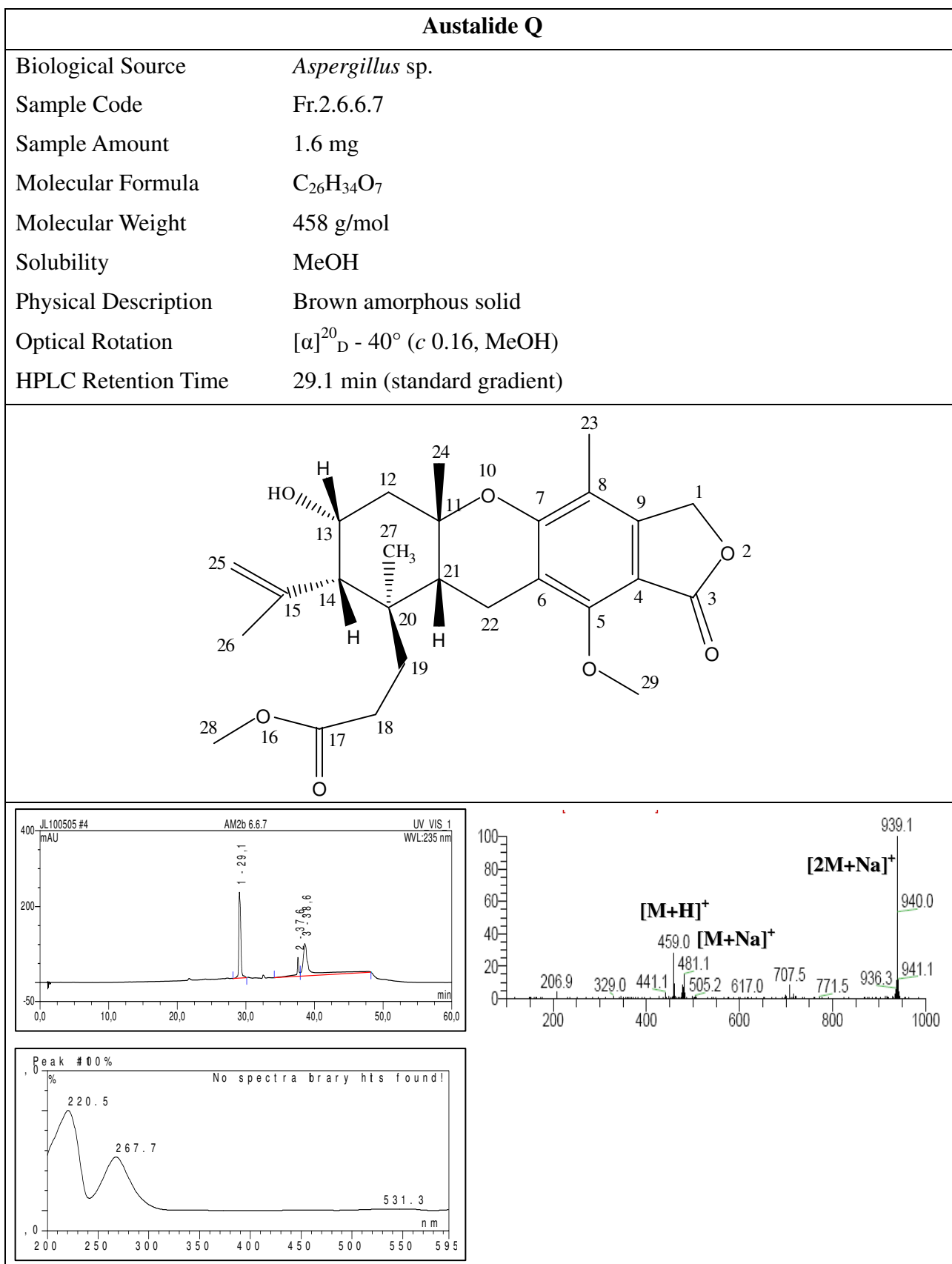


Figure 3.1.26 Experimental ECD spectra of austalide M (10, red), austalide N (11, green), austalide O (12, blue), austalide P (13, black) and austalide Q (14, cyan) in acetonitrile

3.1.14 Austalide Q (compound 14, new)

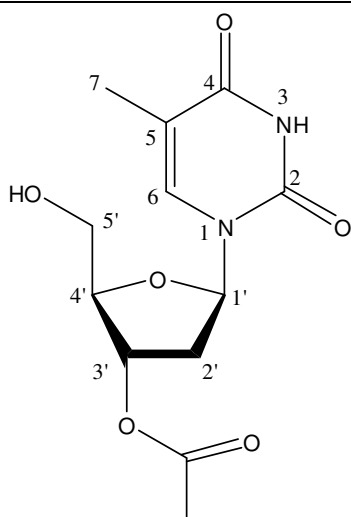
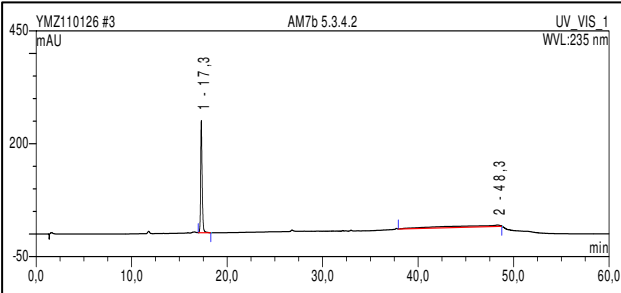
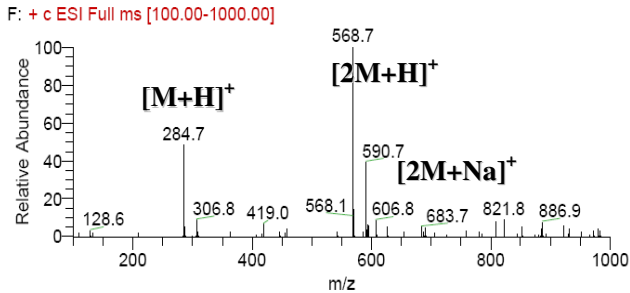
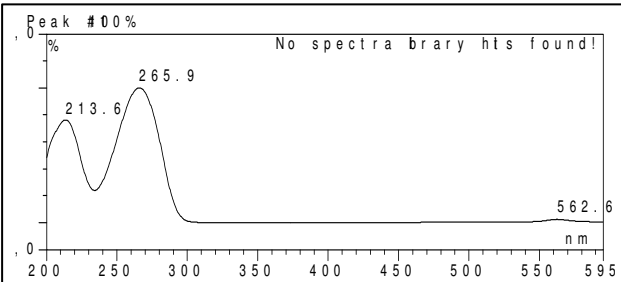


Austalide Q (**14**) was obtained as a brown amorphous solid (1.6 mg) with an $[\alpha]_D^{20}$ value of -40° (c 0.16, MeOH) and its UV spectrum showed maxima at $\lambda_{\max} = 220.5$ and 261.1 nm. The HRESIMS of **14** exhibited a prominent peak at m/z 459.2376 $[M+H]^+$, indicating a molecular formula of $C_{26}H_{34}O_7$. The 1H , ^{13}C NMR and DEPT data of **14** (Table 3.1.15) were similar to those of **13**, apart from the replacement of one of the methylene protons at C-13 by a hydroxyl group in **14**, as evidenced by the chemical shifts of CH-13 (δ_H 4.11, δ_C 72.2). In addition, the hydroxyl group at C-15 of **13** was absent and one of the geminal methyl groups was replaced by an olefinic methylene group instead, the protons of which resonating downfield at δ_H 4.96 and 5.05 ppm (CH₂-25). This was further confirmed by analysis of the 1H - 1H COSY spectrum (Table 3.1.15) which verified the fragment CH₂(12)CH(13)CH(14) derived from the correlations observed between the methylene protons at δ_H 2.02 and 2.41 ppm (CH₂-12), the proton at C-13, and H-14 detected at 2.20 ppm. HMQC and HMBC spectra gave further evidence for the assigned partial structures of **14**. The correlations observed for CH₃-26 (δ_H 1.90) to C-14 (δ_C 54.3), the olefinic quaternary carbon detected at δ_C 148.0 (C-15), and an olefinic methylene carbon at δ_C 116.2 ppm (C-25), confirmed the dehydrogenation of the C-15—C-25 bond in **14** compared to that of **13**. The ROESY spectrum of **14** showed similar correlations to those of **13** indicating (11*S**,13*R**,14*S**,20*S**,21*R**) relative configuration, which regarding the corresponding chirality centers, was homochiral with that of austalide M (**10**). Since compound **14** exhibited nearly identical ECD spectrum with that of **13** and the C-11 and C-21 chirality centers, the closest ones to the substituted chroman chromophore, were the same, its absolute configuration was determined as $(-)-(11*S*,13*R*,14*S*,20*S*,21*R*)$ and it was named austalide Q.

Table 3.1.15 NMR data for austrialide Q (14)

Position	14 CD ₃ OD, δ (ppm), <i>J</i> in Hz		Correlation		
	¹ H (500 MHz)	¹³ C (150 MHz)	COSY	HMBC	ROESY
1	5.21 s	70.7		9	
2					
3		172.1			
4		108.0			
5		154.7			
6		118.0			
7		160.0			
8		117.3			
9		146.2			
10					
11		79.3			
12	2.02 dd (3.9, 15.3) 2.41 dd (2.4, 15.5)	46.6	13		
13	4.11 dd (1.7, 4.5)	72.2	12, 14		
14	2.20 d (1.8)	54.3	13		21
15		148.0			
16					
17		176.7			
18	2.36 t (8.0)	29.9	19	17,19	
19	1.65 m	36.0	18		
20		40.1			
21	1.80 d (7.5)	40.7	22	20	24,14
22	2.87 dd (4.9, 19.3) 2.93 d (18.5)	18.9	21	6, 21	
23	2.08 s	10.8		7, 8, 9	
24	1.25 s	27.8		11, 12, 21	21
25	4.96 d (2.8) 5.05 d (1.8)	116.2			
26	1.90 s	26.4		14, 15, 25	
27	0.86 s	20.7		14, 19, 20, 21	
28	3.67 s	52.4		17	
29	4.05 s	62.7		5	

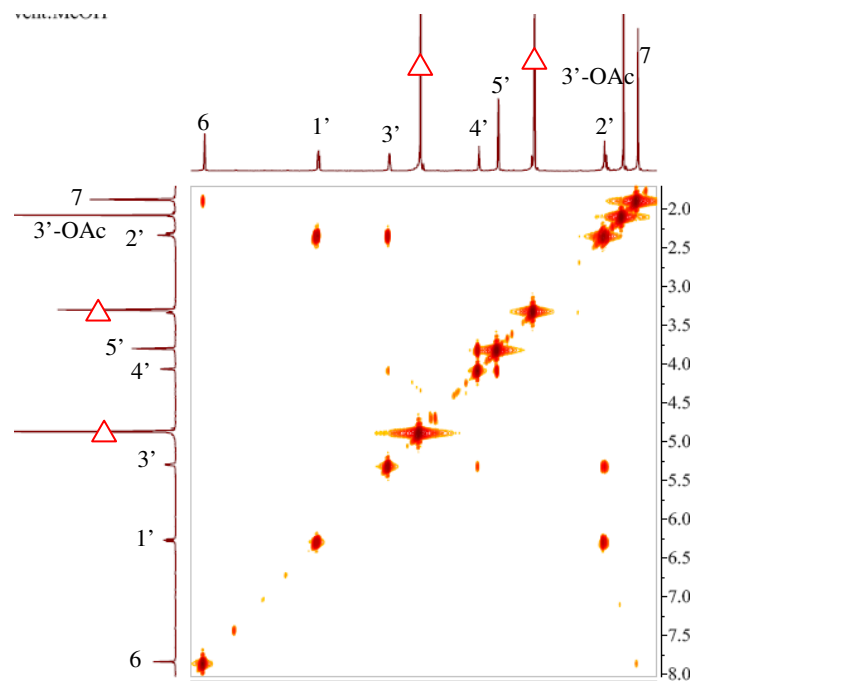
3.1.15 3'-O-Acetylthymidine (compound 15, known)

3'-O-Acetylthymidine	
Biological Source	<i>Aspergillus</i> sp.
Sample Code	Fr.7.5.3.4.2
Sample Amount	6.0 mg
Molecular Formula	C ₁₂ H ₁₆ N ₂ O ₆
Molecular Weight	284 g/mol
Solubility	MeOH
Physical Description	Pale yellow powder
Optical Rotation	$[\alpha]_D^{20} - 28^\circ$ (c 0.4, CHCl ₃)
HPLC Retention Time	17.3 min (standard gradient)
	
<div style="display: flex; justify-content: space-between;"> <div style="width: 45%;">  </div> <div style="width: 45%;">  </div> </div> <div style="margin-top: 10px;">  </div>	

3'-*O*-Acetylthymidine (**15**) was obtained as a pale yellow powder with an $[\alpha]_D^{20}$ value of -28° (c 0.4, CHCl_3). Its UV spectrum showed maxima at $\lambda_{\text{max}} = 213.6$ and 265.9 nm.. Based on its ESIMS (m/z 284.7 $[\text{M}+\text{H}]^+$) and NMR spectral data (Table 3.1.16), the molecular formula of **15** was indicated as $\text{C}_{12}\text{H}_{16}\text{N}_2\text{O}_6$. The ^1H NMR spectrum of **15** exhibited three singlets resonating at δ_{H} 1.87, 2.08 and 7.84 ppm, which were assigned to be the aromatic methyl group (CH_3 -7), the acetoxy methyl group (3'-OAc) and the aromatic proton (H-6), respectively. Furthermore, the signals at δ_{H} 2.32, 3.79, 4.06, 5.30, 6.26 ppm were assigned as H-2', H-5', H-4', H-3', and H-1', respectively. ^{13}C NMR and DEPT spectra revealed the presence of twelve carbon atoms, including two methylene groups one of which being oxygenated (CH_2 -5'), four quaternary including two amide carbonyl carbons, one ester carbonyl carbon and one aromatic quaternary carbon, three oxygenated methine groups, and one aromatic methine group. The carbon signals appearing at δ_{C} 166.4 (C-4), 152.6 (C-2), 137.9 (C-6), 111.8 (C-5) ppm, along with a carbon signal at δ_{C} 12.4 ppm (C-7), and the corresponding proton signals, were thought to be attributable to a thymine base (Davies *et al.*, 1974; Pretsch *et al.*, 1989). The above data, together with ^1H - ^1H COSY and HMBC correlations (Figures 3.1. 27 and 3.1. 28) established the sugar part thus identifying **15** as an acetyl derivative of thymidine. Consequently, on the basis of all the foregoing evidence along with comparison with reported data (Atallan *et al.*, 2006), the structure of **15** was finally characterised as 3'-*O*-acetylthymidine.

Table 3.1.16 NMR data for 3'-O-acetylthymidine (15)

Position	15 CD ₃ OD, δ (ppm), <i>J</i> in Hz		Reference CDCl ₃ , δ (ppm), <i>J</i> in Hz (Atallan <i>et al.</i> , 2006),	
	¹ H (500 MHz)	¹³ C (125 MHz)	¹ H (500 MHz)	¹³ C (125 MHz)
2		152.6		150.2
4		166.4		163.3
5		111.8		111.4
6	7.84 s	137.9	7.50 s	136.2
7	1.87 s	12.4	1.93 s	12.6
1'	6.26 t (6.2)	86.1	6.25 t (6.0)	86.0
2'	2.32 m	38.3	2.42 m	37.2
			2.40 m	
3'	5.30 m	76.3	5.35 m	74.7
4'	4.06 m	86.7	4.10 m	85.0
5'	3.79 d (3.0)	62.9	3.94 dd (12.0, 2.5)	62.6
			3.93 dd (12.0, 2.5)	
3'-OAc	2.08 s	20.7	2.11 s	21.0
		172.1		170.7

**Figure 3.1.27 COSY correlations of 3'-O-acetylthymidine (15)**

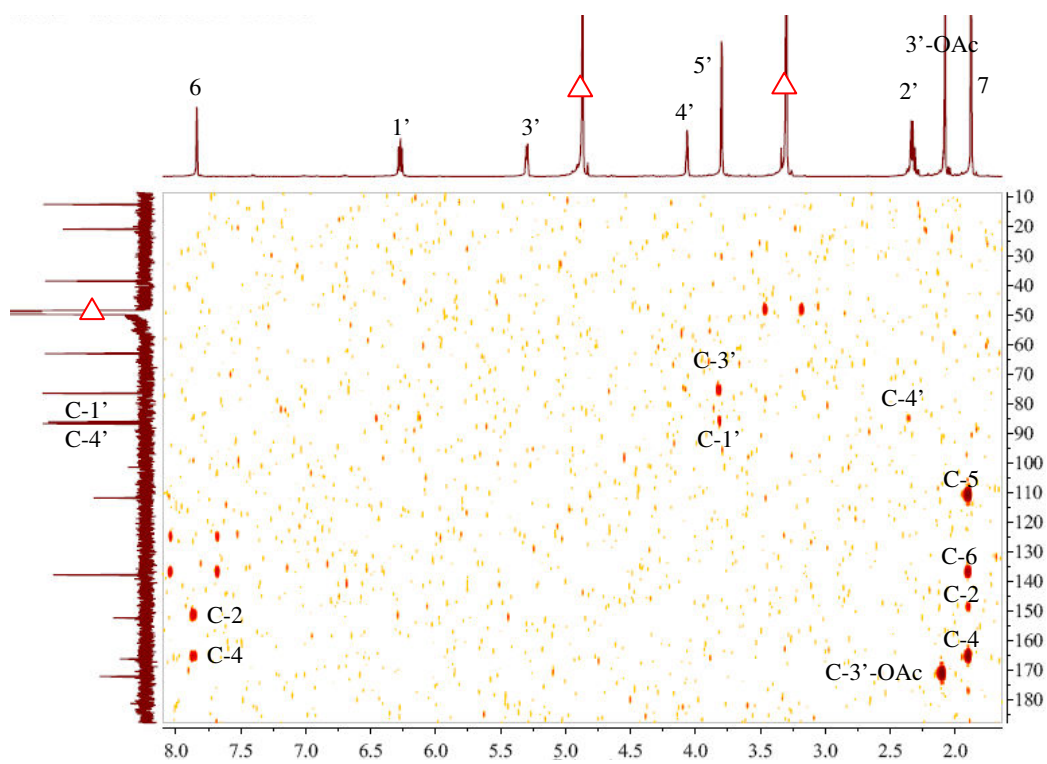
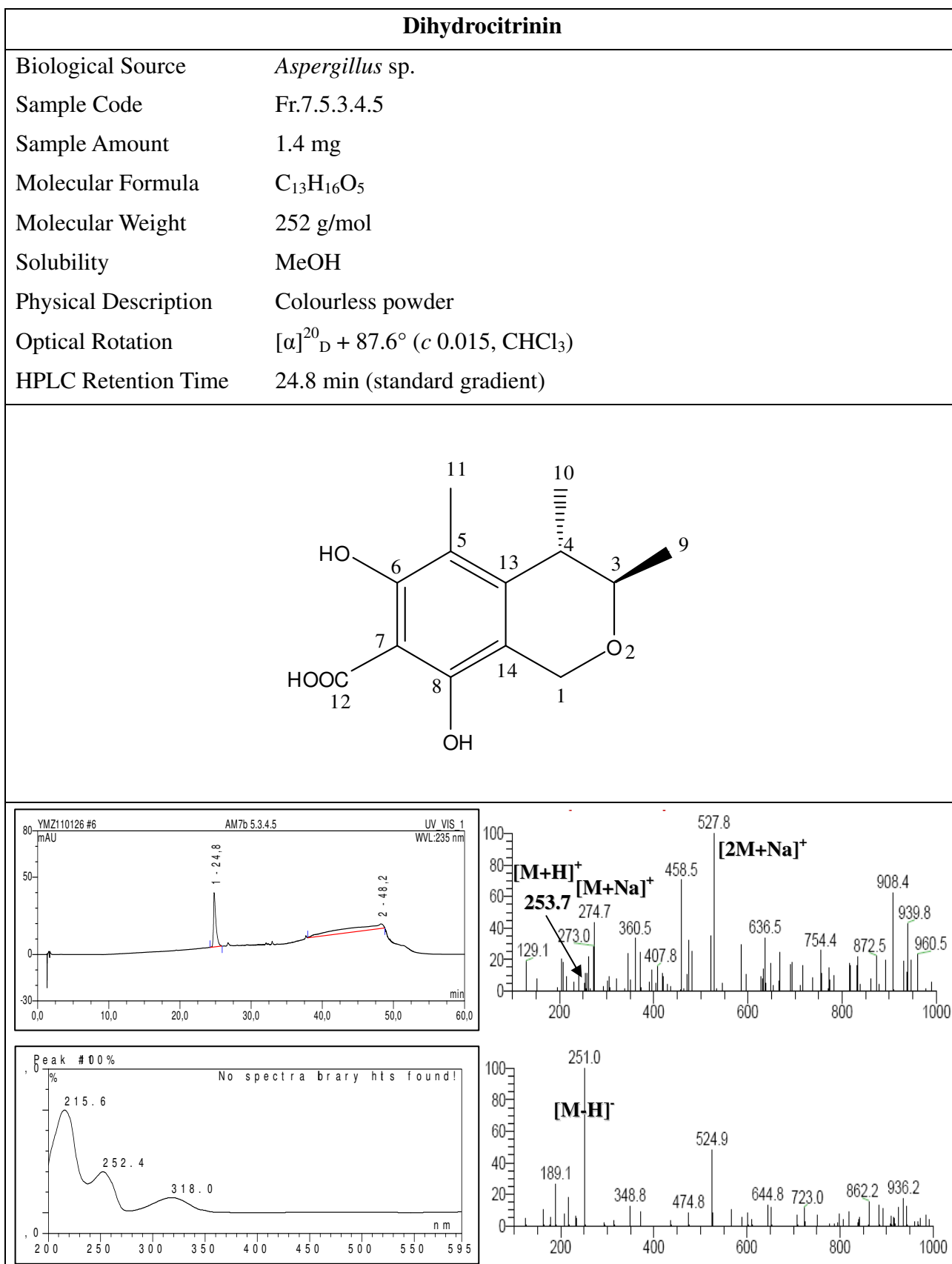


Figure 3.1.28 HMBC correlations of 3'-O-acetylthymidine (15)

3.1.16 Dihydrocitrinin (compound 16, known)



Dihydrocitrinin (**16**) was obtained as a colourless powder (1.4 mg) with an $[\alpha]_D^{20}$ value of + 87.6° (*c* 0.015, CHCl₃) and it displayed UV absorbances at λ_{\max} (MeOH) 215.6, 252.4, and 318.0 nm. Its molecular weight was suggested as 252 g/mol according to the molecular ion peaks observed at *m/z* 253.7 [M+H]⁺ (base peak), 274.7 [M+Na]⁺, and 527.8 [2M+Na]⁺ in the positive mode and at *m/z* 251.0 [M-H]⁻ (base peak) in the negative mode by ESI-MS analysis. The ¹H NMR spectrum (Table 3.1.17) showed an oxygenated methylene group at δ 4.62 ppm (H-1), two methine groups at δ 3.93 and 2.68 ppm (H-3 and H-4, respectively), an aromatic methyl singlet at δ 2.07 ppm (H-11), and two methyl doublets at δ 1.24 and 1.23 ppm (H-9 and H-10, respectively). The ¹³C NMR spectrum indicated the presence of 13 carbon signals, assigned to the carboxyl carbonyl carbon at δ 172.0 ppm (C-12), two oxygenated sp² carbons at δ 158.8 and 155.7 ppm (C-6 and C-8, respectively), four sp² quaternary carbons at δ 144.3, 113.9, 110.7 and 96.2 ppm (C-13, C-5, C-14 and C-7, respectively), two oxygenated methine carbons at δ 73.6 and 60.1 ppm (C-3 and C-1, respectively), one methine carbon at δ 36.6 ppm (C-4), and two methyl carbons at δ 20.6 and 18.2 ppm (C-10 and C-9, respectively), and one aromatic methyl carbon δ 10.1 ppm (C-11). Analysis of ¹H-¹H COSY spectrum of **16** established the presence of one spin system, including the correlations observed for H-3 to H-9, for H-3 to H-4, and for H-4 to H-10. The interpretation of the HMQC spectrum allowed the assignment of proton signals to the corresponding proton-bearing carbon atoms. The connection between the different substructures of **16** was determined by inspection of the HMBC spectrum (Figure 3.1.29). HMBC correlations were observed for the methylene protons CH₃-1 to C-3, C-13, and C-14, for the aromatic methyl group protons CH₃-11 to C-5, C-6, and C-13, for the methyl protons CH₃-9 to C-3 and C-4, and for the methyl protons CH₃-10 to C-3, C-4, and C-13. Accordingly, the structure of **16** was determined as dihydrocitrinin on the basis of its spectroscopic data combined with comparison with reported data (Jack *et al.*, 1992).

Table 3.1.17 NMR data for dihydrocitrinin (16)

Position	16 CD ₃ OD, δ (ppm), J in Hz		Reference CDCl ₃ , δ (ppm), J in Hz (Jack <i>et al.</i> , 1992)	
	¹ H (500 MHz)	¹³ C (75 MHz)	¹ H (250 MHz)	¹³ C (63 MHz)
1	4.62 q (15.1)	60.1	4.73 s	58.6
2				
3	3.93 dq (2.5, 6.6)	73.6	4.04 q	74.0
4	2.68 dq (2.6, 7.0)	36.6	2.69 q	35.7
5		113.9		114.4
6		158.8		157.3
7		96.2		96.8
8		155.7		154.2
9	1.24 d (5.0)	18.2	1.26 d (6.5)	17.9
10	1.23 d (4.7)	20.6	1.26 d (6.5)	19.9
11	2.07 s	10.1	2.10 s	10.0
12		172.0		172.8
13		144.3		146.5
14		110.7		111.7

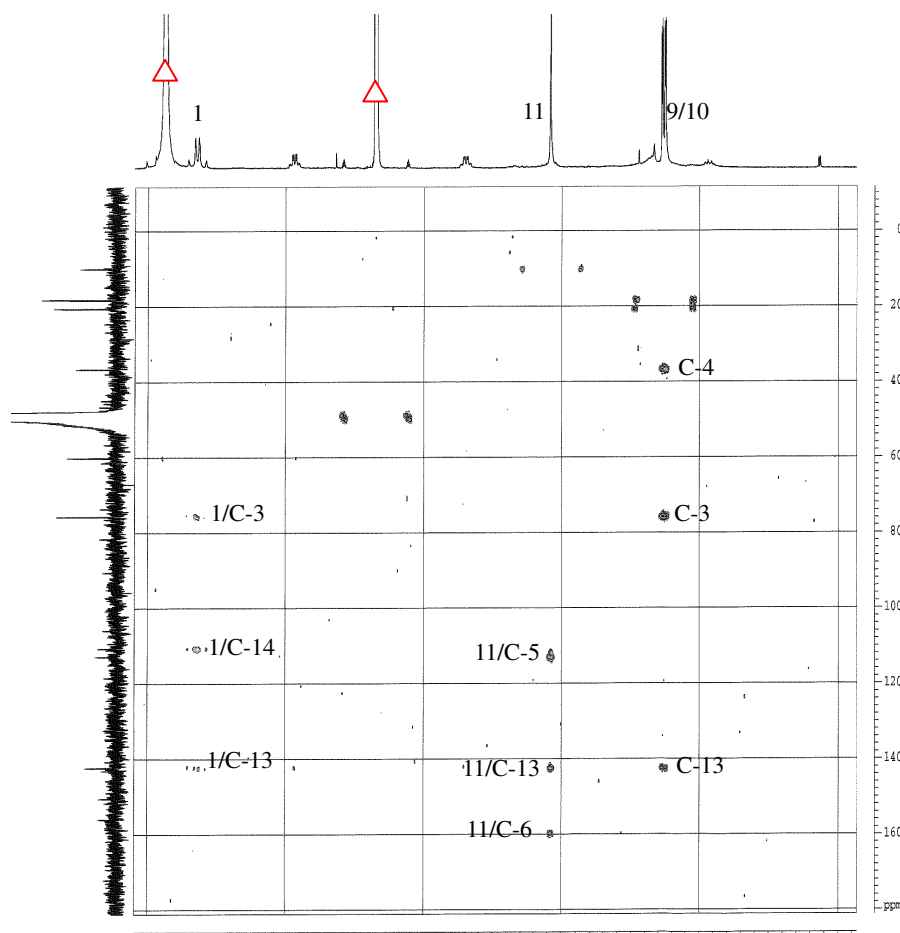
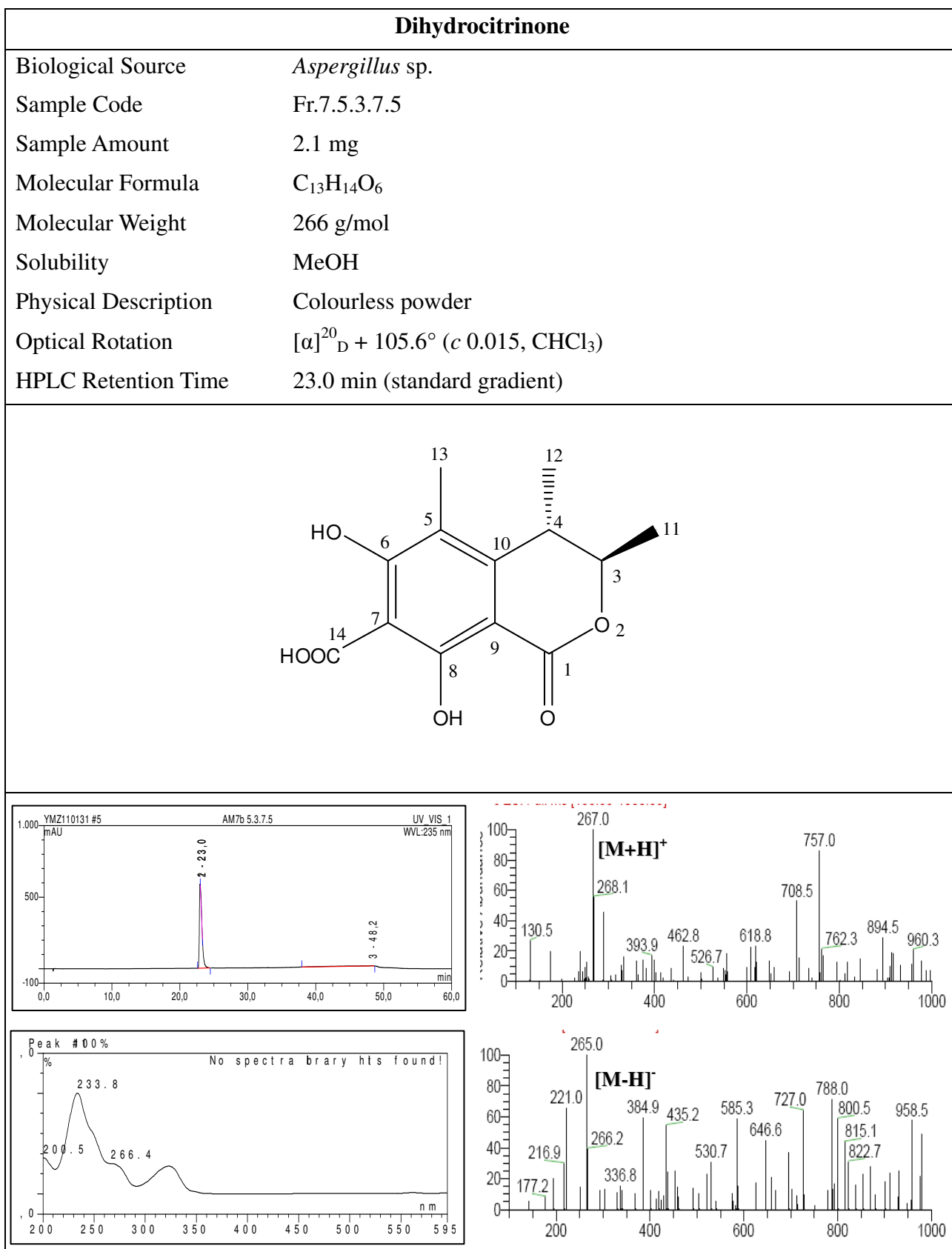


Figure 3.1.29 HMBC correlations of dihydrocitrinin (16)

3.1.17 Dihydrocitrinone (compound 17, known)

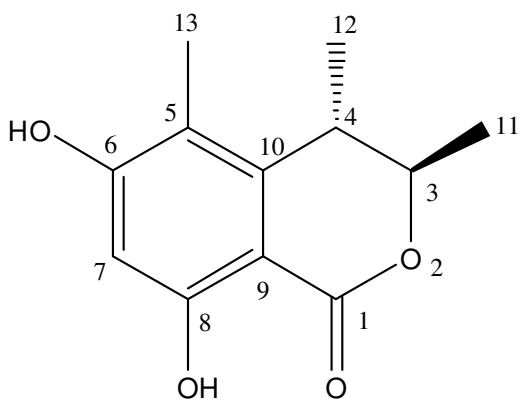
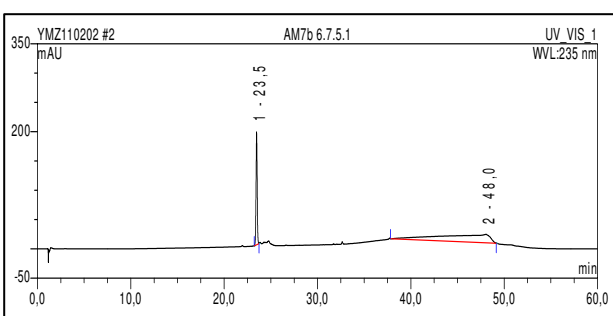
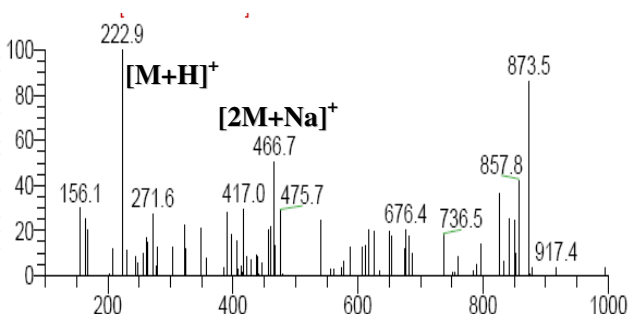
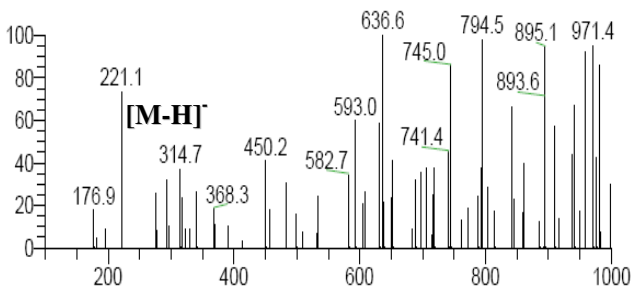
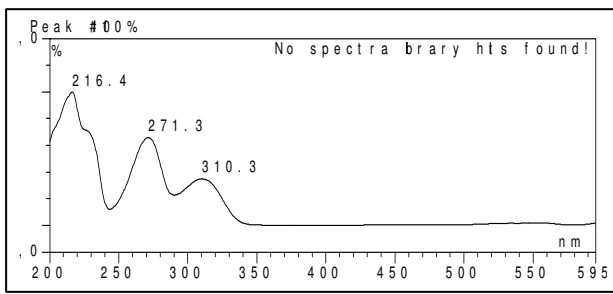


Dihydrocitrinone (**17**) was isolated as a colourless powder (2.1 mg) with an $[\alpha]_D^{20}$ value of + 105.6° (*c* 0.015, CHCl₃) and it displayed UV absorbances at λ_{\max} (MeOH) 200.5, 233.8, and 266.4 nm. Its molecular weight was established as 266 g/mol based on the molecular ion peaks observed at m/z 267.0 [M+H]⁺ (base peak) in the positive mode and at m/z 265.0 [M-H]⁻ (base peak) in the negative mode by ESI-MS analysis, indicating an increase by 14 amu in the molecular weight compared to **16**. The ¹H NMR spectrum (Table 3.1.18) indicated the presence of two methine groups at δ 4.75 ppm and 3.22 ppm (H-3 and H-4, respectively), an aromatic methyl singlet at δ 2.12 ppm (H-13), and two methyl doublets at δ 1.32 ppm and 1.24 ppm (H-12 and H-11, respectively) in analogy to **16**. This suggested that both compounds **16** and **17** have the same basic molecular framework. ¹H and ¹³C NMR spectra of **17** were similar to those of **16** except for the replacement of the methylene group (CH₂-1) by a carbonyl group, which corresponded to the difference in molecular weight between both compounds. Consequently, the structure of **17** was determined as dihydrocitrinone according to its spectroscopic data in addition to comparison with reported data (Xin *et al.*, 2007).

Table 3.1.18 NMR data for dihydrocitrinone (17)

Position	17 CD ₃ OD, δ (ppm), <i>J</i> in Hz		Reference CDCl ₃ , δ (ppm), <i>J</i> in Hz (Xin <i>et al.</i> , 2007)	
	¹ H (300 MHz)	¹³ C (75 MHz)	¹ H (500 MHz)	¹³ C (125 MHz)
1				168.5
2				
3	4.75 m	81.0	4.53 q (6.6)	79.6
4	3.22 m	36.5	3.05 q (6.9)	36.9
5		114.3		113.8
6		166.3		166.6
7				101.7
8				165.8
9				103.8
10		148.7		148.2
11	1.24 d (6.5)	20.5	1.19 d (6.6)	20.9
12	1.32 d (6.5)	20.1	1.24 d (6.9)	20.3
13	2.12 s	10.5	2.04 s	10.9
14				177.9

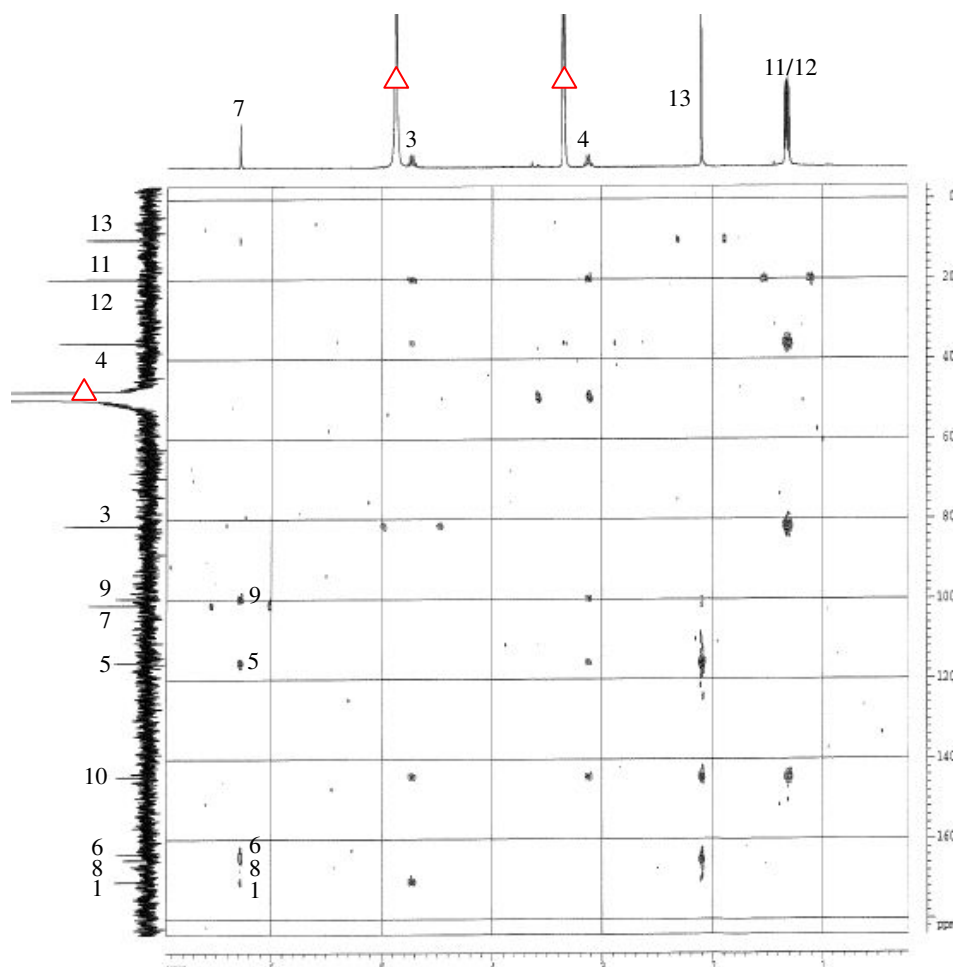
3.1.18 Decarboxydihydrocitrinone (compound 18, known)

Decarboxydihydrocitrinone	
Biological Source	<i>Aspergillus</i> sp.
Sample Code	Fr.7.6.7.5.1
Sample Amount	2.0 mg
Molecular Formula	C ₁₂ H ₁₄ O ₄
Molecular Weight	222 g/mol
Solubility	MeOH
Physical Description	Colourless powder
Optical Rotation	$[\alpha]_D^{20}$ -18.2° (c 0.26, MeOH)
HPLC Retention Time	23.5 min (standard gradient)
	
	
	
	
	

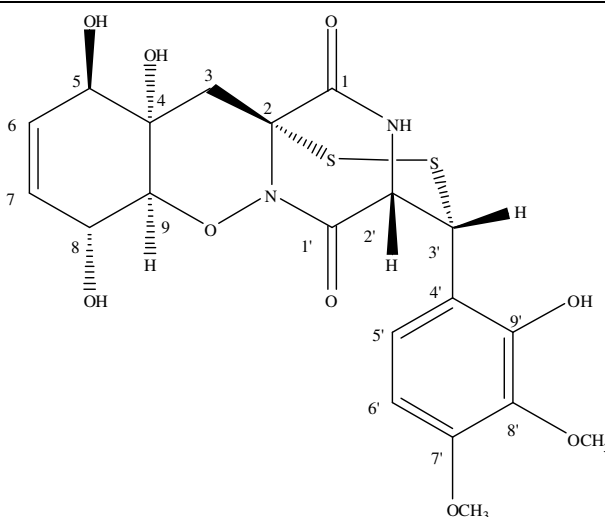
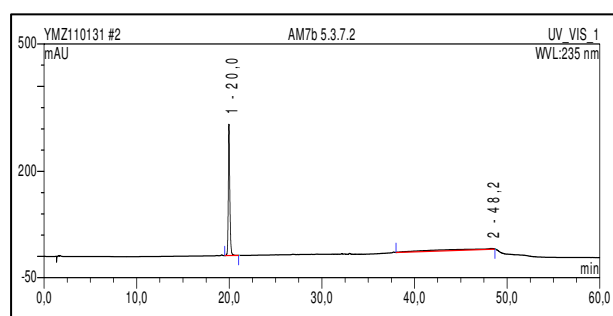
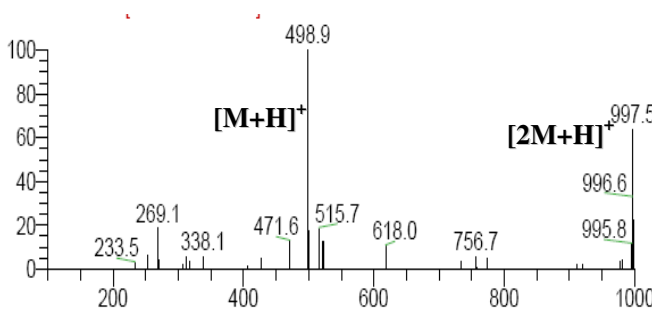
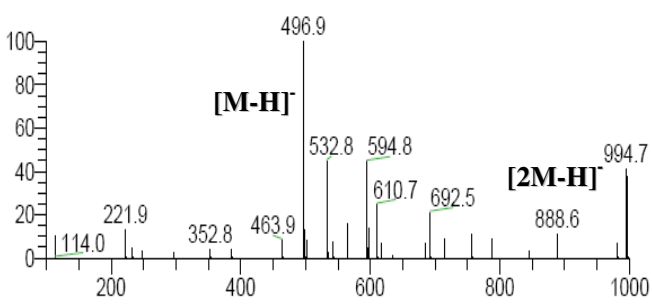
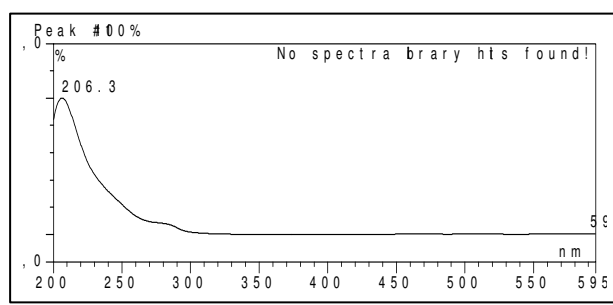
Compound **18** was obtained as a colourless powder (2.0 mg) giving UV absorbances at λ_{\max} (MeOH) 216.4, 271.3, and 310.3 nm and an $[\alpha]_D^{20}$ value of -18.2° (c 0.26, MeOH). Its molecular formula was established as $C_{12}H_{14}O_4$ on the basis of the molecular ion peaks observed at m/z 222.9 $[M+H]^+$ (base peak) and 466.7 $[2M+Na]^+$ in the positive mode and at m/z 221.1 $[M-H]^-$ (base peak) in the negative mode by ESI-MS analysis, thus revealing a 44 amu decrease in the molecular weight compared with **17**. This was further supported by inspection of 1H and ^{13}C NMR spectra. The 1H NMR spectrum (Table 3.1.19) displayed familiar features of compounds **16** and **17** including the presence of two methine groups at δ 4.72 ppm and 3.13 ppm (H-3 and H-4, respectively), an aromatic methyl singlet at δ 2.11 ppm (H-13), and two methyl doublets at δ 1.32 ppm and 1.30 ppm (H-11 and H-12, respectively), in addition to an aromatic proton at δ 6.28 ppm (H-7). The ^{13}C NMR spectrum of **18** (Table 3.1.19) confirmed the presence of 12 carbon atoms in the structure, including six quaternary carbon atoms as indicated by the DEPT experiment. Analysis of 1H - 1H COSY spectrum of **18** established the presence of one spin system, including the correlations observed for H-3 to H-11, for H-3 to H-4, and for H-4 to H-12. Interpretation of the HMQC spectrum allowed the assignment of proton signals to the corresponding proton-bearing carbon atoms. The connection between the different substructures of **18** was determined by inspection of HMBC spectrum (Figure 3.1.30). HMBC correlations were observed for the aromatic proton H-7 to C-5, C-6, C-8, and C-9, as well as the omega correlation to C-1, for the aromatic methyl group protons CH₃-13 to C-5, C-6, and C-10, for the methyl protons CH₃-11 to C-3 and C-4, and for the methyl protons CH₃-12 to C-3, C-4, and C-10. Accordingly, compound **18** has the same basic molecular framework of **17**, apart from the replacement of the carboxyl group at C-7 in **17** by an aromatic proton (H-7), which corresponded to the difference in molecular weight between both compounds. Therefore, the structure of **18** was confirmed as decarboxydihydrocitronone based on its spectroscopic data (Table 3.1.19) and by comparison with reported data (Han *et al.*, 2009).

Table 3.1.19 NMR data for decarboxydihydrocitronone (18)

Position	18 CD ₃ OD, δ (ppm), J in Hz		Reference CDCl ₃ , δ (ppm), J in Hz (Han <i>et al.</i> , 2009)	
	¹ H (300 MHz)	¹³ C (75 MHz)	¹ H (400 MHz)	¹³ C (100 MHz)
1		170.5		170.4
2				
3	4.72 q (6.6)	81.5	4.69 q (6.6)	81.5
4	3.13 q (6.8)	35.8	3.08 q (7.0)	35.7
5		115.6		115.6
6		163.7		163.6
7	6.28 s	101.4	6.25 s	101.3
8		165.0		164.9
9		99.7		99.7
10		144.3		144.2
11	1.32 d (6.0)	19.8	1.28 d (6.1)	19.8
12	1.30 d (6.5)	19.9	1.27 d (6.9)	19.9
13	2.11 s	10.0	2.06 s	10.0

**Figure 3.1.30 HMBC correlations of decarboxydihydrocitronone (18)**

3.1.19 Pretrichoderamide A (compound 19, known)

Pretrichoderamide A	
Biological Source	<i>Aspergillus</i> sp.
Sample Code	Fr.7.5.3.7.2
Sample Amount	5.2 mg
Molecular Formula	C ₂₀ H ₂₂ N ₂ O ₉ S ₂
Molecular Weight	498 g/mol
Solubility	MeOH
Physical Description	Pale yellow solid
Optical Rotation	$[\alpha]_D^{20} -132.0^\circ$ (<i>c</i> 0.10, MeOH)
HPLC Retention Time	20.0 min (standard gradient)
	
	
	
	
	

Compound **19** was isolated as a pale yellow solid (5.2mg) showing a UV absorbance band at λ_{max} (MeOH) 206.3 nm and an $[\alpha]_{\text{D}}^{20}$ value of -132.0° (c 0.1, MeOH). Its molecular weight was determined as 498 g/mol according to the molecular ion peaks observed at m/z 498.9 $[\text{M}+\text{H}]^+$ (base peak) and 997.5 $[2\text{M}+\text{H}]^+$ in the positive mode and at m/z 496.9 $[\text{M}-\text{H}]^-$ (base peak) in the negative mode upon ESI-MS analysis. The molecular formula of **19** was suggested as $\text{C}_{20}\text{H}_{22}\text{N}_2\text{O}_9\text{S}_2$ by ESIMS, ^1H and ^{13}C NMR data. The ^1H and ^{13}C NMR spectra of **19** were very similar to those of gliovirin (**19a**) (Stipanovic *et al.*, 1982). The ^1H NMR spectrum of **19** (Table 3.1.20) revealed the presence of two olefinic AB systems the protons of which appearing at δ 7.52 ppm ($J = 8.8$ Hz, H-5'), 6.56 ppm ($J = 8.9$ Hz, H-6'), 5.68 ppm ($J = 10.2, 1.8$ Hz, H-7) and 5.64 ppm ($J = 10.2, 1.6$ Hz, H-6), five aliphatic methine protons at δ 4.72 ppm (H-3'), 4.57 ppm (H-2'), 4.54 ppm (H-8), 4.38 ppm (H-5), and 4.11 ppm (H-9), one methylene group at δ 2.34 and 2.25 ppm (CH_2 -3), and two methoxy groups at δ 3.88 ppm (OCH_3 -7') and 3.82 ppm (OCH_3 -8'). The ^{13}C NMR (Table 3.1.20) and DEPT spectra revealed the presence of twenty carbon atoms in the structure of **19** including eight quaternary carbon atoms. The ^{13}C NMR spectra displayed two carbonyl groups with chemical shifts characteristic of amides at δ_{C} 168.0 and 169.6 ppm (C-1' and C-1, respectively). Moreover, eight olefinic carbon atoms were observed, including four signals corresponding to the previously mentioned AB systems in addition to four quaternary signals, three of which being oxygenated. The three aromatic carbons with oxygen substituents resonated at δ_{C} 154.8 ppm (H-7'), 149.2 ppm (H-9'), and 137.4 ppm (H-8'). Two methoxyl groups were also detected at δ_{C} 56.3 and 61.1 ppm (OCH_3 -7' and OCH_3 -8', respectively). Analysis of ^1H - ^1H COSY spectrum of **19** established the presence of three spin systems: one spin system including the correlation observed for H-5' to H-6', the second for H-2' to H-3', and the third comprising the five methine protons H-5 to H-9 (Figure 3.1.31).

The interpretation of the HMQC spectrum allowed the assignment of proton signals to the corresponding proton-bearing carbon atoms. In addition, the connection of the different substructures of **19** was determined by interpretation of the HMBC spectrum

(Figure 3.1.32). The methylene protons CH₂-3 correlated with the carbonyl carbon C-1 (δ_C 169.6 ppm), the oxygenated quaternary carbon C-4 (δ_C 72.6 ppm), the quaternary carbon C-2 (δ_C 70.2 ppm), which is connected to the disulfide and to both methine carbons C-5 (δ_C 75.9 ppm) and C-9 (δ_C 88.3 ppm). Correlations observed for the olefinic AB spin systems included those of H-6 to C-4 and C-8 (δ_C 66.6 ppm), of H-7 to C-5 and C-9, of H-5' to C-3', C-7', C-8' and C-9' (δ_C 46.5, 154.8, 137.4, and 149.2 ppm, respectively), and of H-6' to C-4' (δ_C 117.4 ppm), C-7', C-8' and C-9'. Moreover, correlations of H-2' to C-1, C-1' (δ_C 168.0 ppm), C-3' and C-4', and of H-3' to C-1', C-2' (δ_C 61.5 ppm), C-4', C-5' (δ_C 124.2 ppm) and C-9' provided the connections of the third spin system in the structure of **19**. Remaining HMBC correlations were observed for the methoxy group OCH₃-7' to C-7' (δ_C 154.8 ppm) and for the methoxy group (OCH₃-8') to C-8' (δ_C 137.4 ppm). Therefore, based on the above interpretation and by comparison with reported data (Prapairot *et al.*, 2006), compound **19** was finally identified as pretrichodermamide A.

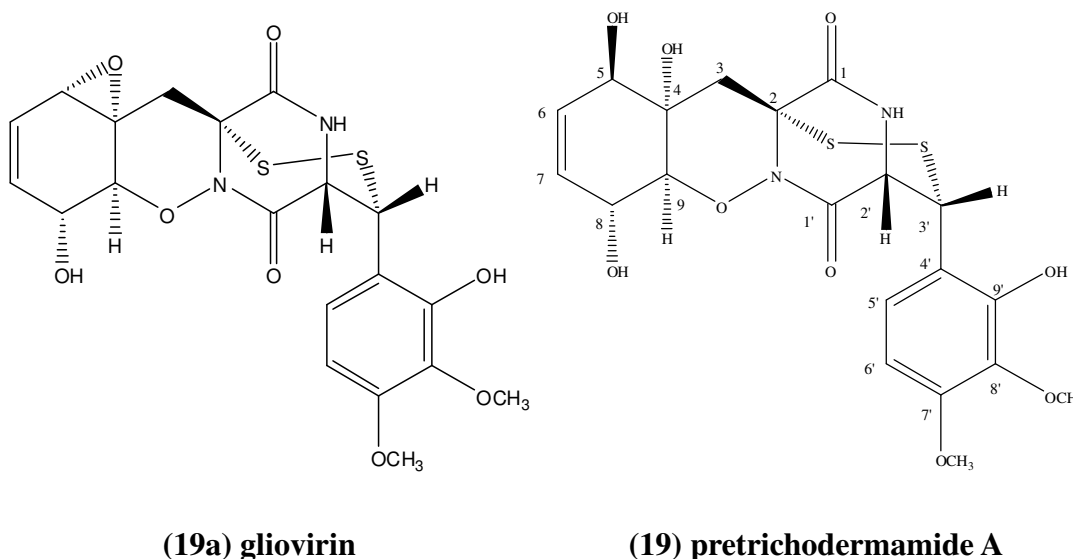


Table 3.1.20 NMR data for pretrichodermamide A (19)

Position	19 CD ₃ OD, δ (ppm), <i>J</i> in Hz		Reference CDCl ₃ , δ (ppm), <i>J</i> in Hz (Prapairat <i>et al.</i> , 2006)	
	¹ H (300 MHz)	¹³ C (75 MHz)	¹ H (400 MHz)	¹³ C (100 MHz)
1		169.6		167.1
2		70.2		69.5
3	2.34 d (16.3) 2.25 d (16.2)	32.1	2.09 d (16.0) 1.96 d (16.0)	31.9
4		72.6		71.0
4-OH			5.09 brs	
5	4.38 m	75.9	4.16 m	74.3
5-OH			5.26 d (5.1)	
6	5.64 dt (10.2, 1.6)	131.2	5.42 brd (10.4)	129.9
7	5.68 dt (10.2, 1.8)	129.0	5.48 dt (10.4, 2.0)	128.9
8	4.54 m	66.6	4.23 m	64.7
8-OH			5.22 d (6.7)	
9	4.11 d (7.1)	88.3	3.93 d (7.2)	85.7
1'		168.0		164.8
2'	4.57 (4.1, 2.0)	61.5	4.41 dd (4.2, 3.0)	59.0
3'	4.72 d (1.8)	46.5	4.49 d 2.7	45.0
4'		117.4		116.6
5'	7.52 d (8.8)	124.2	7.44 d (8.8)	123.1
6'	6.56 d (8.9)	104.4	6.55 d (8.9)	103.5
7'		154.8		153.1
7'-OCH ₃	3.88 s	56.3	3.78 s	55.9
8'		137.4		136.0
8'-OCH ₃	3.82 s	61.1	3.67 s	60.4
9'		149.2		148.0
9'-OH			9.45 s	
NH			9.05 d (4.4)	

Results

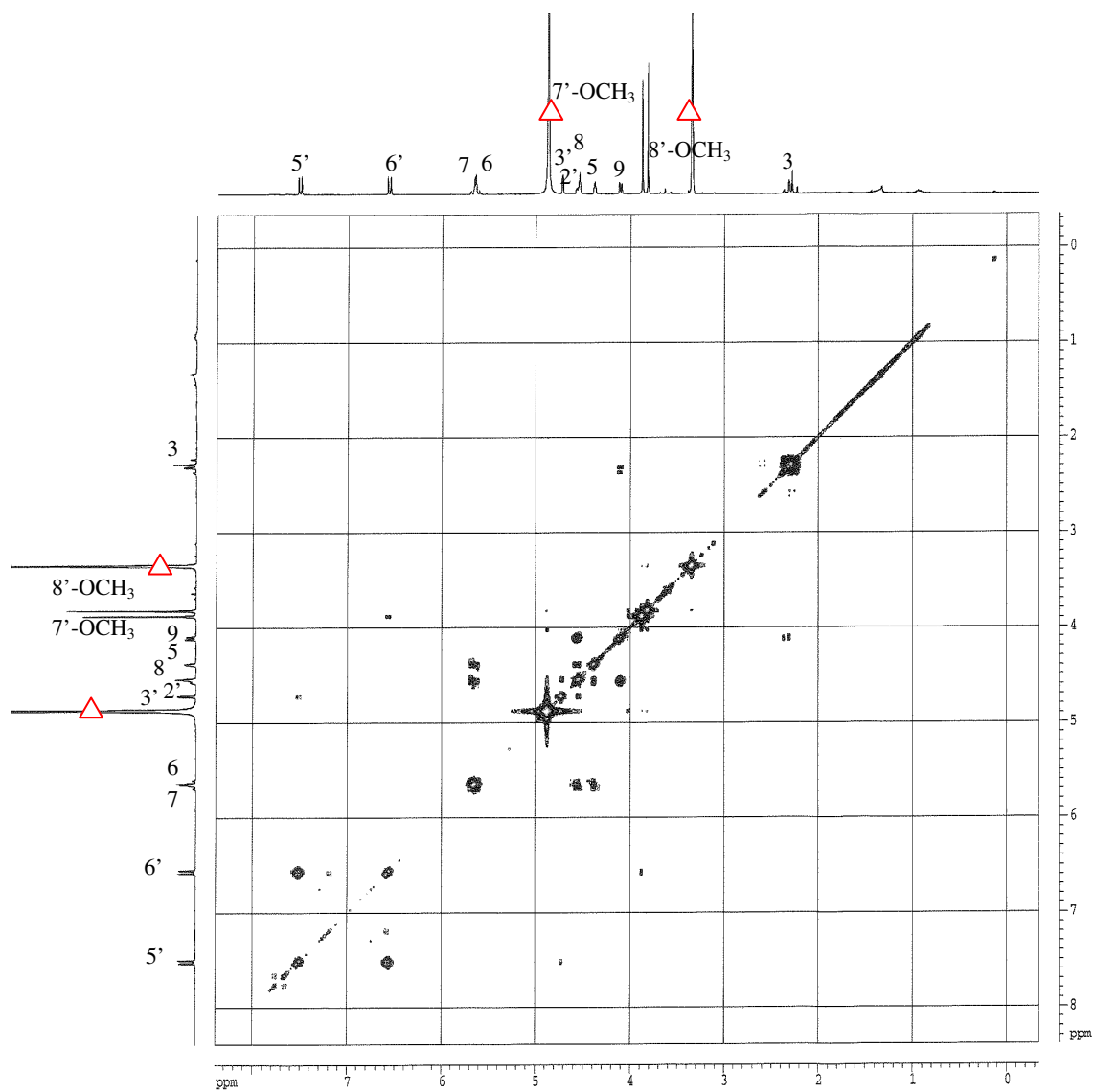


Figure 3.1.31 COSY correlations of pretrichodermamide A (19)

Results

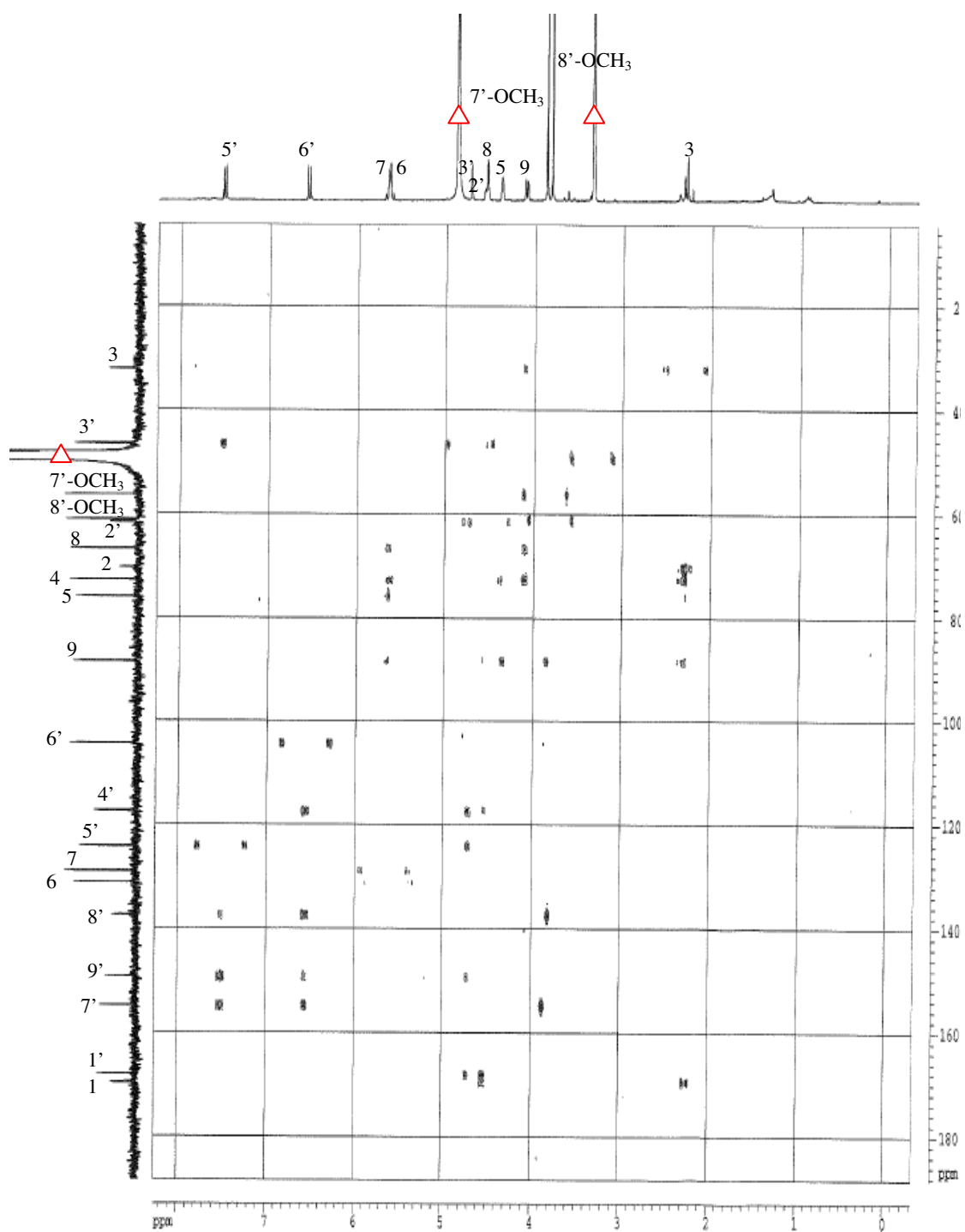
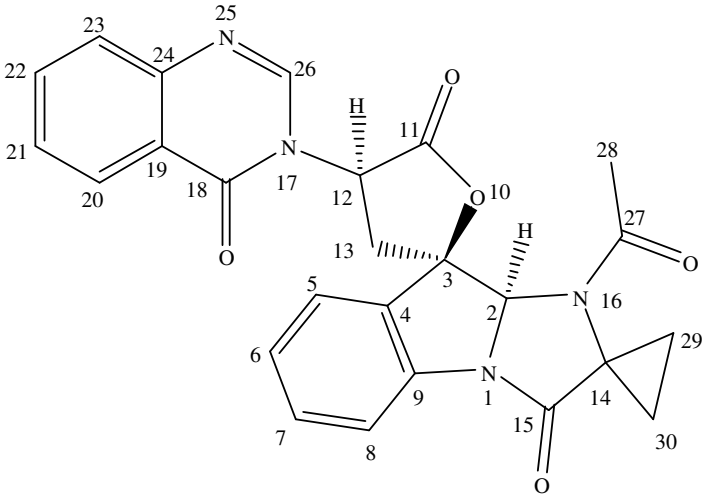
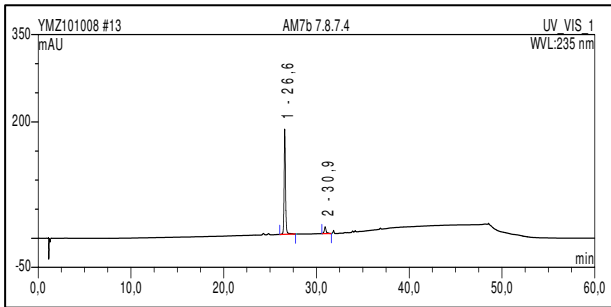
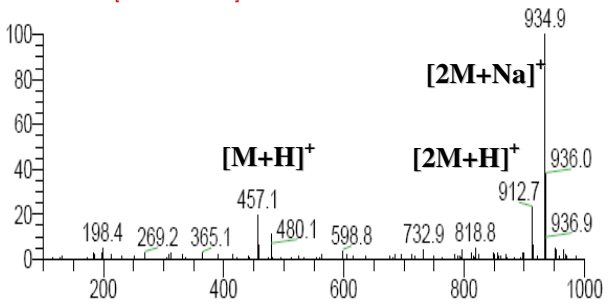
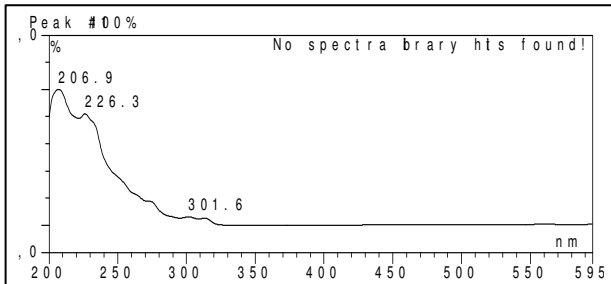


Figure 3.1.32 HMBC correlations of pretrichodermamide A (19)

3.1.20 Tryptoquivaline K (compound 20, new)

Tryptoquivaline K	
Biological Source	<i>Aspergillus</i> sp.
Sample Code	Fr.7.7.8.7.4
Sample Amount	8.0 mg
Molecular Formula	C ₂₅ H ₂₀ N ₄ O ₅
Molecular Weight	456 g/mol
Solubility	MeOH
Physical Description	White amorphous solid
Optical Rotation	$[\alpha]_D^{20} -8.0^\circ$ (c 0.10, MeOH)
HPLC Retention Time	26.6 min (standard gradient)
	
	
	
	

Compound **20** was obtained as a white amorphous solid (8.0 mg) with an $[\alpha]_D^{20}$ value of -8.0° (c 0.10, MeOH) and it displayed UV absorbances at λ_{\max} (MeOH) 206.9, 226.3, and 301.6 nm. Its molecular formula was determined as $C_{25}H_{20}N_4O_5$ by HRESIMS ($[M+H]^+$ observed at m/z 457.1503), indicating 18 elements of unsaturation. Thorough inspection of its UV and NMR data (Table 3.1.21) revealed spectroscopic features comparable to those of tryptoquivaline metabolites, previously reported from *A. fumigatus* (Yamazaki *et al.*, 1976; 1977; 1978). 1H and ^{13}C NMR (Table 3.1.21) indicated the presence of two 1,2-disubstituted benzene rings, an aromatic proton resonating downfield at δ_H 8.45 (δ_C 149.1) ppm (CH-26), three methylene groups, two of which showing upfield chemical shifts characteristic for a cyclopropane moiety at δ_H 1.47/2.12 (δ_C 13.8) and δ_H 1.42/1.74 (δ_C 13.3) ppm (CH₂-29 and CH₂-30, respectively), two methine protons situated on nitrogen-bearing carbon atoms as indicated by their downfield chemical shift values at δ_H 6.16 (δ_C 85.1) and δ_H 5.51 (δ_C 60.0) ppm (CH-2 and CH-12, respectively), and a methyl amide group resonating at δ_H 2.18 (δ_C 21.8) ppm (CH₃-28).

Furthermore, ^{13}C NMR and DEPT spectra disclosed signals for eight sp^2 quaternary carbons, three of which were attributed to the amide carbonyl groups at C-15, C-18 and C-27 (δ_C 173.1, 162.1 and 171.4 ppm, respectively). The upfield chemical shift of C-18 indicated its α,β -unsaturated nature. The remaining signals were assigned to the ester carbonyl group at C-11 (δ_C 173.1 ppm), and to the aromatic carbons (C-4, C-9, C-19 and C-24). The deshielded signals of C-9 and C-24 (δ_C 140.6 and 149.1 ppm, respectively) indicated their nitrogenated nature. In addition, two sp^3 quaternary carbons were detected downfield at δ_C 87.2 and 47.9 ppm (C-3 and C-14, respectively), which implied their attachment to oxygen and nitrogen atoms, respectively. Analysis of the COSY spectrum (Table 3.1.21 and Fig 3.1.33) established the presence of four spin systems, based on correlations of the methylene protons resonating at δ_H 3.42 and 3.54 ppm (CH₂-13) to the deshielded methine group at C-12, for the protons of both methylene groups at C-29 and C-30 to each other, and for the two aromatic ABCD systems (H-5 to H-8 and H-20 to H-23). Assignment of

proton signals to the corresponding proton-bearing carbon atoms was achieved by interpretation of the HMQC spectrum.

The different substructures of **20** were connected based on the correlations observed in the HMBC spectrum (Table 3.1.21 and Fig 3.1.34). The more deshielded aromatic ABCD system (H-20 to H-23) was attributed to a 4-quinazolinone moiety on the basis of the correlations observed for H-23 to C-19 and C-21, for H-22 to C-20 and C-24, for H-21 to C-19 and C-23, for H-20 to C-22, C-24 and to the amide carbonyl group at C-18, for H-26 to C-18 and C-24, in addition to the downfield chemical shift of C-24. Furthermore, correlations of H-26 to C-12, and of H-12 to C-18 and C-26 established the connection to the ethylene group CH(12)CH₂(13) through the nitrogen atom N-17. Both H-12 and CH₂-13 correlated to the ester carbonyl group at C-11, as well as to each other. CH₂-13 correlated also to the oxygenated sp³ quaternary carbon C-3 to close the central γ -butyrolactone ring. Further correlations of CH₂-13 were observed to the aromatic quaternary carbon C-4, and to the downfield shifted tertiary carbon C-2, both belonging to the indoline moiety which also includes the second aromatic ABCD system (H-5 to H-8). This was corroborated by correlations of H-8 to C-4 and C-6, of H-7 to C-5 and C-9, of H-6 to C-4 and C-8, and of H-5 to C-3, C-7 and C-9. Accordingly, the indoline moiety was connected to the γ -butyrolactone ring through a spiro-junction at C-3. Correlations of H-2 to C-3 and C-13 provided additional evidence. Both H-2 and CH₃-28 correlated to the amide carbonyl at C-27 thus establishing the acetamide group at N-16. Furthermore, H-2 and both cyclopropane methylenes (CH₂-29 and CH₂-30) correlated to the quaternary carbon C-14, which was placed adjacent to N-16 due to its downfield chemical shift. Finally, both methylene groups correlated to each other and to the amide carbonyl at C-15, which was connected to N-1 to rationalize the remaining element of unsaturation. Accordingly, the NMR data of **20** indicated an analogue of the known tryptoquivaline J (Han *et al.*, 2007) bearing an additional acetyl function at N-16. Furthermore, the alanine residue in tryptoquivaline J was replaced by a 1-aminocyclopropane-1-carboxylic acid residue in **20**.

The relative configuration of **20** was deduced from analysis of the ROESY spectrum. Key correlations were observed for both H-12 and CH₂-13 to H-2, indicating a *cis* configuration between H-2 and H-12, and thus a relative configuration of (2*S**,3*R**,12*R**) for **20**. The absolute configuration of **20** was determined by TDDFT ECD calculation of its solution conformers. The experimental ECD of **20** showed a strong positive Cotton effect (CE) at 230 nm with positive plateau up to 325 nm and an intense negative CE at 208 nm with a shoulder at 214 nm. The MMFF conformational analysis of **20** provided four conformers, the reoptimization of which at the level of B3LYP/6-31G(d) afforded a major conformer with 99.5% populations. Then TDDFT ECD calculations of (2*S*,3*R*,12*R*)-**20** were performed with TZVP basis set and various functionals (B3LYP, BH&HLYP, PBE0), which consistently reproduced the experimental ECD spectrum with PBE0 giving the best agreement (Figure 3.1.35 and Figure 3.1.36). Hence, the structure of **20** was determined as tryptoquivaline K representing a new natural product.

Table 3.1.21 NMR data for tryptoquivaline K (20)

Position	20 CD ₃ OD, δ (ppm), J in Hz		Correlation		
	¹ H (600 MHz)	¹³ C (125 MHz)	COSY	HMBC	ROESY
1					
2	6.16 s	85.1		3,13,14,27	12,13
3		87.2			
4		134.3			
5	8.17 br d (7.6)	128.0	6	3,7,9	
6	7.47 ddd (1.7, 7.3, 7.4)	128.1	5,7	4,7,8	
7	7.61 ddd (1.3, 7.3, 7.9)	132.6	6,8	5,9	
8	7.64 dd (1.8, 7.9)	117.8	9	4,6	
9		140.6			
10					
11		173.1			
12	5.51 dd (8.6, 10.7)	60.0	13	11,13,18,26	2
13	3.42 dd (8.7, 13.6) 3.54 dd (10.7, 13.6)	36.1	12	2,3,4,11,12	2
14		47.9			
15		173.1			
16					
17					
18		162.1			
19		123.7			
20	8.37 dd (1.6, 8.0)	127.5	21	18,22,24	
21	7.68 ddd (1.1, 7.0, 8.1)	129.0	20,22	19,23	
22	7.94 ddd (1.6, 7.1, 8.2)	136.3	21,23	20,24	
23	7.81 br d (7.9)	128.7	22	19,22,21	
24		149.1			
25					
26	8.45 s	149.1		12,18,24	
27		171.4			
28	2.18 s	21.8		27	
29	1.47 ddd (6.0, 7.0, 10.5) 2.12 m (Σ 24.0)	13.8	30	14,15,30	
30	1.42 ddd (6.0, 8.0, 10.5) 1.74 ddd (6.0, 8.0, 10.4)	13.3	29	14,15,29	

Results

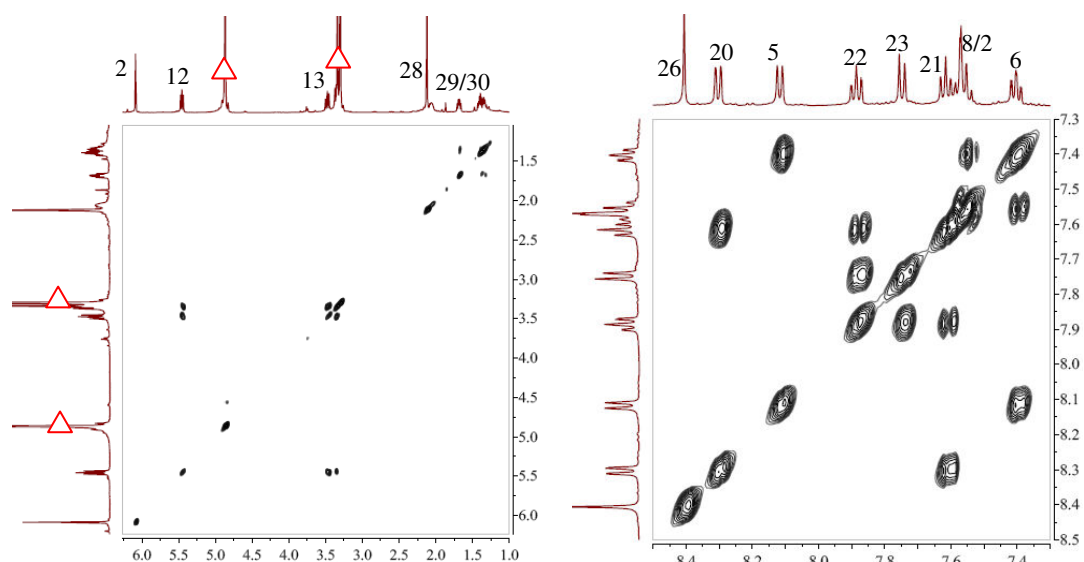


Figure 3.1.33 COSY correlations of tryptoquivaline K (20)

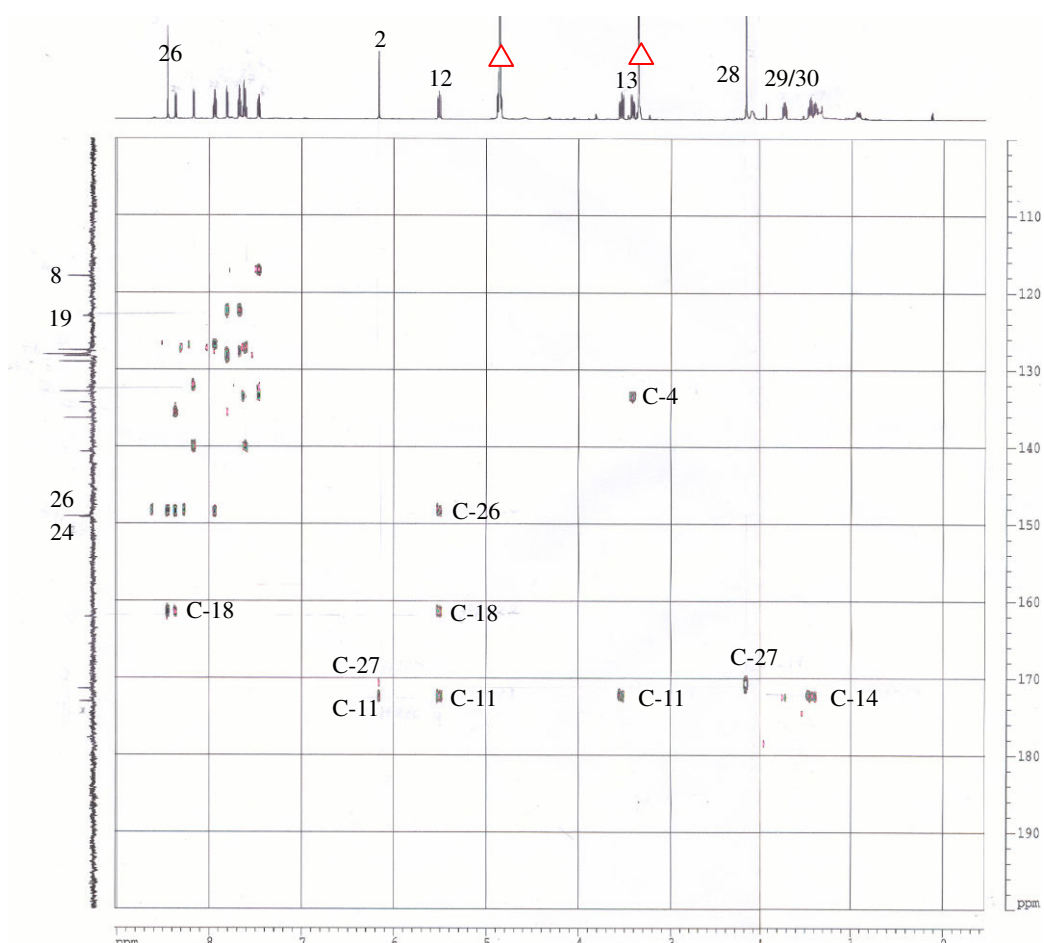


Figure 3.1.34 HMBC correlations of tryptoquivaline K (20)

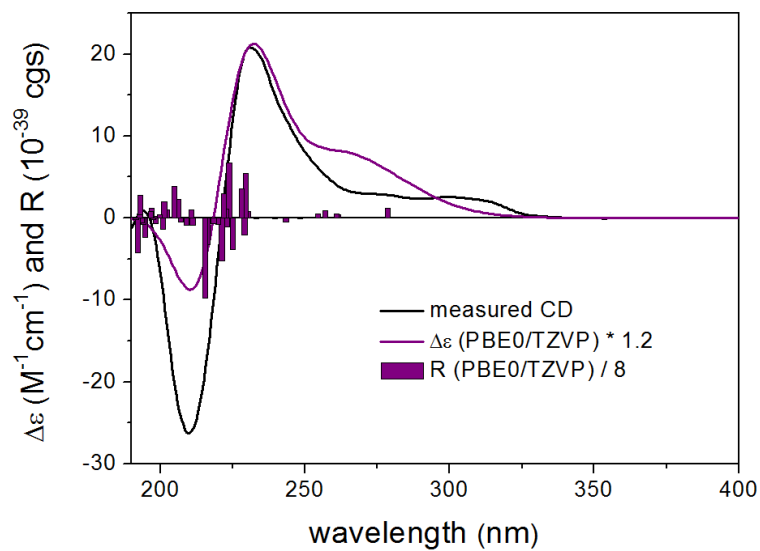


Figure 3.1.35 Experimental ECD spectrum of 20 in acetonitrile compared with the PBE0/TZVP spectrum calculated for the lowest-energy conformer (99.5%) of the (2*S*,3*R*,12*R*)-enantiomer. Bars represent rotational strengths

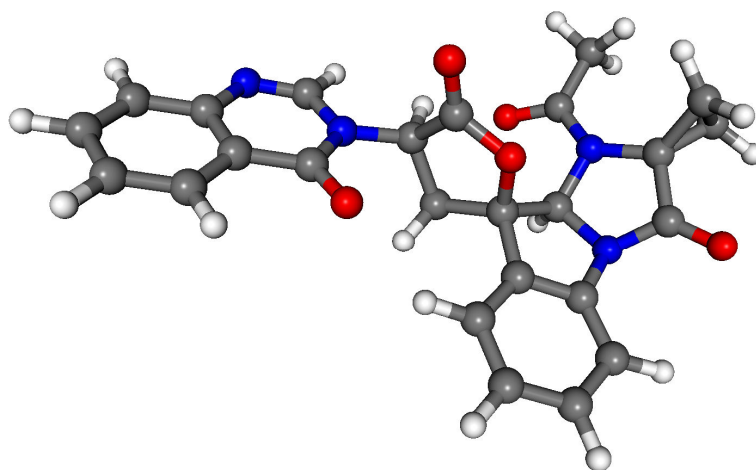
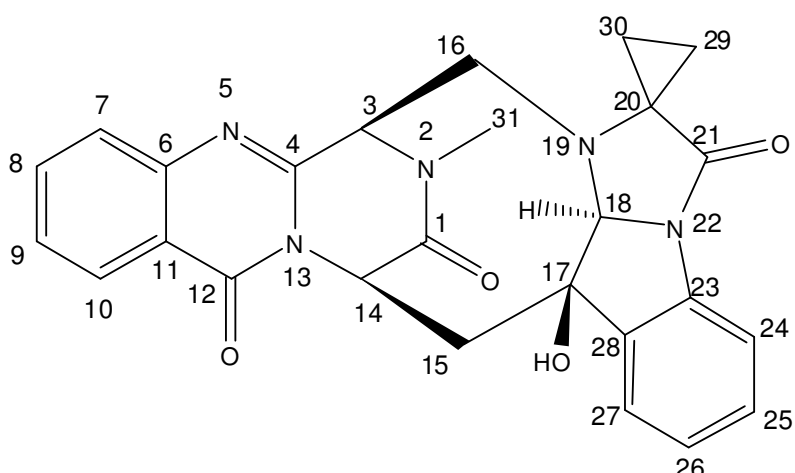
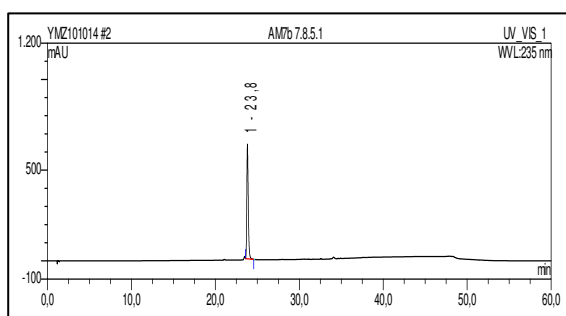
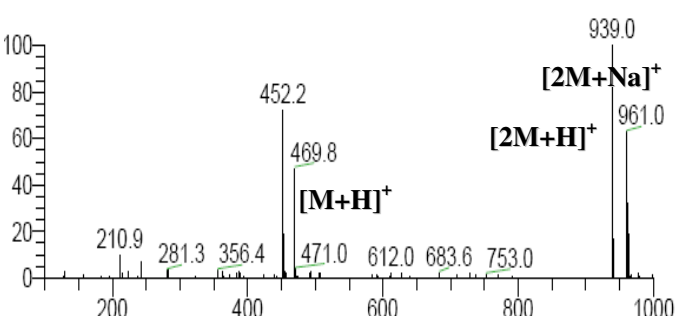
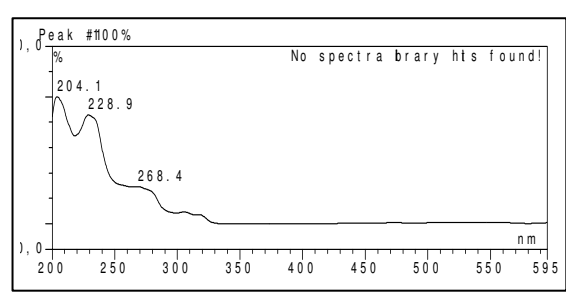


Figure 3.1.36 Computed low-energy conformer of 20 (99.5%)

3.1.21 Fumiquinazoline K (compound 21, new)

Fumiquinazoline K	
Biological Source	<i>Aspergillus</i> sp.
Sample Code	Fr.7.7.8.5.1
Sample Amount	4.2 mg
Molecular Formula	C ₂₆ H ₂₃ N ₅ O ₄
Molecular Weight	469 g/mol
Solubility	MeOH
Physical Description	Yellow amorphous solid
Optical Rotation	$[\alpha]_D^{20} -120.9^\circ$ (<i>c</i> 0.11, MeOH)
HPLC Retention Time	23.8 min (standard gradient)
	
	
	
	

Compound **21** was obtained as a yellow amorphous solid (4.2 mg) with an $[\alpha]_D^{20}$ value of -120.9° (c 0.11, MeOH) and it displayed UV absorbances at λ_{\max} (MeOH) 204.1, 228.9, and 268.4 nm. The $[M+H]^+$ signal at m/z 470.1812 in the HRESIMS of **21** indicated a molecular formula of $C_{26}H_{23}N_5O_4$, thus comprising 18 elements of unsaturation as in **20**. Its physical characteristics were comparable to those of **20**, suggesting a similar basic molecular framework. 1H and ^{13}C NMR (Table 3.1.22) indicated the presence of two 1,2-disubstituted benzene rings, and two methylene groups of a cyclopropane moiety resonating upfield at δ_H 0.15/0.82 (δ_C 14.0) and δ_H 0.90/1.59 (δ_C 11.2) ppm (CH_2 -29 and CH_2 -30, respectively), which were comparable to the respective signals of **20**. In addition, the spectra of **21** displayed signals corresponding to an aliphatic hydroxyl group appearing as a singlet at δ_H 4.47 ppm, three methine protons on nitrogen-bearing carbons at δ_H 5.04 (δ_C 61.8), δ_H 5.24 (δ_C 52.7) and δ_H 5.09 (δ_C 86.2) ppm (CH -3, CH -14 and CH -18, respectively), two methylene groups one of which being adjacent to nitrogen, as indicated by its chemical shift value at δ_H 3.22/3.52 (δ_C 51.1) ppm (CH_2 -16), and a N-methyl group resonating at δ_H 3.06 (δ_C 32.5) ppm (CH_3 -31). Inspection of ^{13}C NMR and DEPT spectra of **21** (Table 3.1.22) revealed the presence of eight sp^2 quaternary carbons as in **20**, including the amide carbonyl groups at C-1, C-12 and C-21 (δ_C 164.9, 160.1 and 174.7 ppm, respectively), and five aromatic carbons (C-4, C-6, C-11, C-23 and C-28), three of which are placed adjacent to nitrogen based on their downfield chemical shifts at δ_C 150.0, 147.4 and 138.0 ppm (C-4, C-6 and C-23, respectively). Moreover, in analogy to **20**, two sp^3 quaternary carbon signals resonating downfield at δ_C 75.9 and 51.1 ppm were assigned to C-17 and C-20, respectively. Examination of the COSY spectrum of **21** (Table 3.1.22 and Fig 3.1.37) disclosed five spin systems, including the familiar aromatic ABCD systems (H-7 to H-10 and H-24 to H-27), the cyclopropane methylene groups (CH_2 -29 and CH_2 -30), and the ethylene group with the deshielded methine $CH(14)CH_2(15)$, which were also detected in **20**, as well as an additional ethylene group $CH(3)CH_2(16)$ possibly flanked by nitrogen as indicated by chemical shift values.

The structural units identified in **21** were connected on the basis of correlations observed in the HMBC spectrum (Table 3.1.22 and Figure 3.1.38). In analogy to **20**, correlations observed for the more deshielded aromatic protons (H-7 to H-10), as well as the downfield chemical shifts of C-4 and C-6, indicated the presence of a 4-quinazolinone moiety. Absence of an aromatic proton singlet and presence of an additional aromatic quaternary carbon implied substitution at C-4 in **21**. Correlations of H-14 to C-4 and C-12 established the connection to the ethylene group CH(14)CH₂(15) through N-13. Both H-14 and CH₂-15 correlated to each other as well as to the amide carbonyl at C-1 and to the tertiary alcohol at C-17. Correlations of CH₃-31 to C-1, C-3, C-4 and C-14 established the additional oxopiperazine ring, which was further corroborated by correlations of H-3 to C-1, C-4 and C-31. CH₂-15 showed further correlations to the aromatic quaternary carbon C-28, and to the downfield shifted tertiary carbon C-18, thus establishing the connection to the indoline moiety through C-17. Correlations observed for 17-OH to C-15, C-17, C-18 and C-28, for H-27 to C-17, and for H-18 to C-15 and C-17, provided additional evidence for the structural assignment. Moreover, H-18 and both cyclopropane methylenes (CH₂-29 and CH₂-30) correlated to the downfield resonating quaternary carbon C-20, as well as to the amide carbonyl at C-21, thus verifying the 1-aminocyclopropane-1-carboxylic acid residue detected in **20**. The remaining correlations of H-3 and H-18 to C-16, together with the downfield chemical shift of CH₂-16, indicating a neighbouring nitrogen (N-19), suggested that N-19 was linked to C-3 through CH₂-16. Correlations of the latter to C-3, C-4, C-18 and C-20 confirmed this connection and hence accounted for the remaining element of unsaturation in the structure of **21**. Consequently, **21** was found to be structurally related to the fumiquinazolines A-J (Liu *et al.*, 2011; Nisho *et al.*, 2000) previously isolated from *A. fumigatus*. More specifically, **21** represents an analogue of the known fumiquinazoline A (Takahashi *et al.*, 1995) differing in the presence of a methyl group at N-2, and the replacement of the methyl groups at C-20 and C-3 in fumiquinazoline A by a cyclopropane moiety and a methylene bridge to N-19.

The relative configuration of **21** was assigned by interpretation of the ROESY spectrum. The presence of the methylene bridge between C-3 and N-19 implied a *cis* configuration of the C-3—C-16 and C-14—C-15 bonds. This was further confirmed by correlations observed for H-18 to CH₂-15, CH₂-16 and CH₃-31, for CH₂-15 to 17-OH and H-27, and for CH₂-16 to CH₂-29 and CH₃-31. Accordingly, a relative configuration of (3*R**,14*R**,17*R**,18*S**) was established for **21**, which is in agreement with the corresponding chirality centers of **20**. The ECD spectrum of **21** was markedly different from that of **20** due to their different skeleton and thus the comparison of their ECD spectra could not be used to determine the absolute configuration of **21**. The ECD spectrum has a broad negative transition above 260 nm consisting of three overlapping CEs, a positive CE at 250 nm, a negative one at 221 nm with shoulder at 233 nm and a strong positive one at 205 nm. The MMFF conformational search and DFT reoptimization afforded a single conformer with 99.9% population for the ECD calculation. The TDDFT ECD spectrum of this conformer with (3*R*,14*R*,17*R*,18*S*) absolute configuration was in agreement with the experimental ECD curve allowing an unambiguous configurational assignment (Figure 3.1.39 and Figure 3.1.40). The corresponding chirality centers of **20** and **21**, C-12/C-14 and C-3/C-17, were found homochiral. Thus, **21** was identified as a new natural product and named fumiquinazoline K.

Table 3.1.22 NMR data for fumiquinazoline K (21)

Position	21 DMSO- <i>d</i> ₆ , δ (ppm), <i>J</i> in Hz		Correlation		
	¹ H (600 MHz)	¹³ C (75 MHz)	COSY	HMBC	ROESY
1		164.9			
2					
3	5.04 d (6.4)	61.8	16	31,16,4,1	
4		150.0			
5					
6		147.4			
7	7.62 br d (7.8)	126.3	8	11,9,6,12	
8	7.82 ddd (1.7, 7.1, 8.2)	134.6	7,9	10,6	
9	7.50 ddd (1.1, 7.0, 8.1)	126.3	8,10	11,7,8,6	
10	8.14 dd (1.7, 8.0)	126.3	9	8,6,12	
11		119.8			
12		160.1			
13					
14	5.24 br d (8.4)	52.7	15	15,17,4,12,1	
15	2.42 dd (1.1, 15.3)	35.6	14	17,28,1,14,18	17,27
	3.56 dd (8.4, 15.3)				
16	3.22 dd (6.4, 13.6)	51.1	3	20,3,18,4	29,31
	3.52 d (13.6)				
17	4.47 s	75.9		15,17,18,28	16
18	5.09 s	86.2		29,15,16,20,17,21	15,16,31
19					
20		51.1			
21		174.7			
22					
23		138.0			
24	7.26 br d (7.6)	116.5	25	26,28	
25	7.32 ddd (1.3, 7.6, 7.6)	129.2	24,26	27,23	
26	7.19 ddd (1.2, 7.6, 7.6)	125.8	25,27	24,28	
27	7.40 dd (1.1, 7.6)	123.7	26	23,25,17	15
28		139.2			
29	0.15 ddd (4.1, 8.5, 10.5)	11.2	30	30, 21, 20	
	0.82 ddd (4.1, 6.5, 10.5)				
30	0.90 ddd (6.0, 8.5, 10.4)	14.0	29	29, 21, 20	
	1.59 ddd (6.0, 6.5, 10.4)				
31	3.06 s	32.5		14,3,4,1	16,18

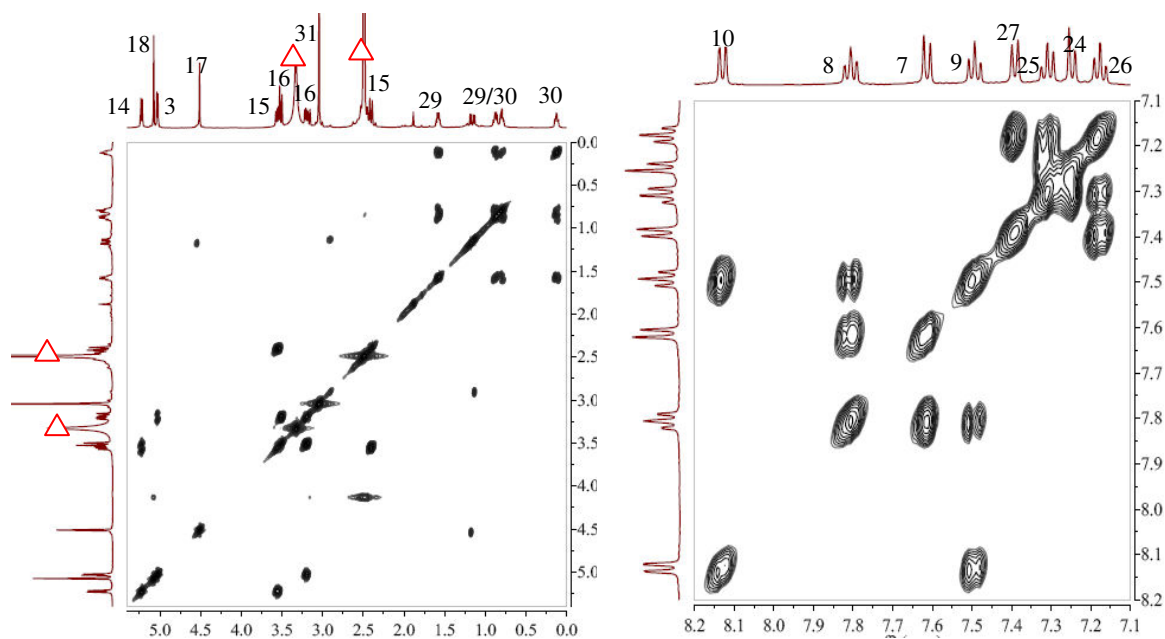


Figure 3.1.37 COSY correlations of fumiquinazoline K (21)

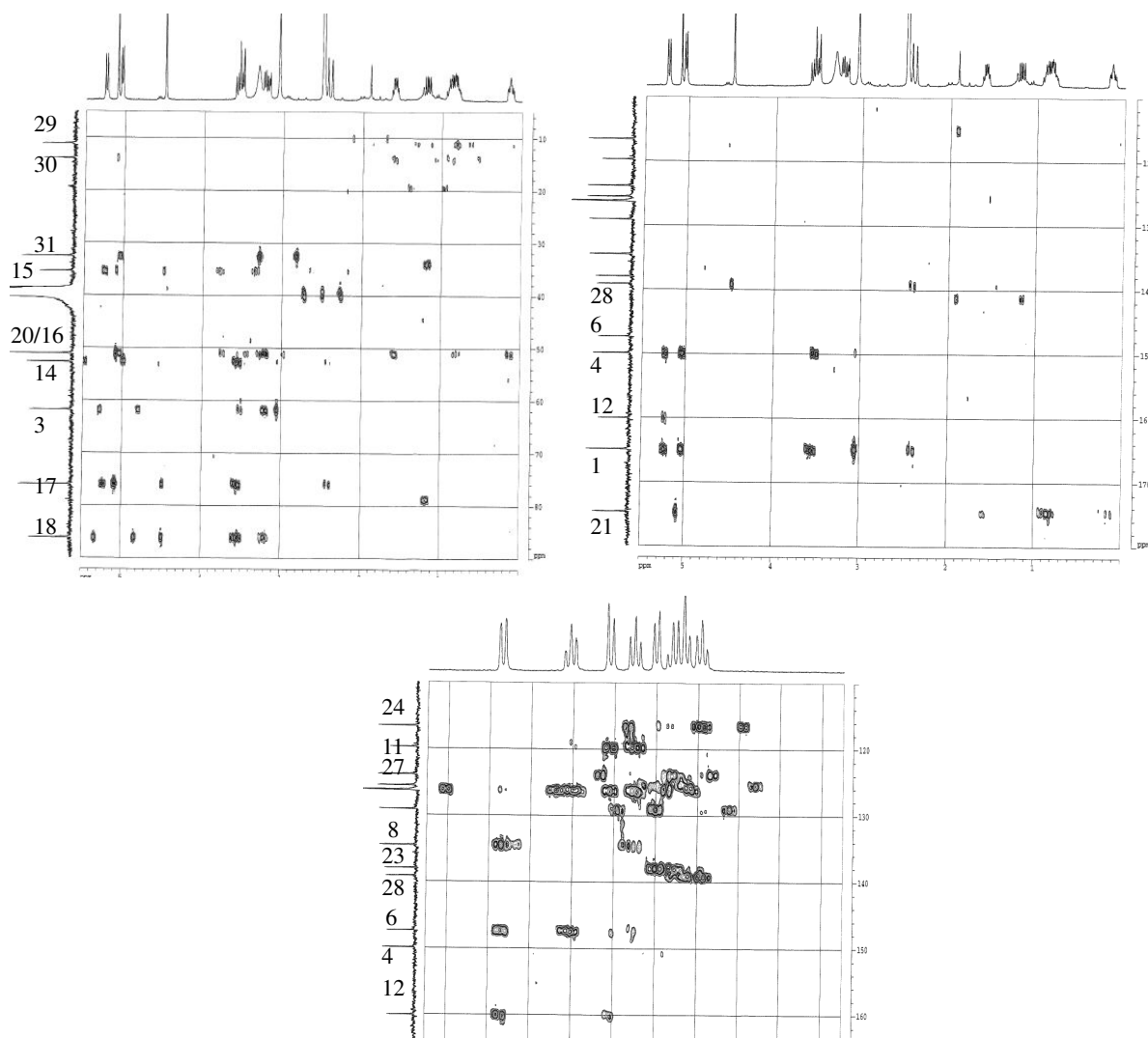


Figure 3.1.38 HMBC correlations of fumiquinazoline K (21)

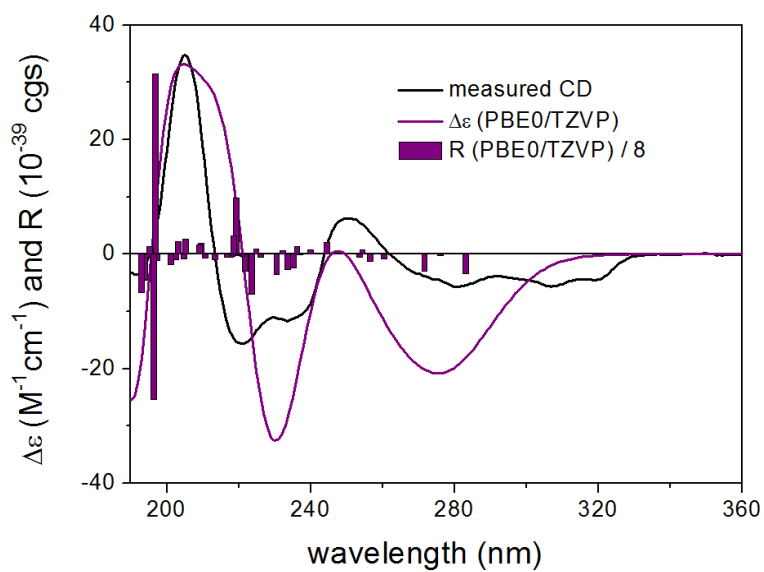


Figure 3.1.39 Experimental ECD spectrum of 21 in acetomitrile compared with the PBE0/TZVP spectrum calculated for the lowest-energy conformer (99.9%) of the (3*R*,14*R*,17*R*,18*S*)-enantiomer. Bars represent rotational strengths

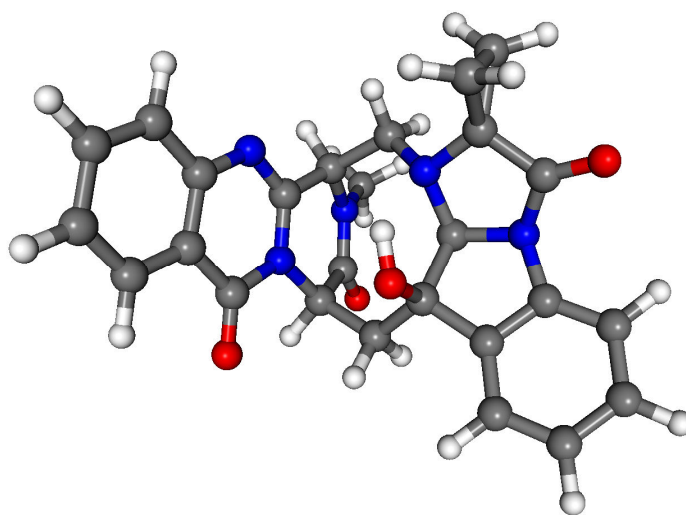


Figure 3.1.40 Computed low-energy conformer of 21 (99.9%)

3.1.22 Fumiquinazoline L (compound 22, new)

Fumiquinazoline L	
Biological Source	<i>Aspergillus</i> sp.
Sample Code	Fr.7.7.8.5.2
Sample Amount	4.4 mg
Molecular Formula	C ₂₅ H ₂₃ N ₅ O ₅
Molecular Weight	473 g/mol
Solubility	MeOH
Physical Description	Yellow amorphous solid
Optical Rotation	[α] _D ²⁰ -30.6° (c 0.14, MeOH)
HPLC Retention Time	24.1 min (standard gradient)

+ c ESI Full ms [100.00-1000.00]

- c ESI Full ms [100.00-1000.00]

Compound **22** was obtained as a yellow amorphous solid (4.4 mg) with an $[\alpha]_D^{20}$ value of -30.6° (c 0.14, MeOH) and it displayed UV absorbances at λ_{\max} (MeOH) 205.9, 231.6, and 304.1 nm. It displayed similar spectroscopic data to those of **21**, suggesting that both compounds have the same molecular skeleton. The molecular formula of **22** was established as $C_{25}H_{23}N_5O_5$ from the prominent signal at m/z 474.1767, corresponding to $[M+H]^+$ in the HRESIMS, thus revealing an increase in the molecular weight of 4 amu and the loss of one double-bond equivalent compared to **21**. The 1H , ^{13}C NMR and DEPT spectra of **22** were similar to those of **21** (Tables 3.1.23) except for the replacement of the C-3 methine proton in **21** by a tertiary methyl group resonating at δ_H 1.87 (δ_C 25.8) ppm (CH₃-16) in **22**. The signal corresponding to the methyl group at N-2 of **21** was absent in the spectra of **22** and a proton of a secondary amide group resonating at δ_H 9.55 ppm (H-2) appeared instead. In addition, the methylene bridge connecting C-3 with N-19 in **21** was not detected in **22**, which accounts for the loss of one element of unsaturation in the structure of **22**. Consequently, exchangeable signals corresponding to a secondary amine proton and a tertiary hydroxyl group resonating at δ_H 3.83 and 7.30 ppm were assigned to H-19 and 3-OH, respectively. The latter was further confirmed by the downfield chemical shift observed for C-3 (δ_C 80.2 ppm) indicating a hydroxyl substituent. H-19 showed a COSY correlation to H-18 and HMBC correlations to C-17, C-18, C-20 and to the cyclopropane methylenes at C-29 and C-30. Correlations of H-2 to C-3, C-4 and C-14, as well as of CH₃-16 to C-3 and C-4 were also observed in the HMBC spectrum of **22** (Table 3.1.23 and Figure 3.1.41).

The relative configuration of **22** was deduced on the basis of the ROESY correlations observed for H-14 to H-18, and for 17-OH to CH₂-15 and H-19. CH₃-16 correlated to H-2, whereas no correlations were observed to H-14 or to CH₂-15, which indicated that the oxopiperazine ring exists in a twist-boat conformation with H-14 and CH₃-16 in equatorial position, while 3-OH and CH₂-15 acquire a coaxial arrangement. Furthermore, the correlation of H-27 to H-14 and CH₂-15 implied that the indoline ring is arranged on a nearly vertical plane to the oxopiperazine ring, hence justifying

the weak correlation observed for H-18 to CH₂-15. Consequently, **22** adopts the same (*3R**,*14R**,*17R**,*18S**) relative configuration as determined for **21**. Since **21** and **22** contain the same 2H-pyrazino[2,1-b]quinazoline-3,6(1H,4H)-dione and tetrahydro-3H-imidazo[1,2-a]indole-3-one chromophores with analogue chirality centers, their ECD spectra could be also compared to establish the absolute configuration of **22**. Compound **22** exhibited the same signs for the corresponding ECD transitions as those of **21**, although the intensities and shapes were somewhat different (Figure 3.1.42). It had three weak negative CEs below 270 nm, a positive one at 249 nm, a negative one at 230 nm and a positive below 210 nm correlating well with the CEs of **21**. Thus the absolute configuration of **22** was established as (*3R*,*14R*,*17R*,*18S*). Consequently, compound **22** was characterized as a new natural product and named fumiquinazoline L.

Table 3.1.23 NMR data for fumiquinazoline L (22)

Position	22 DMSO- <i>d</i> ₆ , δ (ppm), <i>J</i> in Hz		Correlation		
	¹ H (600 MHz)	¹³ C (150 MHz)	COSY	HMBC	ROESY
1		170.1			
2	9.55 s			3, 4, 14	16
3	7.30 d (1.6)	80.2			
4		151.6			
5					
6		146.1			
7	7.63 br d (8.0)	126.9	8	9, 11, 8	
8	7.79 ddd (1.6, 7.2, 8.2)	134.5	7,9	6, 10	
9	7.45 ddd (1.1, 7.0, 8.1)	126.9	8,10	11, 7	
10	7.85 dd (1.6, 8.0)	126.2	9	6, 8, 12	
11		119.8			
12		160.1			
13					
14	5.37 dd (Σ 14.4)	52.9	15	15, 17, 4, 12, 1	18
15	2.78 dd (6.8, 14.7) 2.90 dd (7.6, 14.7)	38.7	14	14, 17, 18, 28, 1	
16	1.87 s	25.8		3, 4	2
17	5.58 s	75.4		15, 17, 28	15,19
18	5.75 d (9.8)	79.7	19	15, 17	14
19	3.83 d (9.9)		18	29, 30, 20, 17, 18	
20		46.5			
21		174.2			
22					
23		138.8			
24	7.23 br d (7.7)	114.4	25	28, 26	
25	7.01 ddd (1.3, 7.6, 7.6)	129.0	24,26	27, 23	
26	6.67 ddd (1.0, 7.6, 7.6)	123.7	25,27	24, 28	
27	7.19 dd (1.0, 7.7)	123.8	26	25, 23, 17	14,15
28		136.9			
29	0.97 ddd (4.0, 7.0, 10.4) 1.07 ddd (4.0, 7.0, 10.3)	13.8	30	30, 20, 21	
30	0.94 ddd (4.0, 7.0, 10.3) 1.03 ddd (4.0, 8.0, 10.4)	11.7	29	29, 20, 21	

Results

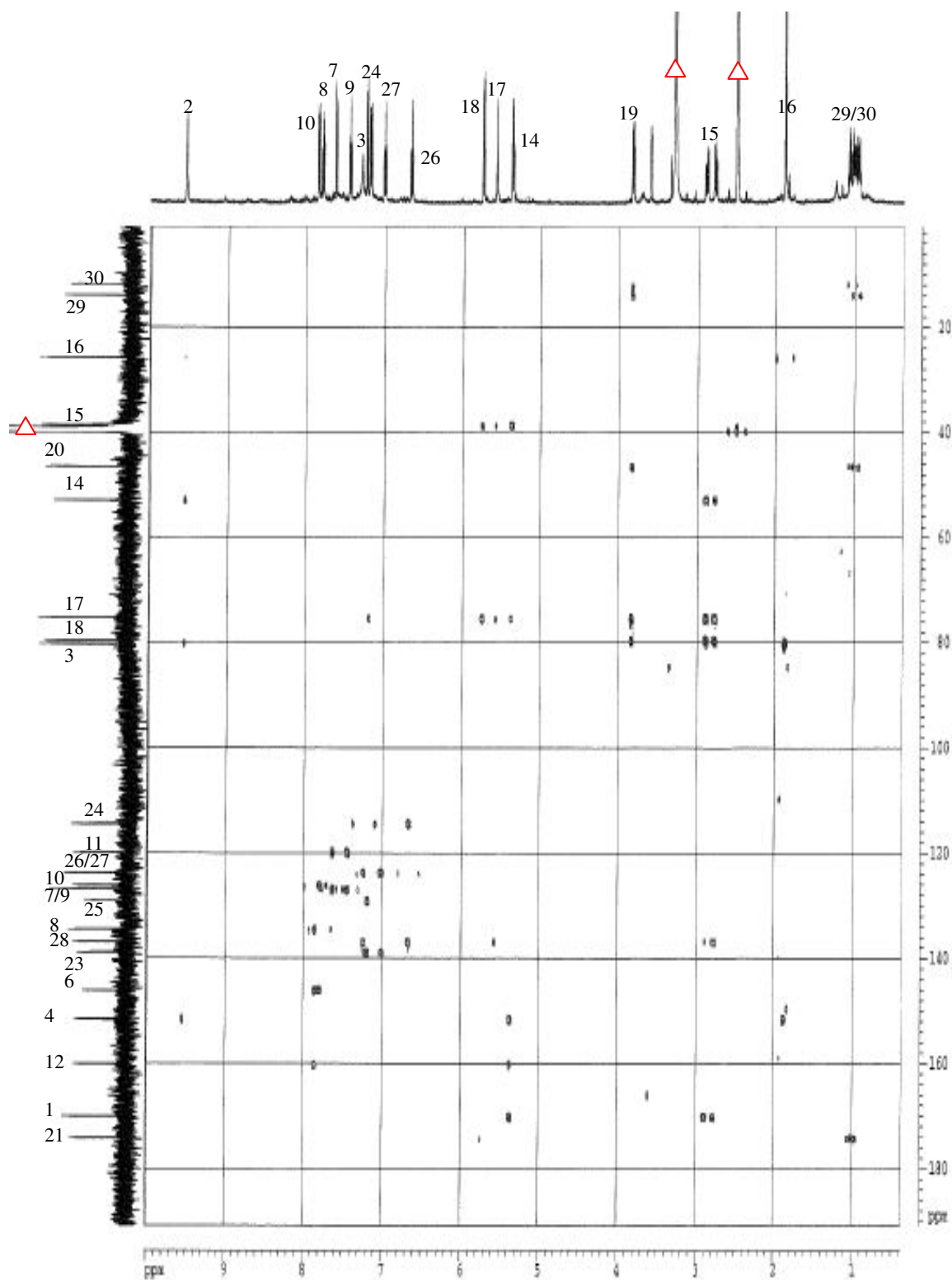


Figure 3.1.41 HMBC correlations of fumiquinazoline L (22)

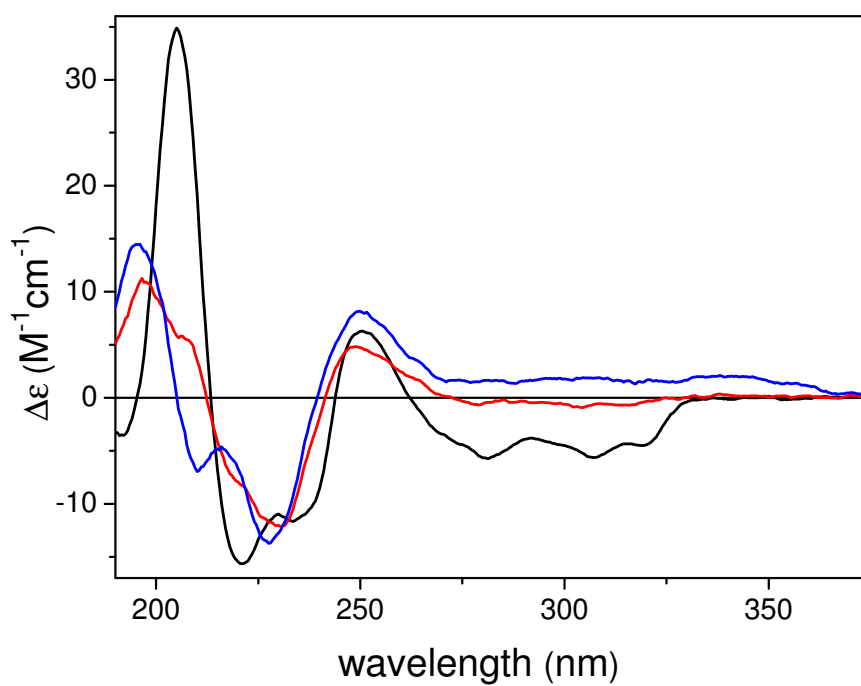
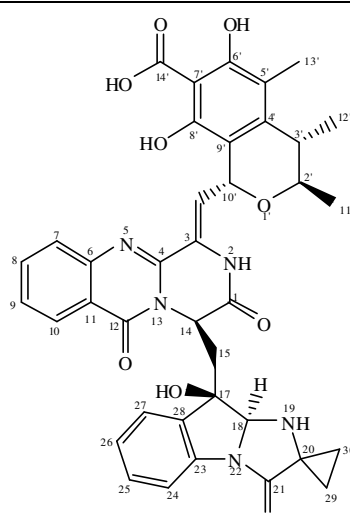
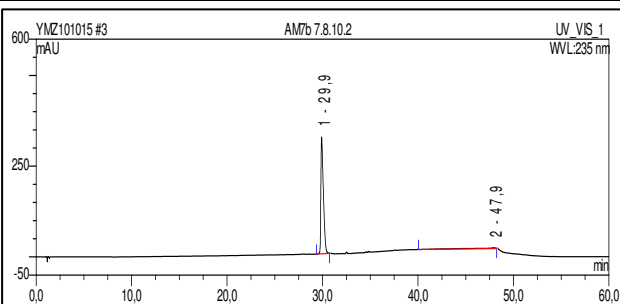
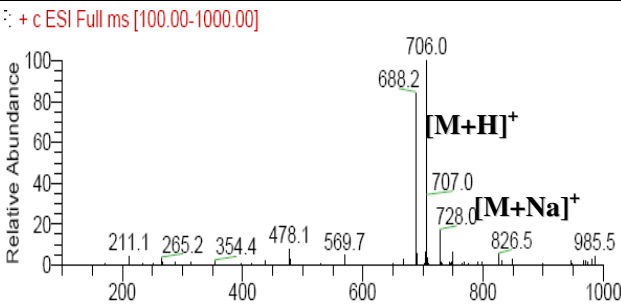
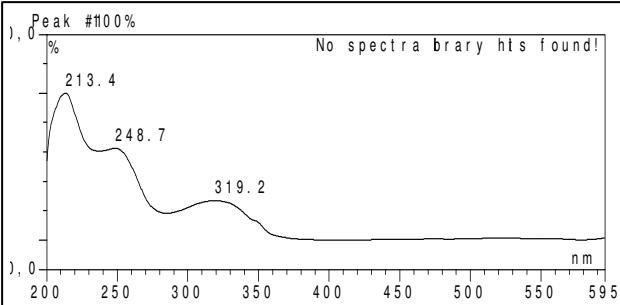
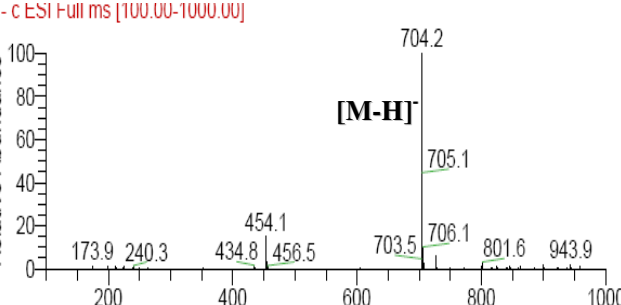


Figure 3.1.42 Experimental ECD spectra of 21 (black), 22 (red) and 23 (blue) in acetonitrile

3.1.23 Fumiquinazoline M (compound 23, new)

Fumiquinazoline M	
Biological Source	<i>Aspergillus</i> sp.
Sample Code	Fr.7.7.8.10.2
Sample Amount	5.4 mg
Molecular Formula	C ₃₈ H ₃₅ N ₅ O ₉
Molecular Weight	705 g/mol
Solubility	MeOH
Physical Description	Yellow amorphous solid
Optical Rotation	[α] _D ²⁰ -24.6° (c 0.11, MeOH)
HPLC Retention Time	29.9 min (standard gradient)
	
	
	
	
	

Compound **23** was obtained as a yellow amorphous solid (5.4 mg) with an $[\alpha]_D^{20}$ value of -24.6° (c 0.11, MeOH) and it displayed UV absorbances at λ_{\max} (MeOH) 213.4, 248.7, and 319.2 nm. The $[M+H]^+$ signal at m/z 706.2508 in the HRESIMS of **23** indicated a molecular formula of $C_{38}H_{35}N_5O_9$, hence including 24 elements of unsaturation. Partial fragmentation observed in the ESIMS spectrum of **23** indicated fragments corresponding to two moieties with molecular weights of 252 and 455 g/mol. Furthermore, 1H NMR and COSY spectra (Tables 3.1.24) showed two different sets of signals implying that the compound consists of two structurally unrelated moieties. The 1H , ^{13}C NMR and DEPT data of one part of the compound (Table 3.1.24) were almost identical to those of **22**, apart from the absence of the hydroxyl group at C-3 of **22**, and the replacement of the methyl group by an olefinic methine group resonating downfield at δ_H 6.31 (δ_C 119.2) ppm (CH-16), which explains the downfield chemical shift of C-3 in **23** (δ_C 128.4 ppm). In contrast, signals due to the other half of the molecule included three aliphatic methine groups resonating at δ_H 2.65, 4.02 and 5.74 (δ_C 35.0, 72.5 and 63.9) ppm (CH-3', CH-2' and CH-10', respectively), denoting the oxygenated nature of the latter two, and three methyl groups including one linked to an aromatic ring which appeared at δ_H 1.98 (δ_C 9.6) ppm (CH₃-13'). In addition, seven sp^2 quaternary carbons, including six aromatic carbons (C-4' to C-9'), two of which being oxygenated as indicated by their downfield chemical shifts at δ_C 158.9 and 156.6 ppm (C-6' and C-8', respectively), and a carboxyl carbon at δ_C 175.5 ppm (C-14') were detected in the ^{13}C NMR spectrum of **23** (Table 3.1.24). The COSY spectrum established a continuous spin system beginning with CH₃-12' through H-3' and the lowfield resonating H-2' to CH₃-11', which is a typical feature of citrinin derivatives (Benjamin *et al.*, 2006). NMR data analysis and the characteristic ESIMS fragment observed at 252 g/mol indicated that dihydrocitrinin constitutes the second partial structure of **23**. This was further confirmed by comparison with data reported for dihydrocitrinin (Jack *et al.*, 1992) and inspection of respective correlations observed in the HMBC spectrum (Table 3.1.24 and Figure 3.1.43). Correlations observed for H-16 to C-4 and C-9', and for H-10' to C-16, indicated that C-10' was connected to C-3 through the olefinic

methine group CH-16. Further evidence for the structural assignment was provided by the direct coupling observed between H-16 and H-10' in the COSY spectrum. Thus, the planar structure of **23** was established as fumiquinazoline M.

The relative configuration of **23** was established by inspection of the ROESY spectrum. The southern part of the molecule showed ROESY correlations similar to those observed for **22**, hence indicating the same configuration at C-14, C-17 and C-18. Correlations observed for H-2' to CH₃-12' and H-16, for H-3' to CH₃-11', and for H-10' to CH₃-11' and H-2 established the relative configuration of the dihydrocitrinin moiety and its connection to the southern part of the molecule. For the dihydrocitrinin part of the molecule the same absolute configuration as previously established for other citrinin derivatives (Richard *et al.*, 1964) was assumed based on biogenetic considerations. In addition, the correlation observed for H-16 to H-7 indicated that the dihydrocitrinin moiety exists in a nearly vertical arrangement to the rest of the molecule. Thus, a relative configuration of (2`R*,3`S*,10`R*,14R*,17R*,18S*) was determined for **23**, in agreement with the corresponding chirality centers of **22** and of dihydrocitrinin (Richard *et al.*, 1964). The ECD spectrum of **23** showed the same positive/negative/positive pattern of transitions below 270 nm as observed for **22**, which indicated that C-14 and the tetrahydro-3H-imidazo[1,2-a]indole-3-one moiety have the same configuration as that of **22** (Figure 3.1.42), while the contribution of the isochroman chromophore is not significant in this range. Above 270 nm, **23** had a broad positive plateau, opposite to the CE of **22**, which is attributed to the contribution of the C-10' chirality center adjacent to the conjugating $\Delta^{3,16}$ double bond. Thus, **23** was identified as a new and structurally unusual dimer of fumiquinazoline L and dihydrocitrinin and was given the name fumiquinazoline M.

Tables 3.1.24 NMR data for fumiquinazoline M (23)

Position	23 DMSO- <i>d</i> ₆ , δ (ppm), <i>J</i> in Hz		Correlation		
	¹ H (600 MHz)	¹³ C (150 MHz)	COSY	HMBC	ROESY
1		166.1			
2	10.3 br s				
3		128.4			
4		146.0			
6		147.1			
7	7.59 br d (8.0)	127.7	8	11,9,8,12	
8	7.74 ddd (1.7, 7.1, 8.2)	134.2	7,9	10,9,6	
9	7.40 ddd (0.9, 7.1, 8.0)	127.3	8,10	11,7	
10	7.89 dd (1.6, 8.0)	127.1	9	6,12,8	
11		120.0			
12		159.9			
14	5.51 dd (Σ 13.5)	51.6	15	15,17,4,12,1	18
15	2.42 dd (7.0, 14.8) 2.66 dd (6.5, 14.8)	39.5	14	14,17,18,28,1	
16	6.31 d (8.5)	119.2	10'	4,9'	2,7
17	5.48 br s	75.1			15,19
18	5.58 d (9.7)	80.1	19	15,17	
19	3.80 d (9.7)		18	29,20,18,17,30	
20		46.5			
21		174.2			
23		138.5			
24	7.21 br d (7.7)	114.4	25	26,28	
25	7.04 ddd (1.0, 7.7, 7.8)	129.2	24,26	24,27,23	
26	6.76 br dd (7.4, 7.7)	124.0	27,25	24,28	
27	7.22 br d (7.4)	124.1	26	25,23,17	14,15
28		136.7			
29	0.98 m 1.08 m (Σ 24.0)	14.1	30	30,20,21	
30	0.98 m 1.02 m (Σ 24.0)	11.7	29	29,20,21	
2'	4.02 dq (2.2, 6.5)	72.5	11',3'	11',12',3',10',4'	12',16
3'	2.65 dq (2.3, 6.9)	35.0	2',12'	5',9',12',4'	11'
4'		139.3			
5'		109.8			
6'	14.82 s	158.9		5',7',6'	
7'		101.9			
8'	15.22 s	156.6		7',9',8'	
9'		108.9			
10'	5.74 d (8.5)	63.9	16	9',16,3,4',8'	11',2
11'	1.17 d (6.5)	18.5	2'	3',2'	
12'	1.28 d (6.9)	20.2	3'	3',2',4'	
13'	1.98 s	9.6		5',4',6'	
14'		175.5			

Results

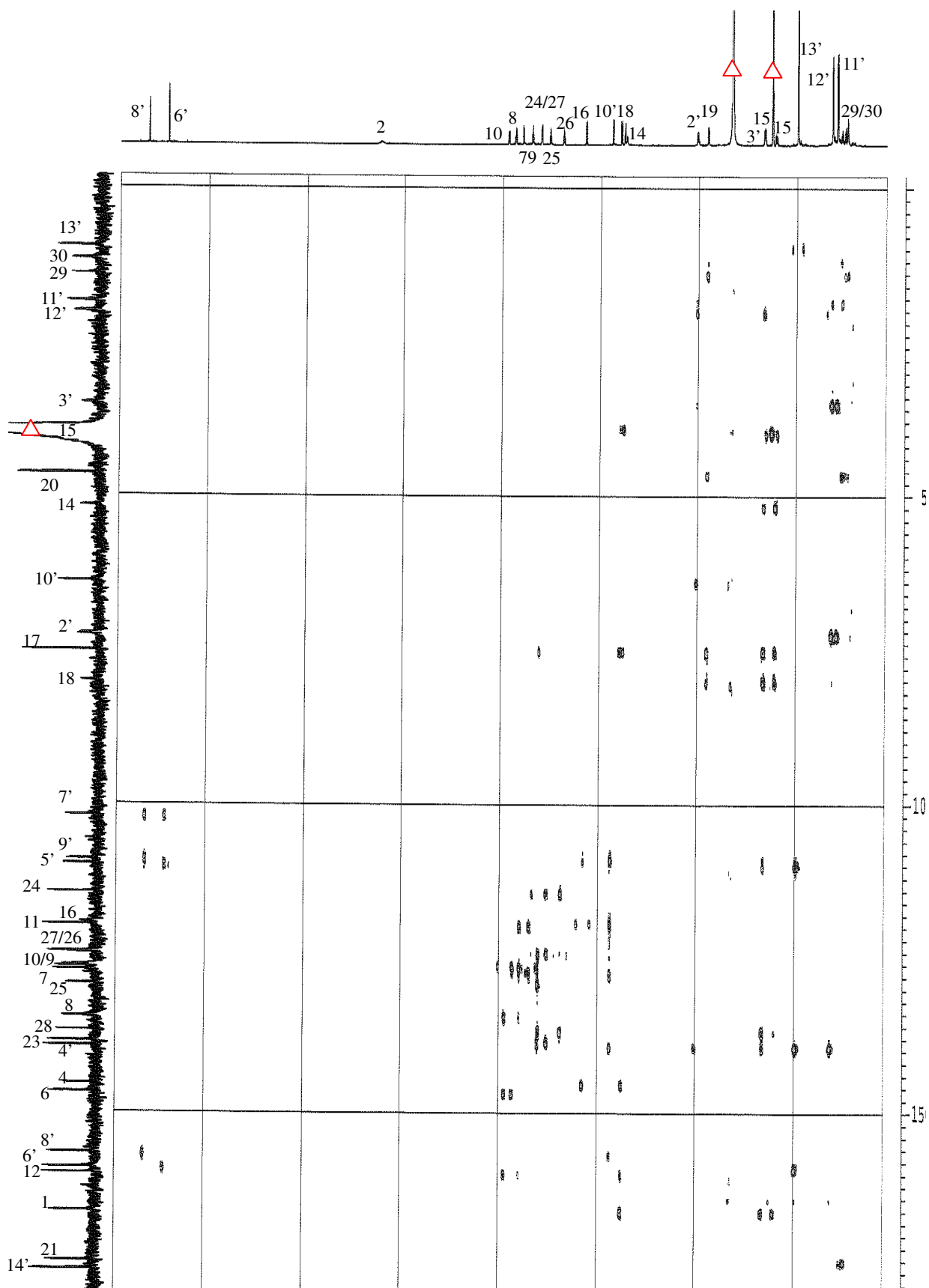
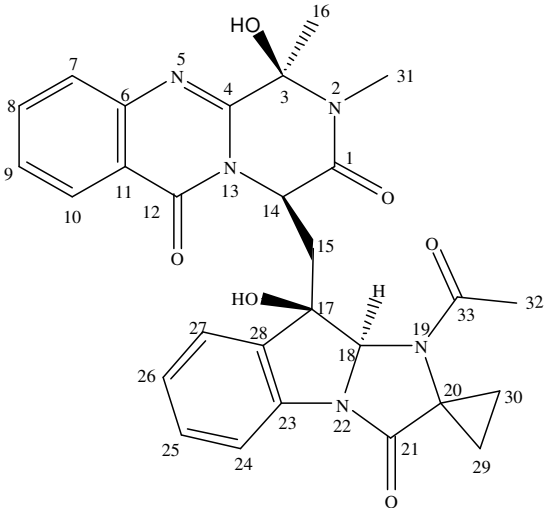
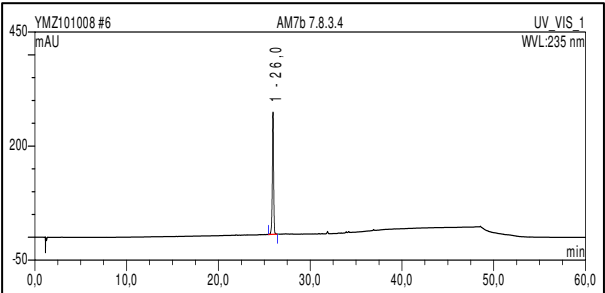
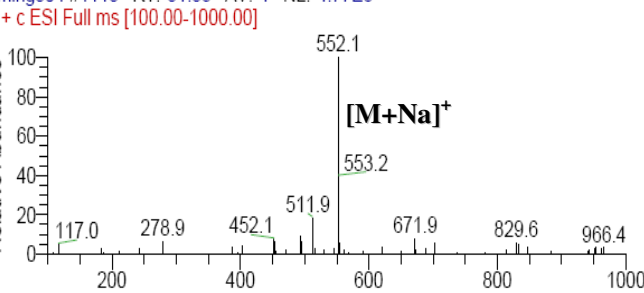
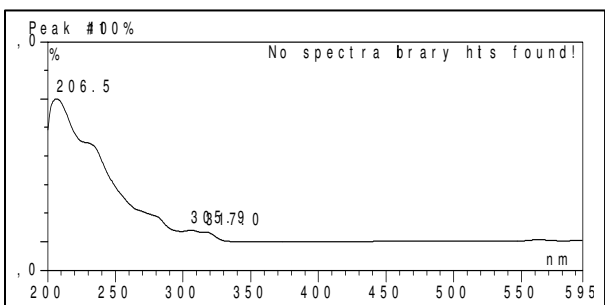
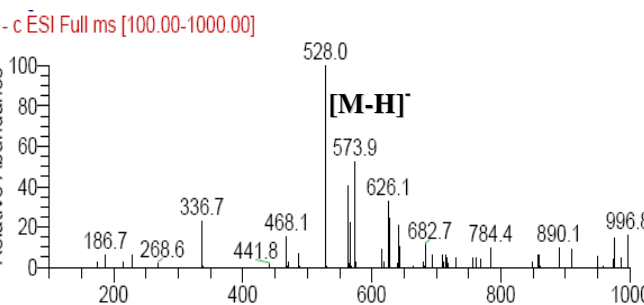


Figure 3.1.43 HMBC correlations of fumiquinazoline M (23)

3.1.24 Fumiquinazoline N (compound 24, new)

Fumiquinazoline N	
Biological Source	<i>Aspergillus</i> sp.
Sample Code	Fr.7.7.8.3.4
Sample Amount	10.0 mg
Molecular Formula	C ₂₈ H ₂₇ N ₅ O ₆
Molecular Weight	529 g/mol
Solubility	MeOH
Physical Description	Yellow amorphous solid
Optical Rotation	$[\alpha]_D^{20} -209.0^\circ$ (c 0.12, MeOH)
HPLC Retention Time	26.0 min (standard gradient)
	
	
	
	
	

Compound **24** was obtained as a yellow amorphous solid (10.0 mg) with an $[\alpha]_D^{20}$ value of -209.0° (c 0.12, MeOH) and it displayed UV absorbances at λ_{\max} (MeOH) 206.5, 305.9, and 317.0 nm. The molecular formula of **24** was determined as $C_{28}H_{27}N_5O_6$, from the prominent signal at m/z 530.2029 corresponding to $[M+H]^+$ in the HRESIMS, indicating a 56 amu increase in the molecular weight and an additional double-bond equivalent compared to **22**. Spectroscopic data of **24** revealed close similarity to **21** and **22**, thus proposing an analogous core structure for **24**. This assumption was confirmed by inspection of 1H , ^{13}C NMR and DEPT spectra (Table 3.1.25), which were almost identical to those of **22**, except for the presence of two additional methyl groups resonating at δ_H 3.14 (δ_C 28.3) and δ_H 1.98 (δ_C 22.4) ppm in **24**, and the absence of signals corresponding to the secondary amide and amine protons (H-2 and H-19, respectively) detected in **22**. Based on chemical shift values, the additional signals were assigned to the N-methyl group at N-2 and the methyl amide group at N-19, respectively. The respective amide carbonyl of the latter was detected at δ_C 169.3 ppm (C-33) thus verifying the additional double-bond equivalent in **24**. Inspection of COSY and HMBC spectra (Table 3.1.25 and Figure 3.1.44) revealed similar structural features as in **22**, in addition to correlations of CH_3 -31 to C-1 and C-3, and of CH_3 -32 to C-33, which confirms the additional functionalities and the planar structure of **24** as shown. Since the corresponding ECD transitions of **24** and **25** had the same sign as those of **21** even above 270 nm, the absolute configuration of **24** was found ($3R,14R,17R,18S$), *i.e.* homochiral with **21** regarding their corresponding chirality centers (Figure 3.1.45). Thus, compound **24** was finally characterized as a new natural product and was named fumiquinazoline N.

Results

Table 3.1.25 NMR data for fumiquinazoline N (24)

Position	24 CDCl ₃ , δ (ppm), <i>J</i> in Hz		Correlation		
	¹ H (600 MHz)	¹³ C (125 MHz)	COSY	HMBC	ROESY
1		169.3			
2					
3		84.7			
4		150.5			
5					
6		146.6			
7	7.69 br d (7.7)	127.9	8	9,11	
8	7.73 ddd (1.6, 6.6, 8.2)	134.7	7,9	6,10	
9	7.43 ddd (1.4, 6.8, 8.1)	127.5	8,10	7,11	
10	8.09 br d (7.9)	126.5	9	6,8	
11		120.3			
12		160.9			
13					
14	5.73 dd (6.5, 8.5)	53.5	15	15,17,4,12,1	
15	3.04 dd (6.4, 14.2)	39.6	14	14,17,18,28,1	32
	3.16 dd (7.0, 14.2)				
16	2.13 s	25.7		3,4	31
17		78.7			
18	6.58 s	80.7		17,33,21,20	14,15,32
19					
20		47.2			
21		172.4			
22					
23		139.3			
24	7.46 br d (7.8)	117.7	25	26,28	
25	7.17 br dd (7.5, 7.6)	130.2	24,26	23,27	
26	7.07 br m	126.4	25,27	24,28	
27	7.72 br d (7.7)	124.0	26	23,25	14,15
28		135.4			
29	1.38 m (Σ 24.0)	13.0	30		
	1.93 m (Σ 24.0)				
30	1.33 m (Σ 24.0)	13.0	29		
	1.45 m (Σ 24.0)				
31	3.14 s	28.3		3,1	
32	1.98 s	22.4		33	
33		169.3			

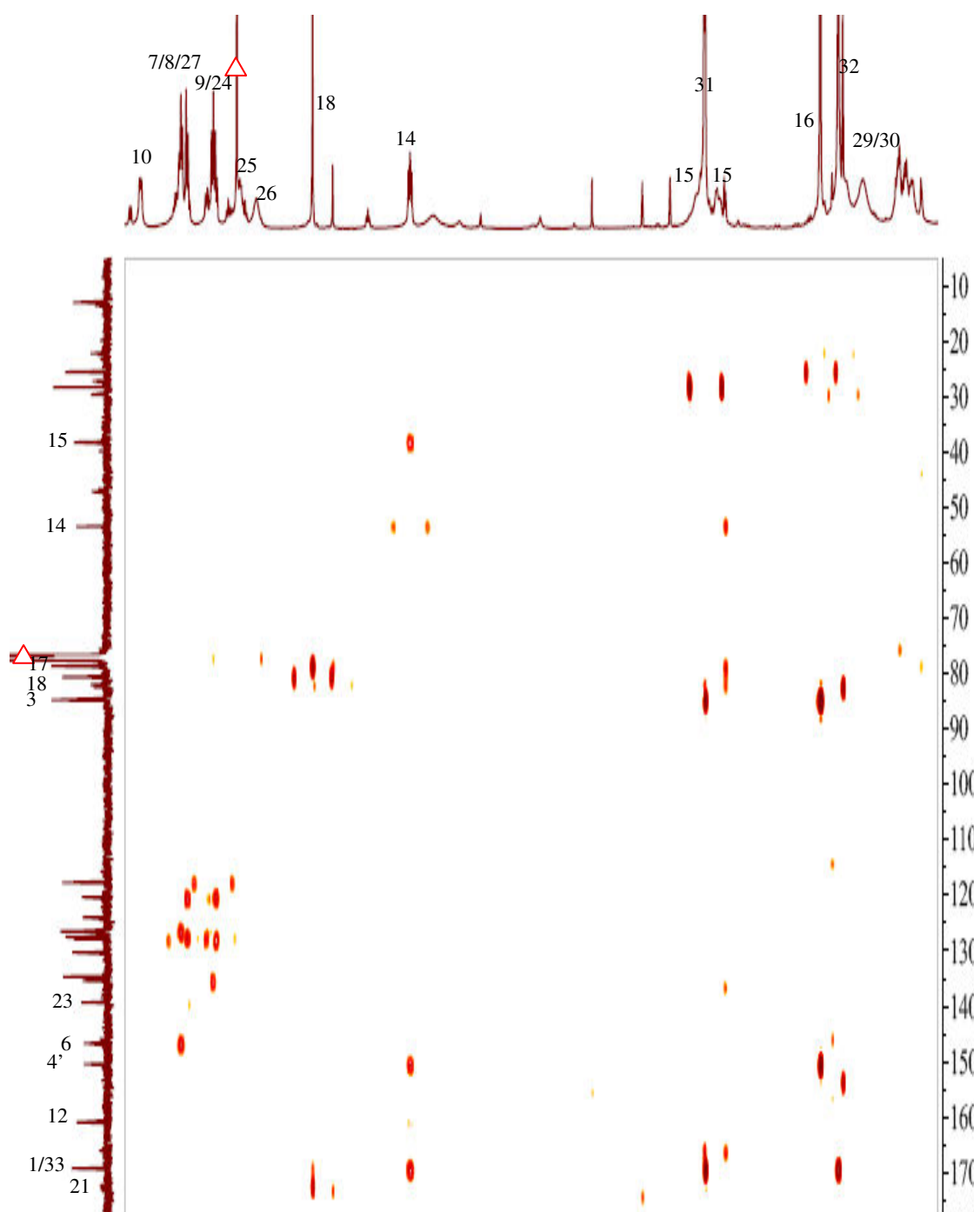


Figure 3.1.44 HMBC correlations of fumiquinazoline N (24)

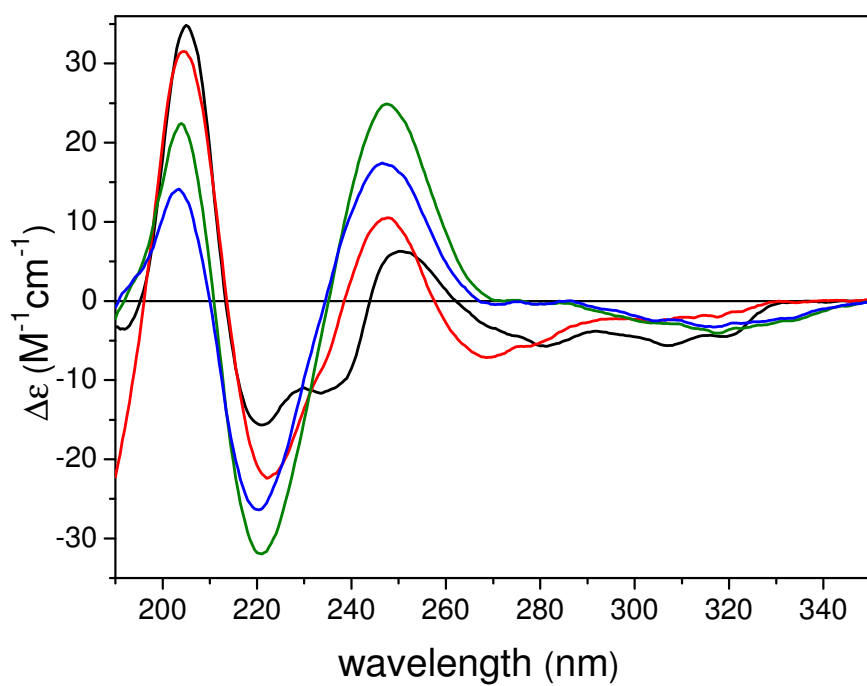


Figure 3.1.45 Experimental ECD spectra of 21 (black), 24 (red), 25 (olive) and 26 (blue) in acetonitrile

3.1.25 Fumiquinazoline O (compound 25, new)

Fumiquinazoline O	
Biological Source	<i>Aspergillus</i> sp.
Sample Code	Fr.7.7.8.3.2
Sample Amount	10 mg
Molecular Formula	C ₂₉ H ₂₉ N ₅ O ₆
Molecular Weight	543 g/mol
Solubility	MeOH
Physical Description	Yellow amorphous solid
Optical Rotation	$[\alpha]_D^{20} -89.0^\circ$ (c 0.12, MeOH)
HPLC Retention Time	24.3 min (standard gradient)

Compound **25** was obtained as a yellow amorphous solid (10.0 mg) with an $[\alpha]_D^{20}$ value of -89.0° (c 0.12, MeOH) and it displayed UV absorbances at λ_{\max} (MeOH) 205.1, 231.2, and 274.5 nm. The molecular formula of **25** was established as $C_{29}H_{29}N_5O_6$ by analysis of its HRESIMS (m/z 544.2186 $[M+H]^+$), indicating an increase by 14 amu compared with **24**. The physicochemical data of **25** were almost identical to those of **24** (Table 3.1.26), apart from the appearance of an additional OCH_3 signal at δ_H 3.03 (δ_C 51.2) ppm in the NMR spectra of **25**, which accounts for the 14 amu molecular weight difference. This suggested that **25** features the same molecular skeleton as **24**, but with a methoxy substituent at C-3 instead of 3-OH as found in **24**. The observed HMBC (Figure 3.1.46) correlation of the methoxy protons (OCH_3 -34) to C-3 supported this assumption. Accordingly, large downfield shifts were observed for C-3 and C-16 (δ_C 89.2 and 27.7 ppm, respectively), whereas CH_3 -16 protons suffered only a slight upfield shift (δ_H 2.03 ppm) compared to the respective values in **24**. Further confirmation of the planar structure of **25** was achieved by comprehensive analysis of 2D NMR spectra (Table 3.1.26). Hence, **25** was characterized as a new natural product and was named fumiquinazolines O.

The relative configurations of **24** and **25** were determined on the basis of ROESY experiments, which showed an identical set of correlations for both compounds. Comparison with ROESY data obtained for **22** indicated identical relative configurations for all three compounds. In analogy to **22**, correlations were observed for both H-18 and H-27 to H-14 and CH_2 -15. In addition, H-18 and CH_2 -15 correlated to CH_3 -32, and CH_3 -16 to CH_3 -31 in **24** and to CH_3 -31 and OCH_3 -34 in **25**. Hence, a relative configuration of $(3R^*,14R^*,17R^*,18S^*)$ was established for **24** and **25**, in agreement with that determined for **21** and **22**. Since the corresponding ECD transitions of **24** and **25** had the same sign as those of **21** even above 270 nm, the absolute configuration of **25** was found $(3R,14R,17R,18S)$, *i.e.* homochiral with **21** regarding their corresponding chirality centers (Figure 3.1.44).

Table 3.1.26 NMR data for fumiquinazoline O (25)

Position	25 CDCl ₃ , δ (ppm), J in Hz		Correlation		
	¹ H (600 MHz)	¹³ C (125 MHz)	COSY	HMBC	ROESY
1		167.4			
2					
3		89.2			
4		149.6			
5					
6		146.8			
7	7.82 dd (1.5, 8.2)	127.8	8	9,11	
8	7.79 ddd (1.6, 6.7, 8.3)	135.1	7,9	6,10	
9	7.49 ddd (1.6, 6.8, 8.1)	127.8	8,10	7,11	
10	8.17 dd (1.1, 7.9)	126.8	9	6,8,12	
11		120.3			
12		160.5			
13					
14	6.15 dd (5.0, 8.6)	52.4	15	15,17,4,1	
15	2.71 dd (5.0, 14.5) 2.88 dd (8.7, 14.5)	40.9	14	14,17,18,28,1	32
16	2.02 s	27.7		3,4	
17		78.8			
18	6.51 s	81.3		15,20,17,33,21	14,15,32
19					
20		46.7			
21		173.1			
22					
23		139.4			
24	7.51 br d (7.6)	117.4	25	26,28	
25	7.27 ddd (1.0, 7.7, 8.2)	130.3	24,26	23,27	
26	7.10 br t (7.5)	126.2	25,27	24,28	
27	7.55 br d (7.5)	123.9	26	23,25	14,15
28		135.9			
29	1.44 ddd (6.2, 7.8, 10.3) 1.93 ddd (6.0, 7.7, 10.1)	13.6	30	30,20,21	
30	1.38 ddd (6.0, 8.0, 10.4) 1.47 ddd (6.1, 8.0, 10.4)	13.3	29	29,20,21	
31	3.09 s	27.3		3,1	34
32	2.03 s	22.6		33	
33		169.2			
34	3.03 s	51.2		3	

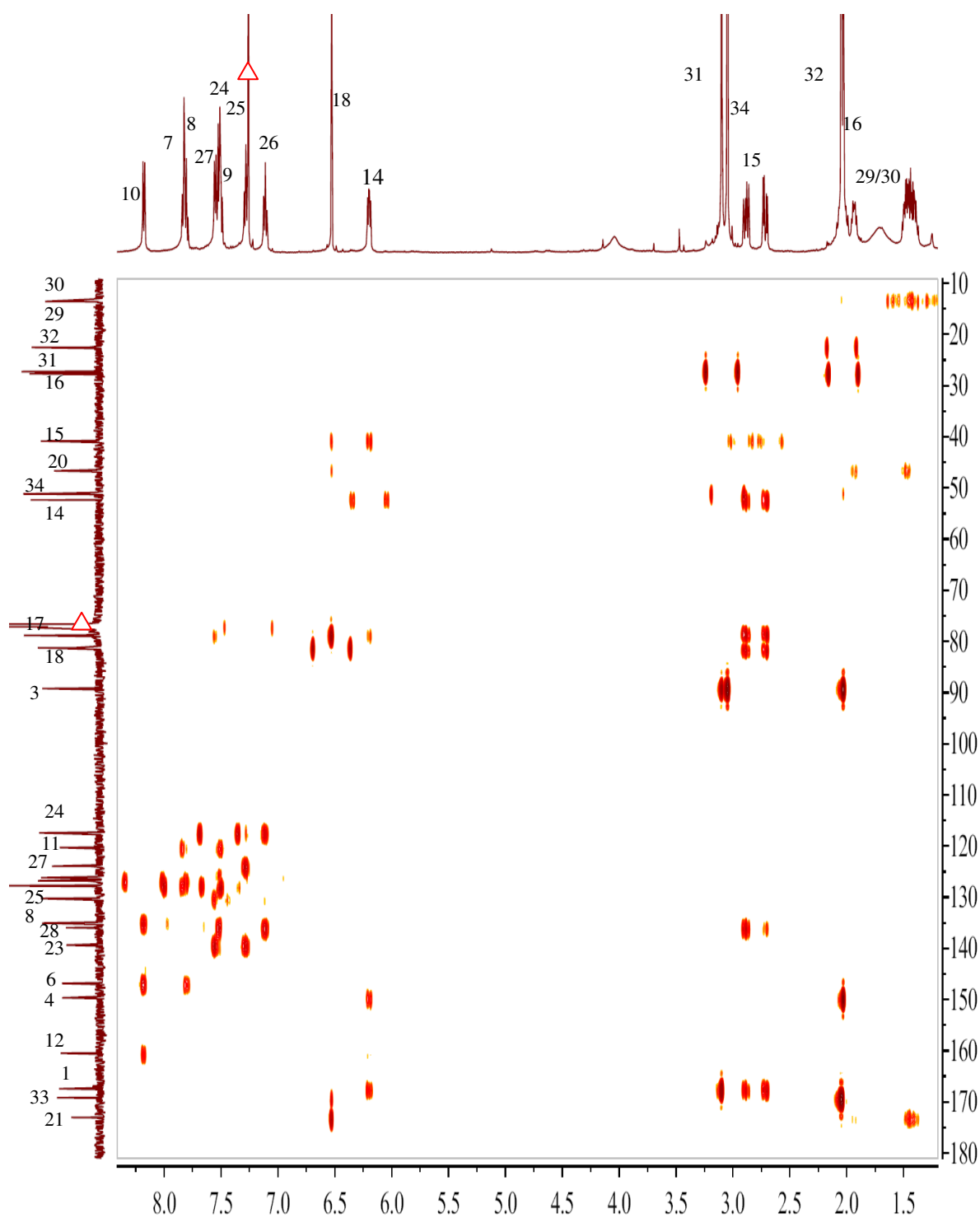
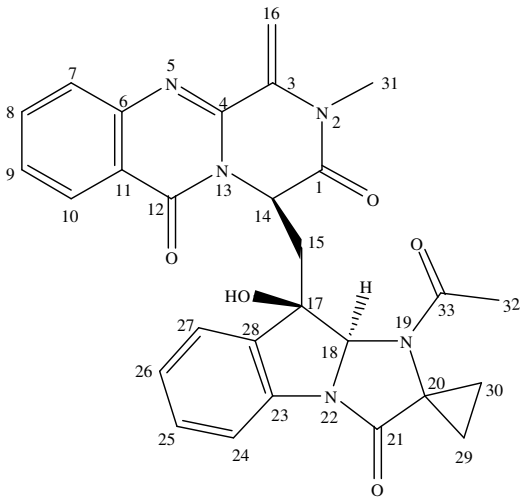
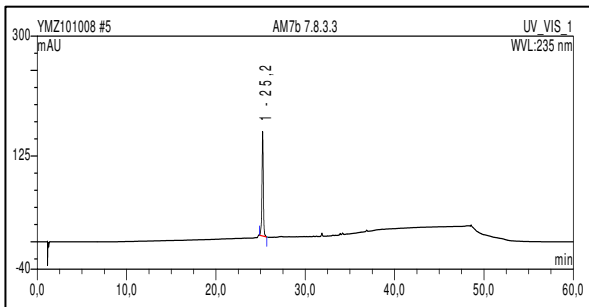
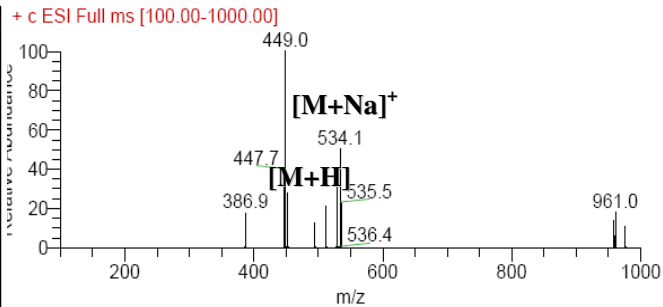
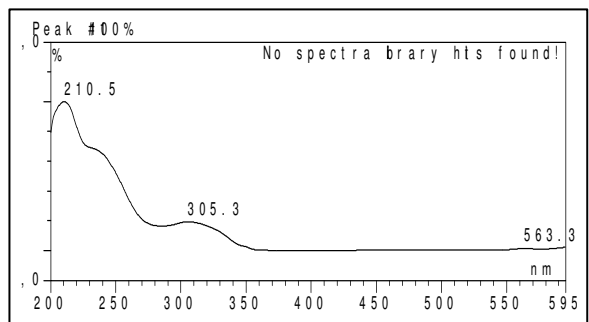
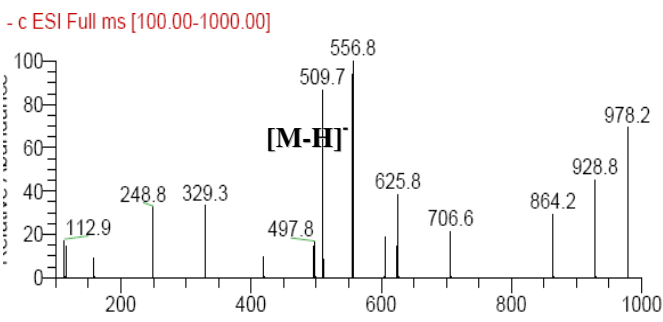


Figure 3.1.46 HMBC correlations of fumiquinazoline O (25)

3.1.26 Fumiquinazoline P (compound 26, new)

Fumiquinazoline P	
Biological Source	<i>Aspergillus</i> sp.
Sample Code	Fr.7.7.8.3.3
Sample Amount	5.2 mg
Molecular Formula	C ₂₈ H ₂₅ N ₅ O ₅
Molecular Weight	511 g/mol
Solubility	MeOH
Physical Description	Yellow amorphous solid
Optical Rotation	$[\alpha]_D^{20} -73.8^\circ$ (<i>c</i> 0.12, MeOH)
HPLC Retention Time	25.2 min (standard gradient)
	
	
	

Compound **26** was obtained as a yellow amorphous solid (5.2 mg) with an $[\alpha]_D^{20}$ value of -73.8° (c 0.12, MeOH) and it displayed UV absorbances at λ_{\max} (MeOH) 210.5, 231.6, and 305.3 nm. HRESIMS of **26** exhibited a prominent peak at m/z 512.1927 $[M+H]^+$, indicating a molecular formula of $C_{28}H_{25}N_5O_5$, including 19 double-bond equivalents. 1H and ^{13}C NMR spectra of **26** showed a set of signals similar to those observed for **24** (Table 3.1.27), apart from the absence of the hydroxyl group at C-3 in **24** and replacement of the methyl group CH_3 -16 by an exocyclic olefinic methylene group, the protons of which resonating downfield at δ_H 5.25 and 6.33 ppm (CH_2 -16) and the corresponding carbon at δ_C 103.7 ppm (C-16). Accordingly, the signal corresponding to C-3 appears downfield at δ_C 138.5 ppm. This was further confirmed by correlations observed for the olefinic methylene protons (CH_2 -16) to C-3 and C-4 in the HMBC spectrum (Table 3.1.27 and Figure 3.1.47). Analysis of ROESY correlations indicated the same relative configuration at C-14, C-17 and C-18 as in the previously discussed compounds (**21-26**), thus establishing a relative configuration of ($14R^*,17R^*,18S^*$) for **26**. Although compound **26** lacks the C-3 chirality center, it exhibited near identical ECD spectrum with **25** (Figure 3.1.44), which confirmed its ($14R,17R,18S$) absolute configuration. Therefore, **26** was characterized as a new natural product and named fumiquinazoline P.

Table 3.1.27 NMR data for fumiquinazoline P (26)

Position	26 CDCl ₃ , δ (ppm), J in Hz		Correlation		
	¹ H (600 MHz)	¹³ C (125 MHz)	COSY	HMBC	ROESY
1		165.0			
2					
3		138.5			
4		144.9			
5					
6		147.0			
7	7.60 br d (8.1)	127.2	8	9,11	
8	7.69 ddd (1.6, 6.8, 8.3)	134.6	7,9	6,10	
9	7.34 ddd (1.3, 6.8, 7.6)	127.3	8,10	7,11	
10	7.87 br d (7.6)	126.8	9	6,8,12	
11		119.6			
12		160.2			
13					
14	6.04 dd (4.9, 9.7)	52.1	15	4	
15	2.66 dd (9.7, 14.5) 3.09 dd (5.1, 14.5)	39.4	14	14,17,18,28,1	32
16	5.25 d (1.8) 6.33 d (1.7)	103.7		3, 4	
17		78.0			
18	6.62 s	80.1		17,33,21	14,15,32
19					
20		47.0			
21		173.1			
22					
23		139.2			
24	7.33 br d	117.0	25	26,28	
25	6.87 br t	130.5	24,26	27,23	
26	6.64 br t	126.1	25,27	24,28	
27	7.07 br d	122.7	26	23,25	14,15
28		134.2			
29	1.38 m (Σ 24.0) 1.92 m (Σ 24.0)	12.6	30		
30	1.33 m (Σ 24.0) 1.50 m (Σ 24.0)	12.6	29		
31	3.34 s	31.3		3, 1	16
32	2.05 s	22.0		33	
33		169.0			

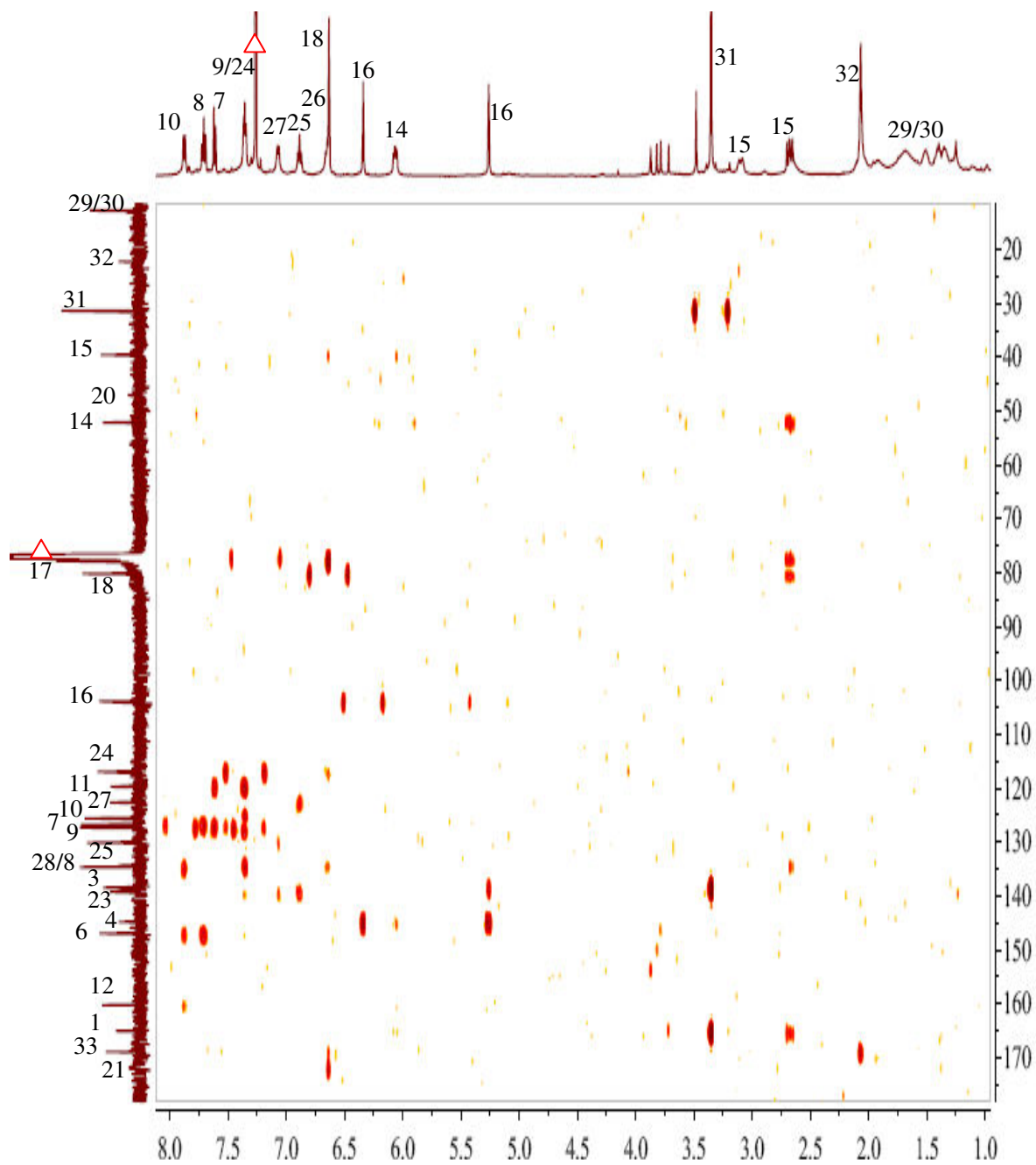
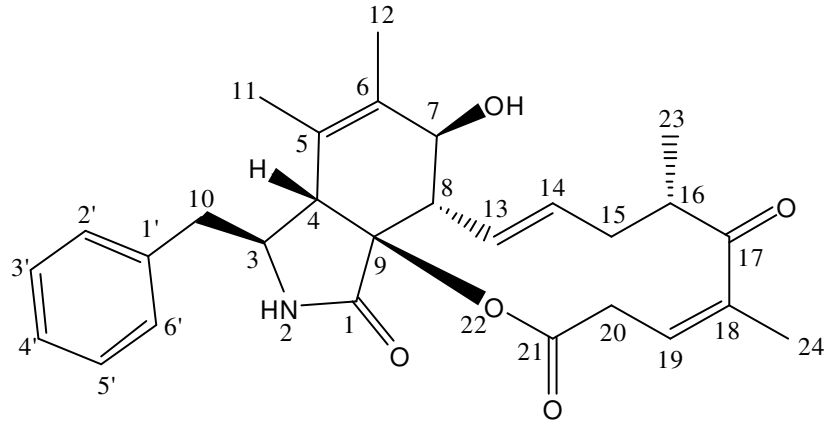
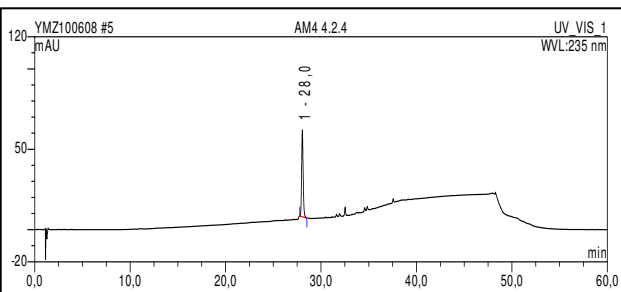
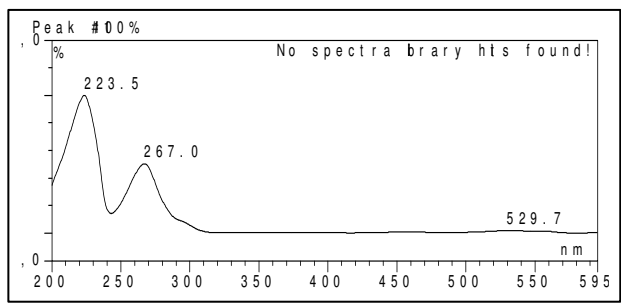


Figure 3.1.47 HMBC correlations of fumiquinazoline P (26)

3.1.27 Cytochalasin Z17 (compound 27, known)

Cytochalasin Z17	
Biological Source	<i>Aspergillus</i> sp.
Sample Code	Fr.4.4.2.4
Sample Amount	5.2 mg
Molecular Formula	C ₂₈ H ₃₃ NO ₅
Molecular Weight	463 g/mol
Solubility	MeOH
Physical Description	Colorless amorphous powder
Optical Rotation	[α] _D ²⁰ + 53.6° (c 0.1, MeOH)
HPLC Retention Time	28.0 min (standard gradient)
	
	
	

Compound **27** was obtained as a colorless amorphous powder (5.2 mg) with an $[\alpha]_D^{20}$ value of + 53.6° (*c* 0.1, MeOH) and it revealed UV absorbances at λ_{\max} (MeOH) 223.5, and 261.0 nm. Its molecular formula was established as C₂₈H₃₃NO₅ according to the [M+H]⁺ signal at *m/z* 464.2431 (calc. for 464.2437) in the HRESIMS. The ¹H-NMR spectrum (Table 3.1.28) of **27** revealed the presence of an amide proton (NH-2) at δ_H 8.36 ppm, three methyl singlets at δ_H 1.73 (CH₃-24), 1.50 (CH₃-12), and 1.17 (CH₃-11) ppm, one methyl doublet at δ_H 0.98 ppm (CH₃-23), three methylene groups at δ_H 2.66 and 2.94 ppm (CH₂-10), 1.68 and 2.19 ppm (CH₂-15), and 2.97 and 3.56 ppm (CH₂-20), five methine groups at δ_H 3.46 (H-3), 3.26 (H-4), 3.58 (H-7), 2.90 (H-8), and 3.54 (H-16) ppm, and one aliphatic hydroxyl group at δ_H 4.59 (7-OH). Moreover, three olefinic hydrogen atoms at δ_H 5.21 ppm (H-14), 5.78 ppm (H-13), and 6.47 ppm (H-19), and five aromatic protons at δ_H 7.15 ppm (H-2' and H-6', respectively), 7.23 ppm (H-4'), and 7.33 ppm (H-3' and H-5', respectively) of a phenyl ring were observed. The observation suggested the presence of one dimethylated 5,6-double bond in the structure of **27**. The ¹³C-NMR spectrum of **27** confirmed the appearance of 28 carbon signals with two carbon signals overlapping in the structure. Furthermore, the DEPT experiment revealed the presence of eight quaternary carbon atoms, three of which were attributed to the carboxyl carbonyl at δ_C 168.8 ppm (C-21), the amide carbonyl at δ_C 171.0 ppm (C-1), and the ketone carbonyl at δ_C 205.4 ppm (C-17), respectively. Inspection and comparison of the NMR spectra of **27** led to the conclusion that compound **27** had the same 10-phenylperhydroisoindol-1-one skeleton identified in cytochalasin Z17 (Table 3.1.28) (Lin *et al.*, 2009; Zhang *et al.*, 2010). The analysis of ¹H-¹H COSY spectrum (Table 3.1.28 and Figure 3.1.48) established the presence of four spin systems including correlations observed for the methine group (H-3) to the methylene protons (CH₂-10), the methine proton (H-4), and the amide proton (NH-2), for the methylene protons (CH₂-20) to the olefinic methine proton (H-19), for the aromatic system (H-2' to H-6'), and for the methine proton (H-8) to H-7 and H-13 as well as for H-13 to H-16 and H-16 to H-23. Interpretation of HMQC spectrum allowed the assignment of proton signals to the corresponding proton-bearing carbon atoms.

The connection between the different substructures of **27** was determined by the HMBC spectrum (Figure 3.1.49). HMBC correlations were observed from the methylene protons (CH₂-10) to C-3, C-4, C-1', C-2', and C-6' (δ_C 58.1, 47.4, 137.5, 129.4, and 129.4 ppm, respectively), from the methine proton (H-4) to C-5 and C-6 (δ_C 124.2 and 134.0 ppm, respectively), from the amide proton (NH-2) to C-1, C-3, C-4, and C-9 (δ_C 171.0, 58.1, 47.4, and 84.2 ppm, respectively), from the proton (CH-8) to C-1, C-4, C-6 (δ_C 134.0 ppm), C-7 (δ_C 69.0 ppm), C-9, C-13 (δ_C 127.5 ppm), and C-14 (δ_C 133.0 ppm), from the methyl group (CH₃-11) to C-4, C-5, and C-6, and from the methyl group (CH₃-12) to C-5, C-6, and C-7. Furthermore, the HMBC spectrum revealed correlations of H-16 to C-14 and C-18 (δ_C 141.6 ppm), of CH₃-23 to C-15 (δ_C 40.1 ppm), C-16 (δ_C 38.9 ppm), and C-17, of CH₃-24 to C-17, C-18, and C-19 (δ_C 133.4 ppm), of H-19 to C-17 and C-24 (δ_C 12.6 ppm), and of H-20 to C-9, C-18, C-19, and C-21.

Inspection of ROESY spectrum showed correlations between CH₂-10 and H-4, H-8 and OH-7, and between H-8 and H-4 indicating the relative configuration of **27** as shown, which was also in accordance with reported data for this compound (Lin *et al.*, 2009). Therefore, compound **27** was finally established as cytochalasin Z17 according to the analysis mentioned above in addition to comparison with reported data (Table 3.1.28) (Lin *et al.*, 2009).

Table 3.1.28 NMR data for cytochalasin Z17 (27)

Position	27 DMSO- <i>d</i> ₆ , δ (ppm), <i>J</i> in Hz		Reference DMSO- <i>d</i> ₆ , δ (ppm), <i>J</i> in Hz (Lin <i>et al.</i> , 2009)	
	¹ H (300 MHz)	¹³ C (75 MHz)	¹ H (600 MHz)	¹³ C (150 MHz)
1		171.0		171.0
2-NH	8.36 s		8.35 s	
3	3.46 m	58.1	3.39 dd (4.8, 9.5)	58.2
4	3.26 m	47.4	3.28 s	47.4
5		124.2		124.2
6		134.0		134.1
7	3.58 m	69.0	3.59-3.61 m	69.0
7-OH	4.59 d (7.6)			
8	2.90 d (10.0)	48.8	2.91-2.94 m	48.8
9		84.2		84.2
10	2.66 dd (10.0, 13.0) 2.94 dd (4.5, 11.8)	42.7	2.69 dd (9.9, 12.8) 2.93-2.95 m	42.7
11	1.17 s	17.1	1.18 s	17.0
12	1.50 s	14.5	1.51 s	14.5
13	5.78 dd (10.1, 15.2)	127.5	5.81 dd (9.8, 15.4)	127.6
14	5.21 m	133.0	5.23 ddd (3.7, 11.0, 15.0)	133.4
15	1.68 d (11.4) 2.19 d (13.6)	40.1	1.70-1.72 m 2.19-2.21 m	40.2
16	3.54 m	38.9	3.45-3.48 m	39.1
17		205.4		205.4
18		141.6		141.6
19	6.47 dd (6.3, 9.3)	133.4	5.48 dd (6.3, 10.3)	133.0
20	2.97 d (5.0) 3.56 d (10.8)	37.2	2.97 m 3.57 m	37.2
21		168.8		168.8
22				
23	0.98 d (6.40)	17.0	0.99 d (6.3)	17.2
24	1.73 s	12.6	1.71 s	12.6
1'		137.5		137.6
2'	7.15 d (7.3)	129.4	7.16 d (7.3)	129.2
3'	7.33 t (7.5)	128.4	7.33 dd (7.3, 7.7)	128.9
4'	7.23 t (7.4)	126.5	7.23 dd (7.3, 7.3)	126.6
5'	7.33 t (7.5)	128.4	7.33 dd (7.3, 7.7)	128.9
6'	7.15 d (7.3)	129.4	7.16 d (7.3)	129.2

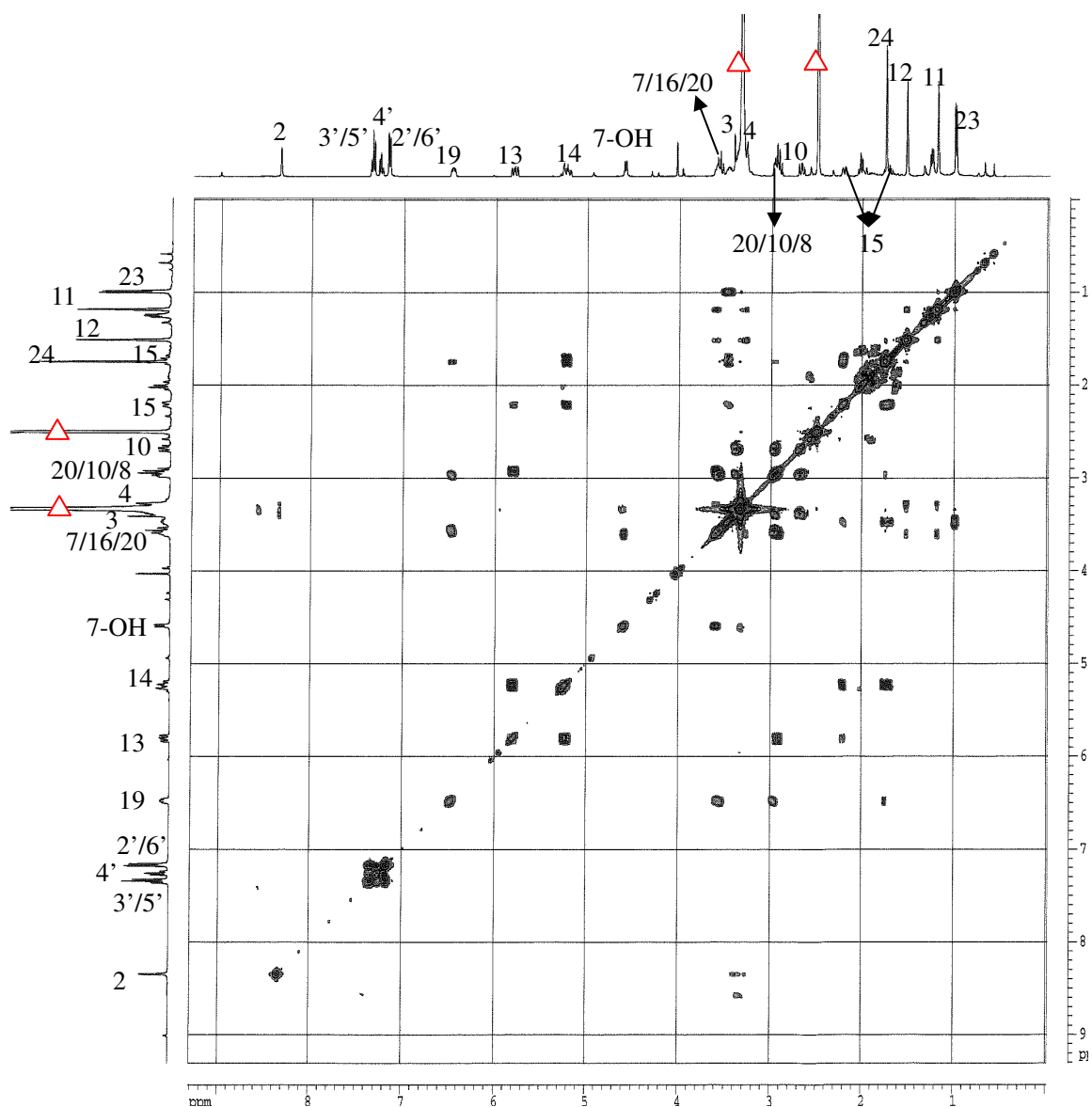


Figure 3.1.48 COSY correlations of cytochalasin Z17 (27)

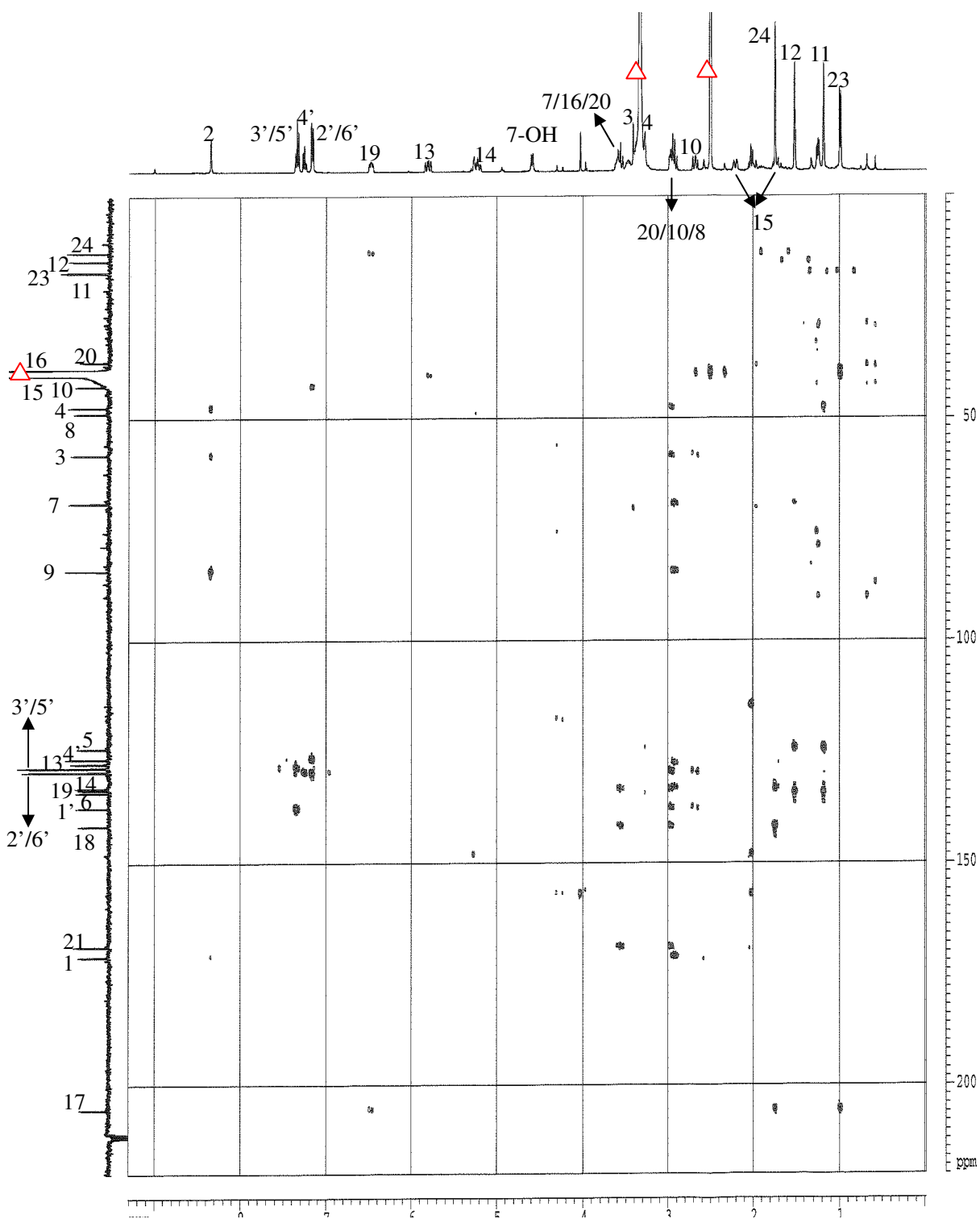


Figure 3.1.49 HMBC correlations of cytochalasin Z17 (27).

3.1.28 Dihydroisoflavipucine (compound 28, known)

Dihydroisoflavipucine	
Biological Source	<i>Aspergillus</i> sp.
Sample Code	Fr.7.6.6.2.2
Sample Amount	12 mg
Molecular Formula	C ₁₂ H ₁₇ NO ₄
Molecular Weight	239 g/mol
Solubility	MeOH
Physical Description	Yellow amorphous solid
Optical Rotation	$[\alpha]_D^{20} -23^\circ$ (c 0.5, MeOH)
HPLC Retention Time	21.7 min (standard gradient)

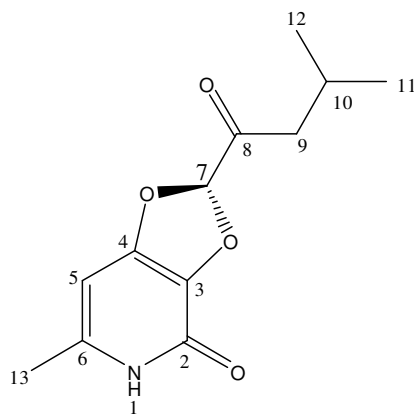
Compound **28** was obtained as a yellow amorphous solid (12 mg) with an $[\alpha]_D^{20}$ value of -23° (c 0.5, MeOH) and it exhibited UV absorbances at λ_{\max} (MeOH) 218.3, 251.8, and 303.9 nm, which suggested that **28** was a pyridione derivative (Loesgen *et al.*, 2011). Its molecular weight was established as 239 g/mol based on the molecular ion peaks observed at m/z 239.8 $[M+H]^+$ (base peak), 261.8 $[M+Na]^+$, 478.9 $[2M+H]^+$, 500.8 $[2M+Na]^+$ and 739.9 $[3M+Na]^+$ upon the positive ionization by ESI-MS analysis. Its molecular formula was determined as $C_{12}H_{17}NO_4$ based on the $[M+H]^+$ signal at m/z 240.1229 (calc. for 240.1231) in HRESIMS, containing two more hydrogen atoms than the isoflavipucine (**28a**). The 1H -NMR spectrum of **28** (Table 3.1.29) revealed the appearance of one olefinic methine proton at δ_H 6.15 ppm (H-5), three aliphatic methine groups at δ_H 6.10 ppm (H-7), 3.91 ppm (H-8) and 1.92 ppm (H-10), one aliphatic methylene group at δ_H 1.33 and 1.41 ppm (CH_2 -9), two methyl groups at δ_H 0.97 ppm (CH_3 -11) and 1.01 ppm (CH_3 -12), and one aromatic methyl at δ_H 2.30 ppm (CH_3 -13). The ^{13}C -NMR and DEPT spectra of **28** displayed 12 carbon signals for three methyl groups, one methylene group, four methine groups, and four quaternary olefinic carbon atoms including one amide carbonyl carbons as well as two oxygenated carbon atoms. The analysis of 1H - 1H COSY spectrum (Table 3.1.29 and Figure 3.1.50) established the presence of one continuous spin system indicating the protons H-7 to CH_3 -12 and CH_3 -11 going through H-8, CH_2 -9 and H-10. Moreover, the interpretation of HMQC spectrum allowed the assignment of proton signals to the corresponding proton-bearing carbon atoms.

Additionally, the connection of different substructures of **28** was determined based on the interpretation of the HMBC spectrum (Figure 3.1.51). HMBC correlations were observed for H-5 to C-3, C-4, C-6, C-13 and even to C-2 (δ_C 132.7, 157.9, 143.5, 18.8, and 155.2 ppm, respectively), corresponding to the pyridone ring, for H-7 to C-3, C-4, C-8 (δ_C 70.5 ppm), and C-9 (δ_C 40.4 ppm) which were assigned to the oxygen-containing five-membered ring, for H-8 to C-7 (δ_C 115.8 ppm), C-9, and C-10 (δ_C 25.2 ppm), for CH_2 -9 to C-7, C-8, C-10, C-11 (δ_C 21.8 ppm), and C-12 (δ_C 24.0 ppm), for CH_3 -11 to C-9, C-10 and C-12, and for CH_3 -12 to C-9, C-10 and C-11,

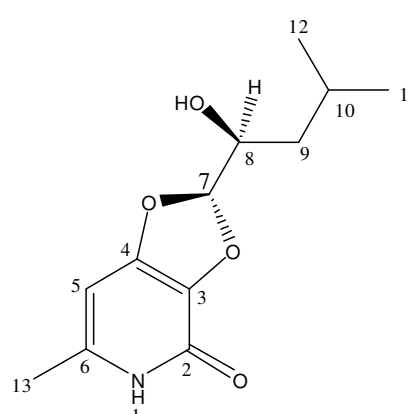
corresponding to the previously mentioned spin system. Besides, correlation of the methylene group protons (CH₂-13) to C-4, C-5, C-6, and even to C-3, revealed that the methyl group was placed at C-6. By comparison of the data obtained for **28** to those of isoflavipucine (**28a**), the only difference was the resonance of an oxygenated saturated carbon atom at δ_C 70.5 (C-8) in **28**, instead of the carbonyl group in **28a**. Therefore, compound **28** was finally established as dihydroisoflavipucine according to the analysis as mentioned above and by comparison with reported data (Table 3.1.29) (Loesgen *et al.*, 2011).

Table 3.1.29 NMR data for dihydroisoflavipucine (28)

Position	28 CD ₃ OD, δ (ppm), <i>J</i> in Hz		Reference CDCl ₃ , δ (ppm), <i>J</i> in Hz Loesgen <i>et al.</i> , 2011	
	¹ H (300 MHz)	¹³ C (75 MHz)	¹ H (600 MHz)	¹³ C (150 MHz)
1				
2		155.2		153.9
3		132.7		130.7
4		157.9		156.5
5	6.15 d (0.7)	95.0	5.96 s	94.2
6		143.5		142.7
7	6.10 d (3.3)	115.8	6.00 d (3.5)	114.1
8	3.91 dt (3.5, 9.3)	70.5	3.92 ddd (4.0, 4.0, 10.0)	69.8
9	1.33 ddd (3.6, 3.6, 9.4)	40.4	1.37 ddd (4.0, 4.0, 10.0)	39.6
	1.41 ddd (3.6, 3.6, 9.4)		1.57 ddd (4.0, 4.0, 10.0)	
10	1.92 m	25.2	1.88 m	24.0
11	0.97 d (6.6)	21.8	0.91 d (6.5)	21.5
12	1.01 d (6.6)	24.0	0.95 d (6.5)	23.5
13	2.30 d s	18.8	2.36 s	19.3



(28a) isoflavipucine



(28) dihydroisoflavipucine

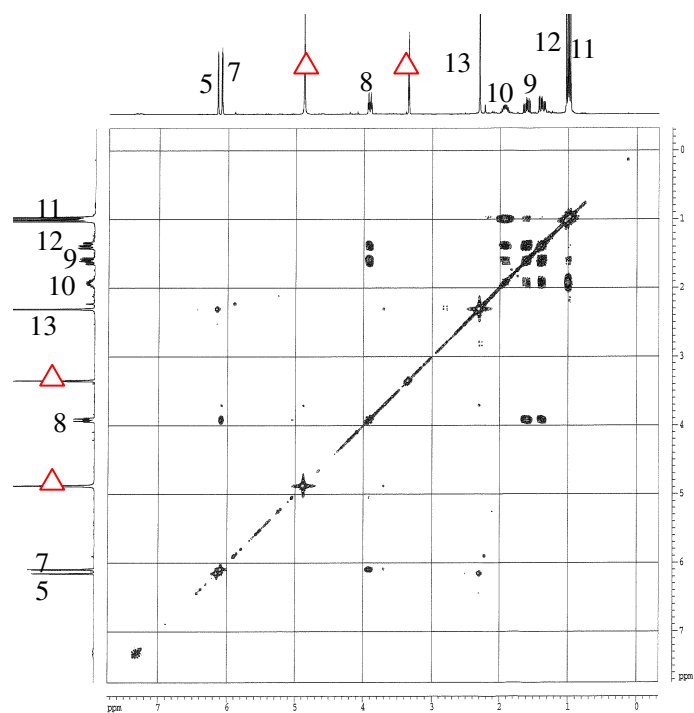


Figure 3.1.50 COSY correlations of dihydroisoflavipucine (28).

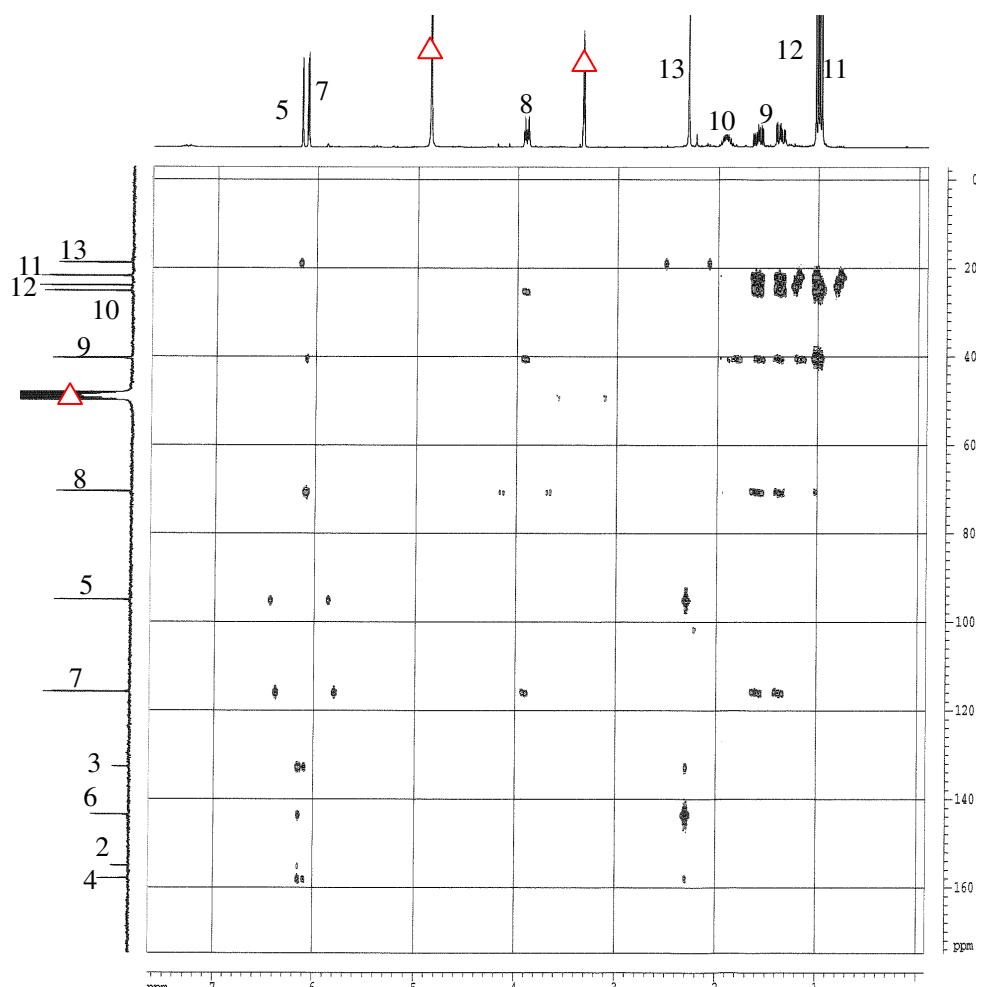
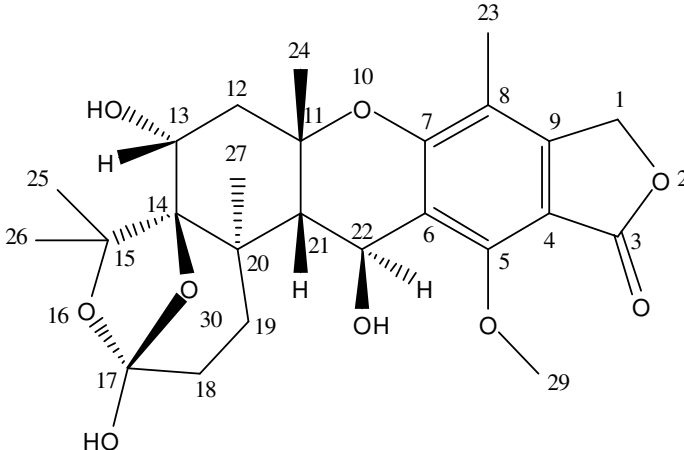
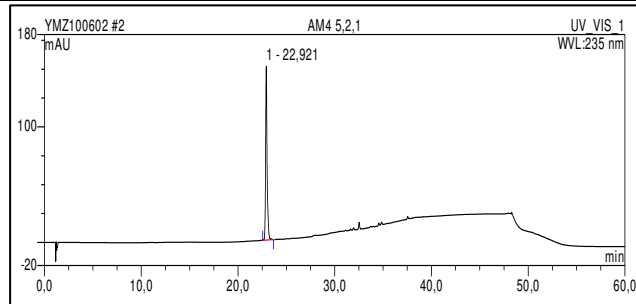


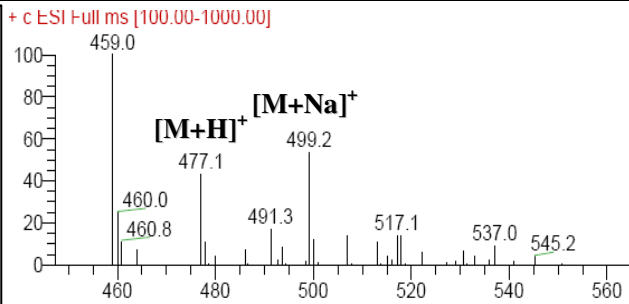
Figure 3.1.51 HMBC correlations of dihydroisoflavipucine (28).

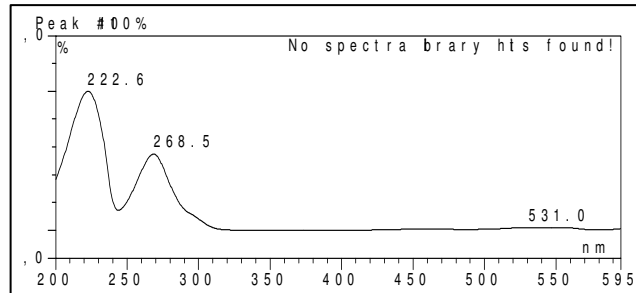
3.1.29 Austalide R (compound 29, new)

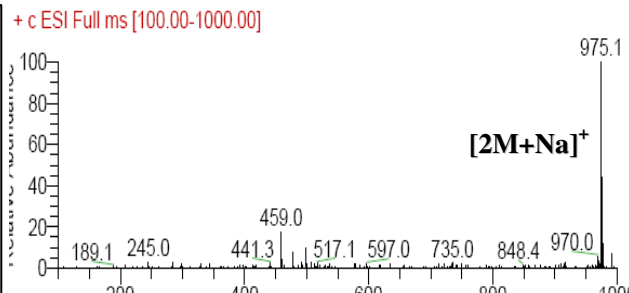
Austalide R	
Biological Source	<i>Aspergillus</i> sp.
Sample Code	Fr.4.5.2.1
Sample Amount	5.4 mg
Molecular Formula	C ₂₅ H ₃₂ O ₉
Molecular Weight	476 g/mol
Solubility	MeOH
Physical Description	Brown amorphous solid
Optical Rotation	$[\alpha]_D^{20} - 57^\circ$ (c 0.15, MeOH)
HPLC Retention Time	22.9 min (standard gradient)











Compound **29** was obtained as a brown amorphous solid (5.4 mg) with an $[\alpha]_D^{20}$ value of -57° (c 0.15, MeOH). Similar to **10-14**, the UV spectrum of **29** showed maxima at λ_{\max} (MeOH) 222.6 and 268.5 nm, which indicated it was a meroterpenoid derivative. Its molecular weight was established as 476 g/mol according to the molecular ion peaks observed at m/z 477.1 $[M+H]^+$ (base peak), 499.2 $[M+Na]^+$, and 975.1 $[2M+Na]^+$ upon positive ionization by ESI-MS analysis. The molecular formula of **29** was determined to be $C_{25}H_{32}O_9$ based on the prominent signal at m/z 477.2119 $[M+H]^+$ (calc. for 477.2125) in the HRESIMS, indicating a loss of 14 amu in the molecular weight compared with **12**. The physicochemical data of **29** were almost identical to those of **12** apart from the disappearance of the methoxy group located at C-17 in **12** in the NMR spectra of **29** (Tables 3.1.30 and 3.1.31). This revealed that **29** possesses the same skeleton as austalide O (**12**) but with a hydroxyl group at C-17 instead of the 17-OMe, which accounts for the 14 amu molecular weight difference. Further confirmation of the planar structure was achieved by analysis of the DEPT, COSY, HMQC, and HMBC spectra (Table 3.1.30 and Figure 3.1.52). Moreover, the ROESY spectrum (Table 3.1.30) exhibited the relative configuration in agreement with those of austalides M-O (**10-12**) (Yaming *et al.*, 2011). Consequently, compound **29** was identified as a new natural product and named austalide R by analysis of all mentioned data and by comparison with reported data (Yaming *et al.*, 2011).

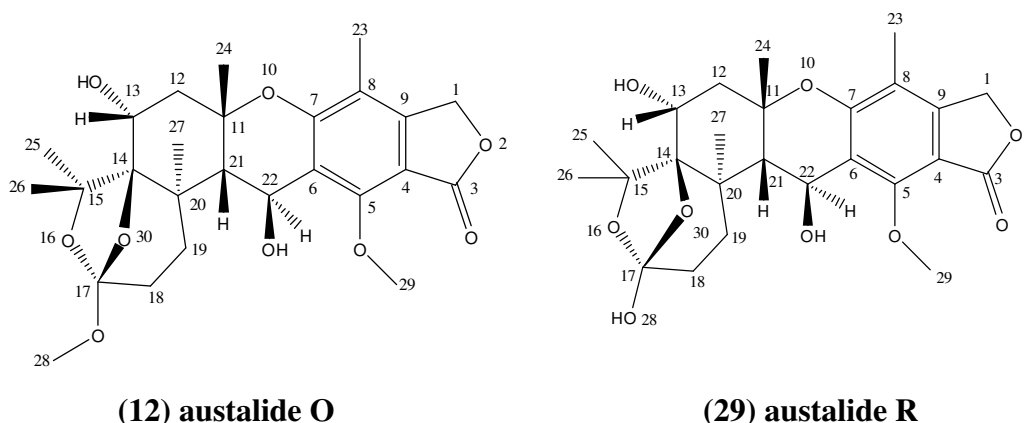


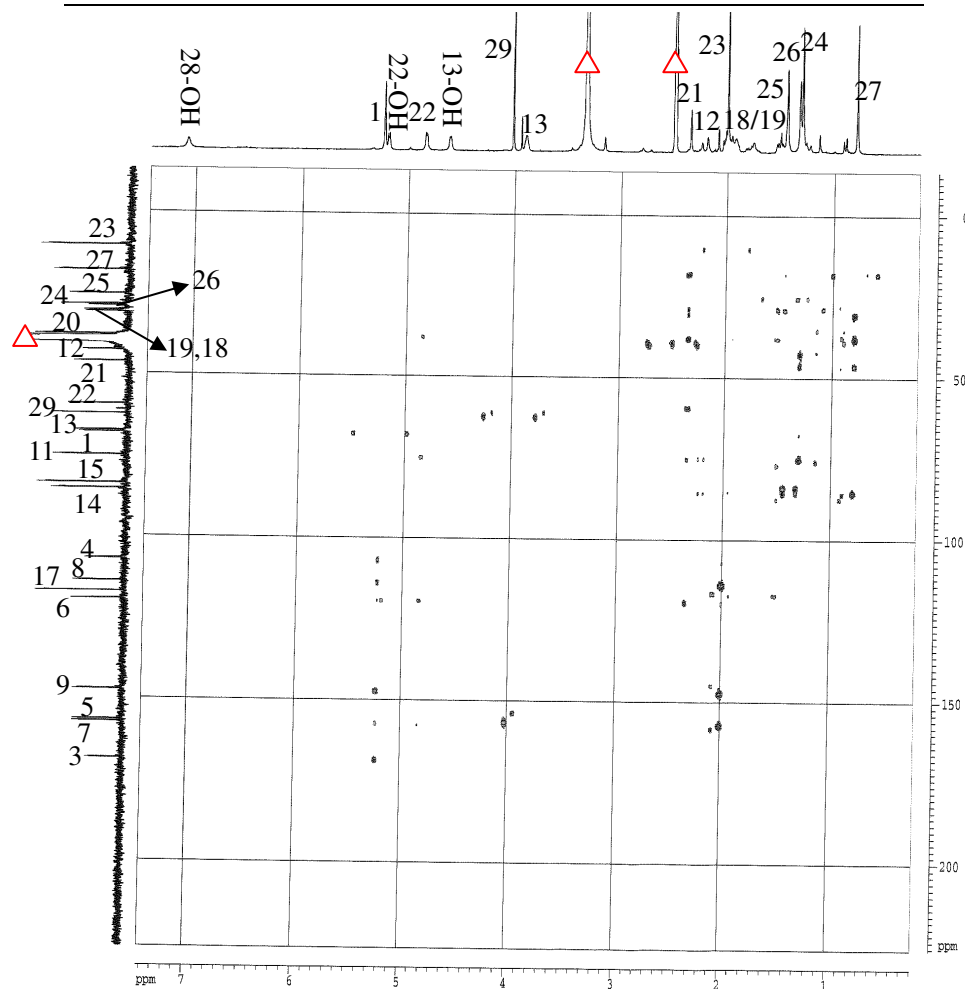
Table 3.1.30 NMR data for austrialide R (29)

Position	29 DMSO- <i>d</i> ₆ , δ (ppm), <i>J</i> in Hz		Correlation		
	¹ H (300 MHz)	¹³ C (75 MHz)	COSY	HMBC	ROESY ^a
1	5.25 s	68.1		3,4,7,8,9	
2					
3		168.6			
4		107.0			
5		156.7			
6		119.4			
7		157.2			
8		113.9			
9		147.3			
10					
11		75.2			
12	2.01 d (4.7) 2.20 d (14.3)	42.8	13		
13	3.89 brs	67.6	12		26
13-OH	4.62 brs				
14		85.5			
15		83.8			
16					
17		117.1			
18	1.50 m, 1.74 m	30.6	19	17,20	
19	1.80 m, 1.93 m	31.0	18	17	
20		38.0			
21	2.34 s	46.3	22	6,11,19,20,22,24,27	24
22	4.83 d (2.8)	59.5	21	6,7,11,20	27
22-OH	5.20 brs			6	
23	1.99 s	10.5		6,7,8,9	
24	1.29 s	28.8		11,12,21	21
25	1.43 s	25.6		14,15,26	27
26	1.32 s	29.1		14,15,25	
27	0.79 s	18.2		14,19,20,21	22,25
28-OH	7.04 brs				
29	4.01 s	62.5		5	

^a CD₃OD (600 MHz)

Table 3.1.31 Comparison between austalide R (29) and austalide O (12)

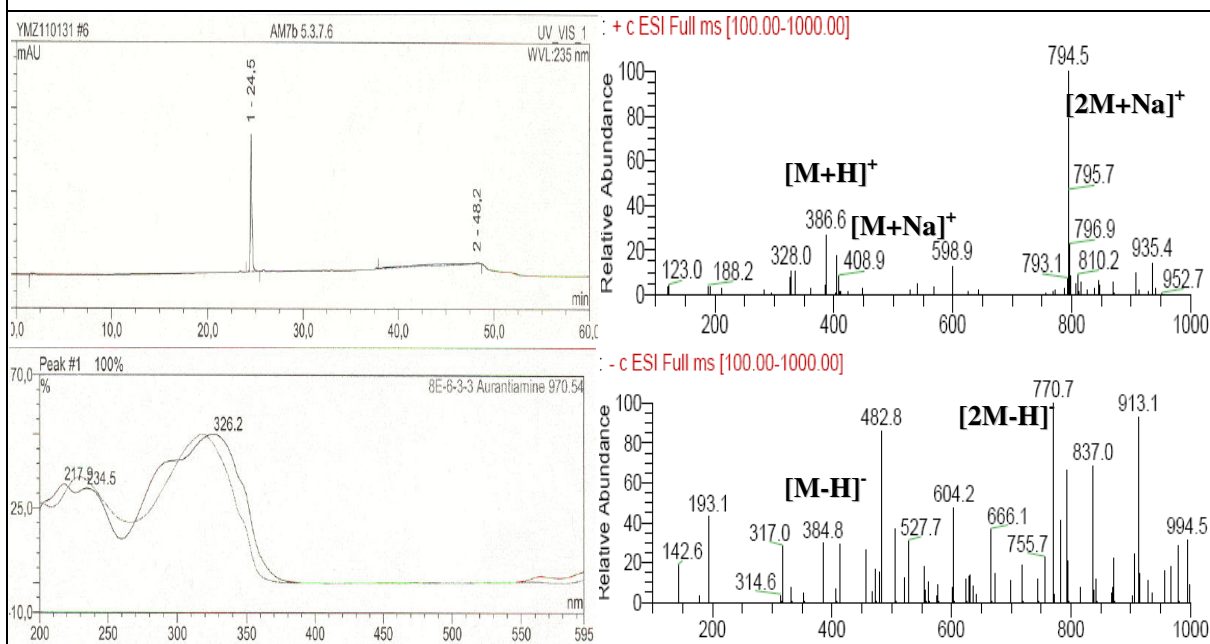
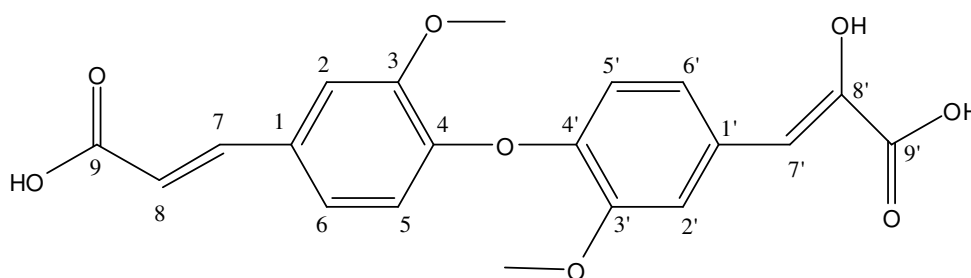
Position	29 CD ₃ OD, δ (ppm), J in Hz	12 CD ₃ OD, δ (ppm), J in Hz
	¹ H (500 MHz)	¹ H (500 MHz)
1	5.25 s	5.23 s
12	2.23 dd (4.2, 15.5)	2.20 dd (4.4, 15.6)
	2.34 dd (2.3, 15.6)	2.32 dd (2.1, 15.7)
13	4.11 dd (2.2, 4.3)	4.09 dd (2.3, 4.3)
18	1.66 m, 1.97 m	1.64 m, 1.96 m
19	1.97 m, 2.14 m	1.96 m, 2.13 m
21	2.52 brs	2.48 brs
22	4.98 brs	4.97 brs
23	2.11 s	2.09 s
24	1.39 s	1.37 s
25	1.59 s	1.60 s
26	1.46 s	1.47 s
27	0.93 s	0.92 s
28		3.38 s
29	4.19 s	4.16 s

**Figure 3.1.52 HMBC correlations of austalide R (29).**

3.1.30 3-(4-(4-(2-Carboxyvinyl)-2-methoxyphenoxy)-3-methoxyphenyl)-2-hydroxyacrylic acid (compound 30, new)

3-(4-(4-(2-Carboxyvinyl)-2-methoxyphenoxy)-3-methoxyphenyl)-2-hydroxyacrylic acid

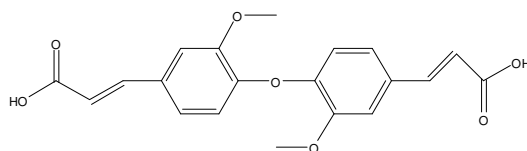
Biological Source	<i>Aspergillus</i> sp.
Sample Code	Fr.7.5.3.7.6
Sample Amount	2.5 mg
Molecular Formula	C ₂₀ H ₁₈ O ₈
Molecular Weight	386 g/mol
Solubility	MeOH
Physical Description	Yellow powder
HPLC Retention Time	24.5 min (standard gradient)



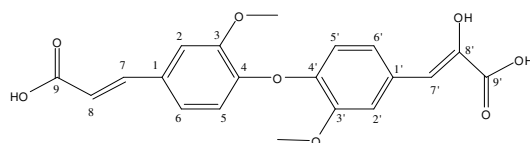
Compound **30** was isolated as a yellow powder (2.5 mg) and it revealed UV absorbances at λ_{\max} (MeOH) 217.9, 234.5, and 326.2 nm. Its molecular weight was established as 386 g/mol based on the molecular ion peaks observed at m/z 386.6 $[M+H]^+$ (base peak), 408.9 $[M+Na]^+$, 794.5 $[2M+Na]^+$, 384.8 $[M-H]^-$ (base peak), and 770.7 $[2M-H]^-$ upon positive and negative ionization by ESI-MS analysis. The molecular formula of **30** was determined as $C_{20}H_{18}O_8$ based on the $[M+H]^+$ signal at m/z 387.1074 (calc. for 387.1080) in the HRESIMS, indicating an increase of 16 amu in the molecular weight compared with 1-feruloyloxy-2-methoxy cinnamic acid (**30a**) (Huang *et al.*, 2000). The 1H -NMR spectrum (Table 3.1.32) of **30** displayed two sets of ABX aromatic systems at δ_H 6.82 ppm (H-5), 7.11 ppm (H-6), and 7.36 ppm (H-2), as well as 6.79 ppm (H-5'), 7.13 ppm (H-6'), and 7.46 ppm (H-2'), which were assigned to the two trisubstituted benzene rings. Two signals resonating at δ_H 3.74 ppm (3'-OCH₃) and 4.01 ppm (3-OCH₃) in the 1H -NMR spectra with two corresponding carbon signals at δ_C 56.1 ppm and 56.8 ppm, respectively, revealed the presence of two methoxyl groups on both rings. Moreover, two trans related olefinic protons resonating at δ_H 6.44 ppm (H-8, $J=13.4$) and 7.65 ppm (H-7, $J=15.9$) revealed the appearance of the $-CH=CH-$ moiety. In addition, the proton signal resonating at δ_H 7.44 ppm was assigned to the olefinic methine group (CH-7). The ^{13}C and DEPT spectra of **30** displayed 18 carbon signals for two methoxy groups, nine olefinic methine groups, and seven quaternary carbon atoms including one carbonyl carbon, whereas two carbon atoms were not detected as indicated by the molecular formula of **30**. The analysis of 1H - 1H COSY spectrum (Table 3.1.32 and Figure 3.1.53) established the presence of two aromatic olefinic AB spin systems corresponding to correlations of H-6 to H-5 and H-2, and of H-6' to H-5' and H-2', as well as one additional olefinic AB system corresponding to correlation of H-7 to H-8. The interpretation of HMQC spectrum allowed the assignment of proton signals to the corresponding proton-bearing carbon atoms. Accordingly, the NMR spectra of **30** revealed signals of two feruloyl moieties. The NMR data of **30** were similar to those of **30a** indicating similar molecular framework for both compounds apart from the appearance of an additional hydroxyl group at C-8' in **30** revealing in an asymmetrical

compound, which accounts for the 16 amu molecular weight difference.

The connection between the different substructures of **30** was achieved by interpretation of the HMBC spectrum (Table 3.1.32 and Figure 3.1.54). The aromatic proton H-2 correlated with two aromatic carbons C-6 (δ_C 123.2 ppm) and C-7 (δ_C 146.0 ppm) as well as three quaternary carbons C-1 (δ_C 130.7 ppm), C-3 (δ_C 150.6 ppm) and C-4 (δ_C 149.3 ppm), two of which being oxygenated. HMBC correlations were also observed for H-5 to C-1 and C-3, for H-6 to C-2 (δ_C 112.9 ppm), C-4 and C-7, and for H-7 to C-1, C-2, C-6, C-8 (δ_C 118.0 ppm), and C-9 (δ_C 170.1 ppm). Moreover, correlations of the aromatic proton H-2' to C-1', C-3', C-4', C-6' (δ_C 126.5 ppm), and C-7', and for the H-5' to C-1' (δ_C 125.8 ppm) and C-3' (δ_C 148.9 ppm), and of H-6' to C-2' (δ_C 113.9 ppm), C-4' (δ_C 149.4 ppm) and C-7' (δ_C 128.6 ppm). Correlations of the methoxy group protons OCH₃-3' and OCH₃-3 to C-3' and C-3, respectively, suggested their location on the aromatic rings. Remaining HMBC correlations were observed for the H-7' to C-2'. Despite of missing carbon signals the structure of **30** was confirmed by HRESIMS and comparison with reported data for 1-feruloyloxy-2-methoxy cinnamic acid (**30a**). Therefore, compound **30** was finally confirmed as a new natural product and was named 3-(4-(4-(2-carboxyvinyl)-2-methoxyphenoxy)-3-methoxyphenyl)-2-hydroxyacrylic acid based on the analysis of the foregoing evidence in addition to comparison with reported data (Huang *et al.*, 2000).



(30a) 1-Feruloyloxy-2-methoxy cinnamic acid (Huang *et al.*, 2000)



(30) 3-(4-(4-(2-Carboxyvinyl)-2-methoxyphenoxy)-3-methoxyphenyl)-2-hydroxyacrylic acid

Table 3.1.32 NMR data for 3-(4-(4-(2-carboxyvinyl)-2-methoxyphenoxy)-3-methoxyphenyl)-2-hydroxyacrylic acid (30)

Position	30 CD ₃ OD, δ (ppm), J in Hz		Correlation	
	¹ H (600 MHz)	¹³ C (150 MHz)	COSY	HMBC
1		130.7		
2	7.36 d (1.3)	112.9	3,6	1,3,4,6,7
3		150.6		
3-OCH ₃	4.01 s	56.8		3
4		149.3		
5	6.82 d (8.0)	114.8	6	1,3
6	7.11 d (7.5)	123.2	2,5	2,4,7
7	7.65 d (15.9)	146.0	8	1,2,6,8,9
8	6.44 d (13.4)	118.0	7	
9		170.1		
1'		125.8		
2'	7.46 d (1.3)	113.9	3',6'	1',3',4',6',7'
3'		148.9		
3'-OCH ₃	3.74 s	56.1		3'
4'		149.9		
5'	6.79 d (8.22)	116.3	6'	1',3'
6'	7.13 dd (1.1, 8.2)	126.5	2',5'	2',4',7'
7'	7.44 brs	128.6		2'
8'				
9'				

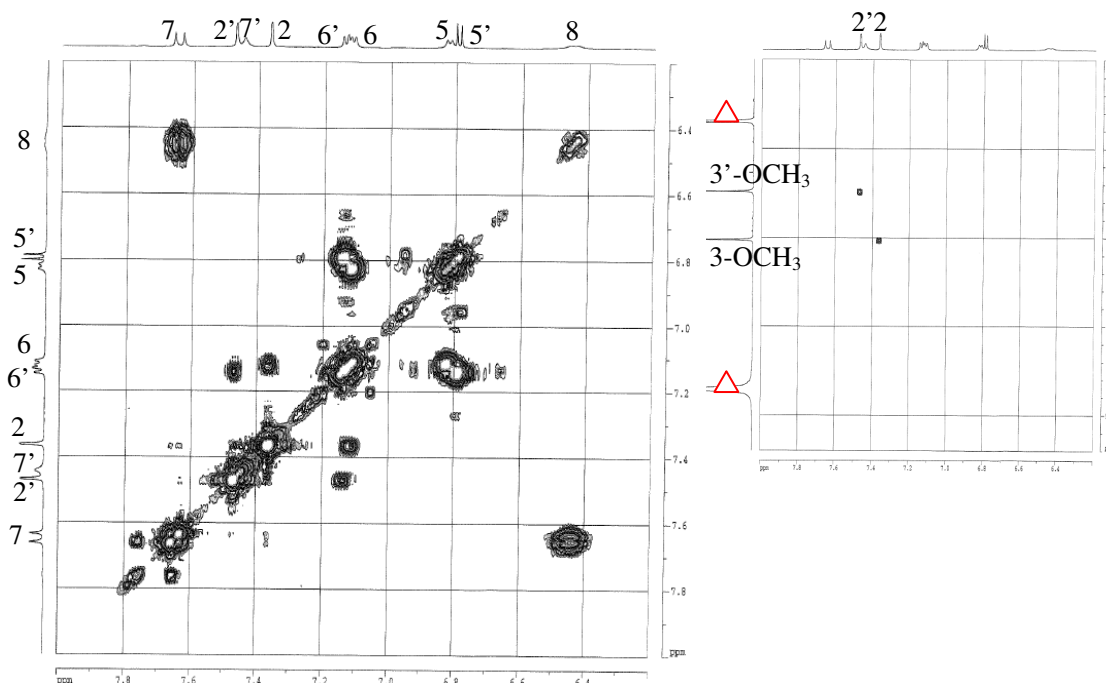


Figure 3.1.53 COSY correlations of 3-(4-(4-(2-carboxyvinyl)-2-methoxyphenoxy)-3-methoxyphenyl)-2-hydroxyacrylic acid (30).

Results

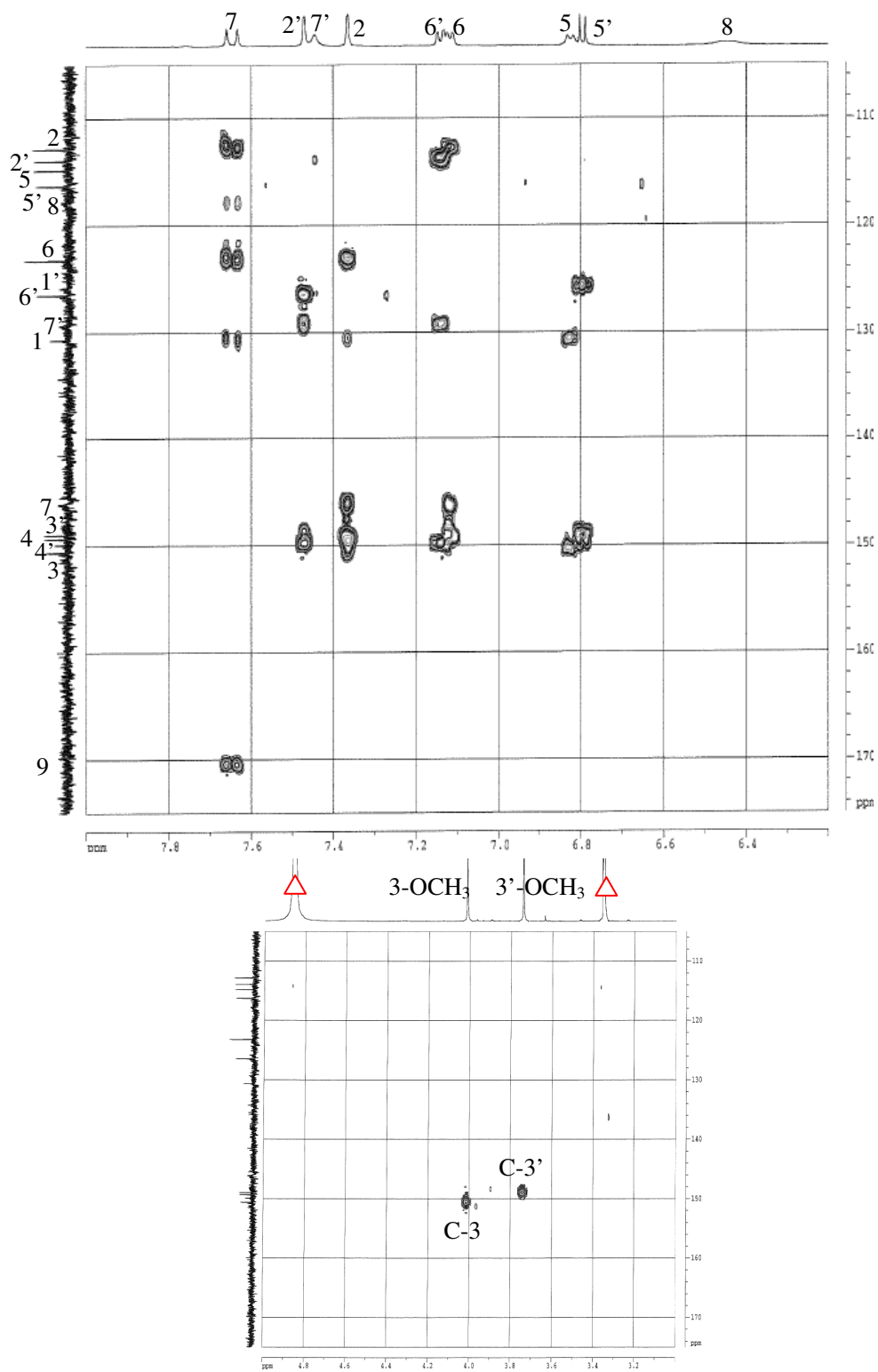
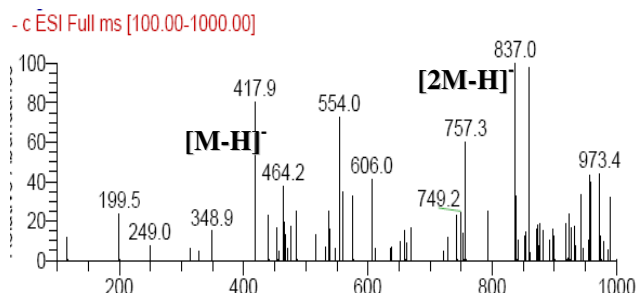
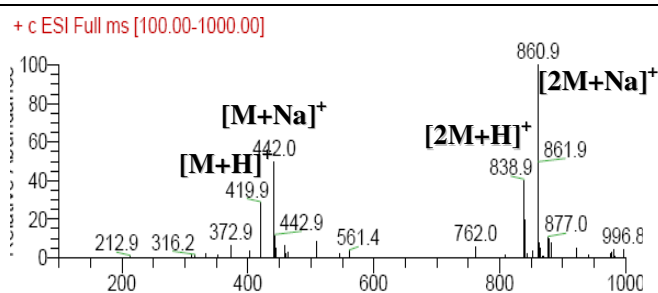
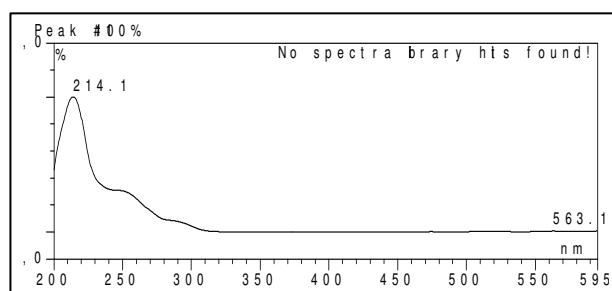
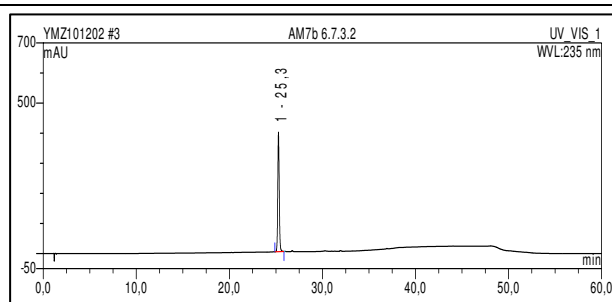
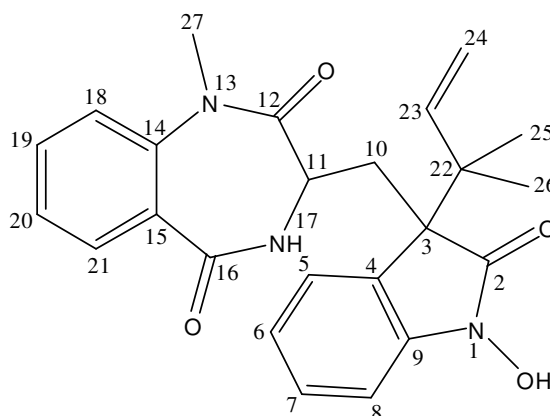


Figure 3.1.54 HMBC correlations of 3-(4-(4-(2-carboxyvinyl)-2-methoxyphenoxy)-3-methoxyphenyl)-2-hydroxyacrylic acid (30).

3.1.31 3-((1-Hydroxy-3-(2-methylbut-3-en-2-yl)-2-oxoindolin-3-yl)methyl)-1-methyl-3,4-dihydro-1H-benzo[e][1,4]diazepine-2,5-dione (compound 31, new)

3-((1-Hydroxy-3-(2-methylbut-3-en-2-yl)-2-oxoindolin-3-yl)methyl)-1-methyl-3,4-dihydro-1H-benzo[e][1,4]diazepine-2,5-dione

Biological Source	<i>Aspergillus</i> sp.
Sample Code	Fr.7.6.7.3.2
Sample Amount	8.0 mg
Molecular Formula	C ₂₄ H ₂₅ N ₃ O ₄
Molecular Weight	419 g/mol
Solubility	MeOH
Physical Description	Colourless amorphous powder
Optical Rotation	$[\alpha]_D^{20} + 62^\circ$ (<i>c</i> 1.0, CHCl ₃)
HPLC Retention Time	25.3 min (standard gradient)



Compound **31** was obtained as a colorless amorphous powder (8.0 mg) with an $[\alpha]_D^{20}$ value of + 62° (*c* 1.0, CHCl₃) and it revealed UV absorbances at λ_{\max} (MeOH) 214.1, 250.1, and 290.0 nm, which suggested the presence of indoline chromophore (Bhat and Harrison, 1986; Kimura *et al.*, 1982). Its molecular weight was established as 419 g/mol based on the molecular ion peaks observed at *m/z* 419.9 [M+H]⁺ (base peak), 442.0 [M+Na]⁺, 838.9 [2M+H]⁺, and 860.9 [2M+Na]⁺ upon positive ionization, and at *m/z* 417.9 [M-H]⁻ (base peak) and 837.0 [2M-H]⁻ upon negative ionization by ESI-MS analysis. The molecular formula of **31** was established as C₂₄H₂₅N₃O₄ on the basis of the [M+H]⁺ signal at *m/z* 420.1917 (calc. for 420.1923) in the HRESIMS. The ¹H NMR spectrum (Table 3.1.33) of **31** showed the presence of eight aromatic protons corresponding to two ABCD aromatic spin systems resonating at δ_H 7.30, 6.90, 7.21, 6.73 ppm (H-5, 6, 7, 8, respectively) and at δ_H 7.24, 7.50, 7.18, 7.27 ppm (H-18, 19, 20, 21, respectively), an olefinic proton at δ_H 6.07 ppm (H-23), a methine signal resonating at δ_H 2.09 ppm (H-11), a methylene group at δ_H 2.30 and 2.70 ppm (CH₂-10), an olefinic methylene group at δ_H 4.94 and 5.02 ppm (CH₂-24), three methyl groups including two aliphatic methyl groups at δ_H 0.98 and 0.98 ppm (CH₃-25 and CH₃-26), and a nitrogen-bearing methyl group at δ_H 3.15 ppm (CH₃-27). Additionally, an amide NH was observed at δ_H 8.18 ppm (H-17) in the ¹H-NMR spectrum. The ¹³C-NMR spectrum (Table 3.1.33) of **31** confirmed the presence of 24 carbon atoms in the structure. Furthermore, the DEPT experiment revealed the presence of ten methine groups, two methylene groups, three methyl groups, and nine quaternary carbon atoms including three amide carbonyl carbons at δ_C 172.3, 169.9, and 166.8 ppm (C-2, C-12, and C-16, respectively). The analysis of ¹H-¹H COSY spectrum (Table 3.1.33 and Figure 3.1.55) established the presence of four spin systems, which included the correlations observed for the aliphatic methylene protons (CH₂-10) to the deshielded methine proton (CH-11), for the olefinic methylene protons (CH₂-24) to the olefinic methine proton (H-23), in addition to the previously mentioned aromatic spin systems H-8 to H-21 and H-5 to H-8. Besides, the analysis of HMQC spectrum allowed the assignment of proton signals to the corresponding proton-bearing carbon atoms.

The connection between the different substructures of **31** was achieved by inspection of the HMBC spectrum (Table 3.1.33 and Figure 3.1.56). The tertiary methyl group CH₃-27 (δ_C 34.9 ppm) correlated with two quaternary carbon atoms C-12 (δ_C 169.9 ppm), C-14 (δ_C 140.1 ppm), whereas the amide proton (NH-17) correlated with the carbon atom C-10 (δ_C 28.9 ppm) as well as with C-11 (δ_C 49.6 ppm) and C-15 (δ_C 128.2 ppm), which indicated that the seven-membered nitrogen-containing ring was fused to a benzene ring. HMBC correlations of the methylene protons (CH₂-10) to C-2 (δ_C 72.3 ppm), C-3 (δ_C 54.7 ppm), C-4 (δ_C 124.8 ppm), C-11 (δ_C 49.6 ppm), C-12 (δ_C 169.9 ppm), and C-22 (δ_C 41.8 ppm), revealed that the indoline moiety was connected with the seven-membered nitrogen-containing ring through CH₂-10. Moreover, the location of CH₃-25 (δ_C 21.3 ppm) and CH₃-26 (δ_C 22.5 ppm) was established on the basis of correlations of both methyl groups to each other and to C-3, C-22, and C-23 (δ_C 142.9 ppm). The olefinic methylene group CH₂-24 (δ_C 113.4 ppm) was assigned by its correlation with C-22 and C-23. Furthermore, remaining HMBC correlations were observed for the aromatic protons as follow: H-5 to C-3, C-7 (δ_C 128.0 ppm), and C-9 (δ_C 142.7 ppm), for H-6 to C-4 (δ_C 124.8 ppm), C-7, and C-8 (δ_C 106.3 ppm), for H-7 to C-5 (δ_C 126.6 ppm), C-8, and C-9, for H-8 to C-4, C-6 (δ_C 120.8 ppm), and C-9, for H-18 to C-15 (δ_C 128.2 ppm) and C-20 (δ_C 125.1 ppm), for H-19 to C-14 (δ_C 140.1 ppm), C-18 (δ_C 121.1 ppm), and C-21 (δ_C 28.8 ppm), for H-20 to C-14, C-15, and C-18 (δ_C 121.6 ppm), and for H-21 to C-14, C-16, and C-19. Hence, compound **31** was determined as a new metabolite based on the analysis of its data as mentioned as above and named 3-((1-hydroxy-3-(2-methylbut-3-en-2-yl)-2-oxoindolin-3-yl)methyl)-1-methyl-3,4-dihydro-1*H*-benzo[*e*][1,4]diazepine-2,5-dione. The relative configuration of **31** is still to be determined..

**Table 3.1.33 NMR data for
3-((1-hydroxy-3-(2-methylbut-3-en-2-yl)-2-oxoindolin-3-yl)methyl)-1-methyl
-3,4-dihydro-1*H* -benzo[*e*][1,4]diazepine-2,5-dione. (31)**

Position	31 DMSO- <i>d</i> ₆ , δ (ppm), <i>J</i> in Hz		Correlation	
	¹ H (300 MHz)	¹³ C (100 MHz)	COSY	HMBC
1				
2		172.3		
3		54.7		
4		124.8		
5	7.30 d (7.8)	126.6	6	3, 7, 9
6	6.90 ddd (0.1, 7.5, 7.5)	120.8	5, 7	4, 7, 8
7	7.21 t (7.7)	128.0	6, 8	5, 8, 9
8	6.73 d (7.6)	106.3	7	4, 6, 9
9		142.7		
10	2.30 dd (7.7, 14.9) 2.70 dd (3.2, 14.9)	28.9	11	2, 3, 4, 11, 12, 22
11	2.90 br m	49.6	10, 17	
12		169.9		
13				
14		140.1		
15		128.2		
16		166.8		
17	8.18 d (5.9)		11	10, 11, 15
18	7.24 d (8.1)	121.6	19	15, 20
19	7.50 ddd (1.7, 8.5, 8.6)	132.0	18, 20	14, 18, 21
20	7.18 t (7.9)	125.1	19, 21	14, 15, 18
21	7.27 d (7.1)	128.8	20	14, 16, 19
22		41.8		
23	6.07 dd (10.8, 17.4)	142.9	24	22, 25, 26
24	4.94 dd (0.1, 17.4) 5.02 dd (0.1, 10.9)	113.4	23	22, 23
25	0.98 s	21.3		3, 22, 23, 26
26	0.98 s	22.5		3, 22, 23, 25
27	3.15 s	34.9		12, 14

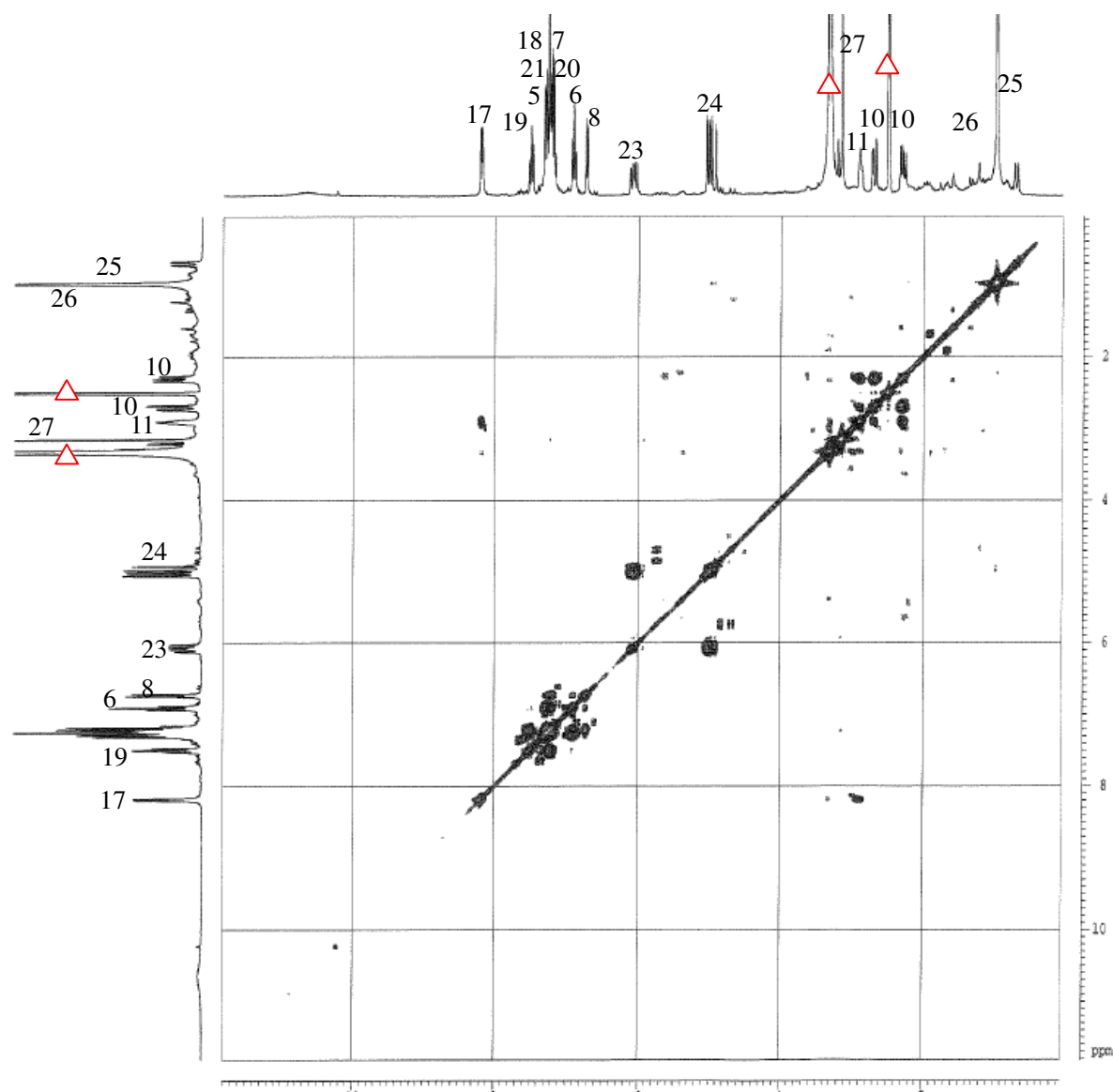


Figure 3.1.55 COSY correlations of 3-((1-hydroxy-3-(2-methylbut-3-en-2-yl)-2-oxoindolin-3-yl)methyl)-1-methyl-3,4-dihydro-1*H*-benzo[*e*][1,4]diazepine-2,5-dione (31).

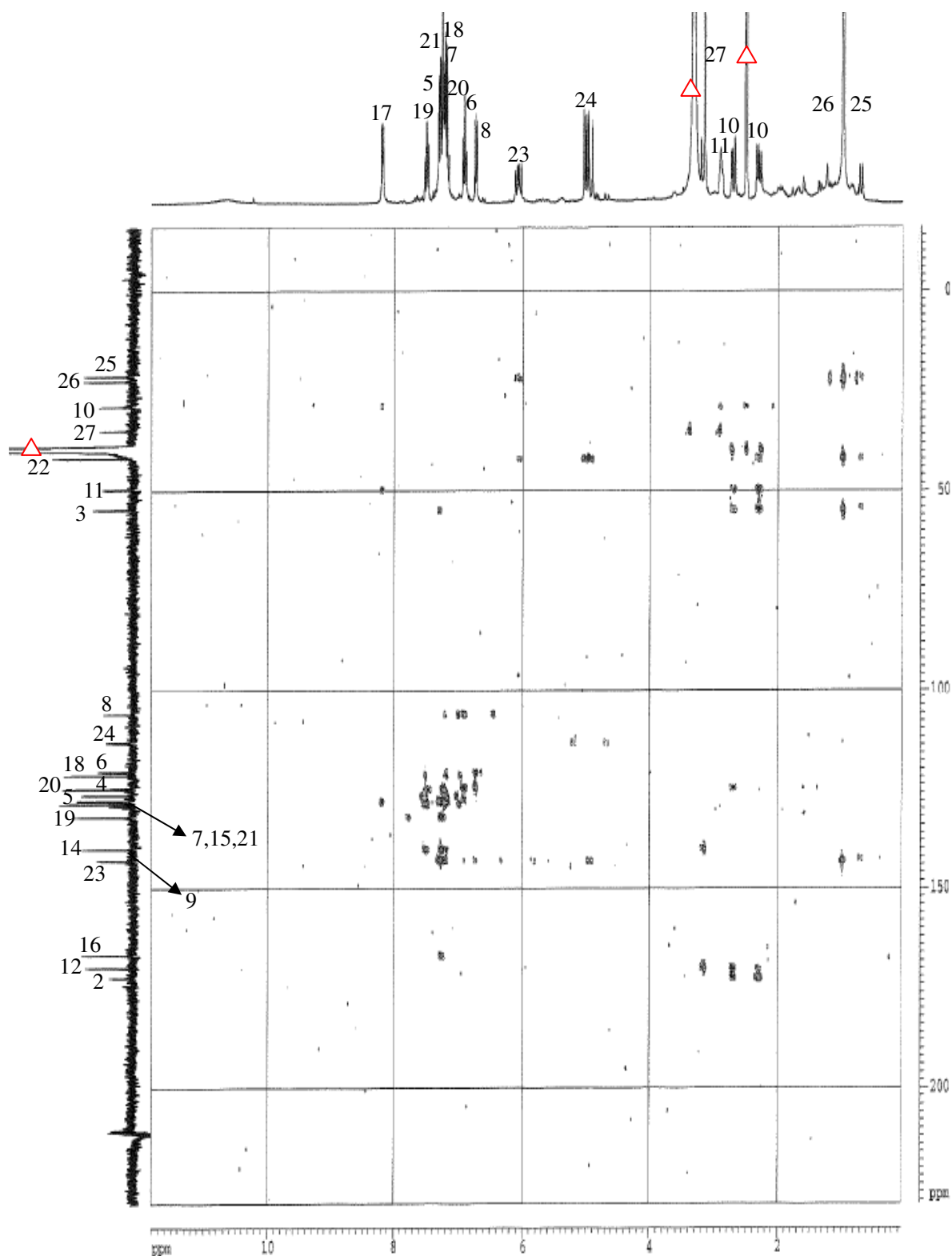


Figure 3.1.56 HMBC correlations of 3-((1-hydroxy-3-(2-methylbut-3-en-2-yl)-2-oxindolin-3-yl)methyl)-1-methyl-3,4-dihydro-1*H*-benzo[*e*][1,4]diazepine-2,5-dione (31).

3.2 Bioactivity test results for compounds isolated from *Aspergillus* sp.

All isolated compounds (**1-31**) from *Aspergillus* sp. were evaluated for their bioactivity against the murine cancer cell line L5178Y using the MTT assay (Aly *et al.*, 2008). Results of the cytotoxicity assay are presented in Table 3.2.1. Compounds **8** and **9** revealed pronounced cytotoxicity against L5178Y with IC₅₀ values of 3.7 and 0.2 μ M, respectively. Compound **5** showed moderate activity with an IC₅₀ value of 39.4 μ M, whereas the remaining investigated compounds showed either weak or no activity in the assay (up to a dose of 10 μ g/mL). (Table 3.2.1).

Compounds **5**, **8**, and **9** were further tested against cell lines human Philadelphia chromosome-positive chronic myelogenous leukaemia (K562), human ovarian carcinoma (A2780sens), and a derived cisplatin-resistant subline (A2780CisR) (Drexler *et al.*, 2000; Klein *et al.*, 1976; Lozzio *et al.*, 1975; Rose *et al.*, 1990), where compounds **8** and **9** exhibited moderate cytotoxic activity with IC₅₀ values of 15.0, 18.5 and 38.8 μ M for **8**, and 19.3, 8.0 and 22.5 μ M for **9**, respectively. However, compound **5** exhibited weak bioactivity in the assay (Table 3.2.1). Compounds **10-14** were also evaluated for their effect on human alveolar basal epithelial cells (A549) viability by XTT viability assay and none of them showed potential bioactivity.

Results

Table 3.2.1 Results of cytotoxicity assay of the isolated compounds (1-31)

Compound tested		% Growth inhibition		IC ₅₀ (μM)		
		(10 μg/mL)		K562	A2780sens	A2780CisR
		L5178Y	L5178Y			
Butyrolactone II	1	49.1				
Dicitrinin A	2	44.6				
4-Acetyl-3,4-dihydro-6,8-dihydroxy-3-methoxy-5-methylisocoumarin	3	9.3				
2,3,4-Trimethyl-5,7-dihydroxy-2,3-dihydrobenzofuran	4	9.1				
4-Acetyl-3,4-dihydro-6,8-dihydroxy-5-methylisocoumarin	5	76.9	39.4	77.7	34.5	79.6
Citrinin	6	35.8				
Phenol A acid	7	0				
Fumiquinazoline J	8	99.1	3.7	15.0	18.5	38.8
Methyl 3,4,5-trimethoxy-2-(2-(nicotinamido)benzamido) benzoate	9	100.1	0.2	19.3	8.0	22.5
Austalide M	10	0				
Austalide N	11	0				
Austalide O	12	28.0				
Austalide P	13	16.2				
Austalide Q	14	41.7				
3'-O-acetylthymidine	15	52.2				
Dihydrocitrinin	16	10.7				
Dihydrocitrinone	17	0				
6,8-Dihydroxy-3,4,5-trimethylisocoumarin	18	8.3				
Pretrichodermamide A	19	24.3				
Tryptoquivaline K	20	22.8				
Fumiquinazoline K	21	0				
Fumiquinazoline L	22	5.8				
Fumiquinazoline M	23	0				
Fumiquinazoline N	24	3.3				
Fumiquinazoline O	25	1.4				
Fumiquinazoline P	26	0				
Cytochalasin Z17	27	25.3				
Dihydroisoflavipucine	28	8.5				
Austalide R	29	3.6				
3-(4-(4-(2-carboxyvinyl)-2-methoxyphenoxy)-3-methoxyphenyl)-2-hydroxyacrylic acid	30	24.3				
3-((1-hydroxy-3-(2-methylbut-3-en-2-yl)-2-oxoindolin-3-yl)methyl)-1-methyl-3,4-dihydro-1H-benzo[e][1,4]diazepine-2,5-dione	31	0				

4 Discussion

4.1 Considerations of natural products research in the present future

In drug discovery programs, the role of natural products or their derivatives has been important and substantial. However, despite of a sustained record of important contributions, the major biopharmaceutical companies have terminated or obviously scaled down their natural products-based discovery projects during the last 15 years. A main reason for the decline of natural product research was attributed to the lengthy time scales to identify or dereplicate promising new lead compounds based on the bioassay-guided pursuit, and one additional reason has been explained by the difficulties encountered upon designing effective natural product-based platforms which would incorporate modern high-throughput screening (HTS) (Baker *et al.*, 2007; Tyler *et al.*, 2011).

Cancer research, however, has mainly kept or renewed the interest of natural products study. In clinical use, 60% of all anticancer agents come from natural products or derivatives thereof. Moreover, around 80% of antibiotics used in clinical treating for bacterial infections are also either natural products or their derivatives (Jacob, 2010; Newman and Cragg, 2007). In recent years, research on the chemistry of marine-organisms has experienced a tremendous increase due to the need for drug discovery, and exhibited a revival of leadfinding marine natural antibiotics (Saleem *et al.*, 2007). This indicates that natural products research is still a promising and important source for drug discovery in pharmaceutical industry.

Traditional natural product research is indeed time consuming and compound availability is very low, which makes it unattractive for pharmaceutical industries. The natural product research and development will not only rely on new findings, but also the rate of making use of the isolated new molecules derived from microorganisms by interdisciplinary approach. Furthermore, it is also very vital to

make a great deal of efforts to find low cost and short term methods for discovering bioactive secondary metabolites.

In the future, natural products research must be based on fast and low cost methods, as well as focusing on biological materials showing high probabilities of finding promising and valuable bioactive compounds. Recently, an approach that incorporates systematic LC-MS-UV-ELSD analysis is reported and used to accelerate identifying compounds with unreported bioactivity and/or new structure (Tyler *et al.*, 2011), which significantly reduces the cycle times required to discover bioactive lead compounds and also illustrates the importance of applying modern HT methods to streamline therapeutic lead discovery projects in natural products research.

4.2 The importance of marine-associated fungi

The marine environment has gained considerable attention as a tremendous source of natural products. Furthermore, many of the isolated compounds from marine macro- and microorganisms revealed obvious biological effects, and some proved to be useful and valuable sources as lead structures for the development of promising anticancer drug candidates (Saleem *et al.*, 2007; Rateb and Ebel, 2011). With the advance in molecular biology in the early 1990s microbial life was found to occupy a vast range of hitherto unexplored environmental extremes including the deep ocean realm. Hence, special attention of natural product chemists was drawn to fungi surviving in the marine environment characterized by its unique ecosystems and harsh living conditions such as total darkness, extreme cold and great pressure. Such marine-derived fungi have proven to be a valuable source for promising drugs and drug lead compounds due to the structural diversity and potent pharmaceutical activities of their secondary metabolites (Debbab *et al.*, 2010; 2010; Rateb and Ebel, 2011; Saleem *et al.*, 2007).

A wide array of bioactive secondary metabolites were characterized from

marine-derived *Aspergillus* species, including the antibiotic and antifungal aculeacins A-G (Mizuno *et al.*, 1977; Satio *et al.*, 1977) and the squalene synthase inhibitor and antifungal agent CJ-15,183 (Watanabe *et al.*, 2001) from *A. aculeatus*, the antibiotic asporozin C from *A. oryzae* (Qiao *et al.*, 2010), the tubulin-depolymerising halimide from *Aspergillus* sp. (Mayer *et al.*, 2010), the NF- κ B inhibiting azonazine from *A. insulicola* (Wu *et al.*, 2010), and the cytotoxic cephalimysin A from *A. fumigatus* (Yamada *et al.*, 2007). Despite more than two decades of intensive investigations, marine-derived members of this genus continue to provide new natural products with novel structures and interesting biological activities (Numata *et al.*, 1992; Rateb and Ebel, 2011; Tyler *et al.*, 2011).

The main interest of this research was the isolation, identification and biological assay of new natural products isolated from sponge-derived *Aspergillus* sp. Fifteen new secondary metabolites and sixteen known ones are reported in this study. The isolated new compounds comprised six meroterpenoids named austalides M-R (**10-14** and **29**), eight alkaloids including tryptoquivaline K (**20**) and fumiquinazolines K-P (**21-26**) bearing a rare amino acid residue, as well as the novel biphenyl ether **30**, and the new tryptophan-derived alkaloid **31**, hence confirming that marine sponge-derived fungi are an important source of novel and interesting secondary metabolites.

4.3 The compounds isolated from *Aspergillus* sp.

In this study, the isolated compounds mainly belong to three different groups on the basis of their structure types and were classified as follow:

4.3.1 Polyketides

From the selected marine sponge-associated endophytic fungus *Aspergillus* sp. eleven polyketide-derived compounds (**1-7**, **16-18**, and **28**) were obtained. For some of them, a closer look will be taken at their structural features together with their biogenetic

origin and bioactivity.

The structure of polyketide antibiotic citrinin (**6**) was proposed and established in 1949, primarily by the investigations of Robertson and his co-workers. Citrinin is a pentaketide and its biosynthesis might proceed through the polyketide way (Curtis *et al.*, 1968). Citrinin is of the first compounds with antibiotic activity isolated as a fungal metabolite from *Penicillium citrinum*. Subsequently, **6** was also obtained from other *Penicillium* and *Aspergillus* species and from the leaves of the Australian plant *Crotalaria crispate*. Due to its high toxicity, its occurrence as mycotoxin in foodstuffs, citrinin has not been broadly exploited in medicine as an antibiotic, despite of promising activity. Moreover, citrinin has been demonstrated to possess nephrotoxic activity in addition to a number of chronic toxic effects (Benjamin *et al.*, 2006; Roedel and Gerlach, 1995). In the course of this study, compound **6** showed weak cytotoxic activity against the murine cancer cell line L5178Y using MTT assay.

Intense biosynthetic research has been performed on compound **6** using a variety of isotopic labeling strategies (Barber *et al.*, 1987; Benjamin *et al.*, 2006). A great deal of citrinin derivatives have been isolated, most famously by Curtis *et al.*, who revealed the isolation of seven metabolites related to citrinin in 1968 (Curtis *et al.*, 1968).

In this study, chemical investigation resulted in the isolation of six citrinin derivatives, which included compounds **4**, **7**, **16**, **17**, **18** and a citrinin dimer dicitrinin A (**2**). All of them may result from the sequential transformation of citrinin into both monomeric and dimeric products. Their proposed biosynthetic schemes are displayed in figures 4.3.1.1 and 4.3.1.2, respectively. Those protocols hypothesize the transformation of citrinin into both monomeric and dimeric derivatives, offering extensive molecular elements for future analytical chemistry investigation (Benjamin *et al.*, 2006; Jill *et al.*, 1981). In the present study, all isolated compounds were tested against the murine cancer cell line L5178Y using the MTT assay. None possessed significant cytotoxic activity, but dicitrinin A (**2**) exhibited the moderate growth inhibition of 44.6% at a

concentration of 10 $\mu\text{g/mL}$.

In addition, compounds **3** and **5** belong to members of the isocoumarin family. Isocoumarins and 3, 4-dihydroisocoumarins are secondary metabolites of a wide variety of insects, plants, and microbial sources. Most isocoumarins have been obtained from different species of the genera *Artemisia*, *Aspergillus*, *Fusarium*, *Penicillium*, and *Streptomyces* etc. Isocoumarins and 3, 4-dihydroisocoumarins have displayed impressive bioactivities (Daigo *et al.*, 2006; Lin and Shen, 2009; Lu *et al.*, 2008; Wang *et al.*, 2011). Herein, the isolated 4-acetyl-3, 4-dihydro-6, 8-dihydroxy -5-methylisocoumarin (**5**) revealed moderate cytotoxicity against the murine cancer cell line L5178Y, whereas, compound **3** showed weak activity in this assay. Comparing the structure of both compounds showed that both have the same framework and the main difference is the presence of an additional substituent at C-3 in **3**, which may result in the difference of the biological activity observed for **3** and **5**.

Butyrolactone II (**1**) belongs to the structure type of saturated dibenzylbutyrolactone lignans (Lin and Shen, 2009). The compound was first isolated from the culture broth of *Aspergillus terreus* IFO 4100 and may be a de-prenyl derivative of butyrolactone I (Keiichi *et al.*, 1983; Kunizo *et al.*, 1983). The biosynthesis of **1** was presumed as shown in Figure 4.3.1.3. Moreover, it was previously reported that **1** exhibited mild or no cytotoxic activity (Rao *et al.*, 2000; Wang *et al.*, 2011), which was in agreement with the bioactivity assay in this study. Additionally, the dihydroisoflavipucine (**28**) was reported for the first time from a sponge-derived fungus (Loesgen *et al.*, 2011) and showed weak activity against murine cancer cell line L5178Y.

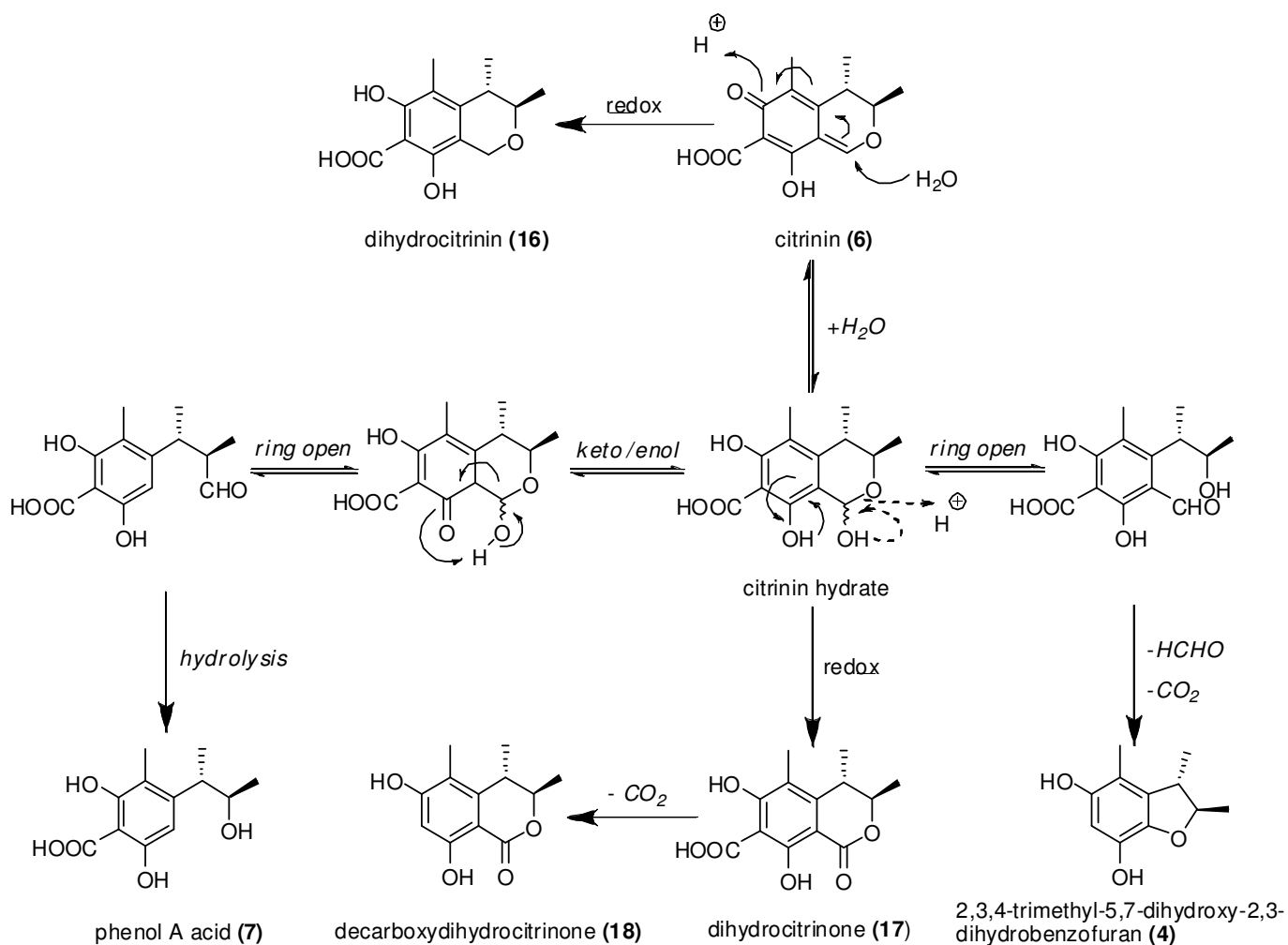


Figure 4.3.1.1 Suggested biosynthetic scheme from citrinin to monomeric species.

(Benjamin *et al.*, 2006)

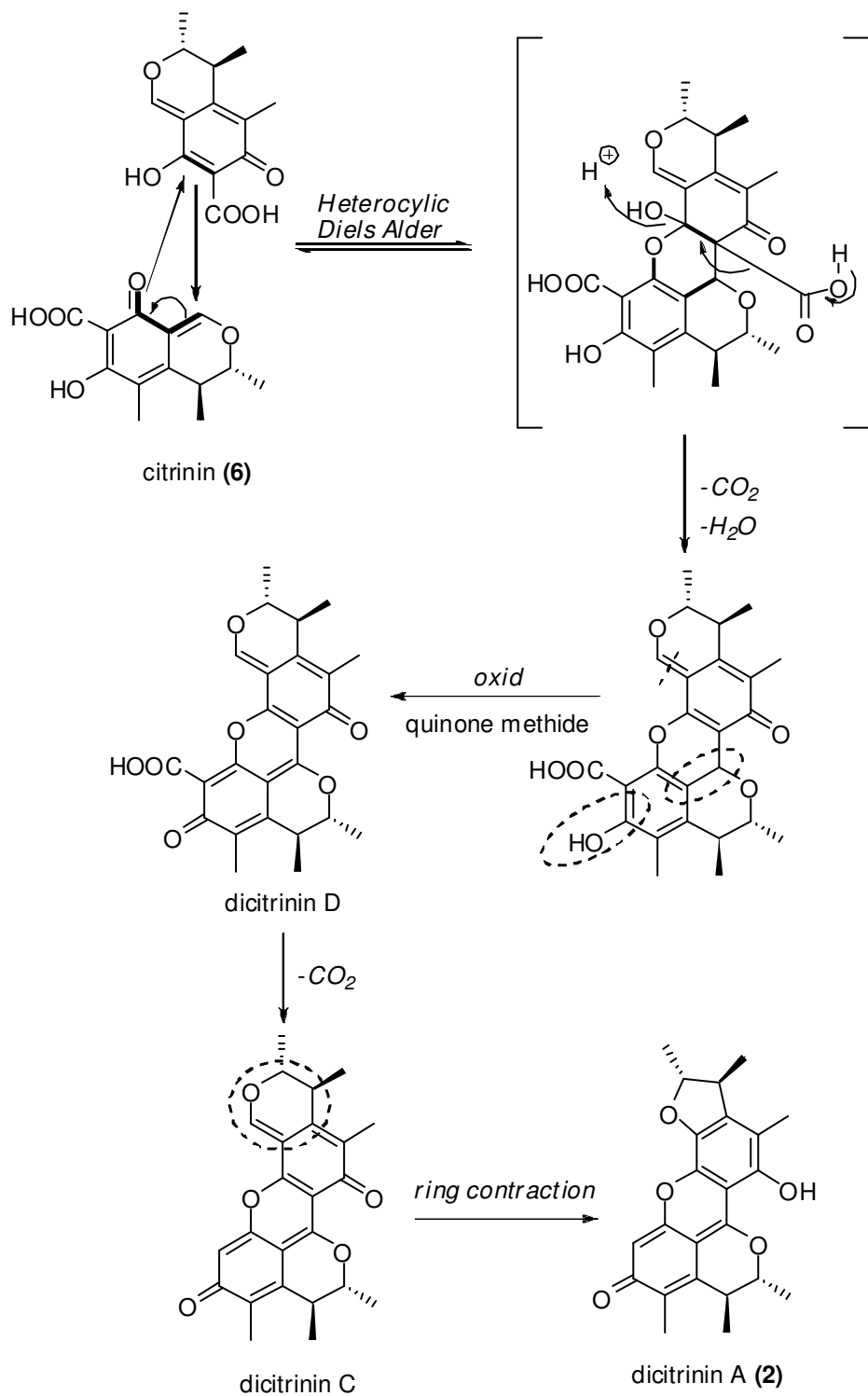


Figure 4.3.1.2 Proposed biosynthetic mechanism for the dicitrinin A (2)
(Benjamin *et al.*, 2006)

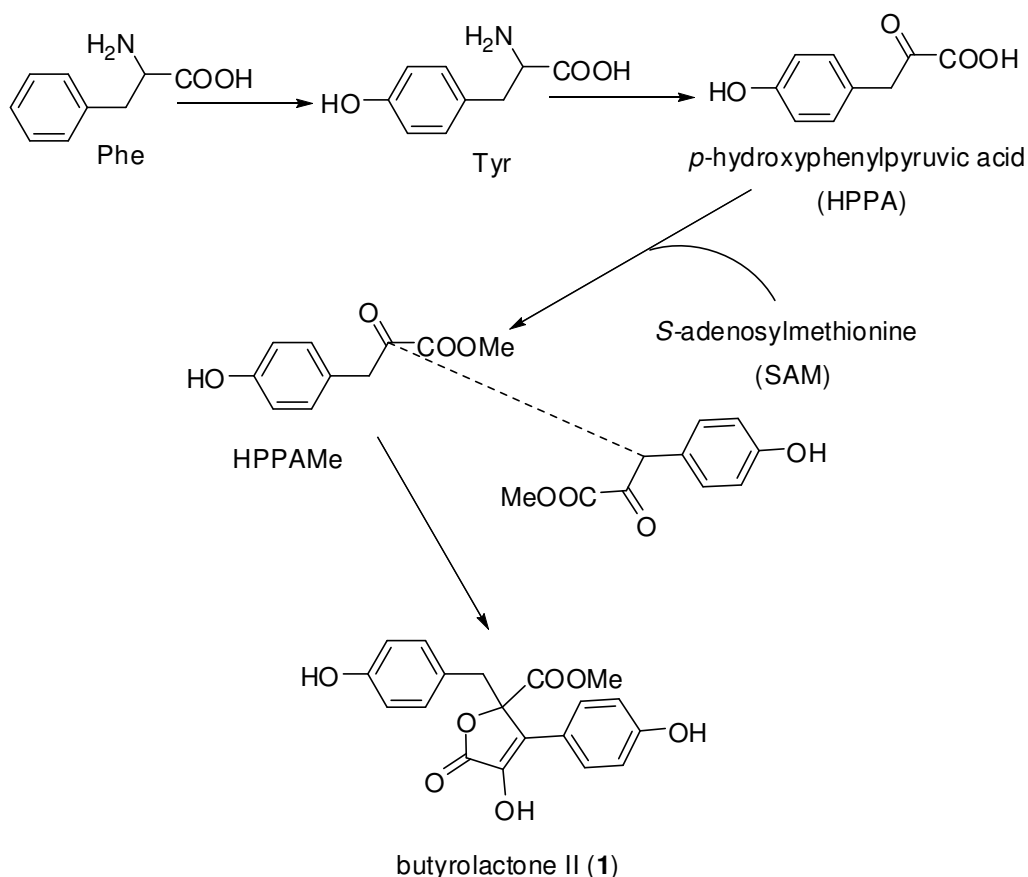


Figure 4.3.1.3 Proposed biosynthesis of butyrolactone II (1)
(Keiichi *et al.*, 1983)

4.3.2 Meroterpenoids

Chromatographic separation yielded six new meroterpenoid metabolites, austalides M-R (**10-14** and **29**). They are a family of mycotoxins previously reported to be produced by whole maize cultures of *Aspergillus ustus* MRC 1163 and arise biogenetically via 6-farnesyl-5, 7-dihydroxy-4-methylphthalide, a key and confirmed intermediate in the biogenesis of mycophenolic acid as well. The molecular architecture of these structurally unique meroterpenoids is endowed with functional group diversity (Horak *et al.*, 1981, 1985; De Jesus *et al.*, 1983, 1987).

The isolation and characterization of twelve biosynthetically related metabolites, austalides A-L was reported from *Aspergillus ustus* (Horak *et al.*, 1985). Austalide M

(10) was determined as the 22-OMe derivative of austalide B. Because the austalide skeleton is originated from the 6-[(2*E*, 6*E*)-farnesyl]-5, 7-dihydroxy-4-methylphthalide, which is biosynthesized through a mixed polyketide-terpenoid pathway with subsequent cyclization and oxidative modification (Horak *et al.*, 1985; De Jesus *et al.*, 1983, 1987), the C-22 benzylic substituent must be introduced after the cyclization. The structure of austalide N (**11**) was similar to **10** except for the replacement of the benzylic C-22 methoxy group by a methyl ester group. In addition, austalide O (**12**) possesses the same skeleton as **10** but with a benzylic 22-OH group instead of the 22-OMe. It is important to note that austalide O (**12**) was kept in ethyl acetate for more than 48 hours, and no formation of the acetate derivatives **11** was detected, which suggested that austalide N (**11**) is a genuine natural product and not an artefact resulting from acetylation of **12**. Austalide R (**29**) possesses the same skeleton as austalide O (**12**) but with a 17-OH group instead of the 17-OMe present in **12**. Consequently, the main structural difference between the austalides **10-12** and **29** and previously isolated austalides with the same molecular framework, is the presence of an additional substituent at C-22. On the other hand, austalides **13 (P)** and **14 (Q)** are similar to the reported austalides G and H. By comparison to the structurally related austalides G and H (Horak *et al.*, 1985), austalides **13 (P)** lacks a substituent at C-13, having a methylene group in this position, whereas **14 (Q)** features a C-15—C-25 double bond, which may have resulted from dehydration.

The absolute configuration of **10** and **13** was determined by time-dependent density functional theory electronic circular dichroism (TDDFT ECD) calculations, which allowed the assignment of the absolute configuration of analogous derivatives **11**, **12**, and **14**. The calculations revealed that the conformation of the benzene-fused phthalide chromophore, which is sensitive to even minor changes in its proximity, is decisive for the ECD parameters, rendering the simple ECD comparison of related homochiral austalides difficult. TDDFT calculations of ECD are being increasingly utilized in determining the absolute configuration of chiral molecule (McCann *et al.*, 2006).

Earlier biosynthetic studies on austalide D, suggested that those meroterpenoid metabolites are derived from 6-[(2*E*, 6*E*)-farnesyl]-5, 7-dihydroxy- 4-methylphthalide. In their original proposal, cyclization of 6-[(2*E*, 6*E*)-farnesyl]-5, 7-dihydroxy-4-methylphthalide (a) is initiated by stereospecific attack of the phenolic oxygen on the *Si* face of the proximal double bond to yield the chromene (b). Subsequent oxygen-centered cyclization is believed to provide a reasonable route to austalide K, whose role is to serve as precursor to the other austalides. Hydroxylation of austalide K gives rise to austalide L. Ensuing an enzymatic Baeyer-Villiger oxidation occurs to yield the seven-membered lactone ring of austalide J and after *O*- methylation with (*S*)-adenosylmethionine, austalide J is transformed to an orthoester. Subsequent hydroxylation and acetylation lead to austalide D (Figure 4.3.2.1). Thus, austalide J, K and L play the intermediary role in the biosynthesis of austalide D (De Jesus *et al.*, 1983, 1987; Paquette *et al.*, 1994). Based on above biosynthetic origin, the biosynthesis of austalides M-O (**10-12**) and R (**29**) is proposed as shown in Figure 4.3.2.1, whereas, the biosynthetic pathway of austalides P-Q (**13-14**), possessing the same molecular framework as austalide G, which probably represent the products of a branch-point in the biosynthetic pathway leading to the highly oxygenated austalides A-F, remain unclear (Horak *et al.*, 1985).

All of these new meroterpenoid compounds, austalides M-R (**10-14** and **29**), showed either weak or no activity in the cytotoxicity assay, and it is interesting to note that no activities were reported for the structurally analogous known austalides A-L isolated from *Aspergillus ustus*.

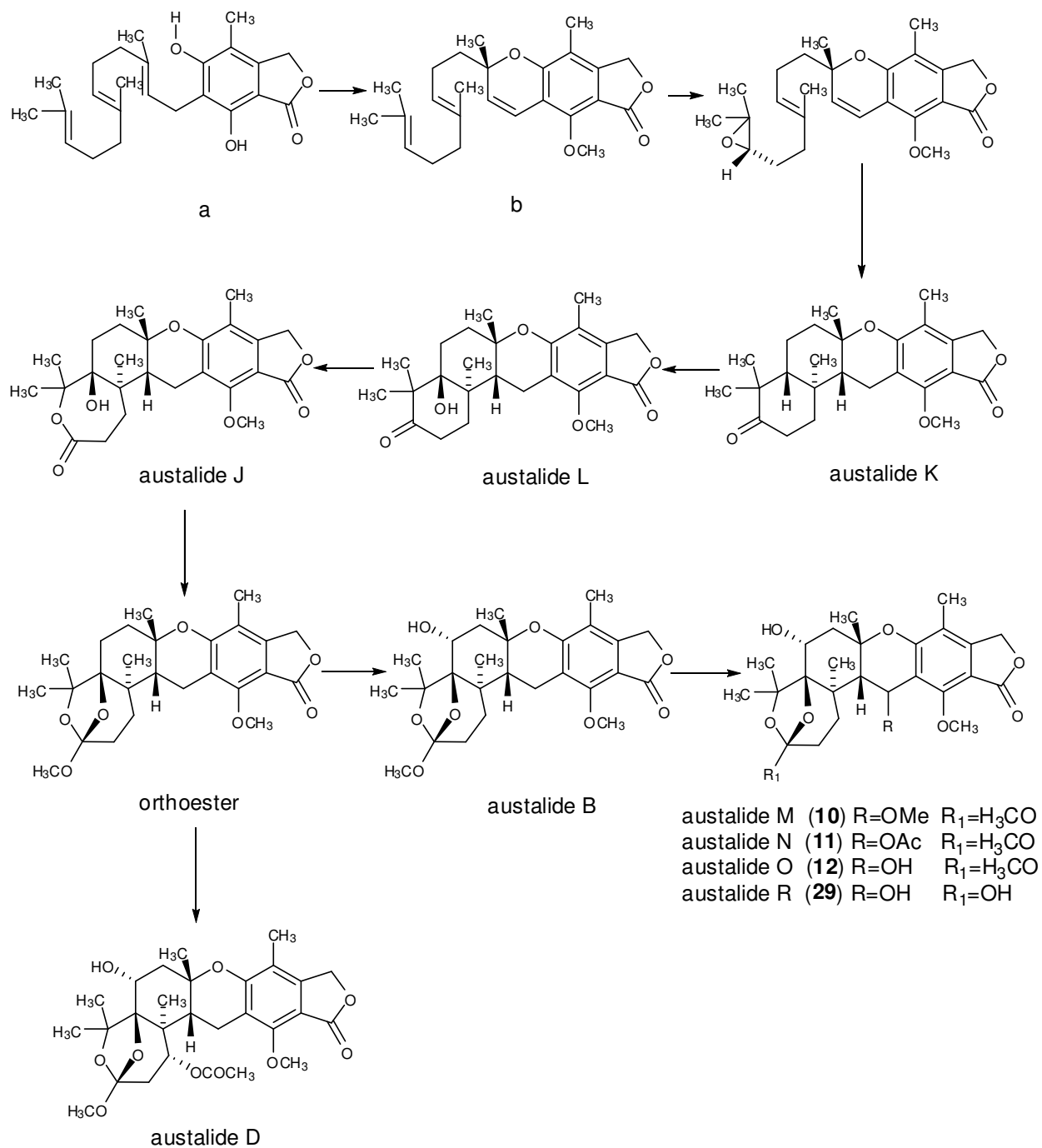


Figure 4.3.2.1 Proposed biosynthetic pathways of australides 10-12 (M-O) and 29 (R) (De Jesus *et al.*, 1983, 1987; Paquette *et al.*, 1994)

4.3.3 Alkaloids

Compounds **20-26** are new tryptoquivaline and fumiquinazoline alkaloids isolated from the selected fungus *Aspergillus* sp. Both of them belong to the subclass of quinazoline alkaloids, which is extensively produced by filamentous fungi. The fumiquinazolines possess a pyrazino[2,1*b*]quinazoline-3, 6-dione core which originated from condensation of anthranilic acid with two additional amino acids. In addition, the main structural difference between the new members (**20-26**) reported in this study and in previously isolated compounds possessing the same molecular framework is the inclusion of a rare amino acid residue, 1-aminocyclopropane-1-carboxylic acid, instead of alanine or methylalanine residues as found in previously reported analogues (Yamazaki *et al.*, 1976, 1977, 1978). Only one analogue bearing a 1-aminocyclopropane-1-carboxylic acid residue, cottoquinazoline D, had been reported in literature so far (Zhuang *et al.*, 2011). The structurally most simple member and proposed biological precursor of fumiquinazolines, fumiquinazoline F with a 6-6-6 tricyclic core, is known to be biosynthetically derived from anthranilic acid, tryptophan and alanine involving a trimodular nonribosomal peptide synthetase (NRPS). Modification of the indole side chain via oxidative coupling of an additional amino acid molecule, commonly alanine or methylalanine, results in the formation of the imidazoindolone part of the compounds. In contrast, unusual oxidative opening of the pyrazinone ring of fumiquinazoline F was suggested as an intermediate step in the biosynthesis of tryptoquivalines (Ames *et al.*, 2010; Gao *et al.*, 2011).

The absolute configuration of tryptoquivaline K (**20**) and fumiquinazolines K (**21**) were determined by TDDFT ECD calculations of their solution conformers and the ECD of the latter was used for the configurational assignment of the related fumiquinazolines L-P (**22-26**).

All new tryptoquivaline and fumiquinazoline alkaloids (**20-26**) together with the

known fumiquinazoline J (**8**) were evaluated for their cytotoxicity against the murine cancer cell line L5178Y. Only fumiquinazoline J (**8**) showed pronounced cytotoxicity with an IC₅₀ value of 3.7 μ M, whereas the remaining investigated compounds showed weak or no activity in this assay. Compound **8** was further evaluated against selected human cell lines and it showed moderate activities as shown in Table 3.2.1. It was worth noting that previously reported fumiquinazolines are moderately cytotoxic and were found to show antitumor activity against several cancer cell lines. In addition, compound **8** was isolated for the first time from a sponge-associated fungus, whereas previous studies reported its isolation from *Aspergillus fumigatus* obtained from sea mud (Ames, *et al.*, 2010; Han *et al.*, 2007).

In addition, two known alkaloids, compound **9** and the unusually bridged epidithiodiketopiperazine, pretrichodermamide A (**19**), were characterized for the first time from a sponge-associated fungus, whereas previous studies reported their isolation from *Aspergillus fumigatus* collected from the air and dust of asthmatic patients' rooms and *Trichoderma* sp. isolated from bamboo leaves, respectively (Prapairat *et al.*, 2006; Yamamoto *et al.*, 1965). Compound **9** displayed pronounced cytotoxicity with an IC₅₀ value of 0.2 μ M against the murine cancer cell line L5178Y, whereas **19** showed weak activity in this assay. Moreover, the novel tryptophan-derived alkaloid **31** exhibited no activity against the murine cancer cell line L5178Y.

The known alkaloid cytochalasin Z17 (**27**) was characterized for the first time from a sponge-associated fungus, whereas previous studies reported its isolation from *A. terreus* collected from the plant *Artemisia annua*, and *A. flavipes* isolated from the mangrove plant *Acanthus ilicifolius* (Lin *et al.*, 2009; Zhang *et al.*, 2010). **27** showed weak cytotoxic activity against the murine cancer cell line L5178Y, whereas previous studies reported its cytotoxic activity against A-549 cell line and against human nasopharyngeal epidermoid tumor KB cell line with IC₅₀ values of 5.6 and 26.2 μ M, respectively (Lin *et al.*, 2009; Zhang *et al.*, 2010).

5. Summary

Marine microorganisms have proven to be a prolific source of structurally interesting and biologically active natural products. In particular, marine fungi have attracted considerable interest because of the diversity in chemical structures and biological activities observed for their secondary metabolites. Marine-derived fungi have been isolated from various organisms, including algae, mollusks and particularly sponges. However, sponge-associated fungi were found to be among the most prolific sources of bioactive compounds. Moreover, most compounds isolated from sponge-associated fungi displayed significant bioactivities in some pharmacological bioassay projects. Therefore, they could be interesting candidates offering lead structures for developing new drugs, primarily in the fields of anti-cancer, anti-inflammatory, anti-infective and analgesic drugs.

Consequently, the aim of this work was to investigate and identify the secondary metabolites from the marine-derived fungus *Aspergillus* sp., isolated from the Mediterranean sponge *Tethya aurantium*, followed by examination of their pharmacological potential. Mass growth of the fungus for the isolation and identification of secondary metabolites was carried out on two different media, namely biomalt agar and spelt barley solid media for 21 days at 22°. The cultures obtained from both media were then lyophilized, extracted with ethyl acetate, and the dry residues left after evaporation were defatted with petroleum ether. The resulting fraction was then subjected to different chromatographic separation techniques in order to isolate the secondary metabolites.

The identification of the secondary metabolites was mainly performed using mass spectrometry (MS) and nuclear magnetic resonance (NMR) experiments to determine the molecular weight and structure, respectively. Moreover, in the case of selected optically active natural products, time-dependent density functional theory electronic circular dichroism (TDDFT ECD) calculations were employed in order to determine

their absolute configuration. Eventually, all of the isolated compounds were subjected to various bioassays to screen their bioactivities, such as cytotoxic and antimicrobial activities.

Chromatographic separation of the crude extract of the sponge-associated fungus *Aspergillus* sp. yielded eleven known polyketide-derived compounds (**1-7**, **16-18**, and **28**), six new meroterpenoid metabolites (**10-14** and **29**), twelve alkaloids including one new tryptoquivaline (**20**), six new fumiquinazolines (**21-26**), one novel tryptophan-derived alkaloid (**31**) as well as four known alkaloids (**8**, **9**, **19**, and **27**), one novel biphenyl ether (**30**), and one known nucleoside (**15**).

Most polyketide-derived compounds isolated in this study were citrinin derivatives. In addition, butyrolactone II (**1**) was isolated as the main secondary metabolite of the investigated *Aspergillus* sp. 4-Acetyl-3,4-dihydro-6,8-dihydroxy-5-methyl isocoumarin (**5**) exhibited pronounced cytotoxic activity against several selected cell lines, whereas the remaining polyketide-derived compounds showed either weak or no activity against L5178Y mouse lymphoma cell line.

The new meroterpenoid compounds, austalides M-R (**10-14** and **29**), were found to be structurally related to the known austalides A-L previously isolated from *Aspergillus ustus*. Structural analysis of the austalides suggested a biosynthetic pathway which involves 6-farnesyl-5,7-dihydroxy-4-methylphthalide, a key intermediate in the biogenesis of mycophenolic acid. Furthermore, TDDFT ECD calculations of austalides M-Q (**10-14**), new metabolites of *Aspergillus* sp., have been presented. ECD calculations of these derivatives afforded their absolute configurations and also revealed that the conformation of the phthalide chromophore was governed by the central chirality elements and that the benzylic center is decisive for the characteristic ECD Cotton effects. The calculations also explain the remarkable difference in the ECD spectra of the structurally related austalides, and demonstrate why the absolute geometry cannot be determined by simple comparison of their ECD spectra. Finally,

they showed either weak or no activity against L5178Y mouse lymphoma cell line.

The known alkaloids **8**, **9** and **19** were characterized for the first time from sponge-associated fungi, whereas previous studies reported their isolation from *Aspergillus fumigatus* obtained from sea mud, *Aspergillus fumigatus* collected from the air and dust of asthmatic patients' rooms, and *Trichoderma* sp. isolated from bamboo leaves, respectively. Compounds **8** and **9** exhibited pronounced cytotoxicity against L5178Y mouse lymphoma cell line with IC₅₀ values of 3.7 and 0.2 μ M, respectively, whereas **19** showed weak activity in this assay. Furthermore, when tested against human cell lines **9** exhibited moderate activity against human ovarian cancer (A2780sens) and human Philadelphia chromosome-positive chronic myelogenous leukemia (K562) cell lines with IC₅₀ values of 8.0 and 19.3 μ M, respectively, whereas **8** exhibited only moderate to weak cytotoxic activity against K562, A2780sens, and A2780CisR cell lines with IC₅₀ values of 15.0, 18.5 and 38.8 μ M, respectively.

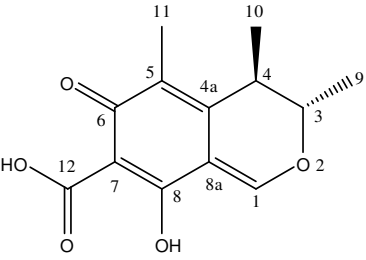
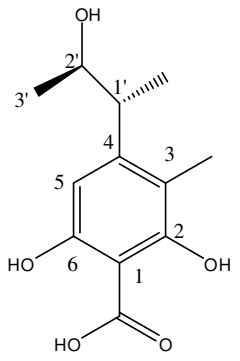
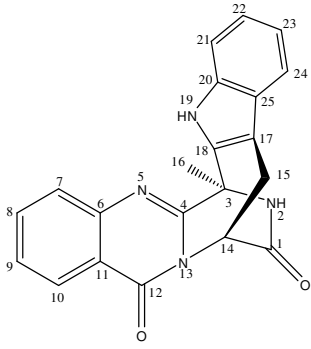
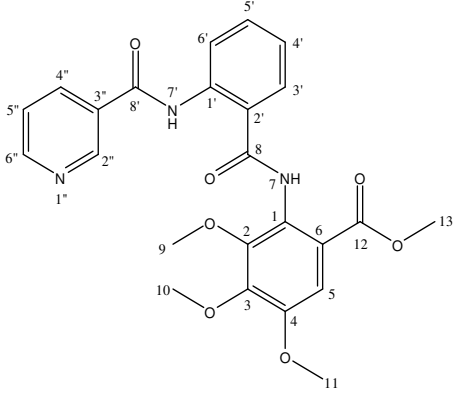
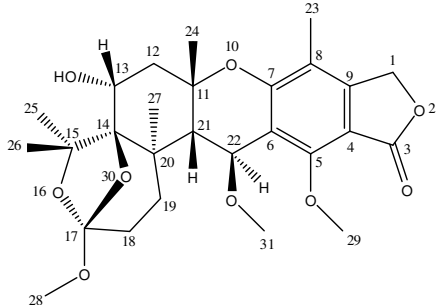
Compounds **20-26** are new tryptoquivaline and fumiquinazoline alkaloids. The main structural difference between the new members reported in this study and previously reported compounds possessing the same molecular framework is the inclusion of a rare amino acid residue, 1-aminocyclopropane-1-carboxylic acid, instead of alanine or methylalanine residues as found in previously reported analogues. The absolute configurations of tryptoquivaline K (**20**) and fumiquinazolines K (**21**) were determined by TDDFT ECD calculations of their solution conformers and the ECD of the latter was used for the configurational assignment of the related fumiquinazolines L-P (**22-26**). In addition, the new alkaloids (**20-26**) were evaluated for their cytotoxicity against the murine lymphoma cancer cell line L517Y and they showed weak or no activity in this assay (up to a dose of 10 μ g/mL).

In conclusion, a total of thirty-one compounds were successfully identified from the sponge-associated fungus *Aspergillus* sp. in this study, to the best of our knowledge, fifteen of which were confirmed as new natural products (Table 5.1).

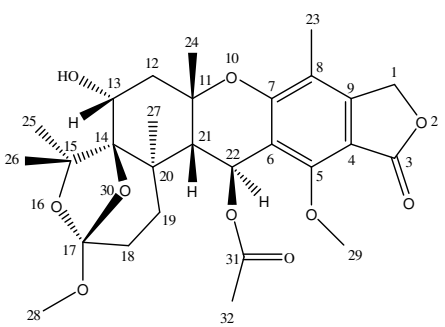
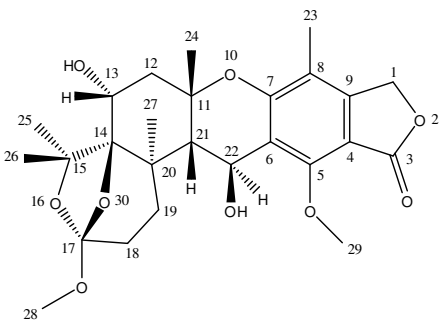
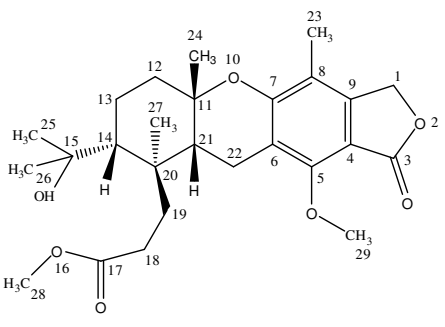
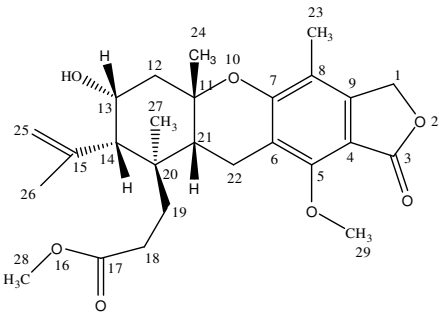
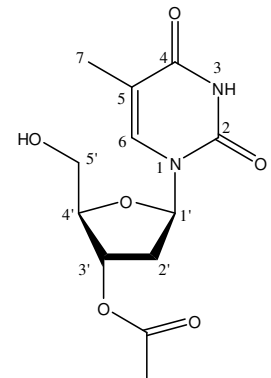
Table 5.1 Summary of the isolated compounds

1	Compound name	Structure	Source	Note	
	Butyrolactone II		<i>Aspergillus</i> sp	Known	
	2	Dicitrinin A		<i>Aspergillus</i> sp	Known
	3	4-Acetyl-3,4-dihydro-6,8-dihydroxy-3-methoxy-5-methylisocoumarin		<i>Aspergillus</i> sp	Known
	4	2,3,4-Trimethyl-5,7-dihydroxy-2,3-dihydrobenzofuran		<i>Aspergillus</i> sp	Known
	5	4-Acetyl-3,4-dihydro-6,8-dihydroxy-5-methylisocoumarin		<i>Aspergillus</i> sp	Known

Summary

6	Citricin		<i>Aspergillus</i> sp	Known
7	Phenol A acid		<i>Aspergillus</i> sp	Known
8	Fumiquinazoline J		<i>Aspergillus</i> sp	Known
9	Methyl 3,4,5-trimethoxy-2-(2-(nicotinamido) benzamido) benzoate		<i>Aspergillus</i> sp	Known
10	Austalide M		<i>Aspergillus</i> sp	New

Summary

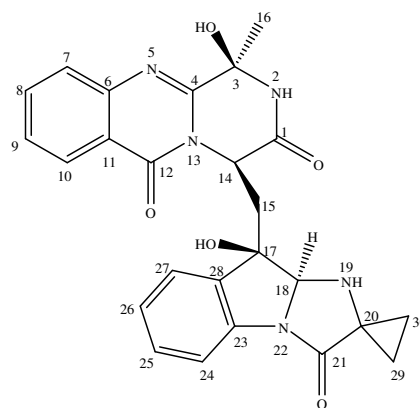
11	Austalide N		<i>Aspergillus</i> sp	New
12	Austalide O		<i>Aspergillus</i> sp	New
13	Austalide P		<i>Aspergillus</i> sp	New
14	Austalide Q		<i>Aspergillus</i> sp	New
15	3'- <i>O</i> -acetylthymidine		<i>Aspergillus</i> sp	Known

Summary

16	Dihydrocitrinin		<i>Aspergillus</i> sp	Known
17	Dihydrocitrinone		<i>Aspergillus</i> sp	Known
18	6,8-Dihydroxy-3,4,5- trimethyl -isocoumatin		<i>Aspergillus</i> sp	Known
19	Pretrichodermamide A		<i>Aspergillus</i> sp	Known
20	Tryptoquivaline K		<i>Aspergillus</i> sp	New
21	Fumiquinazoline K		<i>Aspergillus</i> sp	New

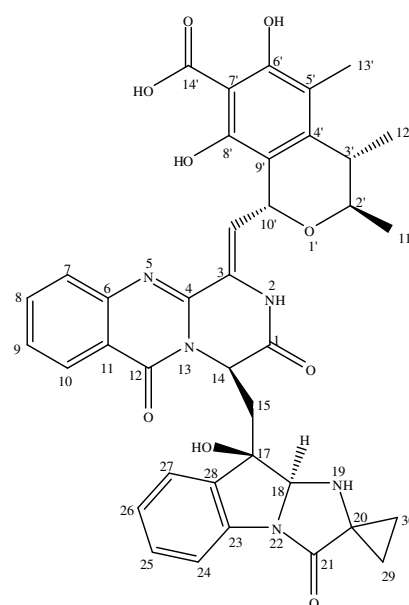
Summary

22 Fumiquinazoline L



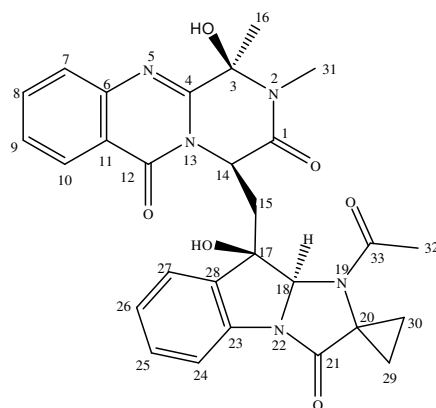
Aspergillus sp New

23 Fumiquinazoline M



Aspergillus sp New

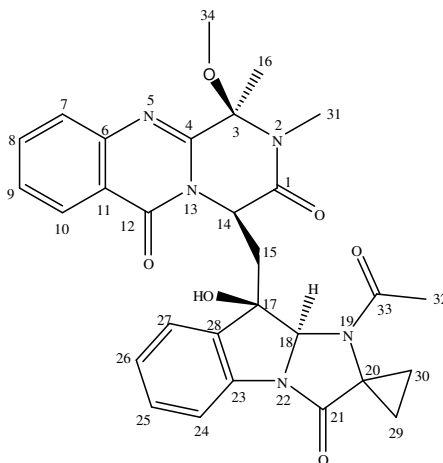
24 Fumiquinazoline N



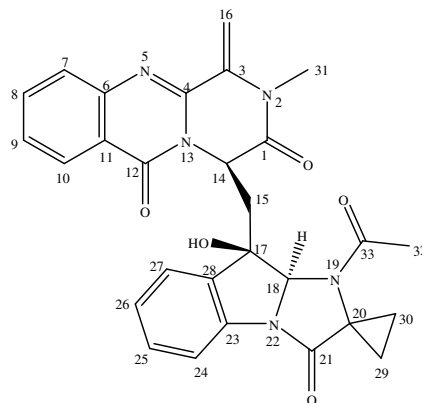
Aspergillus sp New

Summary

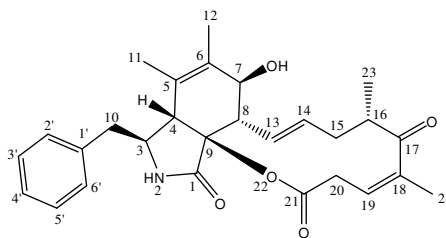
25 Fumiquinazoline O *Aspergillus* sp New



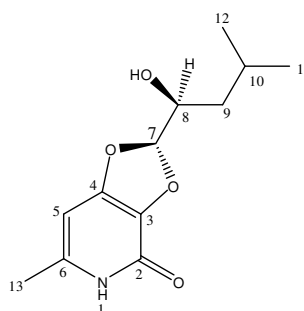
26 Fumiquinazoline P *Aspergillus* sp New



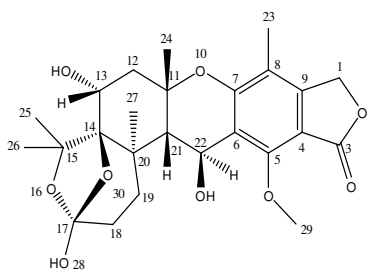
27 Cytochalasin Z17 *Aspergillus* sp Known



28 Dihydroisoflavipucine *Aspergillus* sp Known

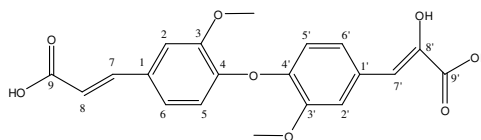


29 Austalide R *Aspergillus* sp New



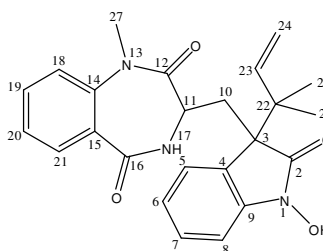
Summary

- 30** 3-(4-(4-(2-Carboxyvinyl)-2-methoxyphenoxy)-3-methoxyphenyl)-2-hydroxyacrylic acid



Aspergillus sp New

- 31** 3-((1-Hydroxy-3-(2-methylbut-3-en-2-yl)-2-oxoindolin-3-yl)methyl)-1-methyl-3,4-dihydro-1*H*-benzo[*e*][1,4]diazepine-2,5-dione



Aspergillus sp New

6. References

- Ahmed, A. F., Wu, M. H., Wu, Y. C., Dai, C. F., and Sheu, J. H. (2006). Metabolites with cytotoxic activity from the formosan soft coral *Cladiella australis*. *J. Chin. Chem. Soc.*, **53**, 489-494.
- Aly, A. H., Debbab, A., Kjer, J., and Proksch, P. (2010). Fungal endophytes from higher plant: a prolific source of phytochemicals and other bioactive natural products. *Fungal Divers.*, **41**, 1-16.
- Aly, A. H., Debbab, A., and Proksch, P. (2011). Fungal endophytes: unique plant inhabitants with great promise. *Appl. Microbiol. Biotechnol.*, **90**, 1829-1845.
- Aly, A. H., Edrada-Ebel, R. A., Indriani, I. D., Wray, V., Mueller, W. E. G., Lin, W. H., Proksch, P., and Ebel, R. (2008). Cytotoxic metabolites from the fungal endophytic *Alternaria* sp. and their subsequent detection in its host plant *Polygonum senegalense*. *J. Nat. Prod.*, **71**, 972-980.
- Ames, B. D., Liu, X. Y., and Walsh, C. (2010). Enzymatic processing of fumiquinazoline F: a tandem oxidative-acylation strategy for the generation of muticyclic scaffolds in fungal indole alkaloid biosynthesis. *Biochemistry*, **49**, 8564-8576.
- Antus, S., Kurtan, T., Juhasz, L., Kiss, L., Hollosi, M., and Majer, Z. (2001). Chiroptical properties of 2, 3-dihydrobenzo[b]furan and chromane chromophores in naturally occurring *O*-heterocycles. *Chirality*, **13**, 493-506.
- Arai, K., Shimizu, S., and Yamamoto, Y. (1981). Metabolic products of *Aspergillus terreus*. VI. Metabolites of the strain IFO 8835. (3). The isolation and chemical structure of colorless metabolites. *Chem. Pharm. Bull.*, **29** (4), 1005-1012.
- Arvigo, R., and Balick, M. (1993). Rainforest Remedies, Lotus Press, Twin Lakes.
- Bacon, C. W., and White, J. F. (2000). Microbial Endophytes, Marcel Dekker inc. New York, pp 341-388.

- Baker, D. D., Chu, M., Oza, U., and Rajgarhia, V. (2007). The value of natural products to future pharmaceutical discovery. *Nat. Prod. Rep.*, **24**, 1225-1244.
- Barber, J., Cornford, J. L., Howard, T. D., and Derek, S. (1987). The structure of citrinin in vivo. *Chem. Soc. Perkin. Trans.*, **1**, 2743-2744.
- Barron, R. L., and Vanscoy, G. J. (1993). Natural products and the athlete: facts and folklore. *Ann. Pharmacother.*, **27** (5), 607-615.
- Benjamin, R., C., Robert, J. C., Ernest, L., Shaun, T., and Jennifer, H. G. (2006). Citrinin revised: from monomers to dimers and beyond. *Org. Biomol. Chem.*, **4**, 1520-1528.
- Bhat, B., and Harrison, D. M. (1986). The total synthesis of (-)-dihydroaszonalenin and the stereochemistry of aszonalenin. *Tetrahedron Lett.*, **27**, 5873-5874.
- Bill, G. F., and Polishook, J. D. (1992). Recovery of endophytic fungi from *Chamaecyparis thyoides*. *Sydowia*, **44**, 1-12.
- Blunt, J. W., Copp, B. R., Munro, M. H. G., Northcote, P. T., and Prinsep, M. R., (2011). Marine natural products. *Nat. Prod. Rep.*, **28**, 196-268.
- Brady, S. F., Singh, M. P., Janso, J. E., and Clardy, J. (2000). Guanacastepene, a fungal-derived diterpene antibiotic with a new carbon skeleton. *J. Am. Chem. Soc.*, **122**, 2116-2117.
- Bringmann, G., Lang G., Steffens, S., and Schaumann, K. (2004). Petrosifungins A and B, novel cyclodepsipeptides from a sponge-derived strain of *Penicillium brevicompactum*. *J. Nat. Prod.*, **67**, 311-315.
- Brown, J. P., Robertson, A., Whalley, W. B., and Cartwright, N. J. (1949). The chemistry of fungi. Part V. The constitution of citrinin. *J. Chem. Soc.*, 867-879.
- Bugni, T. S., and Ireland, C. M. (2004). Marine-derived fungi: a chemically and biologically diverse group of microorganisms. *Nat. Prod. Rep.*, **21**, 143-163.
- Butler, M. S. (2004). The role of natural product chemistry in drug discovery. *J. Nat.*

Prod., **67**, 2141-2153.

Butler, M. S. (2005). Natural products to drugs: natural product derived compounds in clinical trials. *Nat. Prod. Rep.*, **22**, 162-195.

Butler, M. S. (2008). Natural products to drugs: natural product-derived compounds in clinical trials. *Nat. Prod. Rep.*, **25**, 475-516.

Carmichael, J., DeGraff, W. G., Gazdar, A. F., Minna, J. D., and Mitchell, J. B. (1987). Evaluation of a tetrazolium-based semiautomated colorimetric assay: assessment of radiosensitivity. *Cancer Res.*, **47**(4), 943-946.

Carter, G. T. (2011). Natural products and pharma 2011: strategic changes spur new opportunities. *Nat. Prod. Rep.*, DOI: 10.1039/c1np00033k.

Chang, H. M., and But, P. P. H. (1986). Pharmacology and Applications of Chinese Materia Medica, World Scientific Publishing, Singapore, vol **1 & 2**.

Chen, C. H., Shaw, C. Y., Chen, C. C., and Tsai, Y. C. (2002). 2,3,4- Trimethyl-5,7-dihydroxy-2,3-dihydrobenzofuran, a novel antioxidant, from *Penicillium citrinum* F5. *J. Nat. Prod.*, **65**, 740-741.

Clark, A. M. (1996). Natural products as a resource for new drugs. *Pharm. Res.*, **13** (8), 1133-1141.

Cragg, G. M., and Newman, D. J. (2001). Natural product drug discovery in the next millennium. *Pharmaceut. Biol.*, **39** (Suppl.), 8-17.

Cragg, G. M., Newman, D. J., and Snader, K. M (1997). Natural products in drug discovery and development. *J. Nat. Prod.*, **60**, 52-60.

Daigo, W., Tomoo, H., Takeshi, I., Kaoru, O., Galba, M. C. T., Takashi, Y., Kazutaka, F., and Ken-ichi, K. (2006). New citrinin derivatives isolated from *Penicillium citrinum*. *J. Nat. Med.*, **60**, 279-284.

Curtis, R. F., Hassall, C. H., and Nazar, M. (1968). The biosynthesis of phenols. Part XV. Some metabolites of *Penicillium citrinum* related to citrinin. *J. Chem. Soc.*,

- (C), 85-93.
- Dale, J. A., and Mosher, H. S. (1973). Nuclear magnetic resonance enantiomer reagents. Configurational correlations via nuclear magnetic resonance chemical shifts of diastereomeric mandelate, *O*-methylmandelate, and α -methoxy- α -trifluoromethylphenylacetate (MTPA) esters. *J. Am. Chem. Soc.*, **95** (2), 512-519.
- Daferner, M., Anke, T., and Sterner, O. (2002). Zopfiellamides A and B, antimicrobial pyrrolidinone derivatives from the marine fungus *Zopfiella latipes*. *Tetrahedron*, **58**, 7781-7784.
- Davies, D. B., and Danyluk, S. S. (1974). Nuclear magnetic resonance studies of 5'-ribo- and deoxyribonucleotide structures in solution. *Biochemistry*, **13**, 4417-4434.
- Debbab, A., Aly, A. H., and Proksch, P. (2011). Bioactive secondary metabolites from endophytes and associated marine derived fungi. *Fungal Divers.*, **49**, 1-12.
- Debbab, A., Aly, A. H., Lin, W. H., and Proksch, P. (2010). Bioactive compounds from marine bacteria and fungi. *Micob. Biotechnol.*, **3**, 544-563.
- De Jesus, A. E., Horak, R. M., Steyn, P. S., and Vlegaar, R. (1983). Biosynthesis of austalide D, a meroterpenoid mycotoxin from *Aspergillus ustus*. *J. Chem. Soc., Chem. Commun.*, 716-718.
- De Jesus, A. E., Horak, R. M., Steyn, P. S., and Vlegaar, R. (1987). Metabolites of *Aspergillus ustus*. Part 4. Stable-isotope labelling studies on the biosynthesis of the austalides. *J. Chem. Soc. Perkin Trans., I*, 2253-2257.
- Dillen, J. L. M., Horak, R. M., Maharaj, V. J., Marais, S. F., and Vlegaar, R. (1989). Absolute configuration and biosynthesis of the austalides, meroterpenoid metabolites of *Aspergillus ustus*: mode of cyclisation of the farnesyl moiety. *J. Chem. Soc., Chem. Commun.*, 393-394.
- Drexler, H. G. (2000). The leukemia-lymphoma cell line factsbook, San Diego, Academic Press.

- Duke, S. O., Dayan, F. E., Romagni, J. G., and Rimando, A. M. (2000). Natural products as sources of herbicides: current status and future trends. *Weed Res.*, **40** (1), 99-111.
- Endo, A. (1979). Monacolin K, a new hypocholesterolemic agent produced by a *Monascus* species. *J. Antibiot.*, **32**, 852-854.
- Fallarino, M. (1994). Tibetan medical paintings: illustrations to the blue beryl treatise of sangye gyamtso. *Herbalgram*, **31**, 1653-1705.
- Farnsworth, N. R., Akerele, O., Bingel, A. S., Soejarto, D. D., and Guo, Z. (1985). *Bull. WHO*, 1985, **63**, 965.
- Flisiak, R., Horban, A., Gallay, P., Bobardt, M., Selvarajah, S., Wiercinska-Drupal, A., Siwak, E., Cielniak, I., Higersberger, J., Kierkus, J., Aeschlimann, C., Grosgrin, P., and Gilbert, M. R. (2008). Natural products as a robust source of new drugs and drug leads: past successes and present day issues. *Am. J. Cardiol.*, **101** (10A), 43D-49D.
- Frisch, M. J., Trucks, G. W., Schlegel, H. B., Scuseria, G. E., Robb, M. A., Cheeseman, J. R., Montgomery, J. A., Vreven, Jr. T., Kudin, K. N., Burant, J. C., Millam, J. M., Iyengar, S. S., Tomasi, J., Barone, V., Mennucci, Cossi, B., M., Scalmani, G., Rega, N., Petersson, G. A., Nakatsuji, H., Hada, M., Ehara, M., Toyota, K., Fukuda, R., Hasegawa, J., Ishida, M., Nakajima, T., Honda, Y., Kitao, O., Nakai, H., Klene, M., Li, X., Knox, J. E., Hratchian, H. P., Cross, J. B., Bakken, V., Adamo, C., Jaramillo, J., Gomperts, R., Stratmann, R. E., Yazyev, O., Austin, A. J., Cammi, R., Pomelli, C., Ochterski, J. W., Ayala, P. Y., Morokuma, K., Voth, G. A., Salvador, P., Dannenberg, J. J., Zakrzewski, V. G., Dapprich, S., Daniels, A. D., Strain, M. C., Farkas, O., Malick, D. K., Rabuck, A. D., Raghavachari, K., Foresman, J. B., Ortiz, J. V., Cui, Q., Baboul, A. G., Clifford, S., Cioslowski, J., Stefanov, B. B., Liu, G, Liashenko, A., Piskorz, P., Komaromi, I., Martin, R. L., Fox, D. J., Keith, T., Al-Laham, M. A., C. Peng, Y., Nanayakkara, A., Challacombe, M., Gill, P. M. W., Johnson, B., Chen, W., M. Wong, W., Gonzalez,

- C., Pople, J. A., *Gaussian 03, Revision C.02.*, Gaussian Inc., Wallingford CT, 2004.
- Gao, X., Chooi, Y. H., Ames, B. D., Wang, P., Walsh, C. T., and Tang, Y. (2011). Fungal indole alkaloid biosynthesis: genetic and biochemical investigation of the tryptoquialanine pathway in *Penicillium aethiopicum*. *J. Am. Chem. Soc.*, **133**, 2729-2741.
- Gordaliza, M. (2007). Natural products as leads to anticancer drugs. *Clin. Transl. Onco.*, **9**, 767-776.
- Gunatilaka, A. A. L. (2006). Natural products from plant-associated microorganisms: distribution, structural diversity, bioactivity and implication of their occurrence. *J. Nat. Prod.*, **69**, 509-526.
- Guo, B., Wang, Y., Sun, X., and Tang, K. (2008). Bioactive natural products from endophytes: a review. *Appl. Biochem. Microbiol.*, **44**, 136-142.
- Guo, B., Dai, J. R., Ng, S., Huang, Y., Leong, C., Ong, W., and Carte, B. K. (2000). Cytonic acids A and B: novel tridepside inhibitors of hCMV protease from the endophytic fungus *Cytonaema species*. *J. Nat. Prod.*, **63**, 602-604.
- Gusman, J., and Vanhaelen, M. (2000). Endophytic fungi, an underexploited source of biologically active secondary metabolites. *Recent Res. Devel. Phytochem.*, **4**, 187-206.
- Haefner, B. (2003). Drugs from the deep: marine natural products as drug candidates. *Drug Discov. Today*, **8** (12), 536-544.
- Han, X. X., Xu, X. Y., Cui, C. B., and Guo, Q. Q. (2007). Alkaloidal compounds produced by a marine-derived fungus, *Aspergillus fumigatus* H1-04, and their antitumor activities. *Chin. J. Med. Chem.*, **17** (4), 232-237.
- Han, Z., Mei, W., Zhao, Y., Deng, Y., and Dai, H. (2009). A new cytotoxic isocoumarin from endophytic fungus *Penicillium* sp. 091402 of the mangrove plant. *Chem. Nat. Compd.*, **45** (6), 805-807.

- Hanson, J. R. (2008). The chemistry of fungi. Published by The Royal Society of Chemistry, Thomas Graham House, Science Park, Milton Road, Cambridge CB4 0WF, UK.
- Harvey, A. L. (2008). Natural products in drug discovery. *Drug Discov. Today*, **13**, 894-901.
- Hawkesworth, D. L., Sotton, B. C., and Ainsworth, G. C. (1983). Ainsworth & Bisby's Dictionary of the Fungi, Commonwealth Mycological Institute, Kew, UK.
- He, J., Kithsiri, W. E. M., Bashyal, B. P., Zhan, J., Seliga, C. J., Liu, M. X., Pierson, E. E. L., Piesron, S., Vanetten, H. D., and Gunatilaka, A. A. L. (2004). Cytotoxic and other metabolites of *Aspergillus* inhabiting the rhizosphere of sonoran desert plants. *J. Nat. Prod.*, **67**, 1985-1991.
- Heredia, M. L., Cuesta, E., and Avendano, C. (2002). Acid-promoted reactions in 1-hydroxy, 1-dimethylaminomethyl and 1-methylene-4-arylmethyl-2, 4-dihydro - 1*H*-pyrazino[2, 1-*b*]-quinazoline-3, 6-diones. *Tetrahedron*, **58**, 6163-6170.
- Holler, U., Konig, G., and Wright, A. D. (1999). A new tyrosine kinase inhibitor from a marine isolate of *Ulocladium botrytis* and new metabolites from the marine fungi *Asteromyces cruciatus* and *Varicosporina ramulosa*. *Eur. J. Org. Chem.*, **11**, 2949-2955.
- Holt, G. A., and Chandra, A. (2002). Herbs in the modern healthcare environment-an overview of uses, legalities, and the role of the healthcare professional. *Clin. Res. Regul. Aff.*, **19**, 83-107.
- Horak, R. M., Steyn, P. S., Rooyen, P. H. V., and Vlegaar, R. (1981). Structure of the austalides A-E, five novel toxic metabolites from *Aspergillus ustus*. *J. Chem. Soc., Chem. Commun.*, 1265-1267.
- Horak, R. M., Steyn, P. S., and Vlegaar, R. (1985). Metabolites of *Aspergillus ustus*. Part 3. Structure elucidation of austalides G-L. *J. Chem. Soc., Perkin. Trans.*, **1**, 363-367.

- Horak, R. M., Steyn, P. S., and Vlegaar, R. (1985). Metabolites of *Aspergillus ustus*. Part 1. Application of the heteronuclear selective population inversion (SPI) N. M. R. technique to the structure elucidation the of austalides A-F, novel ortho ester meroterpenoids. *J. Chem. Soc., Perkin. Trans.*, **1**, 345-356.
- Huang, J., Ogihara, Y., Gonda, R., and Takeda, T. (2000). Novel biphenyl ether lignans from the rhizomes of *Curcuma chuanyujin*. *Chem. Pham. Bull.*, **48**(8), 1228-1229.
- Hyde, K. D., and Soyong, K. (2008). The fungal endophyte dilemma. *Fungal Divers.*, **33**, 163-173.
- Jack, D., John, M. J., Davis, R. A., and Horace, G. C. (1992). Studies on aldose reductase inhibitors from fungi. I. Citrinin and related benzopyran derivatives. *J. Enzym. Inhib.*, **6**, 201-210.
- Jacob, E. J. (2010). Natural products as lead-structures: a role for biotechnology. *Drug Discov.Today*, **15**, 409-410.
- Jarvis, B. B. (2000). The role of natural products in evolution. *Recent. Adv. Phytochem.*, **34**, 1-24.
- Jill, B., Rachel, H. C., Mary, J. G., and James, S. (1981). The biosynthesis of citinin by *Penicillium citrinum*. *J. Chem. Soc. Perk. I.* 2577-2583.
- Joseph, B., and Priya, R. M. (2011). Bioactive compounds from endophytes and their potential in pharmaceutical effect: a review. *Am. J. Biochem. Mol. Biol.*, **1** (3), 291-309.
- Kapoor, L. D. (1990). CRC Handbook of Ayurvedic Medicinal Plants, CRC Press, Boca Raton.
- Karplus, M. (1963). Vicinal proton coupling in nuclear magnetic resonance. *J. Am. Chem. Soc.*, **85** (18), 2870-2871.
- Kaul, P. N., and Joshi, B. S. (2001). Alternative medicine: herbal drugs and

- their critical appraisal-Part II. *Prog. Drug. Res.*, **57**, 1-75.
- Keiichi, N., Noritaka, F., Tadashi, Y., Kunizo, A., and Yuzuru, Y. (1983). Metabolic products of *Aspergillus terreus*. IX. Biosynthesis of butyrolactone derivatives isolated from strains IFO 8835 and 4100. *Chem. Pharm. Bull.*, **31** (5), 1528-1533.
- Kimura, Y., Hamasaki, T., and Nakajima, H. (1982). Structure of aszonalenin, a new metabolite of *Aspergillus zonatus*. *Tetrahedron Lett.*, **23**, 225-228.
- Klein, E., Ben-Bassat, H., Neumann, H., Ralph, P., Zeuthen, J., Polliack, A., and Vánky, F. (1976). Properties of the K562 cell line, derived from a patient with chronic myeloid leukemia. *Int. J. Cancer.*, **18**, 421-431.
- Kohlmeyer, J., and Kohlmeyer, E. (1979). Marine mycology: the higher fungi. Academic Press, New York.
- Kogel, K. H., Franken, P., and Hueckelhoveb, R. (2006). Endophyte or parasite-what decides? *Cutt. Opin. Plant. Biol.*, **9**, 358-363.
- Krohn, K., Floerke, U., Rao, M. S., Steingroever, K., Aust, H. J., Draeger, S., and Schulz, B. (2001). Metabolites from fungi 15. New isocoumarins from an endophytic fungus isolated from the canadian thistle *Arvensis*. *Nat. Prod. Lett.*, **15**, 353-361.
- Krohn, K., Sohrab, M. D. H., Aust, H. J., Draeger, S., and Schulz, B. (2004). Biologically active metabolites from fungi, 19: new isocoumarins and highly substituted benzoic acids from the endophytic fungus, *Scytalidium* sp. *Nat. Prod. Res.*, **18**, 277-285.
- Kunizo, A., Tadashi, Y., Yoshitaka, I., and Yuzuru, Y. (1983). Metabolic products of *Aspergillus terreus*. VIII. Astepyrone: a novel metabolite of the strain IFO 4100. *Chem. Pharm. Bull.*, **31** (3), 925-933.
- Lee, J. C., Lobkovsky, E., Pliam, N. B., Strobel, G., and Clardy, J. (1995). Subglutinols A and B: immunosuppressive compounds from the endophytic

- fungus *Fusarium subglutinans*. *J. Org. Chem.*, **60**, 7076-7077.
- Li, D., Xu, Y., Shao, C., Yang, R., Zheng, C., Chen, Y., Fu, X., Qian, P., She, Z., Voogd, N. J., and Wang, C. (2012). Antibacterial bisabolane-type sesquiterpenoids from the sponge-derived fungus *Aspergillus* sp. *Mar. Drugs*, **10**, 234-241.
- Lin, T., Lu, C., and Shen, Y. (2009). Secondary metabolites of *Aspergillus* sp. F1, a commensal fungal strain of *Trewia nudiflora*. *Nat. Pro. Res.*, **1**, 77-85.
- Lin, Z., Zhang, G., Zhu, T., Liu, R., Wei, H., and Gu, Q. (2009). Bioactive cytochalasins from *Aspergillus flavipes*, an endophytic fungus associated with the mangrove plant *Acanthus ilicifolius*. *Helv. Chim. Acta.*, **92**, 1538-1544.
- Liu, F., Cai, X., Yang, H., Xia, X., Guo, Z., Yuan, J., Li, M., She, Z., and Lin, Y. (2010). The bioactive metabolites of the mangrove endophytic fungus *Talaromyces* sp. ZH-154 isolated from *Kandelia candel* (L.) Druce. *Planta Med.*, **76**, 185-189.
- Liu, L., Niu, S., Lu, X., Chen, X., Zhang, H., Guo, L., and Che, Y. (2010b). Unique metabolites of *Pestalotiopsis fici* suggest a biosynthetic hypothesis involving a Diels-Alder reaction and then mechanistic diversification. *Chem. Commun.*, **46**, 460-462.
- Liu, H., Edrada-Ebel, R., Ebel, R., Wang, Y., Schulz, B., Draeger, S., Müller, W.E.G., Wray, V., Lin, W., and Proksch, P. (2009). Drimane sesquiterpenoids from the fungus *Aspergillus ustus* isolated from the marine sponge *Suberites domuncula*. *J. Nat. Prod.*, **72**, 1585-1588.
- Liu, H., Edrada-Ebel, R., Ebel, R., Wang, Y., Schulz, B., Draeger, S., Müller, W. E. G. Wray, V., Lin. W., and Proksch, P. (2011). Ophiobolin sesterterpenoids and pyrrolidine alkaloids from the sponge-derived fungus *Aspergillus ustus*. *Helv. Chim. Acta.*, **94**, 623-631.
- Loesgen, S., Bruhn, T., Meindl, K., Dix, I., Schulz, B., Zeek, A., and Bringmann, G.

- (2011). (+)-Flavipucine, the missing member of the pyridione epoxide family of fungal antibiotics. *Eu. J. Org. Chem.*, 5156-5162.
- Lopez-Gresa, M. P., Cabedo, N., Gonzalez-Mas, M. C., Ciavatta, M. L., Avila, C., and Primo, J. (2009). Terretonins E and F, inhibitors of the mitochondrial respiratory chain from the marine-derived fungus *Aspergillus insuetus*. *J. Nat. Prod.*, **72**, 1348–1351.
- Lozzio, C. B., and Lozzion, B. B. (1975). Human chronic myelogenous leukemia cell-line with positive *Philadelphia chromosome*. *Blood*, **45**, 321-334.
- Lu, Z., Lin, Z., Wand, W., Du, L., Zhu, T., Fang, Y., Gu, Q., and Zhu, W. (2008). Citrinin dimers from the halotolerant fungus *Penicillium citrinum* B-57. *J. Nat. Prod.*, **71**, 543-546.
- MacroModel, Schrödinger LLC, 2009.
<http://www.schrodinger.com/Products/macromodel.html>
- Malmstrom, J., Christophersen, C., Barrero, A. F., Oltra, J. E., Justicia, J., and Rosales, A. (2002). Bioactive metabolites from a marine-derived strain of the fungus *Emericella varicolor*. *J. Nat. Prod.*, **65**, 364-367.
- Mayer, A. M., Glaser, K. B., Cuevas, C., Jacobs, R. S., Kem, W., Little, R. D., McIntosh, J. M., Newman, D. J. Potts, B. C., and Shuster, D. E. (2010). The odyssey of marine pharmaceuticals: a current pipeline perspective. *Trends. Pharmacol. Sci.*, **31**, 255-265.
- Mccann, D. M., and Stephens, P. J. (2006). Determination of absolute configuration using density functional theory calculations of optical rotation and electronic circular dichroism: chiral alkenes. *J. Org. Chem.*, **71**, 6074-6098.
- Metz, A. M., Haddad, A., Worapong, J., Long, D. M., Ford, E. J., Hess, W. M., and Strobel, G. A. (2000). Induction of the sexual stage of *Pestalotiopsis microspora*, a taxol-producing fungus. *Microbiology*, **146**, 2079-2089.
- Mizuno, K., Yagi, A., Satoi, S., Takada, M., and Hayashi, M. (1977). Studies on

- aculeacin. I. Isolation and characterization of aculeacin A. *J. Antibiot.*, **30**, 297-302.
- Molinski, T. M., Dalisay, D. S., Lievens, S., and Saludes, J. P. (2009). Drug development from marine natural products. *Nature Reviews: Drug Discovery*, **8**, 69-85.
- Nakanishi, K. (1999). An historical perspective of natural products chemistry. *Comprehensive. Nat. Prod. Chem.*, **8**, xxi-xxxviii.
- Nakanishi, K. (1999). An historical perspective of natural products chemistry. In S. Ushio (Ed.), *Comprehensive. Nat. Pro. Chem.*, **1**. Elsevier Science B.V., Amsterdam, 23-40.
- Newman, D. J., Cragg, G. M., and Snader, K. M. (2000). The influence of natural products upon drug discovery. *Nat. Prod. Rep.*, **17**, 215-234.
- Newman, D. J., Cragg, G. M., and Snader, K. M. (2003). Natural products as source of new drugs over the period 1981-2002. *J. Nat. Prod.*, **66**, 1022-1037.
- Newman, D. J., and Cragg, G. M. (2007). Natural products as sources of new drugs over the last 25 years. *J. Nat. Prod.*, **70**, 461-477.
- Newman, D. J. (2008). Natural products as lead to potential drugs: an old process or the new hope for drug discovery. *J. Med. Chem.*, **51**, 2589-2599.
- Nicolas-Metral, V., Dumont, J. M., Porchet, H., Crabbe, R., and Scalfaro, P. (2008). The cyclophilin inhibitor Debio-025 shows potent anti-hepatitis C effect in patients coinfecting with hepatitis C and human immunodeficiency virus. *Hepatology*, **47**, 817-826.
- Nishio, M., Kohno, J., Sakurai, M., Suzuki, S., Okada, N., Kawano, K., and Komatsubara, S. (2000). TMC-135A and B, new triene-ansamycins, produced by *Streptomyces* sp. *J. Antibiot.*, **53**, 724-727.
- Nitta, K., Fujita, N., Yoshimura, T., Arai, K., and Yamamoto, Y. (1983). Metabolic

- products of *Aspergillus terreus* IX biosynthesis of butyrolactone derivatives isolated from strains IFO 8835 and 4100. *Chem. Pharm. Bull.*, **31** (5), 1528-1533.
- Numata, A., Takahashi, C., Matsushita, T., Miyamoto, T., Kawai, K., Usami, Y., Matsumura, E., Inoue, M., Ohishi, H., and Shingu, T. (1992). Fumiquinazolines, novel metabolites of a fungus isolated from a saltfish. *Tetrahedron lett.*, **33**, 1621-1624
- Ohtani, I., Kusumi, T., Kashman, Y., and Kakisawa, H. (1991). High-field FT NMR application of Mosher's method. The absolute configurations of marine terpenoids. *J. Am. Chem. Soc.*, **113**, 4092-4096.
- Ojima, I. (2008). Modern natural products chemistry and drug discovery. *J. Med. Chem.*, **51** (9), 2587-2588.
- Paquette, L. A., Wang, T. Z., and Sivik, M. R. (1994). Enantioselective synthesis of natural (-)-austalide B, an unusual ortho ester metabolite produced by toxigenic cultures of *Aspergillus ustus*. *J. Am. Chem. Soc.*, **116**, 2665-2666.
- Paquette, L. A., Wang, T. Z., and Sivik, M. R. (1994). Total synthesis of (-)-austalide B. A generic solution to elaboration of the pyran/*p*-cresol butenolide triad. *J. Am. Chem. Soc.*, **116**, 11323-11334.
- Paz, Z., Komon-Zelazowska, M., Druzhinina, I. S., Aveskamp, M. M., Shaniderman, A., Aluma, Y., Carmeli, S., Ilan, M., and Yanden, O. (2010). Diversity and potential antifungal properties of fungi associated with a Mediterranean sponge. *Fungal Divers.*, **42**, 17-26.
- Prapairat, S., Palangpon, K., Samran, P., Masahiko, I., and Yodhathai, T. (2006). Transformation of an irregularly bridged epidithiodiketopiperazine to trichodermamide A. *Org. Lett.*, **8** (14), 3073-3075.
- Pretsch, E., Seibel, J., Simon, W., and Clerc, T. (1989). In spectral data for structure determination of organic compounds; Fresenius, W., Ed.; Springer-Verlag: New

- York, ¹³C-NMR, C210-C212.
- Qiao, M. F., Ji, N. Y., Liu, X. H., Li, K., Zhu, Q. M., and Xue, Q. Z. (2010). Indoloditerpenes from an algicolous isolate of *Aspergillus oryzae*. *Bioorg. Med. Chem. Lett.*, **20**, 5677-5680.
- Rao, K. V., Sadhukhan, A. K., Veerender, M., Ravikumar, V., Mohan, E. V. S., Dhanvantri, S. D., Sitaramkumar, M., Babu, J. M., Vyas, K., and Reddy, G. O. (2000). Butyrolactones from *Aspergillus terreus*. *Chem. Pharm. Bull.*, **48** (4), 559-562.
- Rateb, M. E., and Ebel, R. (2011). Secondary metabolites of fungi from marine habitats. *Nat. Prod. Rep.*, **28**, 290-344.
- Richard, K. H., and Libero, A. G. (1964). The absolute configuration of citrinin. *J. Org. Chem.*, **29**, 766-767.
- Roedel, T., and Gerlach, H. (1995). Enantioselective synthesis of the polyketide antibiotic (3*R*, 4*S*)-(-)-citrinin. *Liebigs Ann.*, 885-888.
- Rollinger, J. M., Langer, T., and Stuppner, H. (2006). Strategies for efficient lead structure discovery from natural products. *Curr. Med. Chem.*, **13**, 1491-1507.
- Rose, W. C., and Basler, G. A. (1990). In vivo model development of cisplatin-resistant and-sensitive A2780 human ovarian carcinomas. *In Vivo*, **4**, 391-396.
- Saleem, M., Ali, M. S., Hussain, S., Jabbar, A., Ashraf, M., and Lee, Y. S. (2007). Marine natural products of fungal origin. *Nat. Prod. Rep.*, **24**, 1142-1152.
- Satio, S., Yagi, A., Asano, K., Mizuno, K., and Watanabe, T. (1977). Studies on aculeacin. II. Isolation and characterization of aculeacins B, C, D, E, F and G. *J. Antibiot.*, **30**, 303-307.
- Schultes, R. E., and Raffauf, R. F. (1990). *The Healing Forest*, Dioscorides Press, Portland.

- Singh, M. P., Janso, J. E., Luckman, S. W., Brady, S. F., Clardy, J., Greenstein, M., and Maiese, W. M. (2000). Biological activity of guanacastepene, a novel diterpenoid antibiotic produced by an unidentified fungus CR115. *J. Antibiot.*, **53**, 256-261.
- Sneader, W. (1996). *Drug Prototypes and Their Exploitation*. Wiley, UK.
- Stephens, P. J., and Harada, N. (2010). ECD cotton effect approximated by the Gaussian curve and other methods. *Chirality*, **22**, 229–233.
- Stierle, A. A., Stierle, D. B., and Bugni, T. (1999). Sequoiatones A and B: novel antitumor metabolites isolated from a redwood endophyte. *J. Org. Chem.*, **64**, 5479-5484.
- Strobel, G. A. (2002). Rainforest endophytes and bioactive products. Critical reviews in biotechnology. *Crit. Rev. Biotechnol.*, **22**, 315-333.
- Strobel, G., and Daisy, B. (2003). Bioprospecting for microbial endophytes and their natural products. *Microbiol. Mol. Biol. Rev.*, **67**, 491-502.
- Strobel, G., Daisy, B., Castillo, U., and Harper, J. (2004). Natural products from endophytic microorganisms. *J. Nat. Prod.*, **67**, 257-268.
- Stipanovic, R. D., and Howell, C. R. (1982). The structure of gliovirin, a new antibiotic from *Gliocladium virens*. *J. Antibiot.*, **35**, 1326-1329.
- Su, B. N., Park, E. J., Mbwambo, Z. H., Santarsiero, B. D., Mesecar, A. D., Fong, H. H. S., Pezzuto, J. M., and Kinghorn, A. D. (2002). New chemical constituents of *Euphorbia quinquecostata* and absolute configuration assignment by a convenient Mosher ester procedure carried out in NMR tubes. *J. Nat. Prod.*, **65**, 1278-1282.
- Sunazuka, T., Hirose, T., and Omura, S. (2008). Efficient total synthesis of novel bioactive microbial metabolites. *Acc. Chem. Res.*, **41**, 302-314.
- Takahashi, C., Matsushita, T., Doi, M., Minoura, K., Shingu, T., Kumeda, Y., and

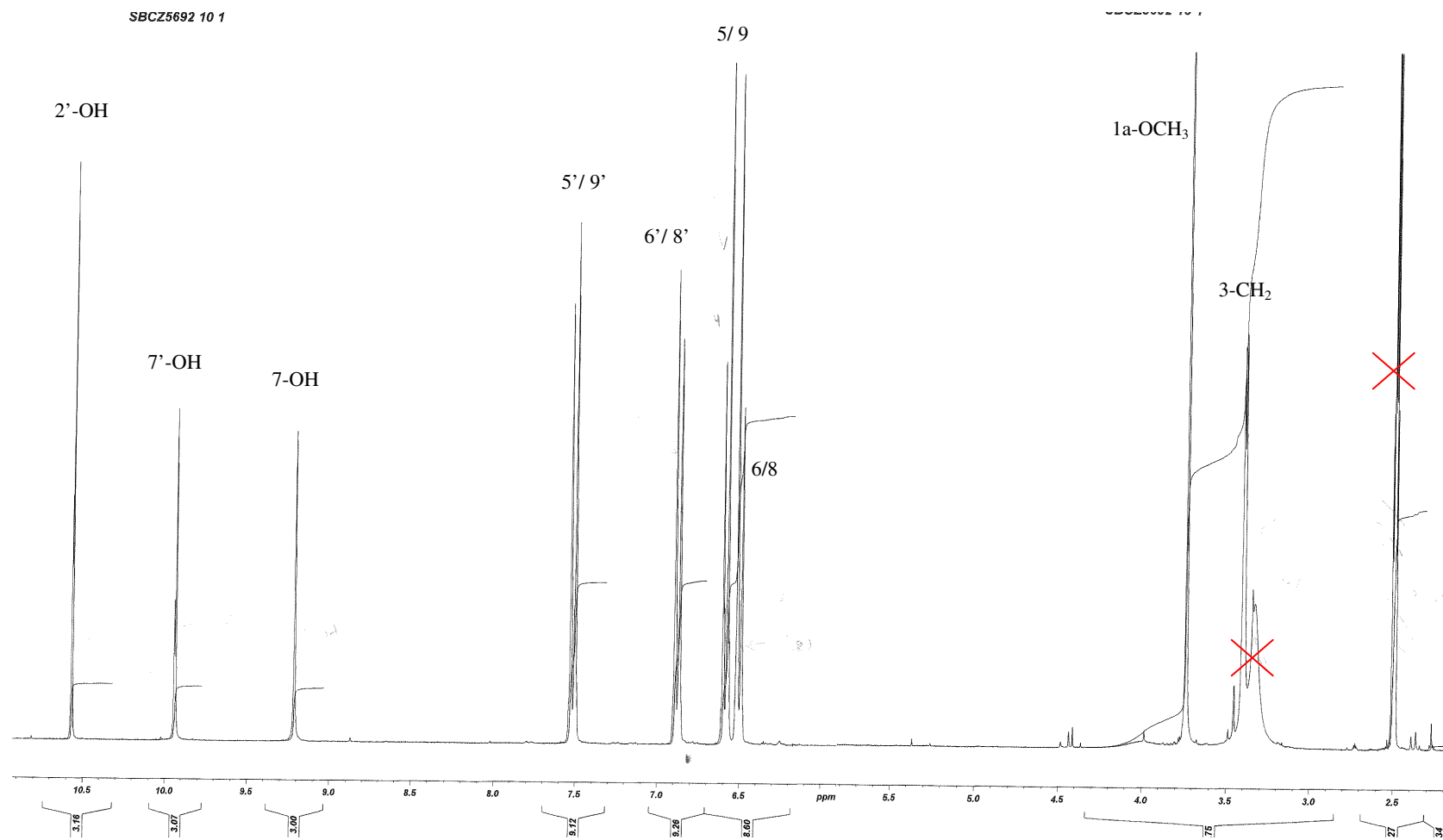
- Numata, A. (1995). Fumiquinazolines A–G, novel metabolites of a fungus separated from a *Pseudolabrus* marine fish. *J. Chem. Soc. Perkin. Trans. I.*, 2345-2353.
- Tan, R. X., and Zou, W. X. (2001). Endophytes: a rich source of functional metabolites. *Nat. Pro. Rep.*, **18**, 448-459.
- Tejesvi, M. V., Nalini, M. S., Mahesh, B., Prakssh, H. S., Kini, K. R., Shetty, H. S., and Subbiah, V. (2007). New hopes from endophytic fungal secondary metabolites. *Bol. Soc. Quim. Mes.*, **1** (1), 19-26.
- Traber, R., Hofmann, H., Kuhn, M., and von Wartburg, A. (1982). Isolierung und Strukturermittlung der neuen Cyclosporin E, F, G, H, und I. *Helv. Chim. Acta.*, **65**, 1655-1677.
- Traber, R., Hofmann, H., Loosli, H. R., Ponelle, M., and von Wartburg, A. (1987). Neue Cyclosporine aus *Tolypocladium inflatum*. Die Cyclosporine K-Z. *Helv. Chim. Acta.*, **70**, 13-36.
- Tyler, A. J., Johann, S., Wayne, D. I., Samarkand, A. E., Steven, T. L., Helene, C. V., Karen, T., Junke, L., Kenny, K. A., Joseline, R., Walter. M. B., Nadine, C. G., Yong, Y. S., Lokey, R. S., James, H. M., Kyria, B., Arif, A., Atit, K., Heddy, J., Leonardus, B. S. K., Leonard, F. B., and Phillip, C. (2011). Natural product libraries to accelerate the high-throughput discovery of therapeutic lead. *J. Nat. Prod.*, **74**, 2545-2555.
- Varetto, U. MOLEKEL 5.4, Swiss National Supercomputing Centre: Manno, Switzerland, 2009.
- Varoglu, M., and Crews, P. (2000). Biosynthetically diverse compounds from a saltwater culture of sponge-derived *Aspergillus niger*. *J. Nat. Prod.*, **63**, 41-43.
- Wang, G. Y. S., Abrell, L. M., Avelar, A., and Borgeson, B. M. (1998). New hirsutane based sesquiterpenes from salt water cultures of a marine sponge-derived fungus and the terrestrial fungus *Coriolus consors*. *Tetrahedron*, **54**, 7335-7342.

- Wang, Y., Zheng, J., Liu, P., Wang, W., and Zhu, W. (2011). Three new compound from *Aspergillus terreus* PT06-2 grown in a high salt medium. *Mar. Drugs*, **9**, 1368-1378.
- Watanabe, S., Hirai, H., Ishiguro, M., Kambara, T., Kojima, Y., Matsunaga, T., Nishida, H., Suzuki, Y., Sugiura, A., Harwood, H. J., Huang, L. H., and Kojima, N. (2001). A new inhibitor of squalene synthase produced by a fungus, *Aspergillus aculeatus*. *J. Antibiot.*, **54**, 904-910.
- Willian, R. S. (2000). The role of natural products in a modern drug discovery program. *Drug Discov. Today*, **5** (2), 39-41.
- Wilson, R. M., and Danishefsky, S. J. (2006). Small molecule natural products in the discovery of therapeutic agents: the synthesis connection. *J. Org. Chem.*, **71**, 8329-8351.
- Wu, Q. X., Crews, M. S., Draskovic, M., Sohn, J., Johnson, T. A., Tenney, K., Valeriote, F. A., Yao, X., Bjeldanes, L. F., and Crews, P. (2010). Azonazine, a novel dipeptide from a hawaiian marine sediment-derived fungus, *Aspergillus insulicola*. *Org. Lett.*, **12**, 4458-4461.
- Xin, Z., Tian, L., Zhu, T., Wang, W., Du, L., Fang, Y., Gu, Q., and Zhu, W. (2007). Isocoumarin derivatives from the sea squirt-derived fungus *Penicillium stoloniferum* QY2-10 and the halotolerant fungus *Penicillium notatum* B-52. *Arch. Pharm. Res.*, **30**, 816-819.
- Yamazaki, M., Fujimoto, H., and Okuyama, E. (1976). Structure determination of six tryptoquivaline-related metabolites from *Aspergillus fumigatus*. *Tetrahedron lett.*, **33**, 2861-2864.
- Yamazaki, M., Fujimoto, H., and Okuyama, E. (1977). Structure of tryptoquivaline C (FTC) and D (FTD). Novel metabolites from *Aspergillus fumigatus*. *Chem. Pharm. Bull.*, **25**, 2554-2560
- Yamazaki, M., Fujimoto, H., and Okuyama, E. (1978). Structure determination of six

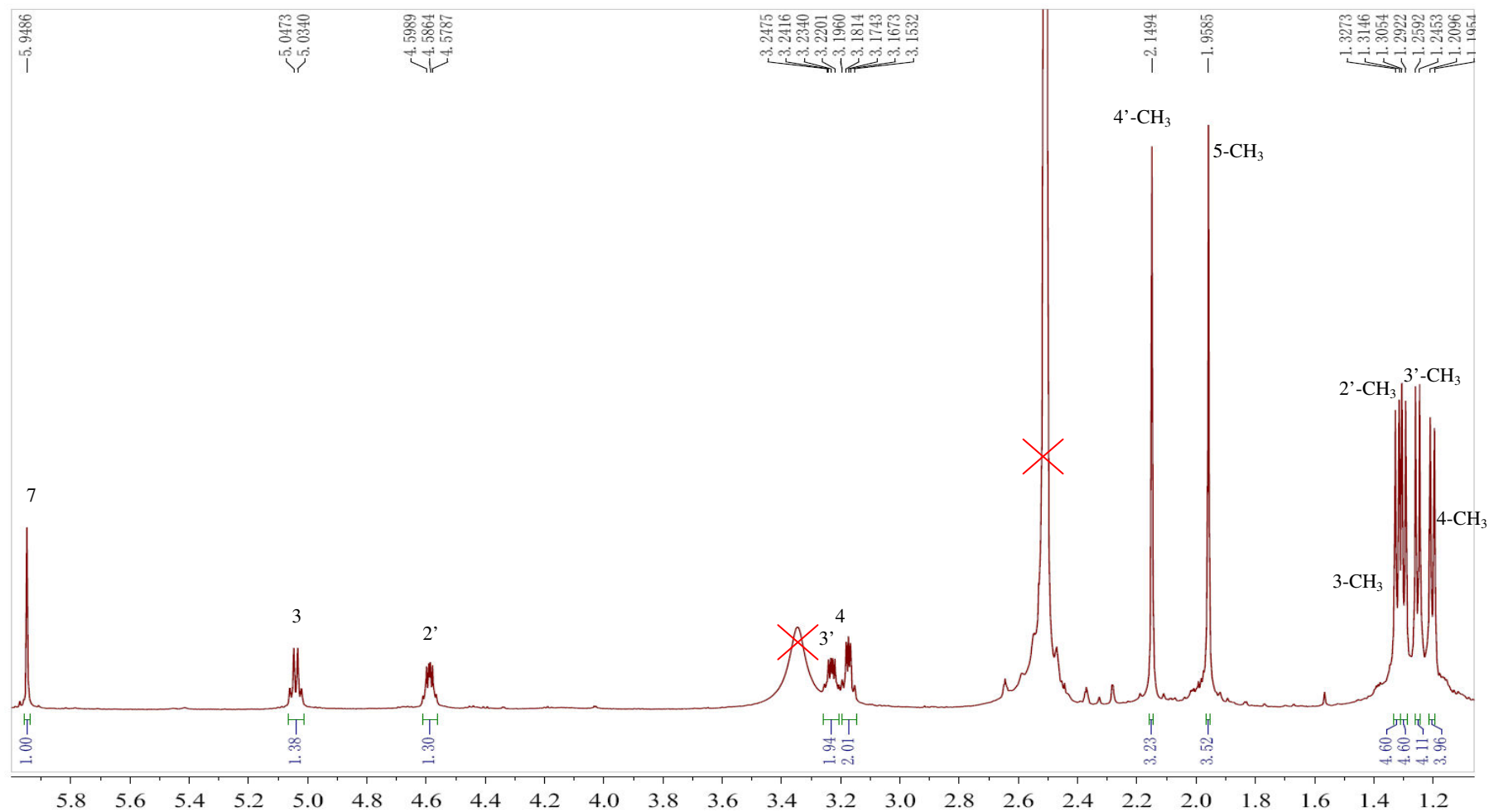
- fungal metabolites, tryptoquivaline E, F, G, H, I and J from *Aspergillus fumigatus*. *Chem. Pharm. Bull.*, **26**, 111-117.
- Yamada, T., Imai, E., Nakatuji, K., Numata, A., and Tanaka, R. (2007). Cephalimysin A, a potent cytotoxic metabolite from an *Aspergillus* species separated from a marine fish. *Tetrahedron lett.*, **48**, 6294-6296.
- Yamamoto, Y., Nitta, K., Tango, K., Saito, T., and Tsuchimuro, M. (1965). Studies on the metabolic products of a strain of *Aspergillus fumigatus* (DH 413). I. Isolation and chemical structures of metabolites. *Chem. Pharm. Bull.*, **13**, 935-941.
- Yu, C. M., Curtis, J. M., Walter, J. A., Wright, J. L., Ayer, S. W., Kaleta, J., Querengesser, L., and Fathi-Afshar, Z. R. (1996). Potent inhibitors of cysteine proteases from the marine fungus *Microascus longirostris*. *J. Antibiot.*, **49** (4), 395-397.
- Zhang, H., Zhang, J., Hu, S., Zhang, Z., Zhu, C., Ng, S. W., and Tan, R. (2010). Ardeemins and cytochalasins from *Aspergillus terreus* residing in *Artemisia annua*. *Planta Med.*, **76**, 1616-1621.
- Zhou, Y., Mándi A., Debbab A., Wray, V., Schulz, B., Müller, W. E. G., Lin, W., Proksch, P., Kurtán, T., and Aly, A. H. (2011). New austalides from the sponge-associated fungus *Aspergillus* sp. *Eur. J. Org. Chem.*, (30), 6009-6019.
- Zhuang, Y., Teng, X., Wang, Y., Liu, P., Li, G., and Zhu, W. (2011). New quinazolinone alkaloids within rare amino acid residue from coral-associated fungus, *Aspergillus versicolor* LCJ-5-4. *Org. Lett.*, **13**, 1130-1133.

7. Attachments

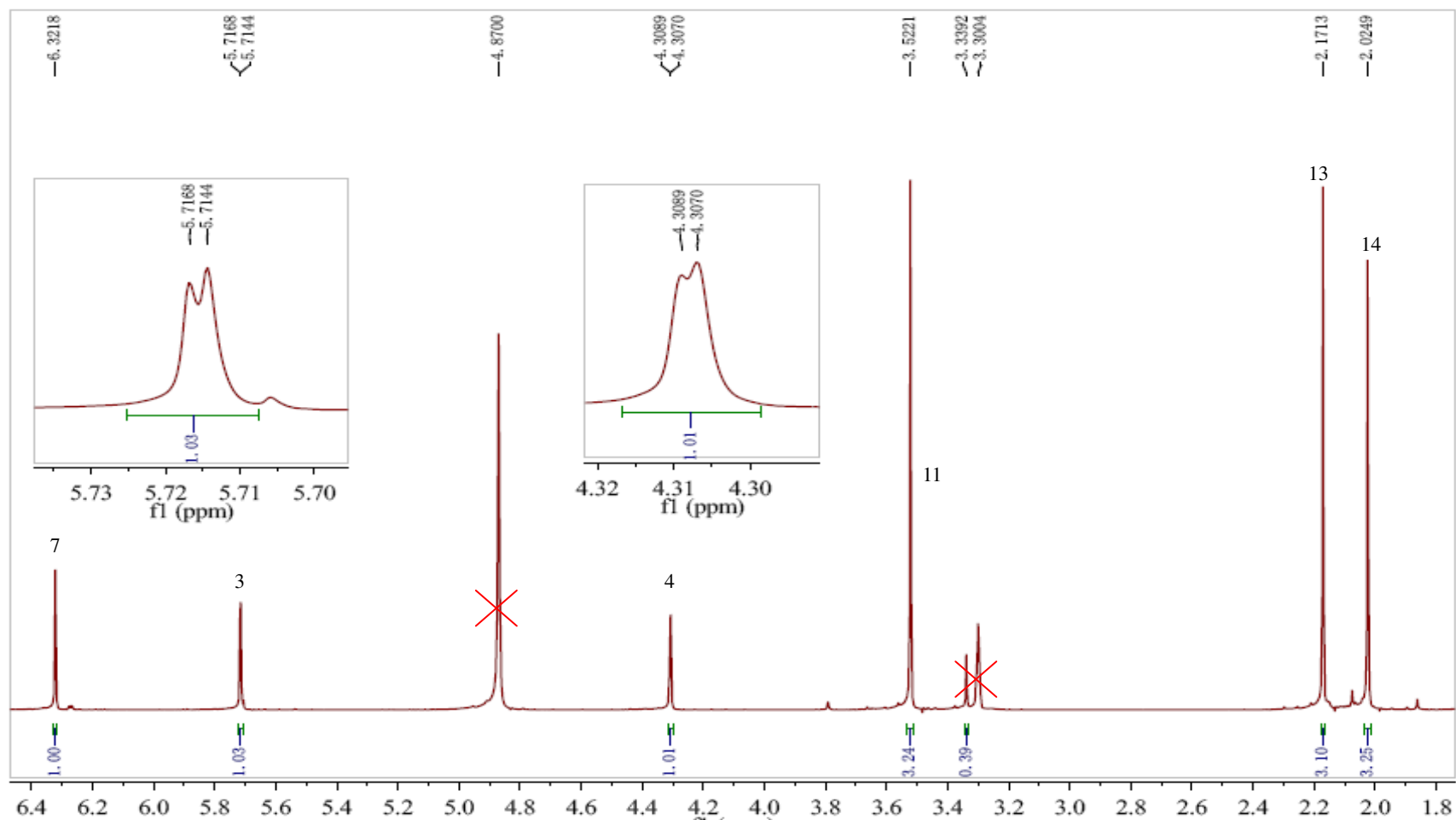
Attachment 1. The ^1H NMR spectrum of butyrolactone II (**1**, known)



Attachment 2. The ^1H NMR spectrum of dicitrinin A (**2**, known)

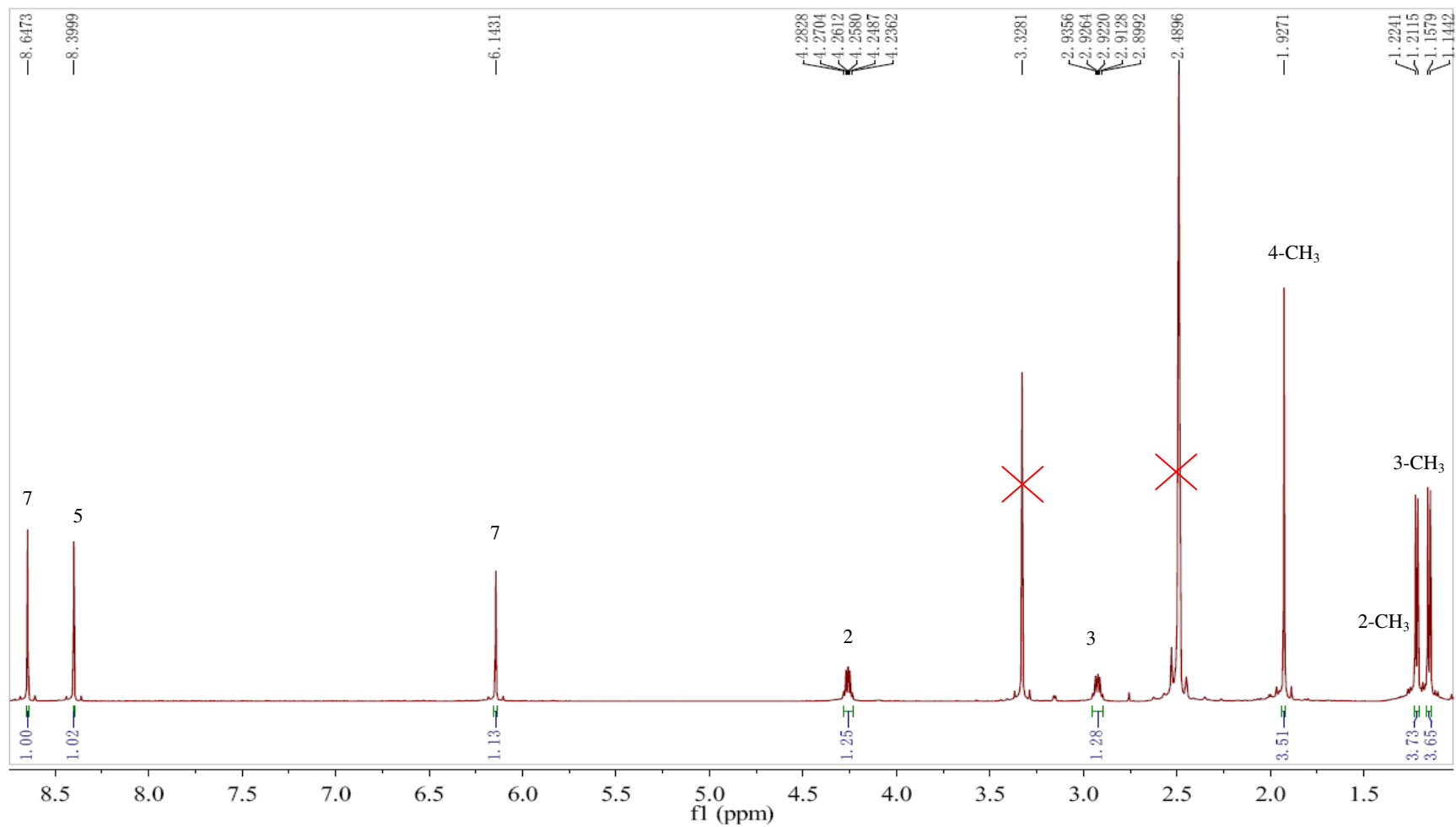


Attachment 3. The ^1H NMR spectrum of 4-acetyl-3,4-dihydro-6,8-dihydroxy-3-methoxy-5-methylisocoumarin (**3**, known)

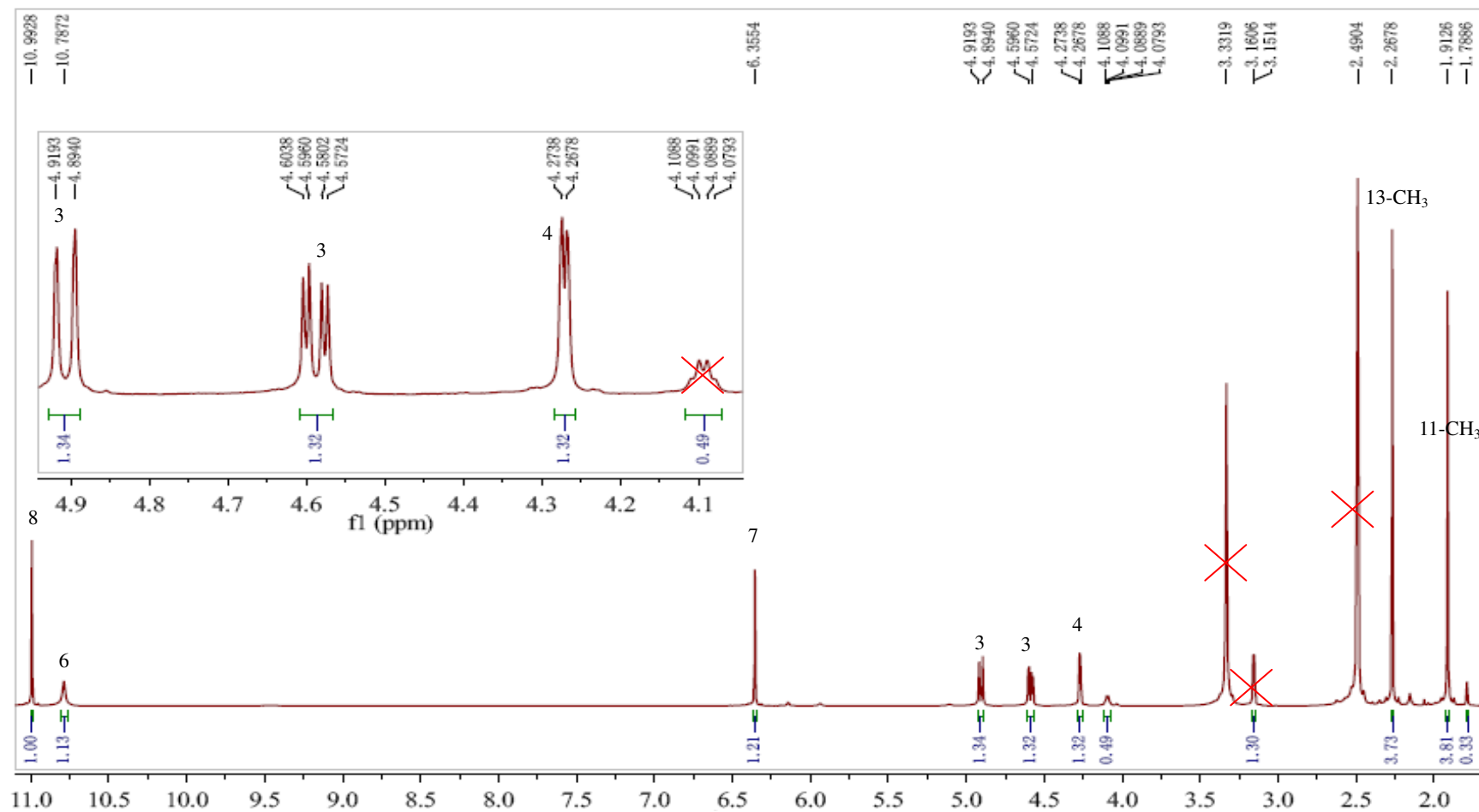


Attachments

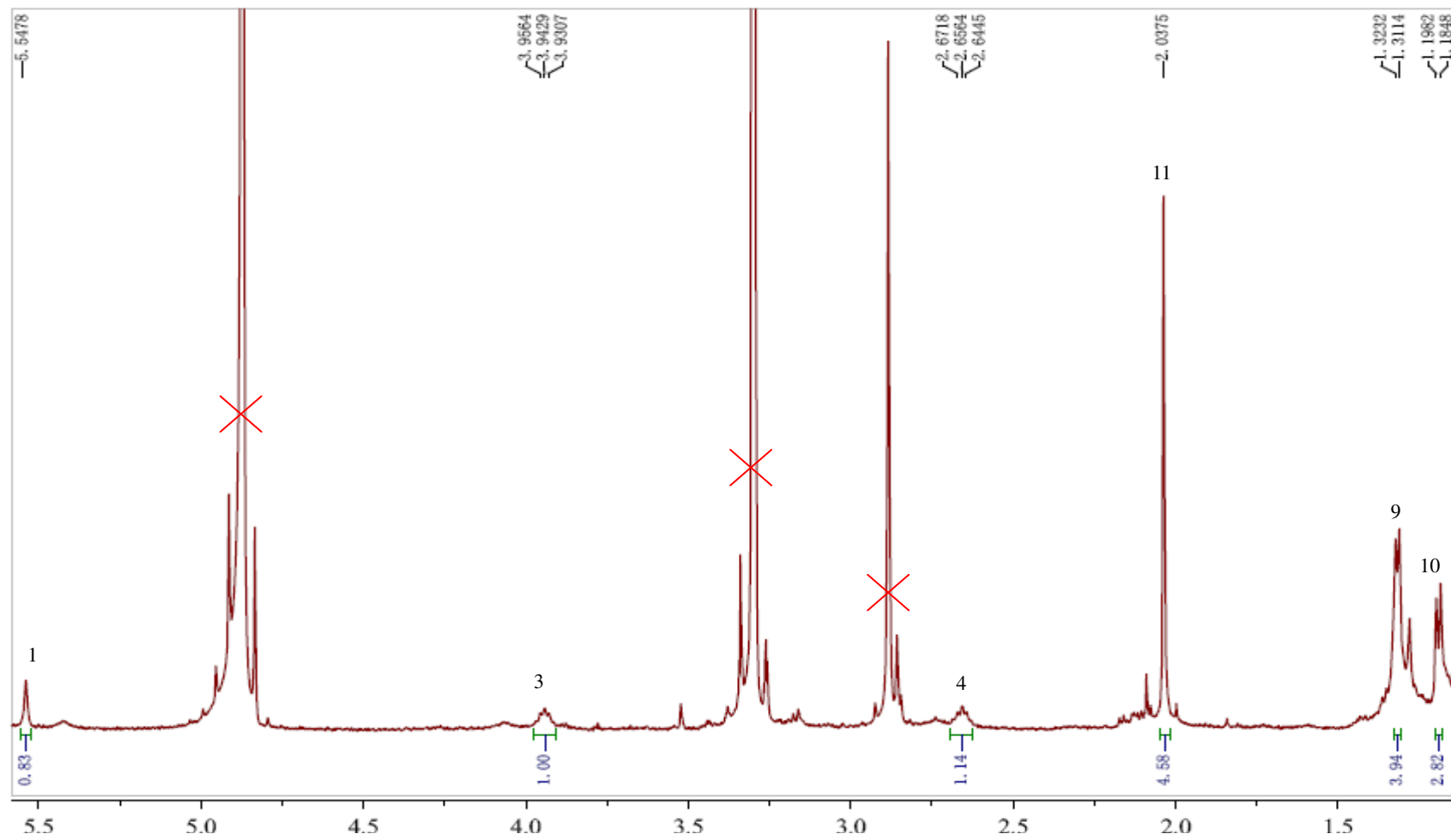
Attachment 4. The ^1H NMR spectrum of 2,3,4-trimethyl-5,7-dihydroxy-2,3-dihydrobenzofuran (**4**, known)



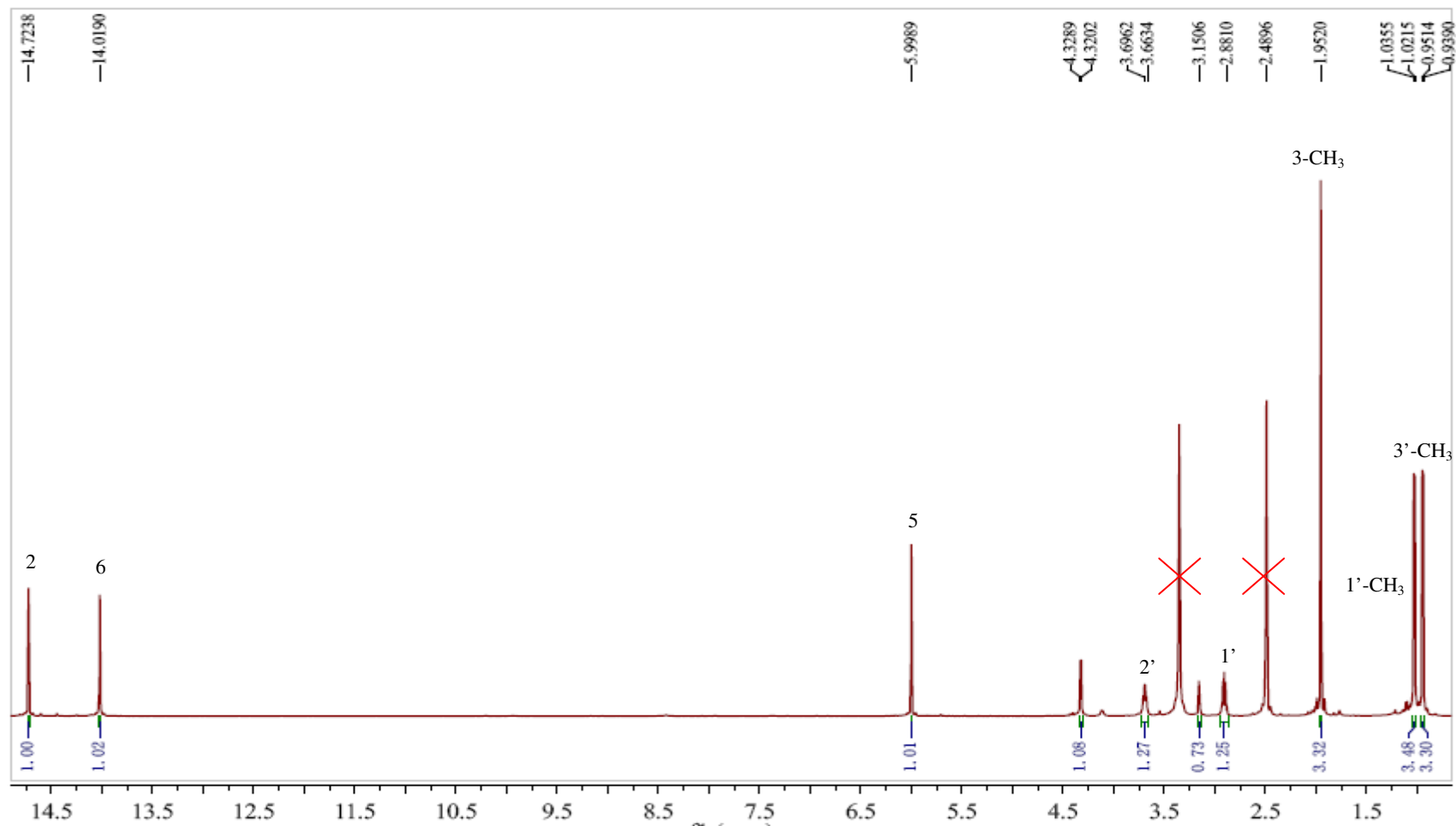
Attachment 5. The ^1H NMR spectrum of 4-acetyl-3,4-dihydro-6,8-dihydroxy-5-methylisocoumarin (**5**, known)



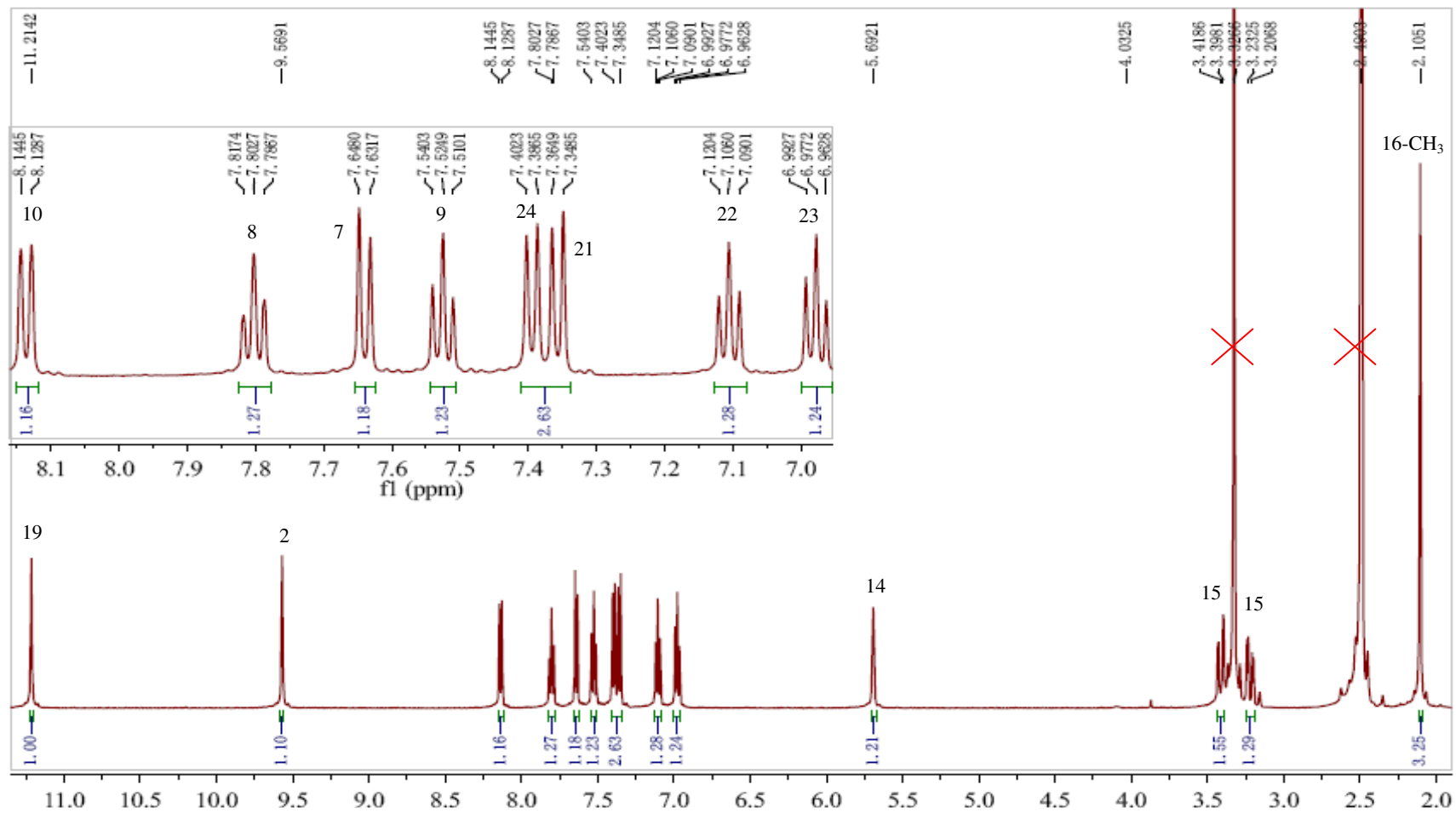
Attachment 6. The ^1H NMR spectrum of citrinin (**6**, known)



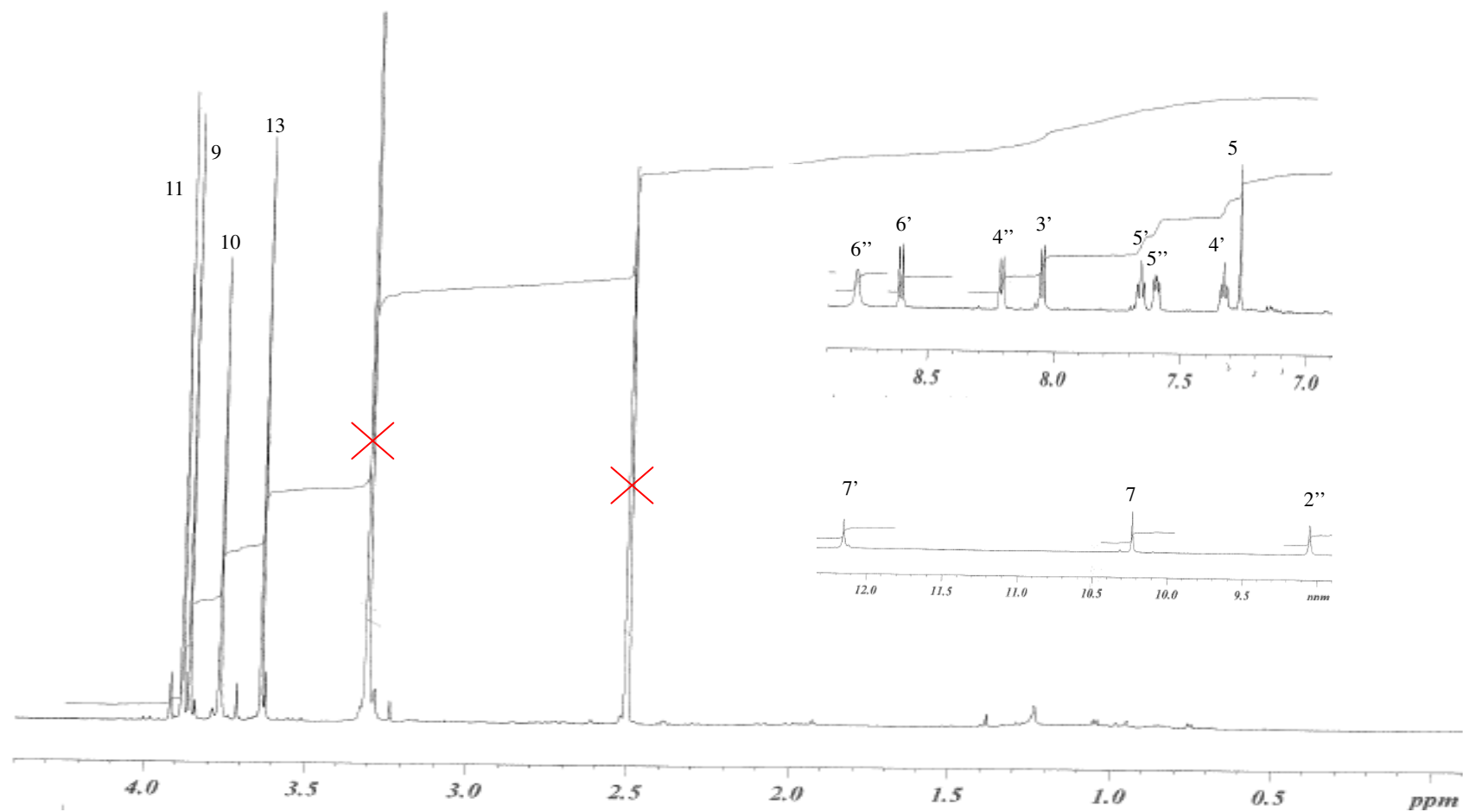
Attachment 7. The ^1H NMR spectrum of phenol A acid (**7**, known)



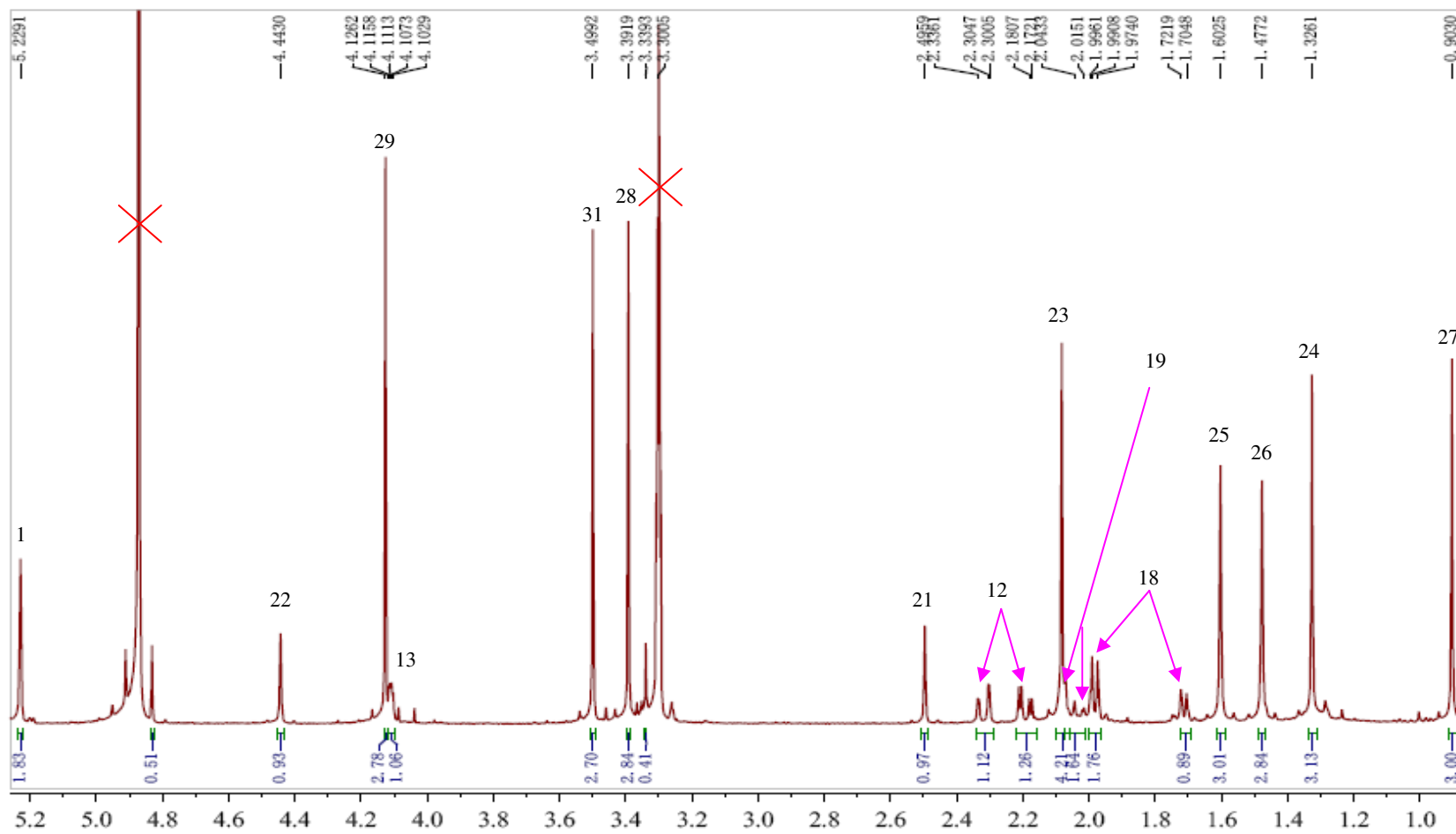
Attachment 8. The ^1H NMR spectrum of fumiquinazoline J (**8**, known)



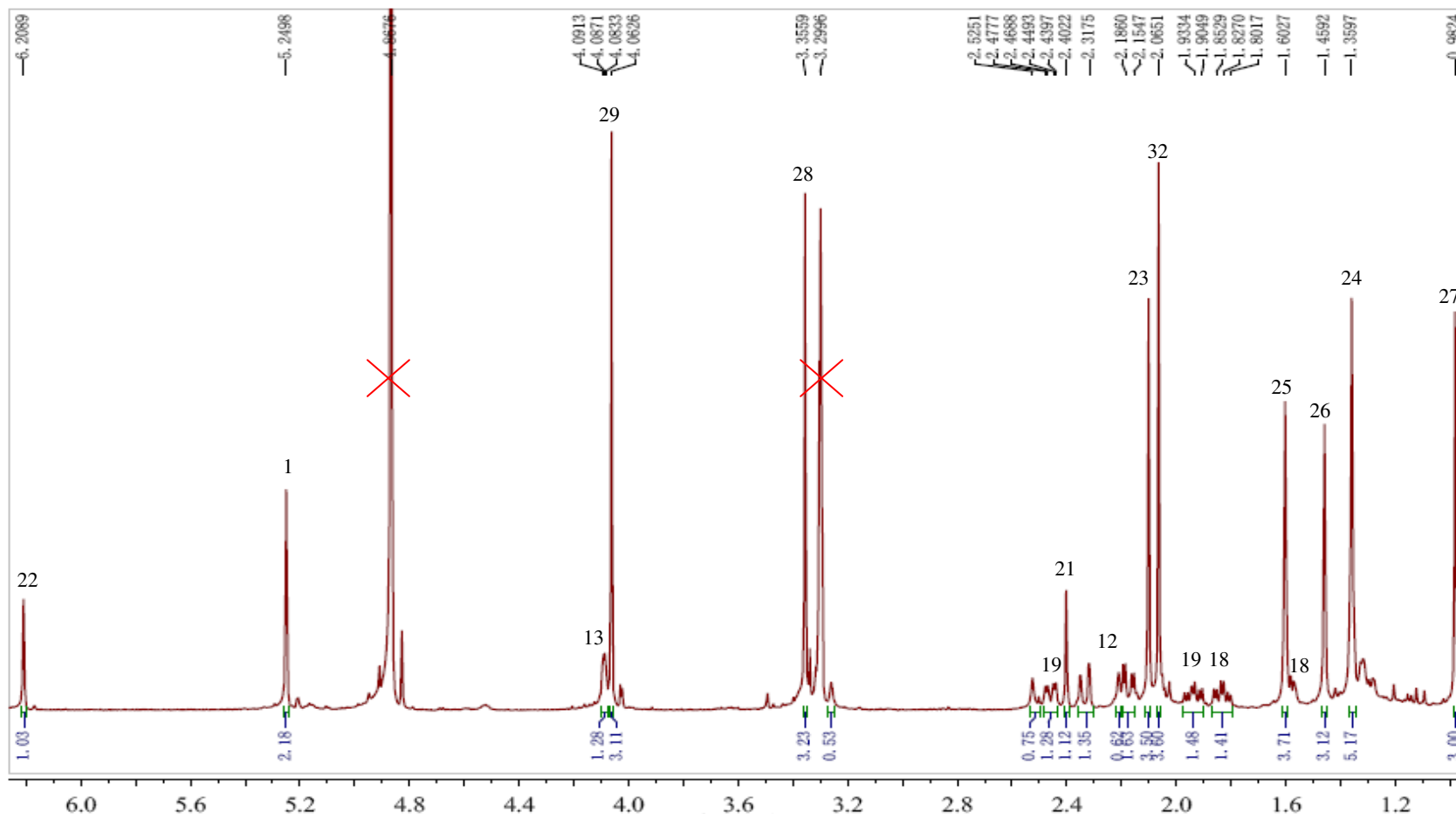
Attachment 9. The ^1H NMR spectrum of methyl 3,4,5-trimethoxy-2-(2-(nicotinamido) benzamido) benzoate (**9**, known)



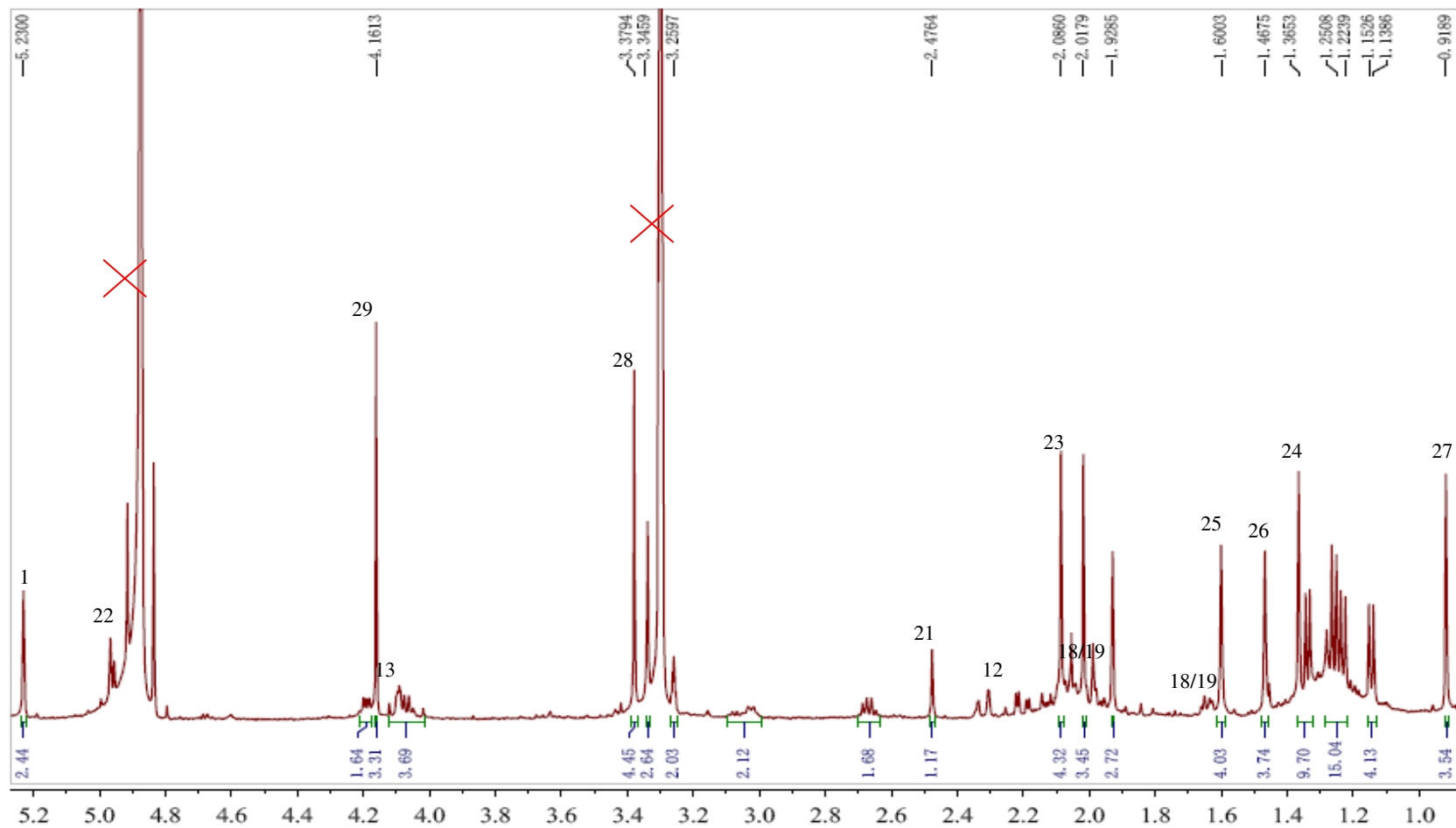
Attachment 10. The ^1H NMR spectrum of austrialide M (**10**, new)



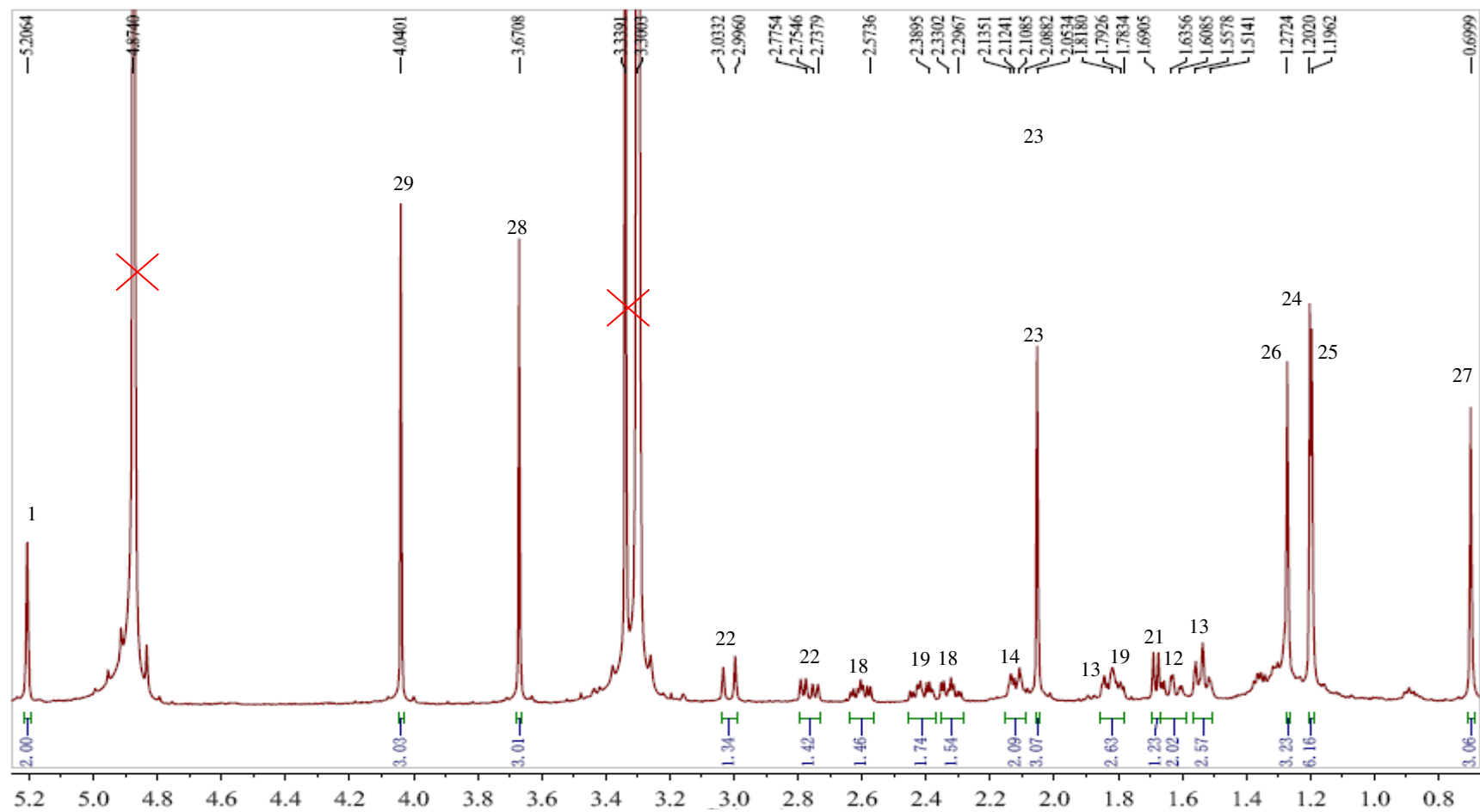
Attachment 11. The ^1H NMR spectrum of austrialide N (**11**, new)



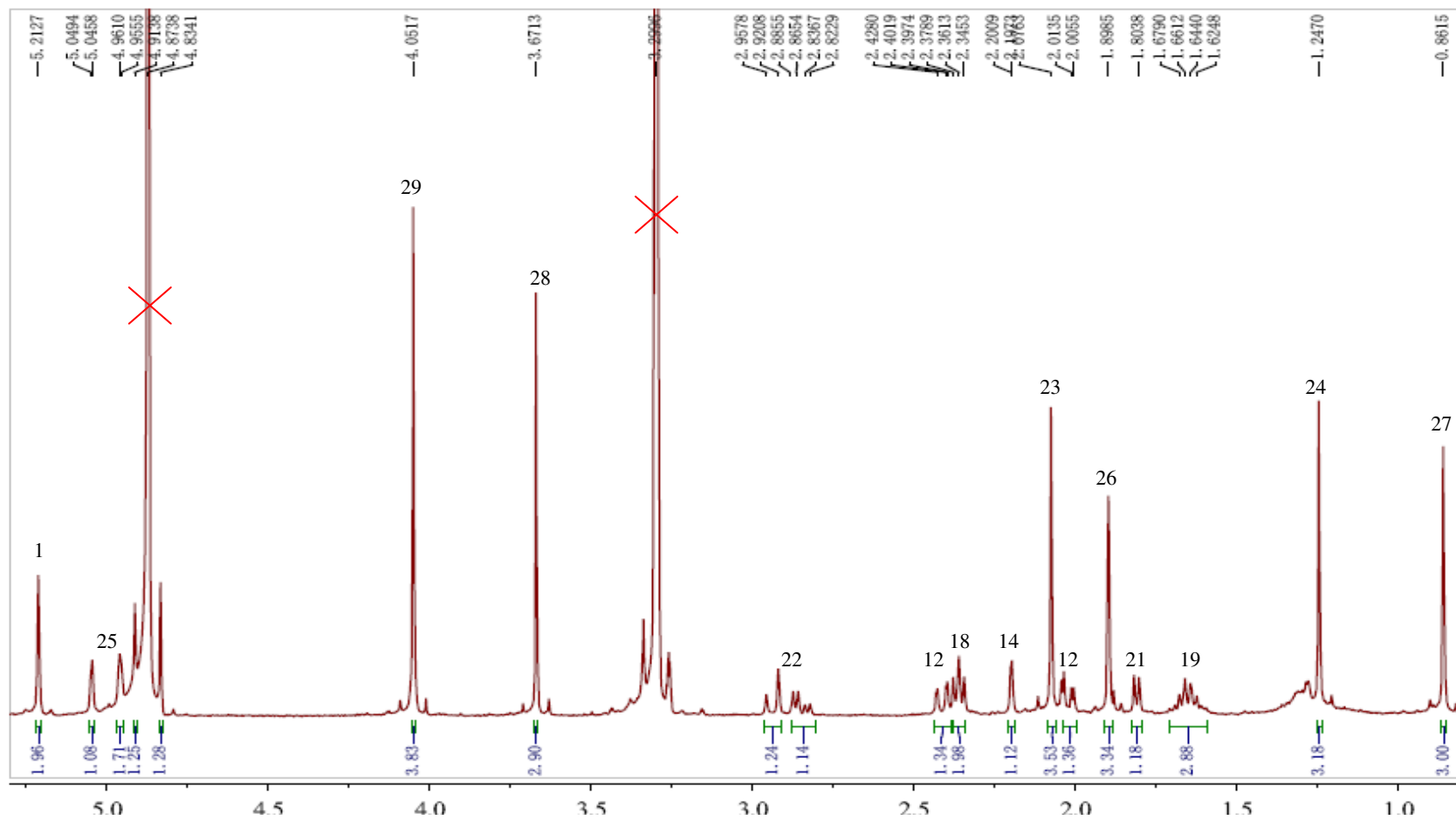
Attachment 12. The ^1H NMR spectrum of austalide O (**12**, new)



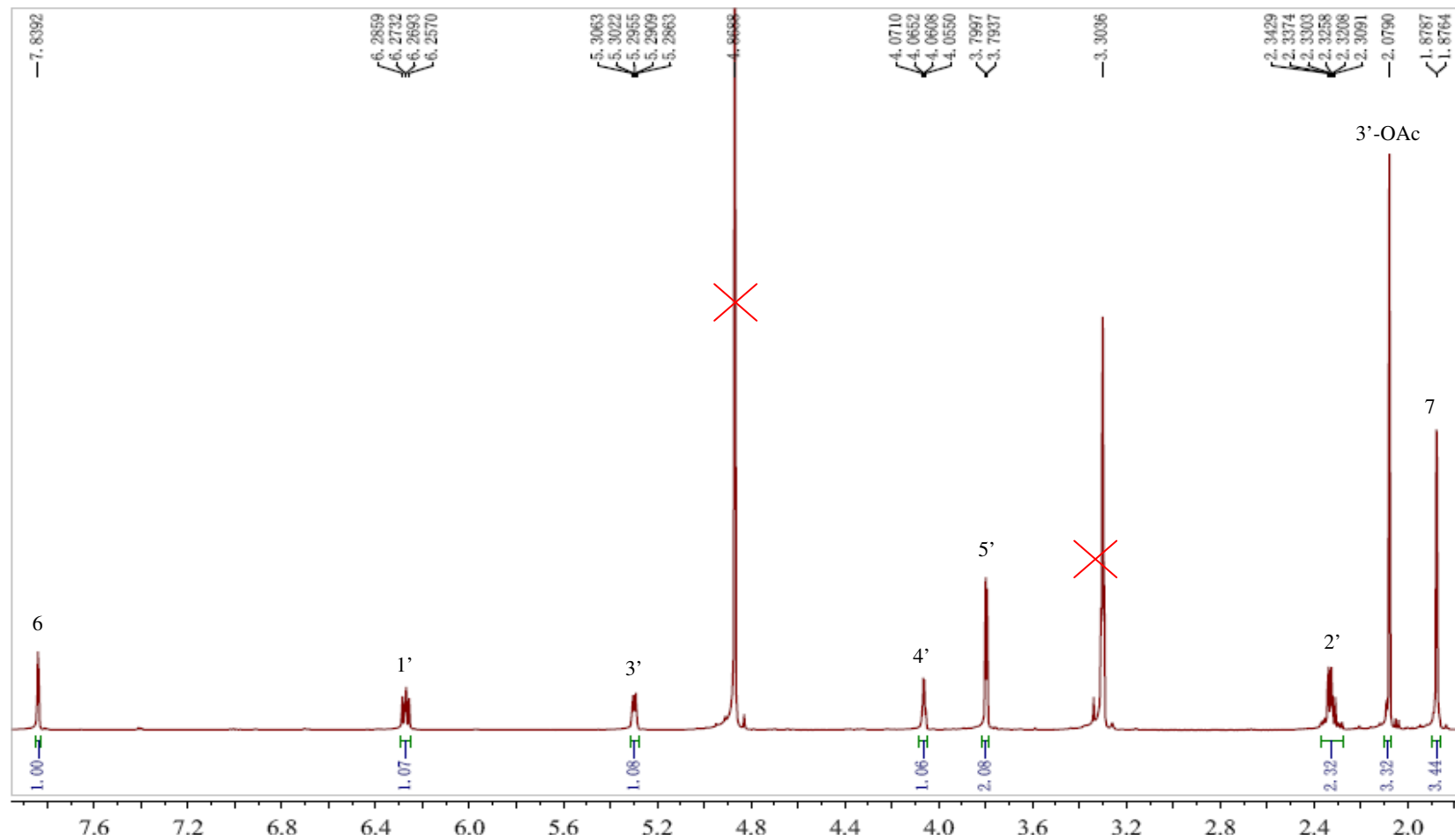
Attachment 13. The ^1H NMR spectrum of austrialide P (**13**, new)



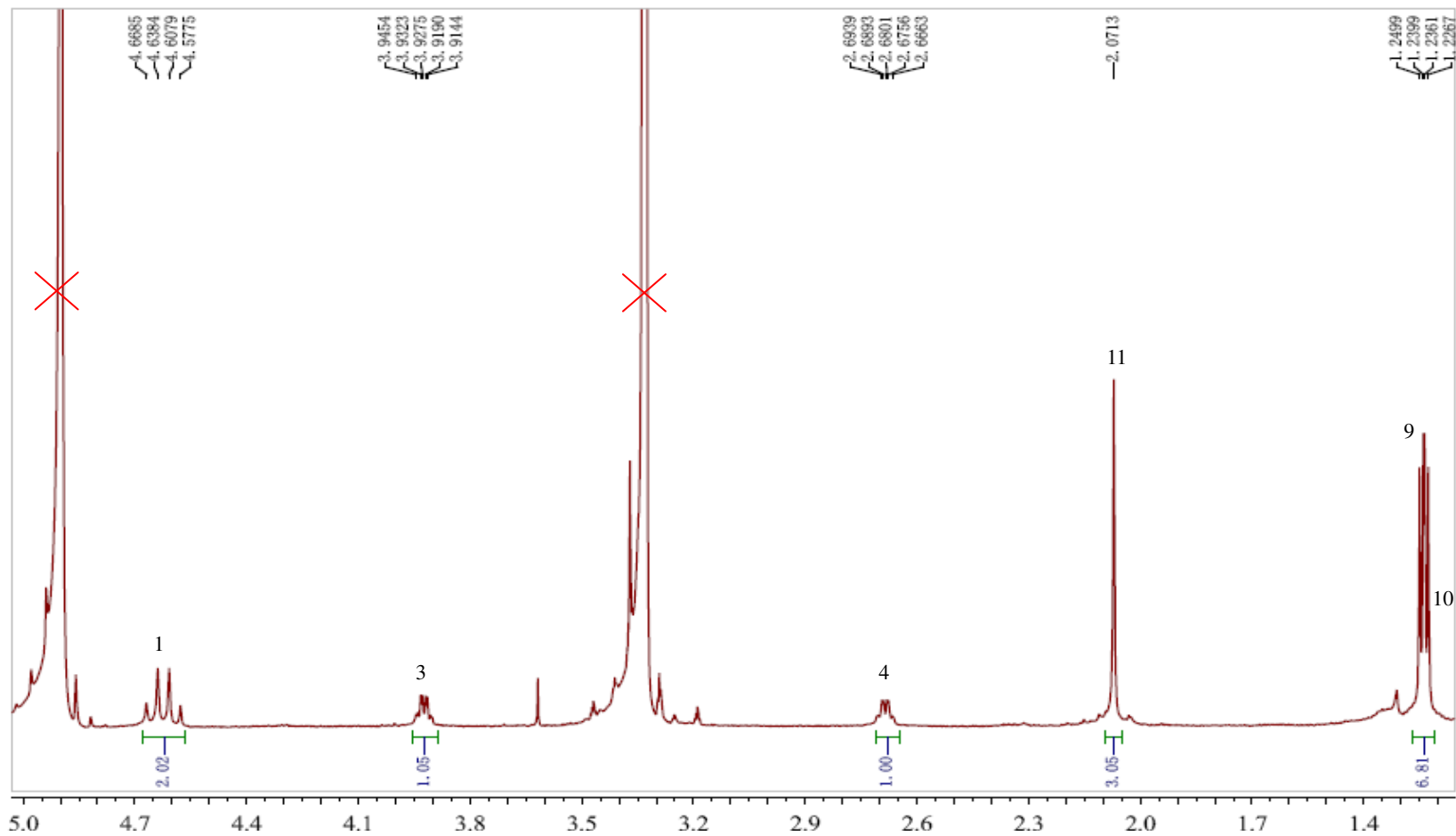
Attachment 14. The ^1H NMR spectrum of austrialide Q (**14**, new)



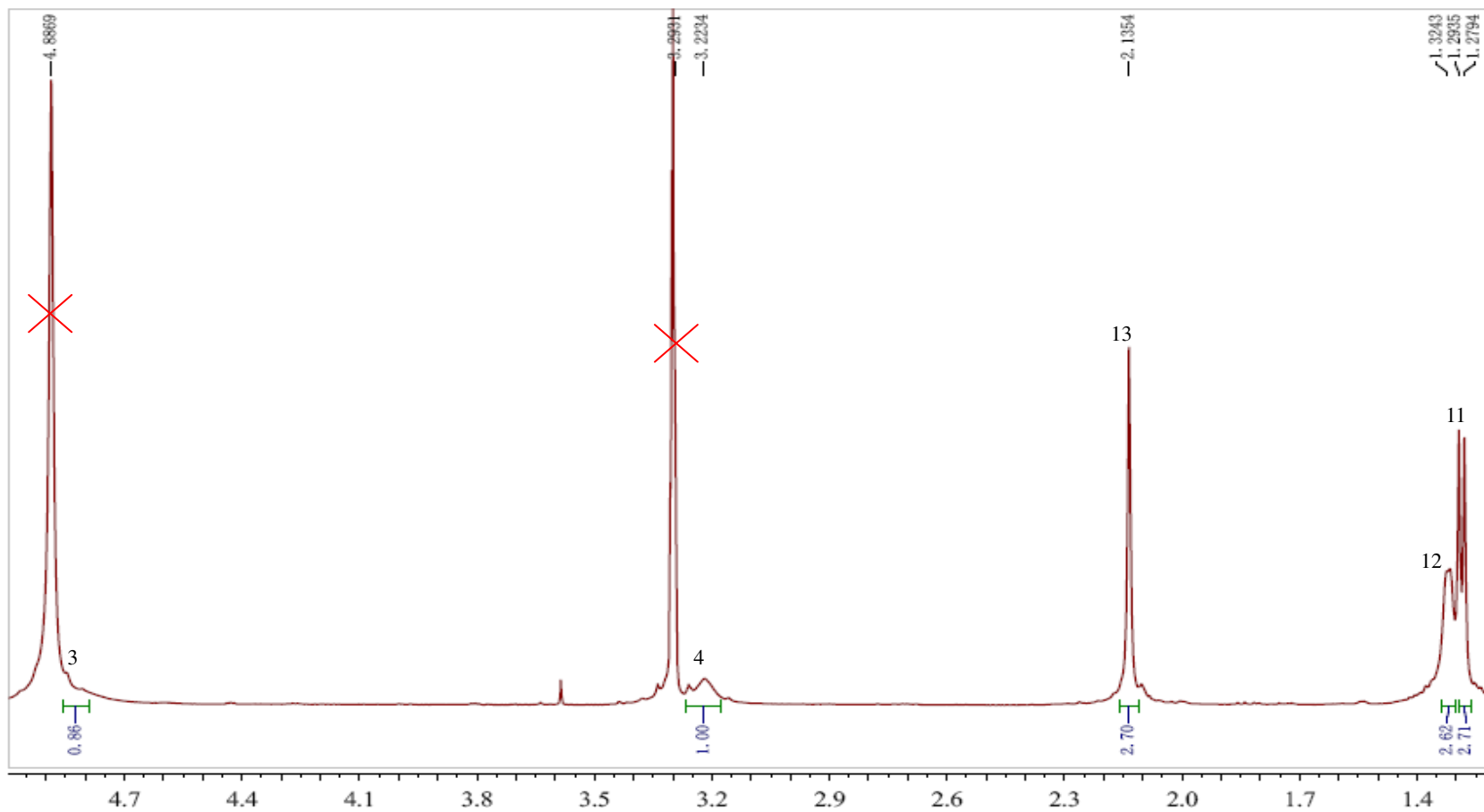
Attachment 15. The ^1H NMR spectrum of 3'-*O*-acetylthymidine (**15**, known)



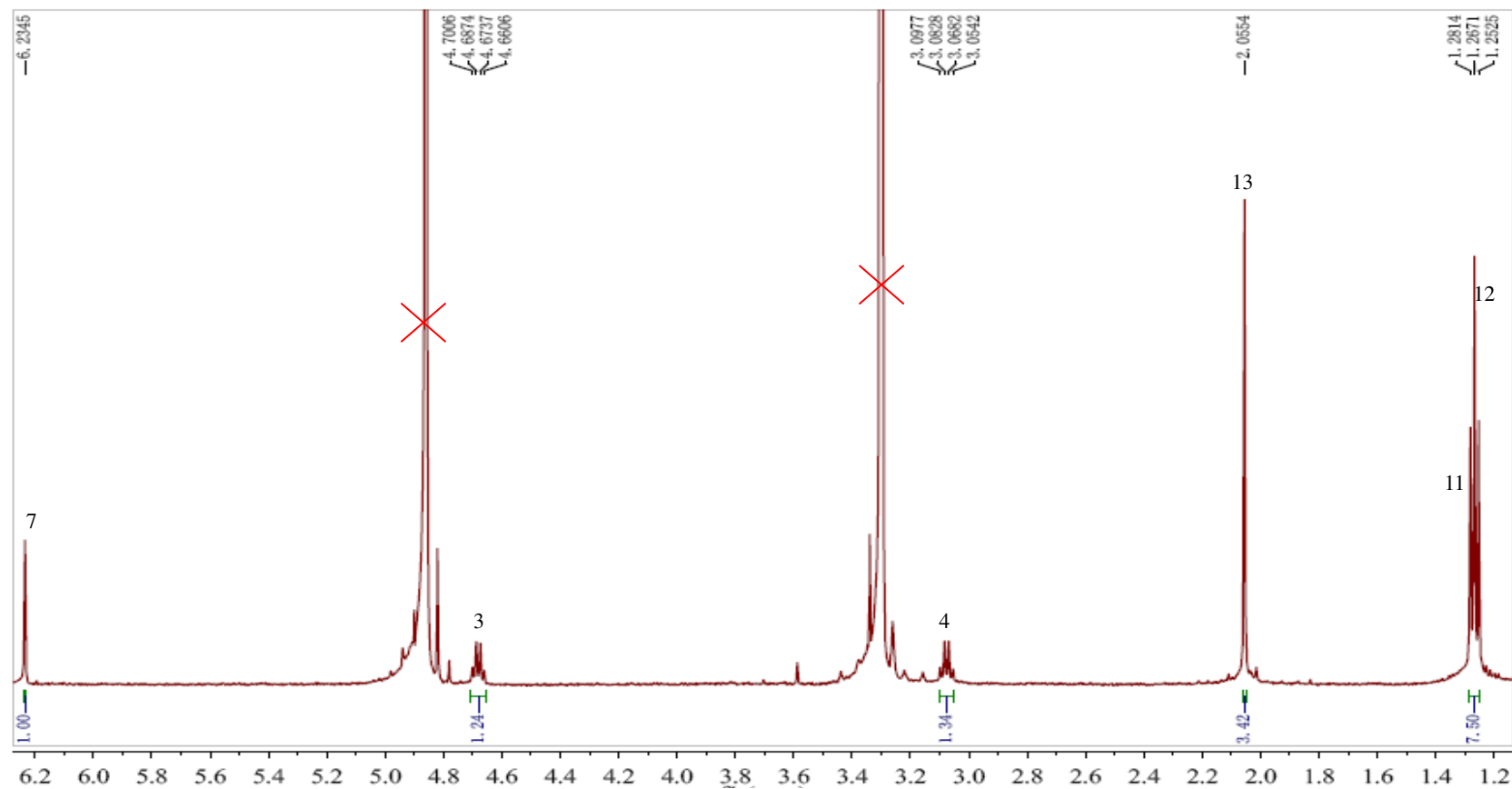
Attachment 16. The ^1H NMR spectrum of dihydrocitrinin (**16**, known)



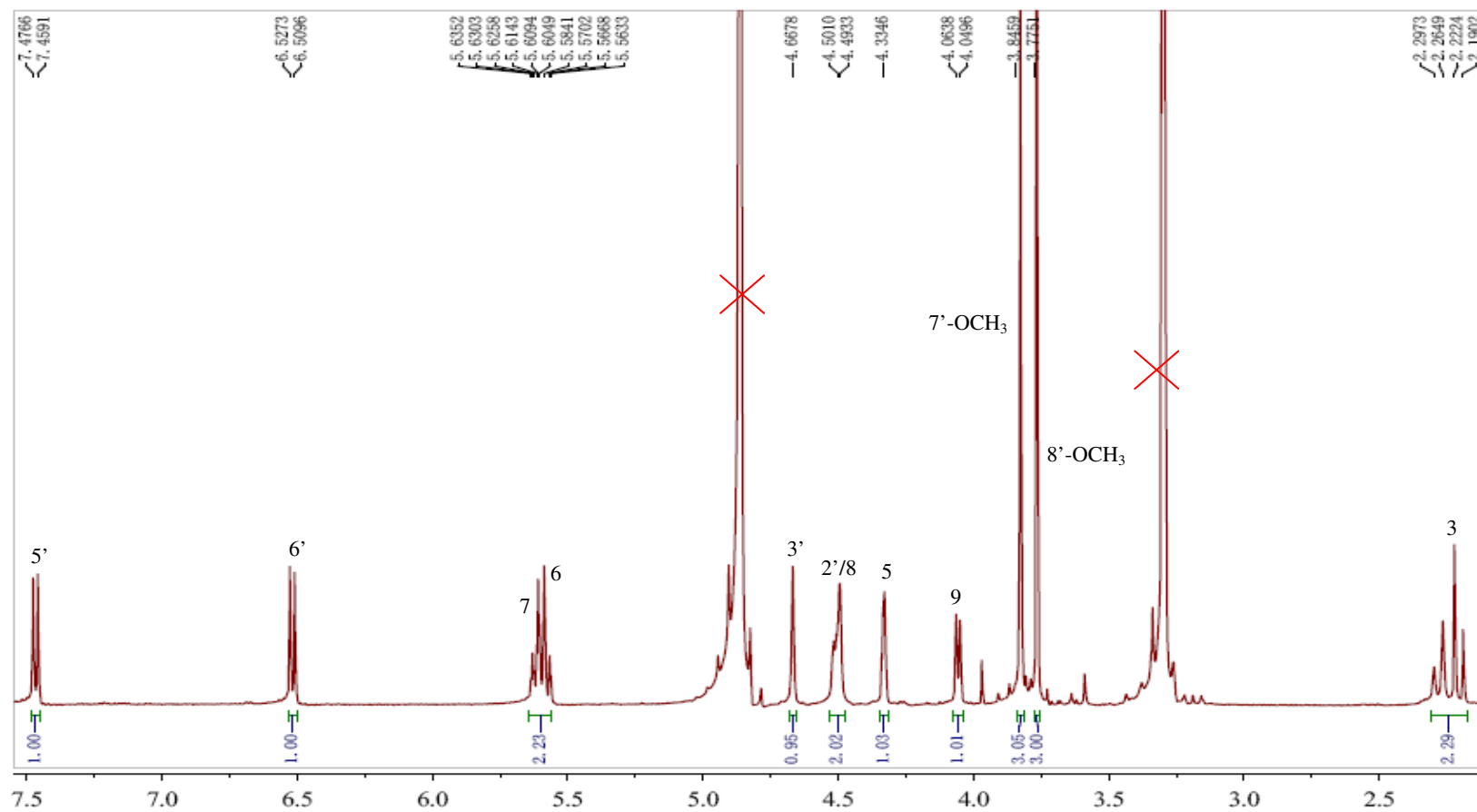
Attachment 17. The ^1H NMR spectrum of dihydrocitrinone (**17**, known)



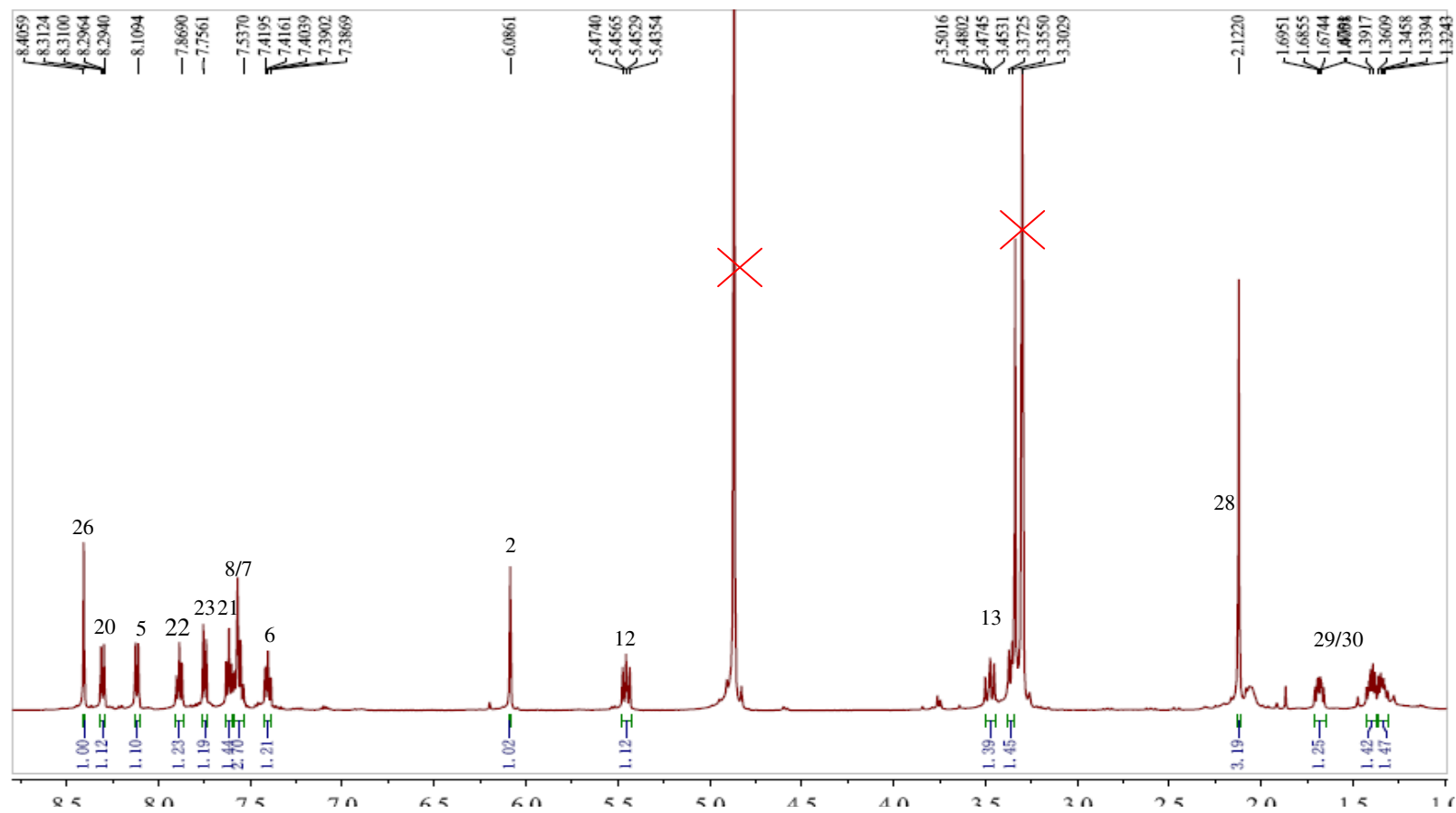
Attachment 18. The ^1H NMR spectrum of decarboxydhycitrinone (**18**, known)



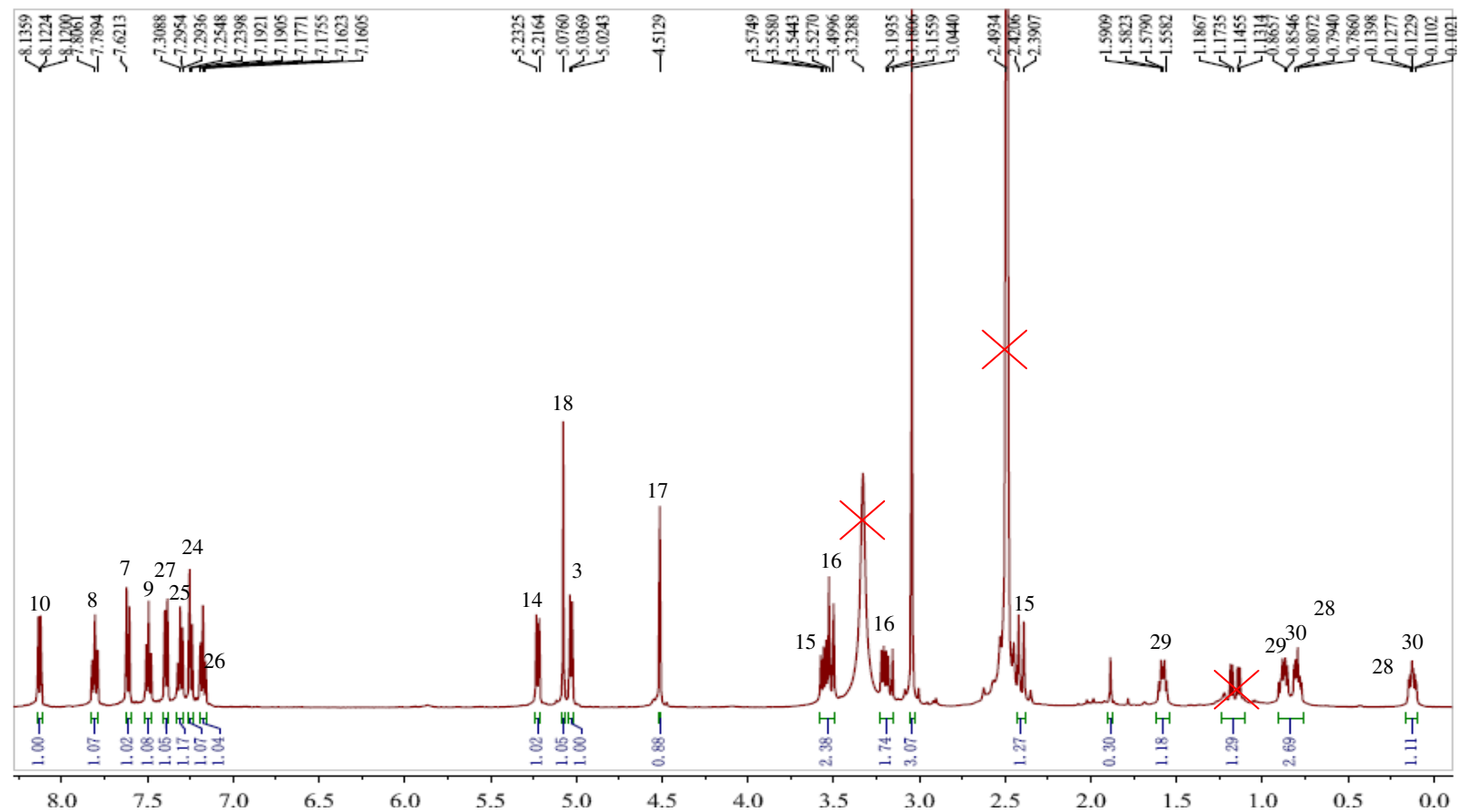
Attachment 19. The ^1H NMR spectrum of pretrichodermamide A (**19**, known)



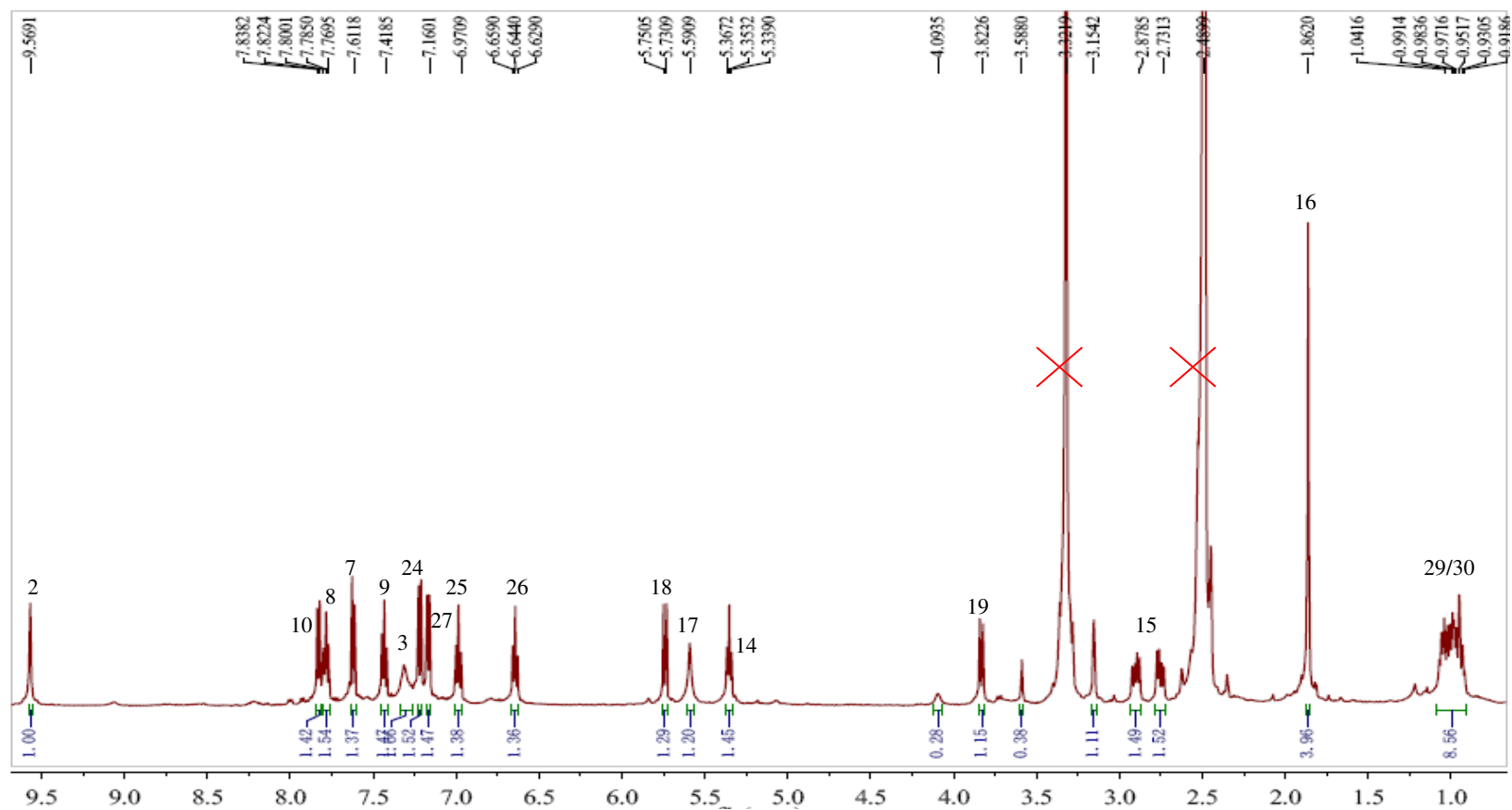
Attachment 20. The ^1H NMR spectrum of tryptoquivaline K (**20**, new)



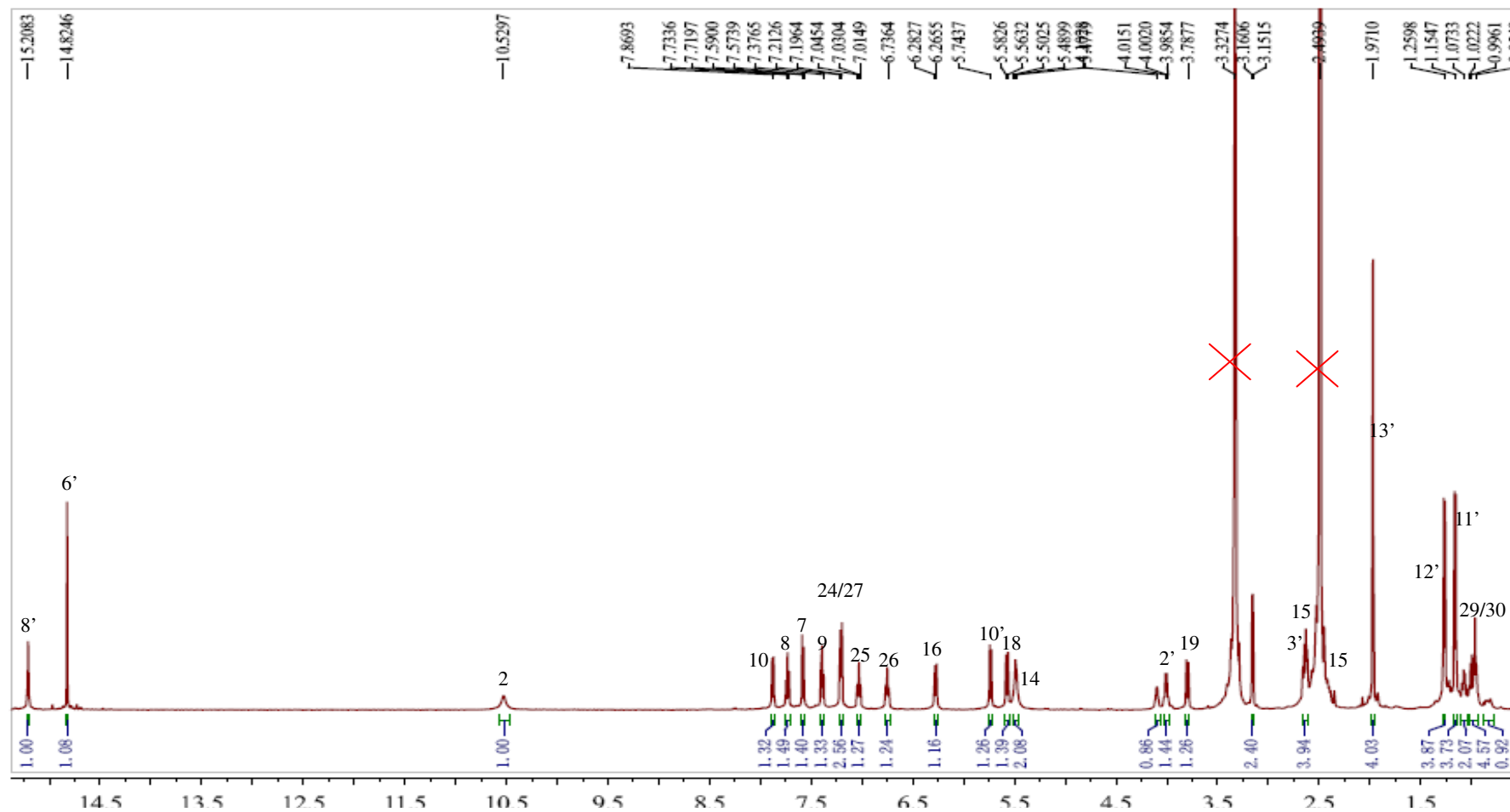
Attachment 21. The ^1H NMR spectrum of fumiquinazoline K (**21**, new)



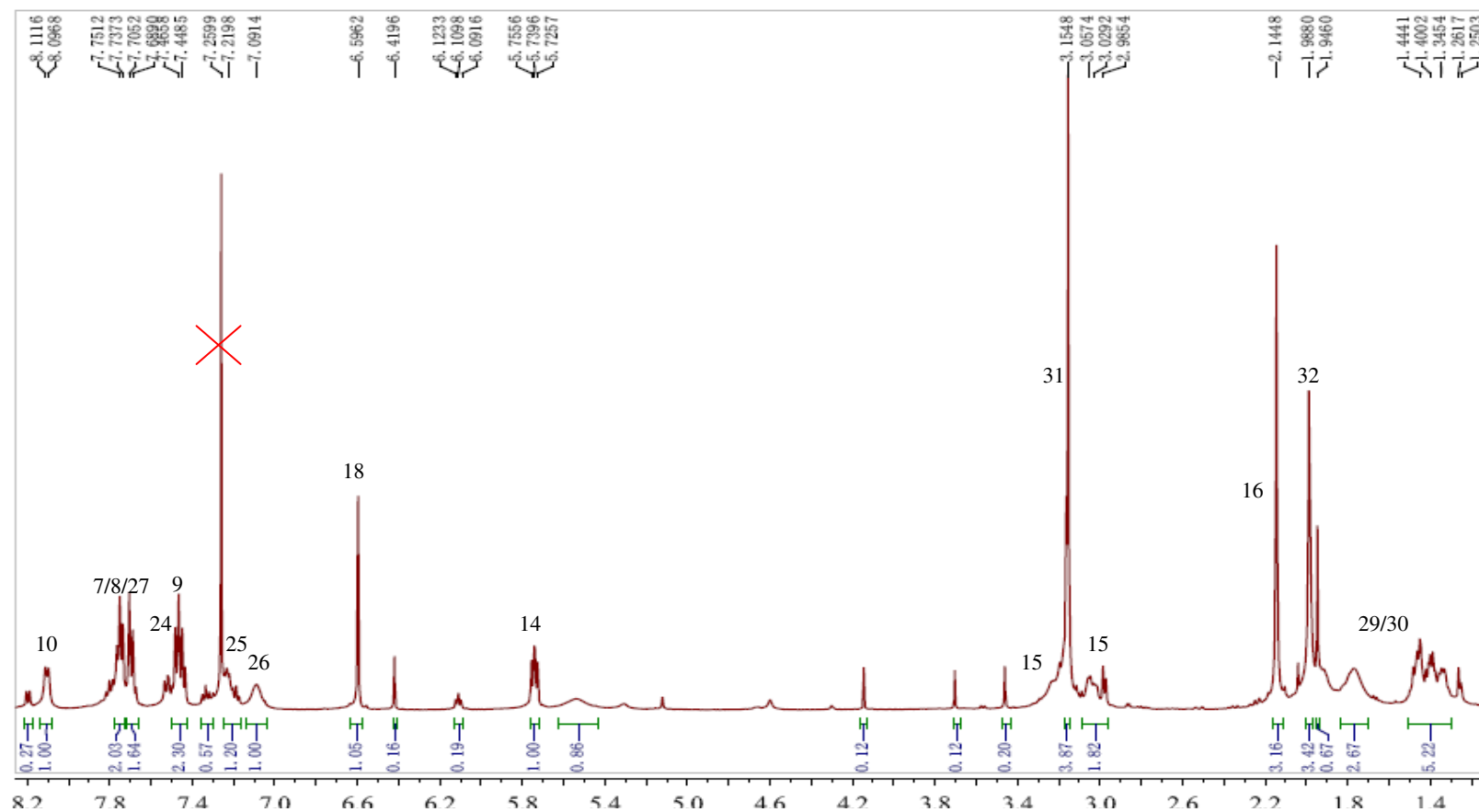
Attachment 22. The ^1H NMR spectrum of fumiquinazoline L (**22**, new)



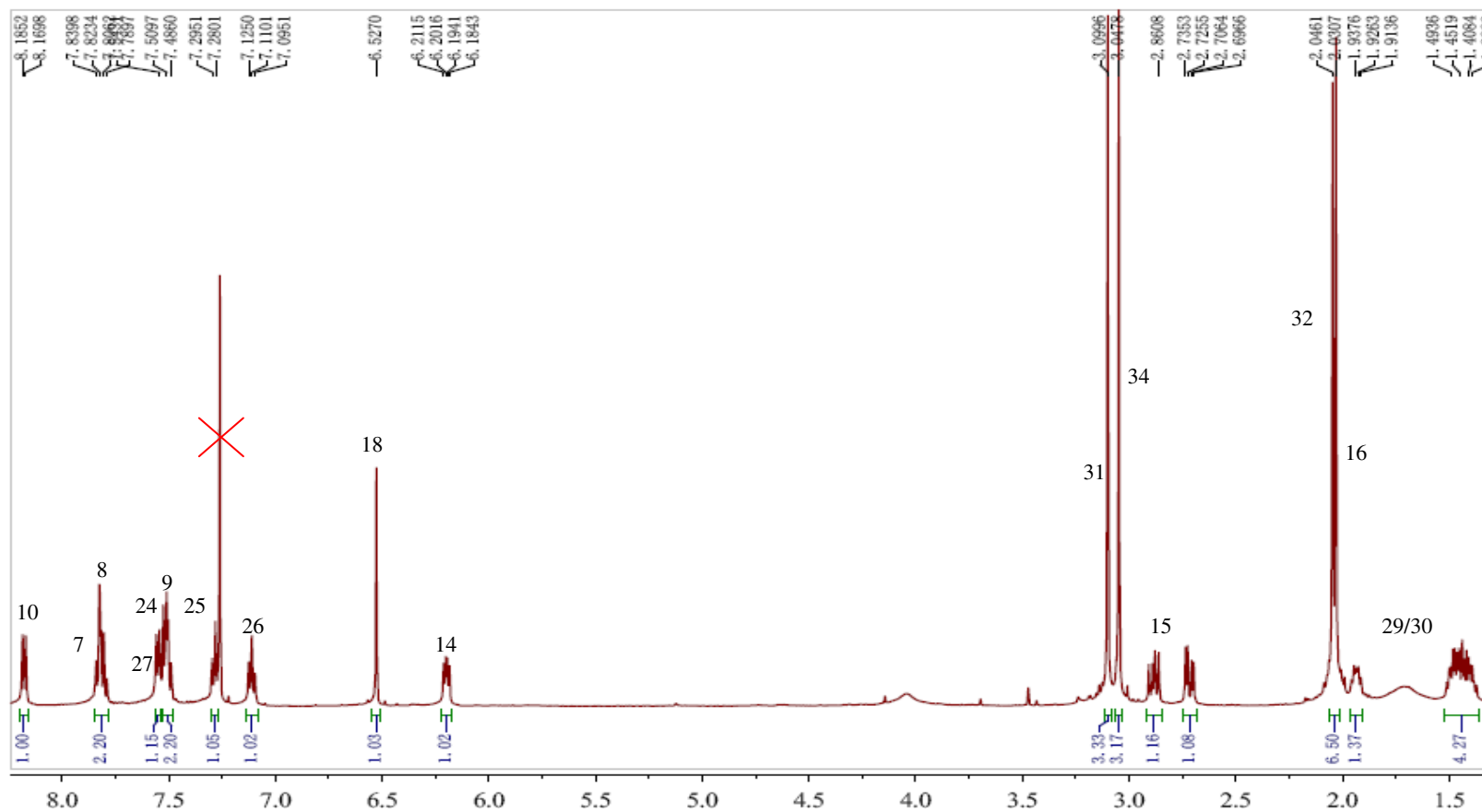
Attachment 23. The ^1H NMR spectrum of fumiquinazoline M (**23**, new)



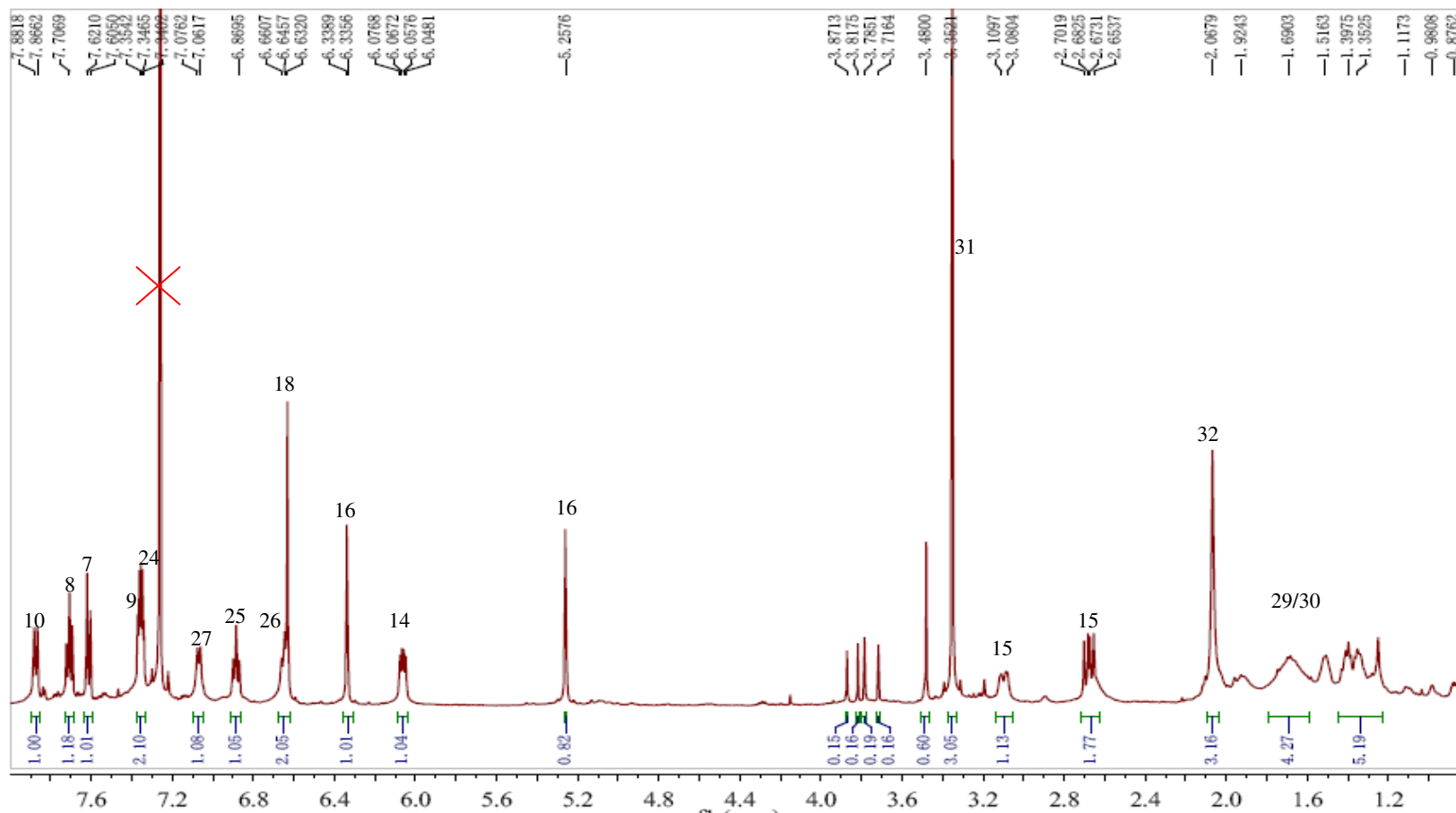
Attachment 24. The ^1H NMR spectrum of fumiquinazoline N (**24**, new)



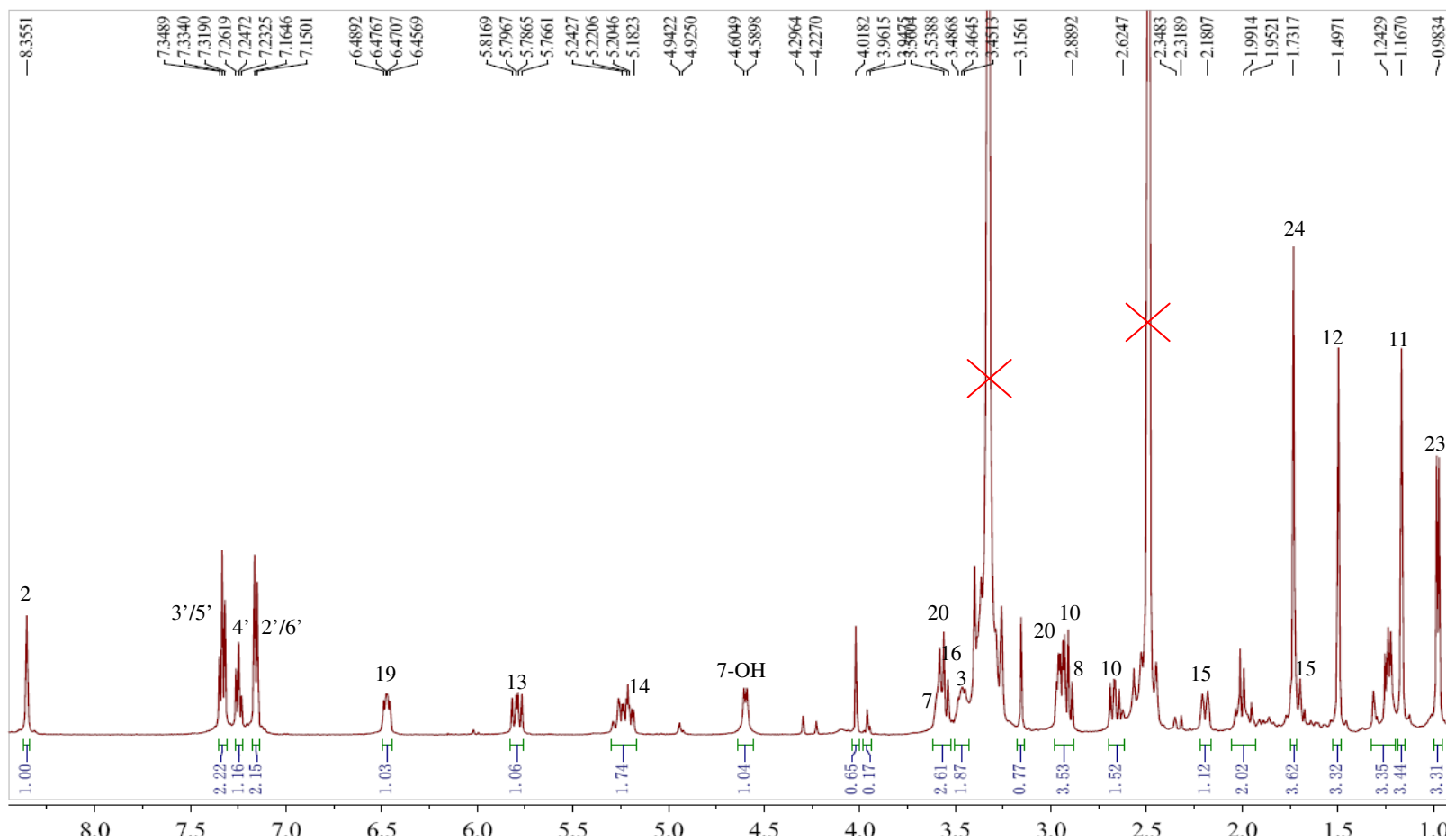
Attachment 25. The ^1H NMR spectrum of fumiquinazoline O (**25**, new)



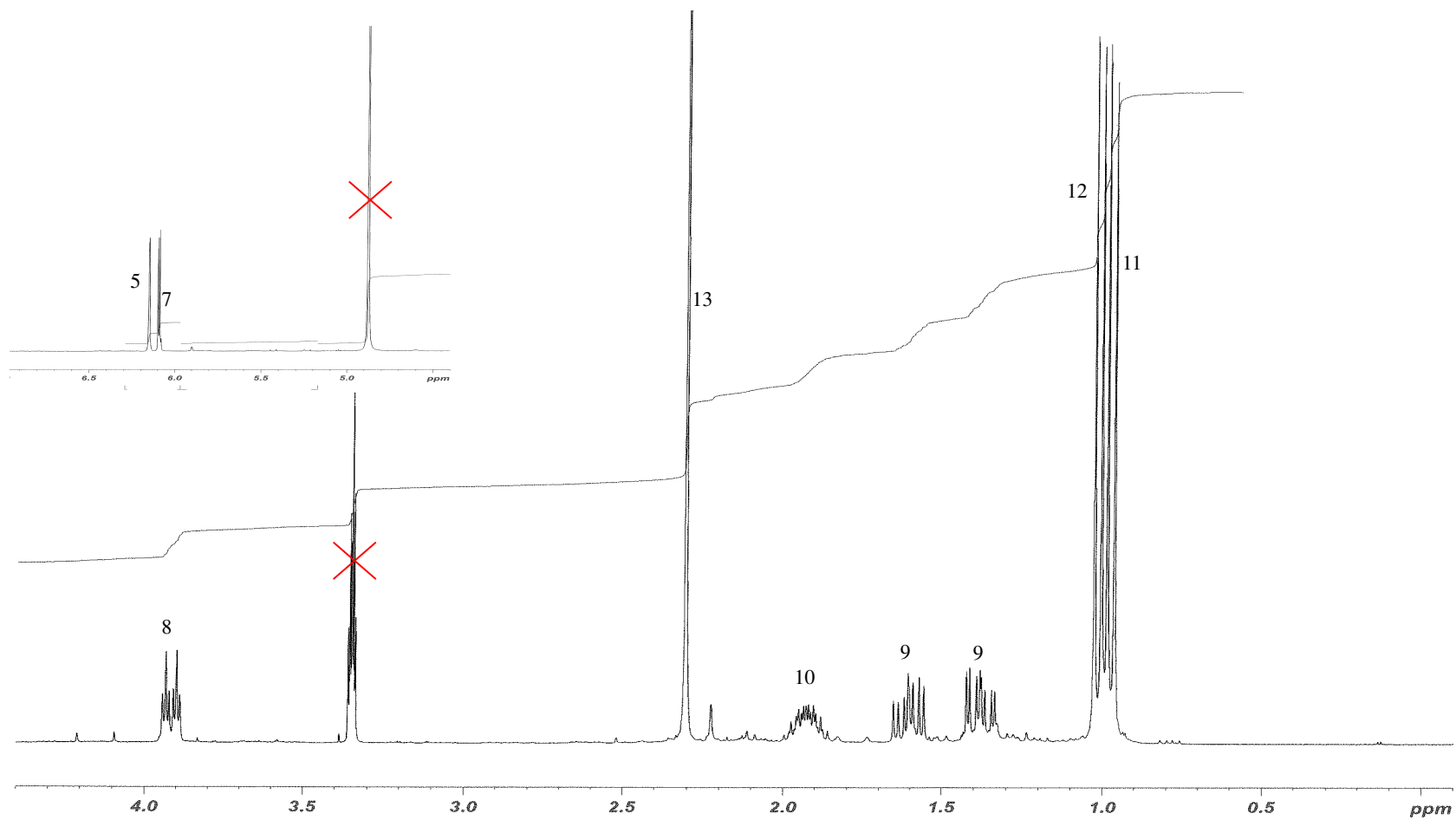
Attachment 26. The ^1H NMR spectrum of fumiquinazoline P (**26**, new)



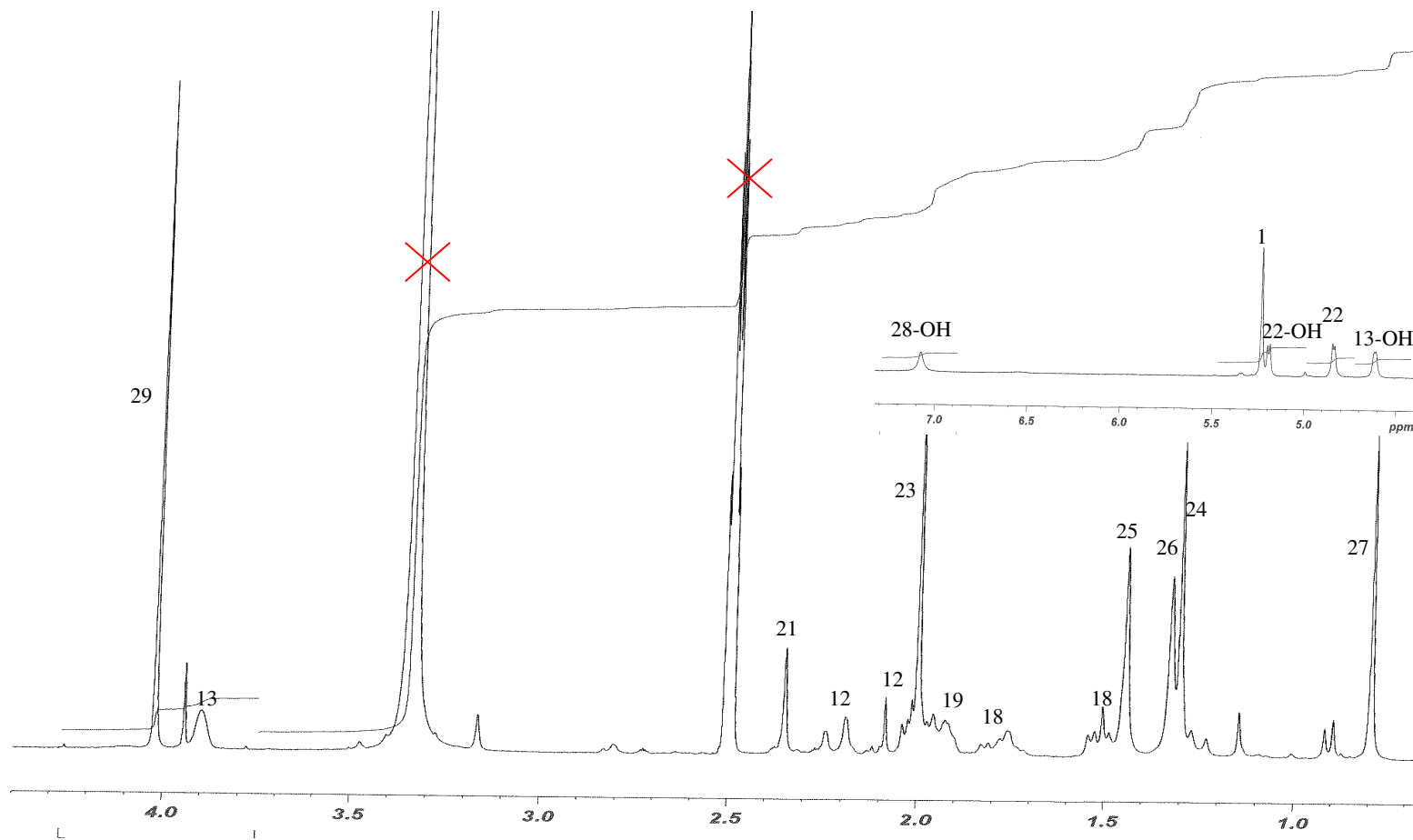
Attachment 27. The ^1H NMR spectrum of cytochalasin Z17 (**27**, known)



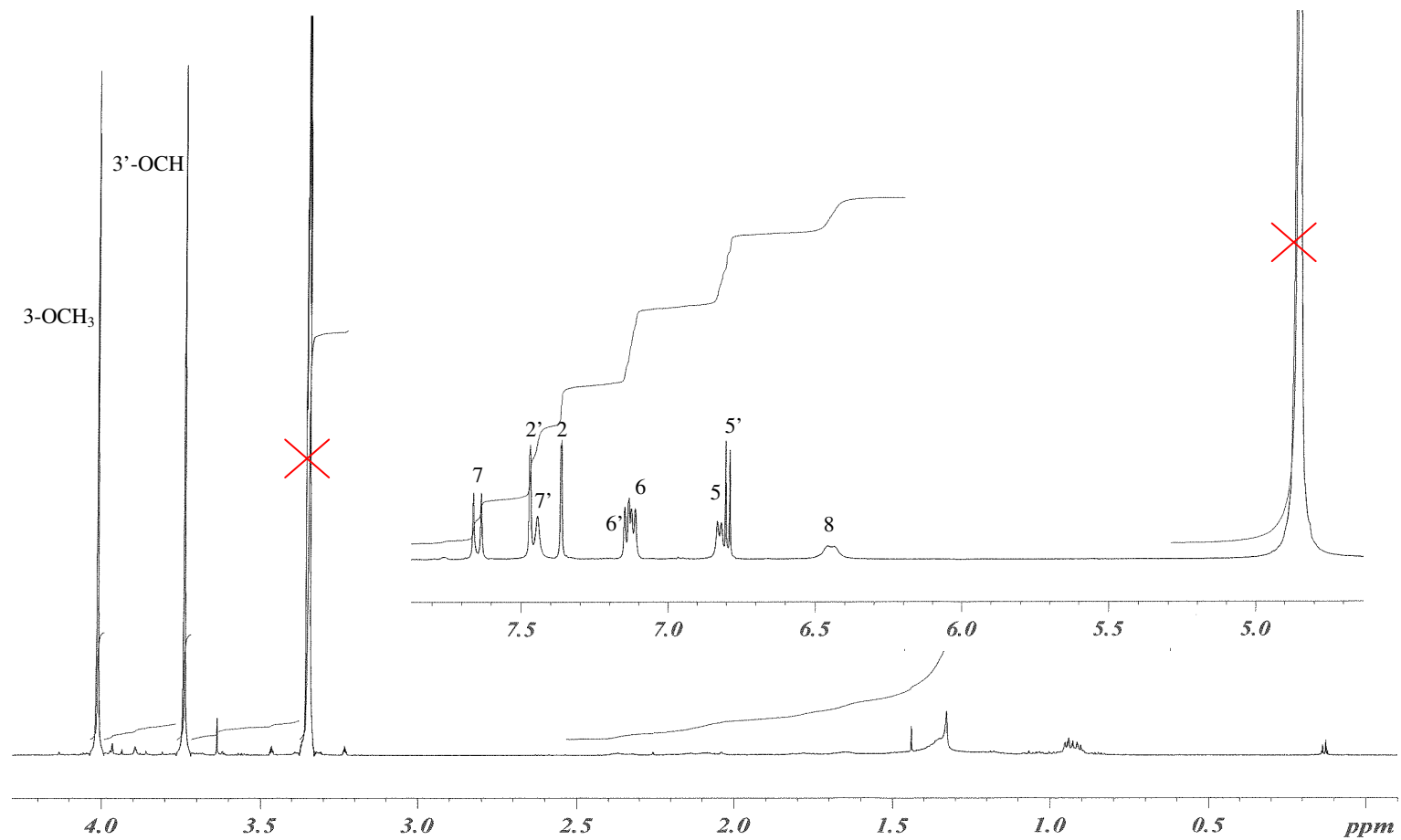
Attachment 28. The ^1H NMR spectrum of dihydroisoflavipucine (**28**, known)



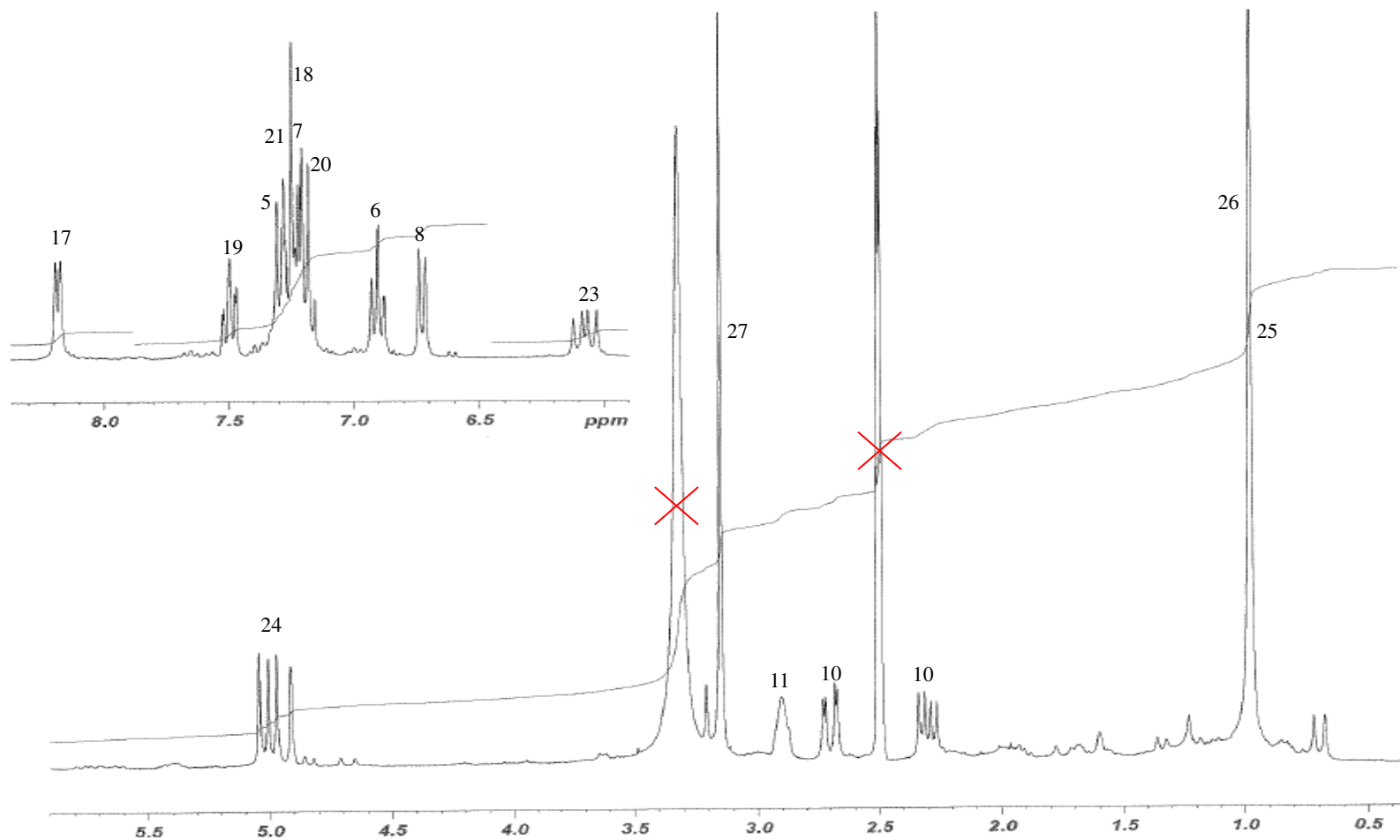
Attachment 29. The ^1H NMR spectrum of austrialide R (**29**, new)



Attachment 30. The ^1H NMR spectrum of 3-(4-(4-(2-carboxyvinyl)-2-methoxyphenoxy)-3-methoxyphenyl)-2-hydroxyacrylic acid (**30**, new)



Attachment 31. The ^1H NMR spectrum of 3-((1-hydroxy-3-(2-methylbut-3-en-2-yl)-2-oxindolin-3-yl)methyl)-1-methyl-3,4-dihydro-1*H*-benzo[*e*][1,4]diazepine-2,5-dione (**31**, new)



8. List of abbreviations

$[\alpha]_D^{20}$	Specific rotation at the sodium D-line
amu	Atomic mass unit
Approx.	Approximately
br	Broad signal
CC	Column chromatography
$CDCl_3$	Deuterated chloroform
$CHCl_3$	Chloroform
CI	Chemical ionization
COSY	Correlation spectroscopy
d	Doublet
DAD-HPLC	HPLC with diode array detector
dd	Doublet of doublet signal
DEPT	Distortionless enhancement by polarization transfer
DMSO	Dimethyl sulfoxide
e.g.	<i>exempli gratia</i> (for the sake of example)
EI	Electron impact ionization
ESI	Electron spray ionization
<i>et al.</i>	et altera (and others)
EtOAc	Ethyl acetate
eV	Electron Volt
FAB	Fast atom bombardment
g	Gram
HMBC	Heteronuclear multiple bond connectivity
HMQC	Heteronuclear multiple quantum coherence
H_2O	Water
HPLC	High performance liquid chromatography
HR-MS	High resolution-mass spectrometry
Hz	Hertz
IC_{50}	Half maximal inhibitory concentration
L	Liter
LC	Liquid chromatography
LC-MS	Liquid chromatography-mass spectrometry
m	Multiplet signal
MeOD	Deuterated methanol
MeOH	Methanol

List of abbreviations

mg	Milligram
MHz	Mega Hertz
min	Minute
mL	Milliliter
MS	Mass spectrometry
MTT	3-(4,5-Dimethylthiazol-2-yl)-2,5-diphenyltetrazolium bromide
<i>m/z</i>	Mass per charge
μ g	Microgram
μ L	Microliter
μ M	Micromolar
MW	Molecular weight
ng	Nanogram
<i>n</i> -BuOH	<i>n</i> -Butanol
NMR	Nuclear magnetic resonance
NOE	Nuclear Overhauser effect
NOESY	Nuclear Overhauser and exchange spectroscopy
ppm	Part per million
q	Quartet signal
ROESY	Rotating frame Overhauser enhancement spectroscopy
RP-18	Reversed phase C 18
s	Singlet signal
SAM	<i>S</i> -adenosyl methionine
Si	Silica
t	Triplet signal
TFA	Trifluoroacetic acid
TLC	Thin layer chromatography
UV	Ultra-violet
VLC	Vacuum liquid chromatography

9. Curriculum Vitae

Name: Yaming Zhou

Address: Institute of Pharmaceutical Biology and Biotechnology,
Heinrich-Heine-Universitaet Duesseldorf,
Universitaetsstraße 1, Geb. 26.23,
D-40225, Duesseldorf, Germany

Office Telephone: 0049-211-8111739

E-Mail: zhoyaming94@gmail.com

Current Research Subject

Bioactive marine natural products from the sponge-derived endophytic fungus *Aspergillus* sp.

Educational Background

- 10.2008 ~ Present Ph.D. student in Pharmacy, Institute of Pharmaceutical Biology and Biotechnology, Heinrich-Heine-Universitaet Duesseldorf, Germany
- 09.2005 ~ 07.2008 Master of Science in Plant Pathology, College of Agriculture & Biotechnology, China Agricultural University
- 09.2001 ~ 07.2005 Bachelor of Science in Food Science and Engineering, College of Food Science & Nutritional Engineering, China Agricultural University

Research Experience

- ✧ Ph.D. student in marine natural products at the Institute of Pharmaceutical Biology and Biotechnology, Heinrich-Heine University Düsseldorf, Germany, since 2008.
Supervisor: Prof. Dr. Peter Proksch
Fields: studies means useful for isolation, purification, and cultivation of endophytic fungi associated with various organisms (sponges and plants). Most importantly, work at the extraction, isolation, characterization and structure elucidation of biologically active secondary metabolites together with the preliminary evaluation of their pharmacological properties based on rapid screening system.
- ✧ Key laboratory of Plant Pathology, Ministry of Agriculture, P. R. China, College of Agriculture & Biotechnology, China Agricultural University, 06.2006 ~ 06.2008.
Supervisor: Prof. Dr. Ligang Zhou
Fields: research on plant antimicrobial compounds in addition to work with fungi and bacteria subculture and storage, identification of fungi, and preliminary antimicrobial assays of the extractions, fractions and compounds in Plant-Microbe Interactions Group.

Honors

Granted a full scholarship from Program of Governmental Graduate Students Scholarship launched by China Scholarship Council (2008)

Self-Evaluation

- ✧ Progressive, strong self-learning ability and team spirit
- ✧ Hard-working and strong ability to forge ahead
- ✧ Effective communicative and totally adaptive abilities
- ✧ Energetic and strong sense of responsibility

References

1. **Yaming Zhou**, Attila Mándi, Abdessamad Debbab, Victor Wray, Barbara Schulz, Werner E. G. Müller, WenHan

- Lin, Peter Proksch, Tibor Kurtán, Amal H. Aly. New austalides from the sponge-associated fungus *Aspergillus* sp., *European Journal of Organic Chemistry*, 2011, (30): 6009-6019.
2. **Yaming Zhou**, Attila Mándi, Abdessamad Debbab, Victor Wray, Barbara Schulz, Werner E. G. Müller, WenHan Lin, Tibor Kurtán, Amal H. Aly, Peter Proksch. New alkaloids from the sponge-associated fungus *Aspergillus* sp. (Submitted)
 3. **Yaming Zhou**, Hao Liu, Jianglin Zhao, Manliang Tan, Peng Sui, Jingguo Wang, Ligang Zhou. Poplar stem blister canker and its control strategies by plant extracts, *World Journal of Microbiology and Biotechnology*, 2008, 24 (8): 1579-1584.
 4. **Yaming Zhou**, Hao Liu, Lingyun Zhong, Ligang Zhou, Peng Sui, Zejian Guo. Inhibitory activity of extracts and fractions of *Populus × euramericana* on plant pathogenic fungi in vitro, *Guihaia*, 2009, 29 (2): 275-278.
 5. **Yaming Zhou**, Hao Liu, Yuan Zhao, Ligang Zhou, Peng Sui, Zejian Guo. In vitro inhibitory activity of extracts and fractions of *Populus × euramericana* cl. 'Zhonglin 46' on plant pathogenic fungi, *Acta Agriculturae Boreali-occidentalis Sinica*, 2008, 17 (3): 308-311, 323.
 6. Jianping Wang, **Yaming Zhou**, Yujie Ye, Xianmei Shang, Yaling Cai, Chaomei Xiong, Yunxia Wu, Haixing Xu. Topical anti-inflammatory and analgesic activity of kirenol isolated from *Siegesbeckia orientalis*, *Journal of Ethnopharmacology*, 2011, 137 (3): 1089-1094.
 7. Jianping Wang, **Yaming Zhou**. Kirenol production in hairy root culture of *Siegesbeckia orientalis* and Its antimicrobial activity, *Pharmacognosy Magazine*, 2012, 8 (30): 149-154.
 8. Hongbing Yang, **Yaming Zhou**, Hao Liu, Hua Du, Zhanhong Ma, Chun Li, Ligang Zhou. Inhibitory activity of extracts and fractions from six chenopodiaceae plants on plant pathology, *Natural Product Research and Development*, 2009, 21: 744-747.
 9. Lingyun Zhong, Ligang Zhou, **Yaming Zhou**, Yuanquan Chen, Peng Sui, Jingguo Wang, Mingan Wang. Antimicrobial flavonoids from the twigs of *Populus nigra × Populus deltoids*, *Natural Product Research*, 2012, 26 (4): 307-313.
 10. Hongbing Yang, Hua Du, **Yaming Zhou**, Hao Liu, Zhanhong Ma, Chun Li, Ligang Zhou. Antifungal activity of the extracts and fractions of six chenopodiaceae plant species, *Abstracts/Journal of Biotechnology*, 2008, 136, Supplement, S89.
 11. Jing Tang, Ligang Zhou, **Yaming Zhou**, Hua Du, Hao Liu, Zejian Guo, Jingguo Wang. Inhibitory effects of *Phellodendron chinense* Schneid extracts on some phytopathogenic fungi, *Natural Product Research and Development*, 2008, 20: 505-507.
 12. Jing Tang, Ligang Zhou, Xiaodong Cao, Guanghui Xie, Peng Sui, Manliang Tan, **Yaming Zhou**. Inhibition of plant extracts, sodium carbonate and sodium bicarbonate on the pathogen of poplar canker *Botryosphaeria dothidea*. *Acta Phytopathologica Sinica*, 2006, 36 (5): 446-453.

Conferences

1. ScieTalk NRW: Cutting-Edge Technologies in Molecular Life Sciences, November 23th, 2011, Münster, Germany. (Poster presentation)
2. 6th Annual Meeting of The Chinese Association for Life Science and Biotechnology in Germany, September 24-25th, 2011, Bonn.
3. 4th Asia-Link Meeting & 10th Anniversary of Proksch Group at HHU, September 20-22th, 2010, Duesseldorf.
4. Annual Meeting of Chinese Society for Plant Pathology, August 5-9th, 2007, Sian. (Oral presentation)